Vibro-acoustic study of the clavichord

Jean-Théo Jiolat

École doctorale de Sciences Mécaniques, Acoustique, Électronique et Robotique de Paris (ED 391)

Thèse

pour obtenir le grade de docteur de

Sorbonne Université

Spécialité "Acoustique"

Vibro-Acoustic Study of the Clavichord

Par Jean-Théo Jiolat

Soutenue le 25 juin 2021 devant le jury composé de :

Rapporteur :	Emmanuel Foltête,	Professeur, ENSMM, Besançon
Rapporteur :	François Gautier,	Professeur, ENSIM, Le Mans
Examinateur :	José Antunes,	Principal Researcher, C2TN, Bobadela
Examinateur :	Régis Marchiano,	Professeur, SU, Paris
Examinatrice :	Caroline Traube,	Professeure, Université de Montréal, Montréal
Directeur de thèse :	Christophe D'Alessandro,	Directeur de Recherche CNRS, SU, Paris
Co-directeur de thèse :	Jean-Loïc Le Carrou,	Maître de Conférences HDR, SU, Paris
Invitée :	Théodora Psychoyou,	Maîtresse de Conférences, SU, Paris
Invité :	Thomas Steiner,	Chercheur associé, Université de Bâle, Bâle

Bin ich dann gleich von Schmerz umgeben,
So schaffest du mir Trost und Ruh.
O wäre doch mein ganzes Leben
So freudenvoll und sanft wie du.

Dank, Dank sey dem der dich erfunden,
Mein silbertönendes Klavier!
Durch dich versüss' ich trübe Stunden
Durch deine sanfte Töne mir.

Ernestine Krüger (1767-1843), "An das Clavier wenn es rein gestimmt is".[1]

Ted Rosenthal: *When I was listening to your "Book of Ways,"(clavichord improvisations) there were a number of pieces that were in a contrapuntal, perhaps baroque or early classical style. So I thought you were improvising in that style.*

Keith Jarrett: *Well, when sound takes me there, then it's not improvising in a style to me. It's the sound (and) how it relates to what I've heard maybe. It can turn into that especially if the instrument is so provocatively historical which, of course the clavichord is.*

Interview between Keith Jarrett and Ted Rosenthal, 'The Insanity of Doing More than One Musical Thing', *Piano and Keyboard Magazine* (January 1997).

[1]Georg Jacob Decker, *Anleitung zur Singkomposition*, Berlin, 1781, Allgemeine Musik-Gesellschaft Zürich, Signatur: AMG III 711, Dauerleihgabe in der Zentralbibliothek Zürich.

Remerciements

Je souhaite remercier François Gautier et Emmanuel Foltête pour avoir accepté d'être les rapporteurs de cette thèse. Je remercie également Régis Marchiano et Caroline Traube qui ont accepté d'être les examinateurs de ce travail. En particulier, je remercie José Antunes avec lequel j'ai collaboré. Ses enseignements en matière de modélisation et simulation de systèmes vibratoires ont été d'une aide précieuse. Je remercie Théodora Psychoyou d'avoir accepté l'invitation à ma soutenance de thèse et pour ses remarques sur les aspects musicologiques de mon sujet de recherche. Je remercie également Thomas Steiner pour l'attention qu'il a portée à mon travail de rédaction. Ses remarques sur l'organologie du clavicorde ainsi que sur les traités portant sur cet instrument ont permis d'améliorer la qualité du manuscrit. Les questions et les remarques qui ont été avancées par le jury ont été très enrichissantes.

Ce travail de thèse fait suite à un stage de M2 porté sur une étude vibratoire préliminaire des cordes sympathiques du clavicorde, proposé par Christophe d'Alessandro ainsi que Jean-Loïc Le Carrou. Je remercie Christophe, déjà parce qu'il a construit le clavicorde sur lequel j'ai pu faire mes recherches ! Mais surtout, je le remercie pour son encadrement, sa sollicitude, et sa présence. Compte tenu de son savoir musical et de sa pratique des instruments à clavier, il m'a apporté une ressource symbolique et des connaissances considérables autour du clavicorde. Je remercie Jean-Loïc pour l'encadrement rigoureux dont il a fait preuve, l'expertise qu'il m'a apportée dans le domaine de la vibro-acoustique, son accompagnement, ainsi que pour le dynamisme qu'il a insufflé à ce travail de thèse. Cette équipe encadrante a été déterminante dans la bonne conduite de mes recherches sur la vibro-acoustique du clavicorde.

Je remercie mes collègues de bureau Youssri El Majaty ainsi que Xiasu Yang pour les nombreuses discussions qu'on a pu avoir, soit autour de sujets sur l'ingénierie mécanique en général, soit autour de sujets divers et variés au cours de nos déjeuners journaliers. Je remercie Manuel Gaulhiac pour les discussions passionnantes que j'ai pu avoir avec lui durant ces années de thèse. Les études de philosophie que j'ai effectuées en cours du soir à l'Institut Catholique de Paris durant ces mêmes années ont permis d'enrichir nos entretiens sur l'esthétique musicale, ou sur des sujets proprement philosophiques. Je remercie également Grégoire Locqueville avec lequel j'ai pu m'entretenir occasionnellement et avec beaucoup plaisir autour de l'enregistrement musical. Je remercie Antoine Monier pour son assistance s'agissant de la diffusion en ligne et en direct de ma soutenance de thèse.

Je remercie les membres de l'IJLRA, et spécifiquement l'équipe LAM. Je remercie en particulier Laurent Quartier pour son aide technique, ainsi que Sandrine Bandeira pour son aide administrative. Je remercie également Héloïse Lafont et Damien Bestard qui ont participé à un projet de Master 1 que j'ai encadré. Je remercie Sébastien Guy avec qui j'ai travaillé à l'occasion d'un stage. Je remercie Armand

Schwarz pour son assistance au clavicorde durant ma soutenance de thèse ainsi que pour son travail de stage que j'ai dirigé. Je remercie également Yvan Giro pour le travail de recherche sur l'étude du couplage des cordes sympathiques du hardingfele que j'ai pu encadrer avec Jean-Loïc Le Carrou et Louise Condi. Je les remercie de m'avoir proposé de participer à cet encadrement.

Je remercie mes amis de longue date de sciences et musicologie qui sont venus à ma soutenance : Noé, Louise, Louis ainsi que Tristan. Ça m'a fait vraiment plaisir de les revoir après une longue absence : *Long time no see* comme on dit. Merci aussi à une de mes vielles connaissances, Téo du M1 d'ingénierie mécanique, d'être venu également.

Je souhaite également remercier Charlotte de la licence de philosophie d'avoir assisté en ligne à ma soutenance de thèse. Merci à Morgane pour les moments qu'on a passés ensemble durant nos révisions de philosophie, qui ont eu lieu durant la fin de ma thèse.

Je remercie enfin ma famille pour m'avoir soutenu durant ces années.

Contents

List of Symbols

M	Number of particles
$\mathbf{M}$	Mass matrix (kg)
$\boldsymbol{M}$	Modal mass matrix (kg)
m_n^s	Modal mass of substructure s (kg)
P	Number of constraints
P_h	Number of holonomic constraints
P_{nh}	Number of non-holonomic constraints
t	Time (s)
Y	Dynamic response (m)
$\mathbf{y}$	Coupled system displacement vector (m)
$\mathbf{y}_u$	Uncoupled system displacement vector (m)
$\mathbf{v}$	Coupled system velocity vector ($\mathrm{m.s^{-1}}$)
$\mathbf{F}_e$	Constraining forces vector (N)
$\mathbf{F}_c$	Constraining forces vector (N)
φ	Holonomic constraints
ψ	Non-holonomic constraints
$\mathbf{A}$	Constraint matrix
$\boldsymbol{A}$	Modal constraint matrix
$\mathbf{b}$	Constraint vector
$\mathbf{r}$	Rank of the constraint matrix
λ	Lagrange multipliers
$\mathbf{F}_{nl}$	Non-linear force vector (N)
$\boldsymbol{F}_{nl}$	Modal non-linear force vector (N)
F_{nl}	Non-linear force (N)
$\mathbf{F}_{ext}$	Excitation force vector (N)
$\boldsymbol{F}_{ext}$	Modal excitation force vector (N)
$\mathbf{r}$	Coordinate vector (m)
q_n	Modal amplitude
$\mathbf{q}$	Coupled system modal amplitude vector
$\mathbf{q}_u$	Uncoupled system modal amplitude vector
N	Number of modes
$\boldsymbol{C}$	Modal damping matrix ($\mathrm{kg.s^{-1}}$)
c_n^s	Modal damping of substructure s ($\mathrm{kg.s^{-1}}$)
$\boldsymbol{K}$	Modal stiffness matrix ($\mathrm{N.m^{-1}}$)
k_n^s	Modal stiffness of substructure s ($\mathrm{N.m^{-1}}$)
ρ	Mass density ($\mathrm{kg.m^{-3}}$
ω_n	Modal pulsation ($\mathrm{s^{-1}}$)
ξ_n	Modal damping ratio (%)

L	String length (m)
f_0	Fundamental frequency (Hz)
f_n	Modal frequency (Hz)
μ	Linear density (kg.m^{-1})
T_0	String tension at rest (N)
S	string cross-section area (m^2)
T_{dyn}	Dynamic tension (N)
T_{stat}	Static tension (N)
E	Young modulus (Pa)
I	Second moment of inertia (m^2)
B	Inharmonic coefficient
c_0	velocity of the string transverse wave (m.s^{-1})
Q	Quality factor
δ_{ve-te}	Dissipation of the visco-elastic effects
R	Mechanical resistance (N.s.m^{-2})
η_{air}	Dynamic viscosity of the air (Pa.s)
L_T	Length of the key (m)
L_{tg}	Distance between the key extremity and the tangent (m)
L_p	Distance between the key extremity and the pivot on the key (m)
L_f	Distance between the key extremity and the finger on the key (m)
ϵ_n	Relative error at mode n
E_e	Energy (J)
W	Mechanical work (J)
Δt	Time step (s)
F_s	Sampling frequency (Hz)
EDC	Energy decay curve
SC	Spectral centroid (Hz)
a_k	spectral amplitude
A_k	Residu
k_n	String wave number of mode n (m^{-1})
Y_c	Coupling admittance between the string and the bridge (m.s^{-1}.N^{-1})
H	Mobility of the bridge (m.s^{-1}.N^{-1})
Ω	Dynamic matrix (s^{-1})
ϵ	Mistuning between two strings
Z_0	Characteristic admittance of the string (N.s.m^{-1})
$\beta_\pm$	Eigen values of the dynamic matrix

Part I

Introduction

Chapter 1

Context and positioning of the PhD

This PhD is devoted to the vibro-acoustic study of the clavichord. It aims at highlighting the specific vibro-acoustic features of this instrument from its excitation system to the vibration of the sympathetic strings. The excitation system is significantly different from that of the other keyboard instruments. It is possible to control the pitch of the clavichord vibrating string after exciting it. No other acoustic keyboard instrument is able to create such an effect. This is the reason why the clavichord was commonly considered, mostly in the XVIII$^{\text{th}}$ Germany, as the most expressive keyboard instrument. Indeed, the clavichord player can take advantage of this control to enhance the expressivity of its musical playing, for example by producing vibrato. Also, because of its mechanical constraints, this clavichord excitation system imposes a specific gesture to achieve this expressivity. One has to play fast in order to play loudly, while mastering the control of the produced sound pitch. As a result, keyboard players used this instrument to shape their musical gesture. The clavichord pedagogical quality was especially acknowledged by Carl Philipp Emmanuel Bach, who claimed that it was his most favoring instrument [1]. The sympathetic strings play a significant role in the acoustic functioning of the clavichord. The sound produced by the clavichord is not very loud, largely outmatched by that of the piano and the harpsichord. The reverberation effect created by the sympathetic strings is often used in the case of the clavichord to increase the produced sound loudness. Also, some of these sympathetic strings can resonate because of frequency coincidence with the excited string. This is generally avoided by the clavichord makers because this resonance could be detrimental for the musical sound. The excitation system of the clavichord and its sympathetic strings vibration creating reverberation and resonance are the two main topics studied in the work. A modelling of the clavichord is proposed by means of a formulation conceived to model coupled mechanical systems. To study these vibro-acoustic features, the model is simulated and compared with measurements.

The aim of the present chapter is to introduce the clavichord, considering its organological and acoustic features, along side with the presentation of the clavichord studied in this PhD, and setting the context related to the scientific study of this instrument. To start with, a brief organological description of the clavichord is given in section 1.1. An historical account of the organological evolution of this instrument is given in section 1.2. Then, the specific clavichord chosen for our study is presented in section 1.3 whose instrument making is based on a specific clavichord historical model. The differences between the two are underlined in the same section. All

the scientific studies that have been done so far on the clavichord is summed up in section 1.4. Considering that the clavichord is an acoustic keyboard instrument, a brief state of the art of musical acoustic studies on the piano and the harpsichord is given in section 1.5. Since this PhD focuses on the modelling of the clavichord by considering it like a mechanical coupled system, an overview of coupling models used in musical acoustics is provided in section 1.6. Finally, the specific objectives of this PhD are presented in details in section 1.7.

1.1 Organological description of the clavichord

Along a time span of five centuries, the clavichord has undergone a few organological evolutions of different kinds with respect to the different European and South American countries. Nevertheless, there are organalogical invariants regarding this instrument which forge its identity. First of all, the clavichord has rectangular dimensions, except for some instruments which are polygonal. Even wing-shaped clavichords dating back to at least 1470 have existed [2]. In the right hand side of the instrument, there is the soundboard whose dimensions vary depending on the different clavichords. In its left hand side and at its centre, all the organological elements constituting the excitation system are found. Namely, these are the keys whose extremities are located below the strings. The stringing occupies the whole dimensions of the instrument (see figure 1.1).

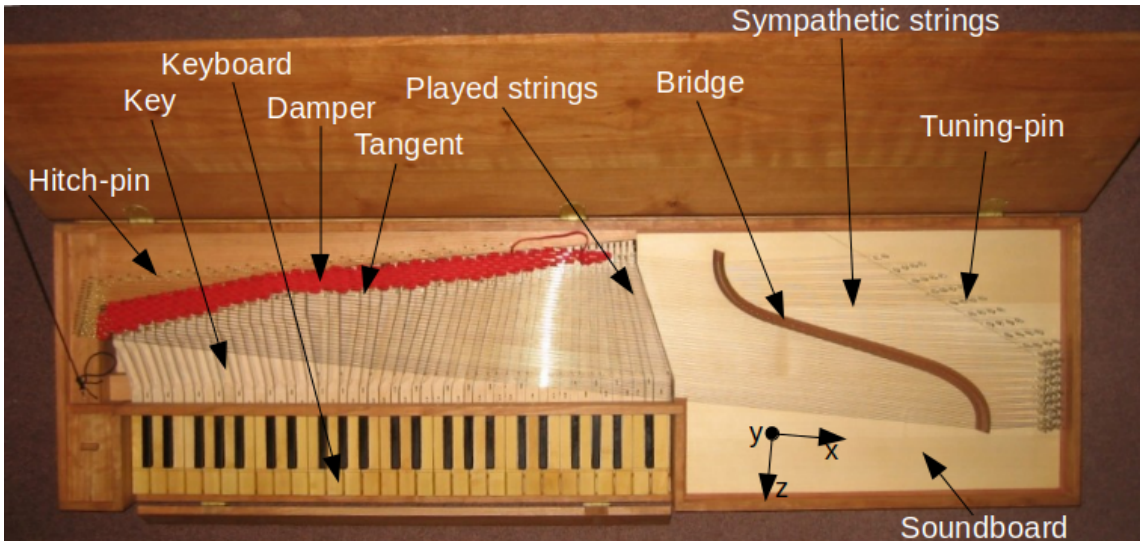

Figure 1.1: A view from above of the LAM1 clavichord (copy of a model designed by Christian Gottlob Hubert, see section 1.3) designed by E. Dancet and M. Ducornet, with the principal parts.

The strings are stretched by means of tuning pins laid out on the soundboard. The other strings' extremity is placed at the left hand side of the clavichord by means of hitch-pins. It is possible to divide the strings in three parts : 1. the part which goes from the hitch-pin to the tangent (damped part of the string), 2. the part which goes from the tangent to the bridge pin (played part of the string), 3. and the part which goes from the bridge pin to the tuning pin, which is commonly called the sympathetic part of the string. A strip of cloth is laid out at the extremity of the strings, near the hitch-pin, in order to damp the strings' vibration once their corresponding keys are released. This instrument is usually double strung, which means that each note is produced by the excitation of a pair of strings. As to the clavichord presented in figure 1.1, it is fretted from the $F_2 - F\#_2$ pair of strings up to the final treble string, which means that two tangents strike the same string at two different locations to produce two different notes separated by a half tone.

The way this instrument functions is simple : a small metal blade called the tangent is laid out at the extremity of each key (see figure 1.2). Once the musician finger presses one of the keys, the tangent is uplifted on the basis of the lever principle. As the tangents are located below the strings, the uplifted tangent impacts a pair of strings. As long as the finger pressure on the key remains, the tangent remains in contact with the pair of strings. Then, the tangent becomes a boundary condition working like a nut. Following the impact, the pair of strings is put into vibration according to a length bounded by the tangent and the bridge. The instrument strings are pressed vertically on the bridge and pressed horizontally on the pins laid out along the bridge (see figure 1.2). This contact leads to the coupling of the strings with the clavichord soundboard. By means of this coupling, the vibratory energy of the excited strings is transmitted to the soundboard whose role is to radiate the sound in the air. The tangent is in contact with the string as long as the musician finger remains pressed on the key. After the tangent impact, it uplifts the string with a height determined by the finger force exerted on the key. By uplifting the key, the excited string tension increases. This increase in tension leads to the increase in the string fundamental frequency. The frequency variation created by the variation of the finger pressure is audible [3]. Thus, this excitation mechanism leads to a direct control on the excited string frequency by the musician. This is the most singular acoustic feature of the clavichord, which is not found in any other keyboard string instruments. To play the clavichord with rigour, one must develop a specific gesture adapted to the mechanical constraints imposed by the excitation system [4].A summary of all the main vibratory components is present with a block diagram presented in figure 1.3. This diagram summarises the interaction of each of these components from the input given to the system up to the output produced by it. To model the instrument, only a few of these components can be taken into account: The key-tangent substructure, the muffled strings, the played strings, the sympathetic strings and the bridge. This reduction of the clavichord can be simulated in order to focus on the interested physical phenomena. The selected components are pointed out by the red color.

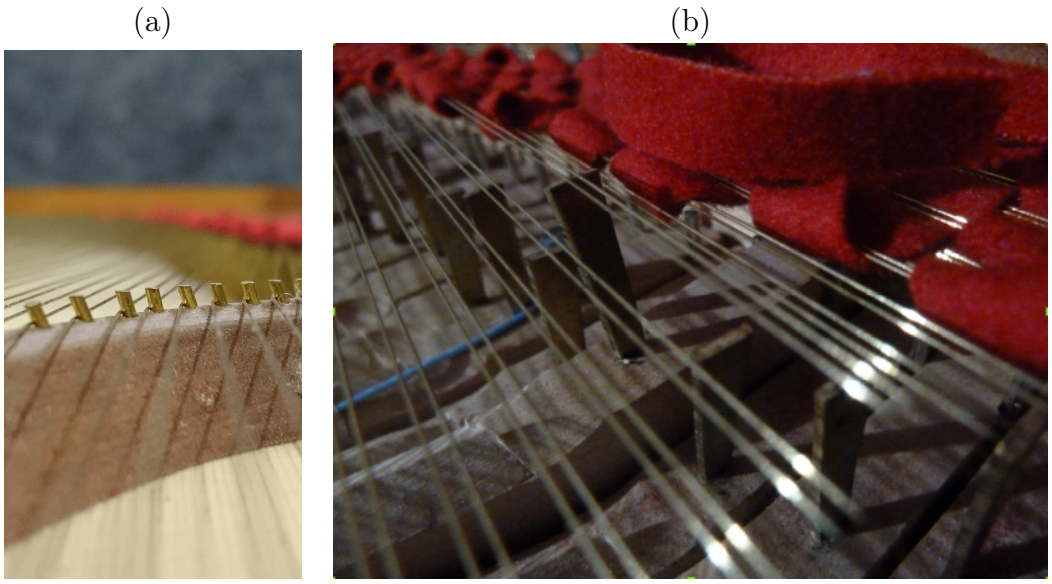

Figure 1.2: Coupling point of the string and the pin laid out on the bridge (a), Tangent impacting the string (b).

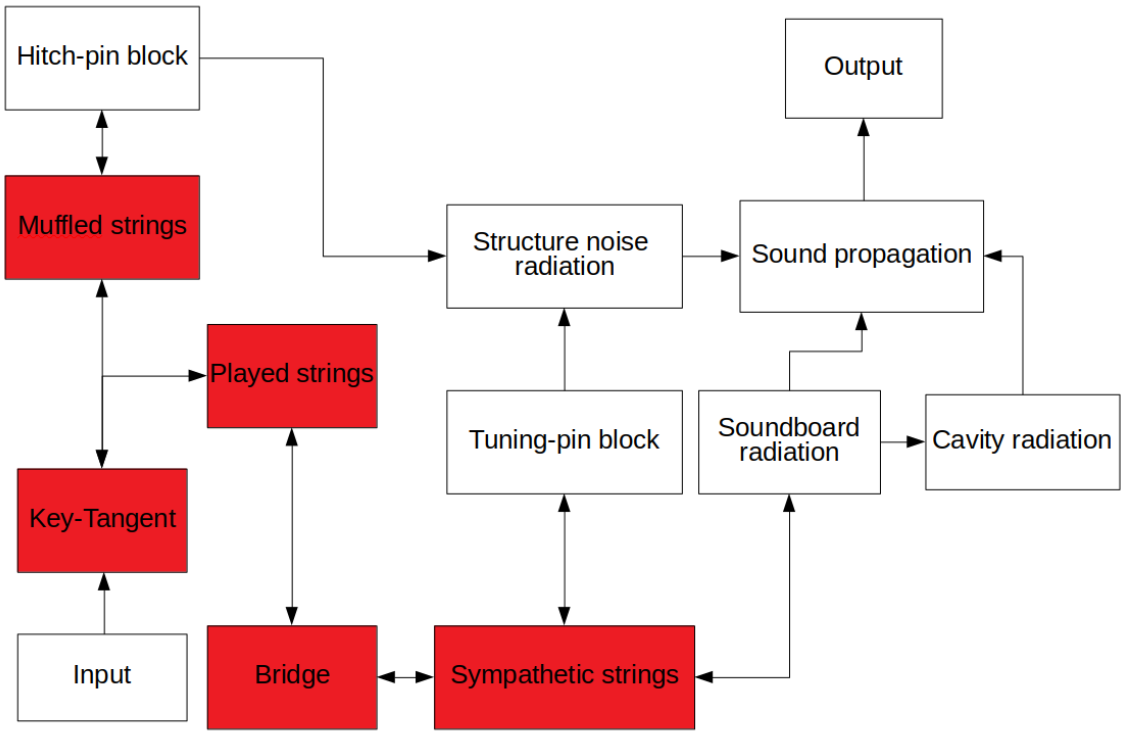

Figure 1.3: Block diagram of the vibro-acoustic functioning of the clavichord, where the part in red refers to the components that are modelled in this work.

1.2 Historical account of the clavichord

In this section, a historical overview of the clavichord focused on its organological evolution is presented. The amount of information gathered here comes from the monograph written by B. Brauchli [1].

1.2.1 Origin of the clavichord

The origin of the clavichord comes from the monochord, a medieval instrument. It consists in a soundboard where a string is stretched at its two extremities. The bridge coupling the string with the soundboard is not fixed. It can be displaced at different points of the string. This unfixed bridge was a tool for theoreticians of the time to study the harmonic relations between partials and string lengths. The arithmetic ratios put forward by this instrument brought its contribution during the medieval period to spread the Pythagorean theory, which postulate that the intervals' ratios in the case of musical instruments (*musica instrumentalis*) are analogous to the proportions of the human body (*musica humana*) and ultimately to the harmony of the cosmos (*musica mundana*) [5, 1]. Different instruments are derived from the monochord. By adding more strings to the same soundboard, it gave birth to the psaltery. Also, a keyboard has been added to the monochord. The origin of the keyboard comes from the organ, which was invented by Ctesibius in the IIIth century before Christ. With a parallel stringing and with a fixed bridge, the purpose was to excite the different strings having different lengths by means of the keyboard to play different notes. This is the way the clavichord came into being. One of the first occurrence of the term "clavichord" (*clavicordium*) in the treaties is found in the *Minne Regel* (The Rules of the *Minnesinger*) written in 1404 by Eberhard Cerne de Minden. Given the date of this treaty, the first medieval clavichords date back at least to the end of the XIVth century.

1.2.2 XVth century clavichords

Among all the clavichords built in the XVth century, none of them have survived. These clavichords have been studied and reconstructed by means of iconographic documents, treaties and textual sources. The oak carving of the altarpiece in the Cathedral of Minden, dating back to 1425, presents one of the first representation of the clavichord. These medieval clavichords have only a few strings (between 12 and 13 strings). At that period, the clavichord had the dimensions of a rectangular box with a small size. All the strings are fretted, that means that many tangents strike the same string at different locations in order to play many notes on the same string. As a result, these clavichords possess more keys than strings. Also, all the strings have the same length and the stringing is parallel to the keyboard. The soundboard is placed underneath the key levers and occupies all the length of the instrument. The first organological treaty dealing with the clavichord, among other instruments, is the one written by Arnault de Zwolle (c. 1440). In this treaty, stringing dimensions of the clavichord are indicated. It contains a diagram indicating the distribution of the tangents and that of the strings, as well as a detailed plan of construction of the instrument. This clavichord is tuned with respect to the Pythagorean temperament. The treaty puts forward that the unison tuning of all the strings, the one that was used before, has been abandoned in order to change

the distances between the tangents. One of the most important representation of the clavichord at that time is the intarsia of Urbino (1479-1482), which is found in the Urbino ducal palace walls. It was done under the direction of Baccio Pontelli during the reign of Duke Federigo da Montefeltro (see figure 1.4).

Figure 1.4: Intarsia of the Urbino ducal palace representing a clavichord (1479-1482) (ref : http://www.gutenberg-e.org/kirkbride/detail/us_clavichord.html [consulted in 06/01/2021])

1.2.3 XVIth century clavichords

When it comes to the XVIth century, five clavichords of this period remains (to see an iconographic example, see figure 1.5; as for a real clavichord, see figure 1.6). One of the major evolution of the clavichord is the development of the soundboard. Medieval clavichords possess a soundboard located underneath the key levers. Because of this, the bridge was lengthened in height in order to support adequately the strings. However, a high bridge as such is inadequate to transmit vibratory energy from the strings to the soundboard. That is the reason why the soundboard was displaced to the right hand side of the instrument. Also, to enhance the sound quality of the bass strings, they were lengthened. By lengthening these strings, their tension needs to be higher to obtain the same note. This increase in tension implies a stronger static charge from the string on the bridge. This enables a better transmission of the vibratory energy to the soundboard, hence these bass strings can sound better in such a way. Because of this lengthening, the whole stringing needed to be lengthened, which led to an enlargement of the clavichor dimension. Then, new strings were added at the treble range. The XVIth century clavichord ended up with an ambitus of 4 octaves or more. In addition to the main soundboard laid out at the right hand side of the instrument, these clavichords still possess another soundboard underneath the key levers, in accordance with the legacy of the XVth century clavichords.

An important treaty of that period is the *Musica getutcht* (1511) by Sebastian Virdung [6]. According to the author, it is possible to have as much strings on a

Figure 1.5: Woman playing a clavichord, by Van Hemessen (c. 1575), conserved at the Worcester art museum (ref : https://worcester.emuseum.com/objects/10587/young-woman-playing-a-clavichord [consulted in 06/01/2021])

clavichord as wished, as long as all the strings are tuned in unison. On the basis of Virdung's model, a clavichord does not need more than twenty keys. The diagram presented in this treaty shows a way to divide the tones of the instrument in a chromatic way, especially by means of a particular lay out of the tangents. Each string is struck by three tangents at different lengths. Because of the unison tuning of the strings, The ambitus of Virdung's clavichord became limited necessarily. It has an ambitus of three octaves and a half, which is inferior to those of most XVIth century clavichord. Finally, Virdung remarked the substantial acoustic role of the sympathetic part of the strings, which vibrate sympathetically (*Resonanz)* and then help to provide a richer sound [6].

1.2.4 XVIIth century clavichords

The XVIIth century witnesses a non-linear evolution of the clavichord, that is to say an evolution which is differentiated with respect to the different European countries. In general, the instrument ambitus enlarged. The secondary soundboard placed underneath the key levers was abandoned, probably because its acoustical contribution is negligible. It is interesting to note that the clavichord market at that time, in whichever country, was less popular than that of the harpsichord. The clavichord market was less structured, given the fact that it took shape by the initiative of isolated and small workshops. To build a clavichord was considered as a secondary activity for the instrument makers of this period, in comparison to the construction of harpsichords and organs. The importance of clavichord making arises in Germany during the XVIIIth century, where the most important instrument making workshops were considerably devoted to clavichords. Eight clavichords of the XVIIth century

remains (see for instance figure 1.7). The unfretted clavichord is introduced at the end of this century. When a clavichord is unfretted, each pair of strings is struck only by one tangent, as opposed to a fretted clavichord. Furthermore, the XVIIth century fretted clavichords possess some unfretted pairs of strings, namely all the strings corresponding to the D and A notes of all octaves. The only exception to this is the unfretted clavichords made in the Iberian countries, where the unfretted pairs of strings correspond to the E and B notes of all octaves. In any case, the purpose of unfretting the strings is to diminish the number of tangents used for each string. By comparing the XVIIth century clavichords with those of the preceding centuries, it is possible to note a diminution of the key number striking the same string as well as an increase of the pair of strings' number enlarging the ambitus in bass and in the treble. To give an idea of this evolution, the clavichord of the Urbino intarsia (1482) have seventeen pair of strings. In comparison, a clavichord dating back to the end of the XVIIth century possesses thirty five pairs of strings. By this augmentation of the string number, the stringing has taken more space on the instrument. Thus, the enlargement of the clavichord dimensions was necessary. This change in size of the instrument led to a redistribution of the strings. Instead of being parallel to the key levers, the stringing became laid out in an oblique way. This particular layout has two advantages : 1. the total length of the strings can be progressively differentiated, 2. this layout leads to a better harmonisation of key levers' disposition. However, this kind of stringing has one drawback : it undermines the instrument stability. When the strings were parallel to the key levers, they were also parallel to the wood fibers of the soundboard. This alignment is an efficient way to support the static charge of the strings applied on the bridge. Having lost this propriety because of the oblique layout, deformation of the soundboard became more frequent.

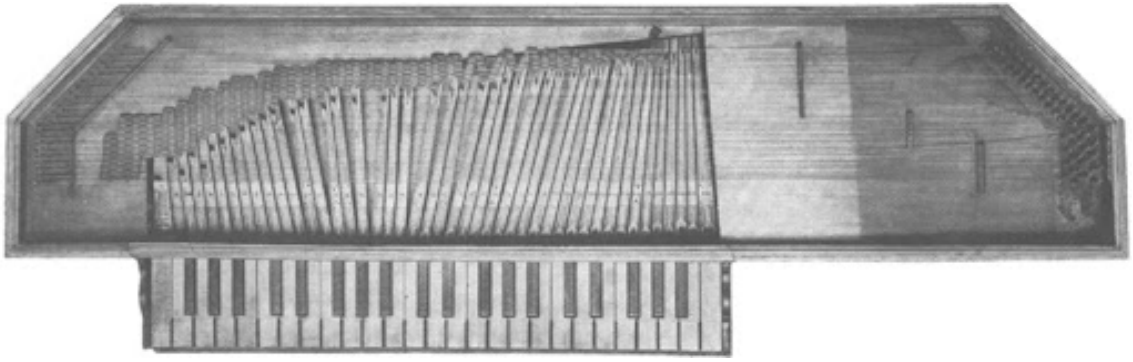

Figure 1.6: Clavichord by Dominicus Pisaurensis, 1543. Henkel cat. no. 1. Musikinstrumenten-Museum der Universität Leipzig (ref : http://www.claviantica.com/Publications_files/Pisaurensis_clavichord_files/Pisaurensis_Introduction_files/Introduction.htm [consulted 06/01/2021])

Most of the XVIth century clavichords possess many straight bridges, laid out differently depending on the ambitus (see figure 1.6). These bridges with a straight line shape led to bringing the coupling points of the treble and bass strings closer to the soundboard boundaries. Given the fact that the amplitude of the soundboard vibration nearby these boundaries is small, the acoustic radiation of the aforementioned strings were undermined. In comparison, for most of the XVIIth century

clavichords, only one bridge is used (see figure 1.7). This bridge is in shape of an S, placed diagonally on the soundboard. Often, the bridge height decreases around the treble strings to compensate for the decrease of the strings' diameter. When the strings are laid out parallel to the key levers, they press the bridge vertically, which is characteristic of XVIth century clavichords. In the XVIIth century, a deviation angle was introduced between the played part of the string and its sympathetic part. It was introduced without aligning the bridge pin, the hitch pin and the tuning pin. Thus, the string presses horizontally the bridge pin. Then, the vertical pressure is ensured by tightening the string by means of a tuning pin placed at an altitude inferior to that of the bridge pin. To reinforce the soundboard stability with an oblique stringing, ribs were added to the soundboard. The way the ribs were placed depends on the different clavichords. Yet, one common solution was to place ribs parallel and underneath the bridge. Thus, the soundboard and the bridge could be stiffened at specific places.

Figure 1.7: Clavicorde, anonyme, c. 1620., St Cecilia Hall, Édinburgh (ref : https://collections.ed.ac.uk/mimed/record/17226?highlight=mirrey [consulted 06/01/2021]

Among the significant treaties on clavichord making, there is the *Harmonie Universelle* (1636) by Marin Mersenne [7]. The author points out that the clavichord is not a loud instrument, producing a soft sound. He accounts for this softness of sound in the following way :

> But one should notice what is singular to this instrument, namely the pieces of cloth, which are present around the strings in the space bounded by ONPM [points in space] and which muffle the sound so much so that it cannot be heard from afar, and this sound becomes really soft : that

> is why this instrument is suited for those who wish to play the spinet without being heard by the neighbours; therein it can be called the muffled spinet[1].

By virtue of this low sound level, Mersenne bestows to the clavichord the name "muffled spinet". It is interesting to point out that the clavichord is not a concert instrument. It was only played in living rooms, which gave the opportunity to practice freely this instrument without disturbing the neighbourhood. Nevertheless, the argument used by Mersenne to account for this low sound level is wrong. The clavichord is the only instrument where the sound is not produced by the entire length of the string, given the fact that the tangent defines the boundary of one of the string extremities while it sets the string into vibration at the same time. In order words, the tangent is a boundary condition of the string. Yet at the same time, it excites the string. As a result, the string is excited at a vibratory node point. This causes the clavichord acoustic sound level to be low. In addition to this, the little soundboard surface available for the acoustic radiation, compared to that of a harpsichord soundboard, can also account for this low sound level.

1.2.5 XVIIIth century clavichords

In the XVIIIth century, the clavichord lost its fame in France, Italy and England because of the empowering dominance of pluck instruments. These countries developed a musical style specifically elaborated to value the technical possibilities of the harpsichord, the spinet and the virginal as opposed to countries such as Spain, Portugal, Scandinavia and Germany. At that time, it is in Germany that clavichord making reached a high level of craftsmanship and technicality which is comparable to that of harpsichord making. Thus, great families of clavichord making came into light, like for example the Silbermann, Stein, Hass, Schmahl, Schiedmayer, Horn and Friederici families.

The tension of the oblique stringing tends to provoke soundboard deformations, because the string number for unfretted clavichords is higher than for fretted ones. The static charge of the strings was such that instrument deteriorated quite fast. Then, a reinforcement of the structure needed to be introduced. In particular, stiffer ribs to sustain the soundboard were necessary (see figure 1.8). The stringing became more spaced, which led to longer keys levers. Typically, the distance between the keyboard and the tangent, for the bass strings as well as for the treble strings, more than doubled. Because of this increase in key levers' length, the regulation of the finger pressure exerted on the key changed, which undermines the playability. To resolve partially this problem, the alignment of the key levers' pivots was displaced by an angle. As such, the total key length could be reduced in order to reduce

[1] (*Mais il faut remarquer ce qui est de plus particulier en cet instrument, à savoir les morceaux d'escarlatte ou d'autre drap, qui courent toutes les cordes dans l'espace compris entre ONPM et qui étouffent tellement leur son, qu'il ne se peut entendre de loin, et qu'il est fort doux : c'est pourquoi il est fort propre pour ceux qui désirent d'apprendre à jouer de l'épinette sans que les voisins le puissent apercevoir; de là vient que l'on peut la nommer épinette sourde*) Marin Mersenne, 1636, dans Christophe d'Alessandro, « Le clavicorde dans l'Encyclopédie (CLARICORDE, MANICORDE ou CLARICORDE, MANICORDION) » *Édition numérique collaborative et critique de l'*Encyclopédie, online since January 4 2020, consulted in April 20 2020 (http://enccre.academie-sciences.fr/encyclopedie/dossier/D00-37540b24699b/) [Personal translation]

the necessary finger pressure to play the instrument. Notwithstanding the fame of unfretted clavichords, the construction of fretted clavichords continued until the end of the XVIIIth century.

Jacob Adlung is one of the most important theoretician of this period. His treaties *Anleitung zu der musikalischen Gelahrtheit* (1758) [8] and *Musica Mechanica Organoedi* (1768) [9] describe the instruments, their historical evolution, as well as their musical practice at Adlung's time. In the *Anleitung*, the term "*Clavier*" is used. In XVIIIth century Germany, the term "*Clavier*" could be considered as synonymous to the term "*Klavichord*". Indeed, the clavichord was considered as the classical keyboard instrument, whose musical quality was praised and recognised in the German speaking countries. According to Adlung, among the advantages of the clavichord, these can be found : there is no plectrum to harmonise, the tuning lasts long enough, and it is easy to tune the instrument since many keys strike the same string. Also, the strings should not be too thick, and the angle between the portion of the string coming from the tangent and arriving at the bridge and the portion of the string leaving the bridge and continuing to the wrestpin should not be too sharp (Adlung, Jacob, *Musica Mechanica Organoedi*, 1768, §581, in [1], pp. 197). The tangents should have the same height (Adlung, Jacob, *Musica Mechanica Organoedi*, 1768, §584) and should stand vertically (Adlung, Jacob, *Musica Mechanica Organoedi*, 1768, §591, in [1], pp. 200). A technique recommended by Adlung consists in increasing the bridge height at the bass strings, which became a standard feature for late clavichords. Finally, this theoretician insists on the importance of the sympathetic part of the strings, putting forward the embellishment of the sound provided by the resonant effect (*Nachsingen*) produced by sympathetic vibration (*cum sympathia*).

Figure 1.8: Clavichord by Christian Gottfried Frederici, 1773, Musée de la musique, Paris (ref : https://collectionsdumusee.philharmoniedeparis.fr/doc/MUSEE/0160057 [consulted in 06/01/2021]

There is also another treaty entitled *Beitrag zu einer allgemeinen Verbesserung der Claviere, aus mechanischen Gründen hergeleitet* written by J.B.v.H, an unidentified author. Among the positions taken by this author, one of those claims that favouring the maximum tension possible of the clavichord stringing leads to obtaining the best sound possible. Furthermore, the stringing tension should be balanced for all the strings in order to obtain a sound equilibrium between the different strings. In the treaty *Clavierschule* (1789) by Daniel Gottlob Türk [10], an insistence is given on the duration and the sound level of the clavichord sound. Its sound should be loud enough but not percussive, and having a long duration at the same time. As a result, the compromise between duration and sound loudness is an important criteria when it comes to making a good clavichord.

1.2.6 Reappearance of the clavichord

In the course of the XIXth century, the clavichord has been considered as an old and ancient instrument. Even though this instrument was still practised by a small number of musicians at that time, it lost its fame on the European musical scene. The piano became the keyboard instrument of reference in the XIXth century. Because of its large acoustic radiation, its large ambitus and its associated aesthetics, the piano remained very dominant brushing aside all the other keyboard instruments. Nonetheless, at the end of the XIXth century, these forgotten instruments were rediscovered, including the clavichord. In England, one of the pioneers of this rediscovery motion is A.J. Hipkins (1826-1903) who presented in his book *A Description and History of the Pianoforte and the Older Keyboard Stringed Instruments* (1896) [11] this renewal of interest in the clavichord. Carl Engel (1818-1882), in his article "Some Accounts of the Clavichord with Historical Notices" dating back to 1879 and published in *The Musical Times*, mentions his fretted clavichord inviting musicians to play J.S. Bach's fugues with this instrument [12] :

> I therefore invite my musical friends and my musical enemies also, if I have any to go and examine it; or, still better, to play on it Bach's fugues precisely as he himself played them on the clavichord.

Another pioneer of this rediscovery motion is Arnold Dolmetsch (1858-1940), who built six different clavichords between the years 1894 and 1897 [13]. This interest in the clavichord at the end of the XIXth century was only present in England and in the United States. In the course of the XXth century, German musicologists mostly began publishing articles on the clavichord and its musical practice [1].

The clavichord decline can be explained, given the fact that the piano acoustic radiation and musical possibilities outweighs that of the clavichord. However, it is interesting to note the reemergence of this instrument and the regain of interest in it since the end of the XIXth century up to now. The clavichord possesses its proper instrument-making and some specific organological aspects. As a result a specific musical aesthetics and a long tradition of musical interpretation for keyboard instruments are related to this instrument.

1.3 The studied instrument

The studied clavichord in this work has been built at The Paris Workshop, in Montreuil, by C. d'Alessandro (it was the second clavichord that he built) and C. Besnainou (a professional luthier) in 2007 (see figure 1.11). It has been built by means of a kit designed by E. Dancet and M. Ducornet conceived on the basis of the clavichords built by Christian Gottlob Hubert. This specific clavichord is not an exact replica of a Hubert clavichord, but it contains the main essential features of this instrument maker's clavichords dating back to the last quarter of the XVIIIth century. The instrument is of good musical and mechanical quality. This clavichord has been made specifically for vibro-acoustic investigations. The overall characteristics of this instrument are shown in table 1.1 (see also annex A) and the dimensions of its strings are presented in annex B. Figure 1.9 shows the sketch of this clavichord sides and figure 1.10 shows a precise and scaled sketch of the whole clavichord. The name given to this instrument studied in this PhD is "LAM1 clavichord".

Range	C_1-D_5, 51 strings
Stringing	double strung
Soundboard	268 × 227
Dimensions	1267 × 358 × 112
Tuning	A_3 : 415 Hz
Materials of the strings	yellow brass with the CuZn30 alloy
Fretting	double fretted

Table 1.1: Overall characteristics of the LAM1 clavichord.

Christian Gottlob Hubert (1714-1793) is one of the major clavichord and keyboard instrument makers of the XVIIIth century. He is famous for making clavichords, fortepianos, and also for building organs like that of the Catholic chapel at Ansbach [14]. His craftsmanship was recognised as one of the finest, and his instruments were praised for their durability and their beautiful tones. Many clavichords have remained up to now [15], among which the clavichord dating back to 1784 and preserved at the Cecilia Hall museum, at the University of Edinburgh (see figures 1.12). Although Dancet and Ducornet used this model to conceive the kit used by C. d'Alessandro and C. Besnainou to make the clavichord of study, some differences can be noticed between the two instruments. In overall, the played string lengths are approximately similar. Furthermore, the range of the original 1784 Hubert clavichord goes from C_1 to F_5, which amounts to 4 and a half octaves with 54 notes. The range of the LAM1 clavichord is a bit smaller, going from C_1 to D_5, which amounts to 51 notes. The two clavichords are double strung and fretted, except for the D and A notes which are unfretted. Then the LAM1 clavichord has an amount of 74 strings, which is 6 strings less than the original Hubert clavichord stringing. The tangents for the lowest 11 notes are thicker than the others for the original clavichord, which is not the case for the LAM1 clavichord. The dimensions of the lid for the two instruments are not the same, and the lid of the original clavichord is panelled as opposed to that of the LAM1 clavichord.

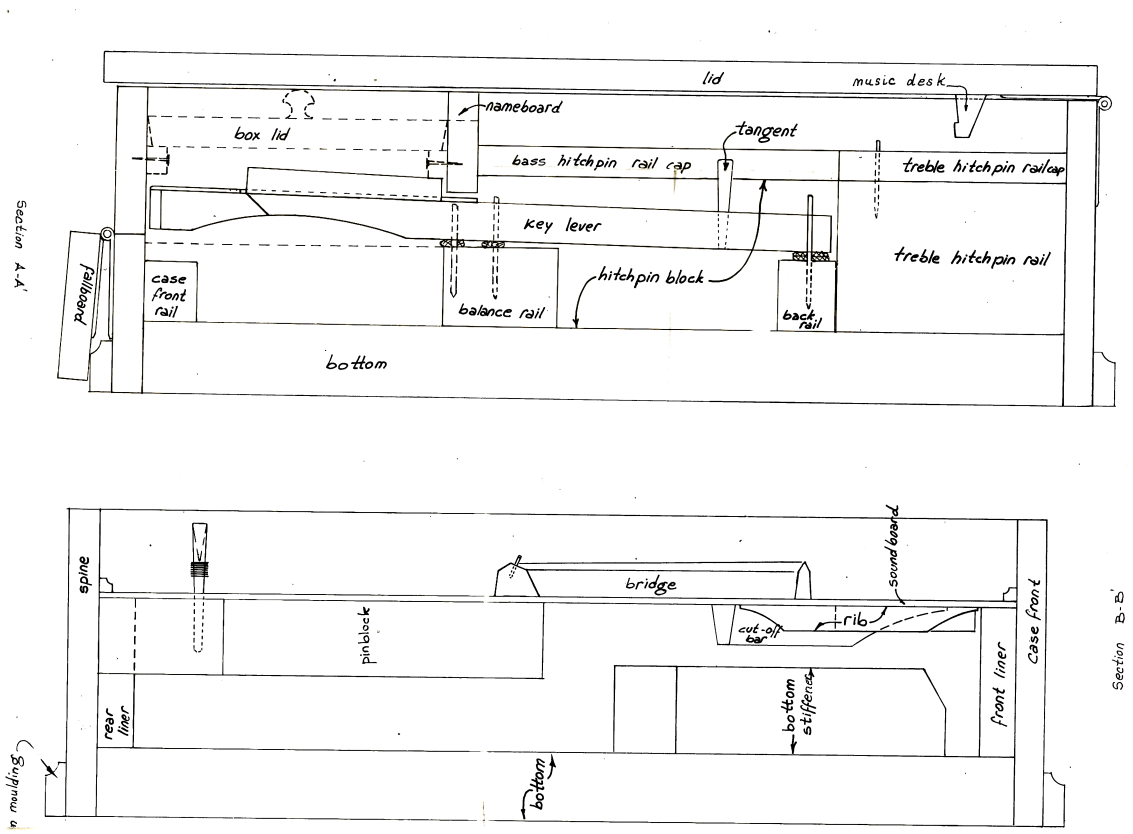

Figure 1.9: Construction plan of the kit designed by Dancet and Ducornet seen from the sides (copyright Dancet and Ducornet, The Paris Workshop).

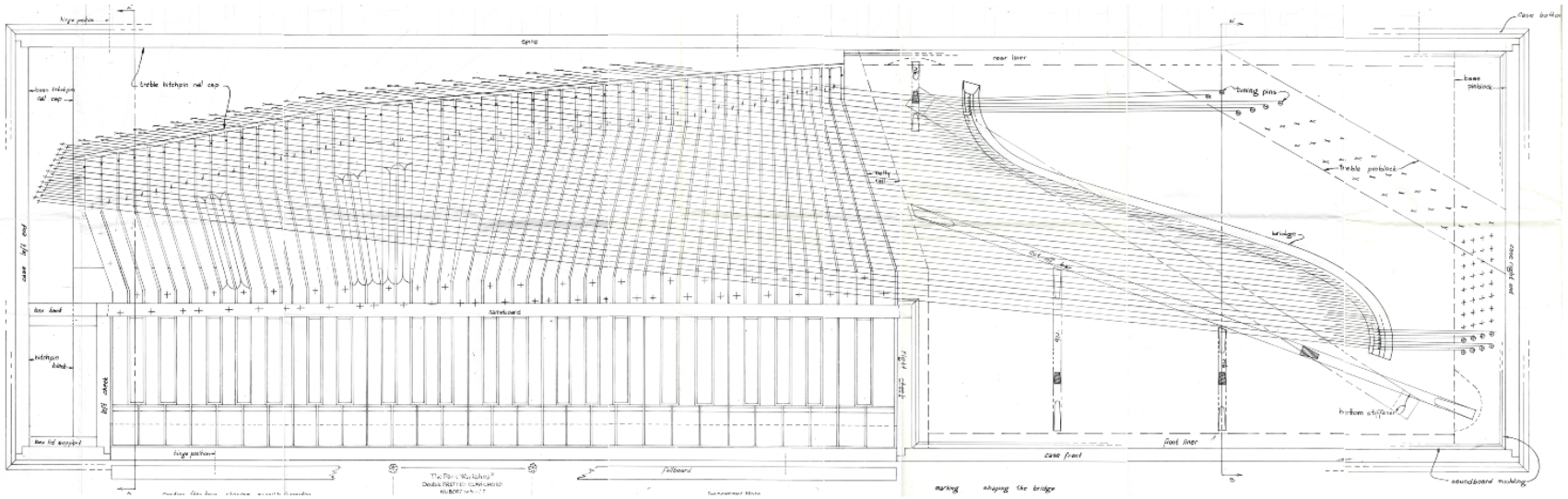

Figure 1.10: Construction plan of the kit designed by Dancet and Ducornet seen from above (copyright Dancet and Ducornet, The Paris Workshop).

Figure 1.11: Picture of the LAM1 clavichord.

Figure 1.12: Picture of the original 1784 Hubert clavichord conserved at the St Cecilia Hall museum, at the Edinburgh university (ref : https://collections.ed.ac.uk/mimed/record/18264?highlight=hubert [consulted in 14/10/2020]).

1.4 A review of the acoustics of the clavichord

To our knowledge, the oldest scientific study of the clavichord dates back to 1940 and was done by Trendelenburg [16]. It indicates that, as opposed to the piano, it is possible to change lightly the timbre of the clavichord after the excitation by means of the clavichord player's action on the tangent in contact with the string without changing the sound level.

In 1967, R.A. Hands published a scientific study on the clavichord, where the clavichord excitation system is described [17]. This study accounts for the low acoustic level of the instrument by means of impact energy splitting at the moment when the tangent impacts the string. All the impact energy is not transmitted to the played part of the string, but some of this energy goes to its damped part. This is opposed to the harpsichord where all the energy given by the plucking goes entirely to the played part of the string.

In 1973, because of this low sound level, R.W. Burhans proposed an electro-acoustic way to amplify adequately the sound of the clavichord so that it could compete with that of the piano [18].

The first study which takes into consideration the overall acoustic aspects of the clavichord is that of Thwaites and Fletcher [19]. Specifically, this study aimed at investigating theoretically as well as experimentally different aspects of this instrument acoustic functioning. It showed that the excitation force spectrum level produced has a smooth slope of 6 dB/octave, and the radiated spectrum depends greatly on the properties of the soundboard. It is on the basis of this result that D.E. Hall tried to elaborate a physical synthesis model of the clavichord, trying to reproduce the 6 dB/octave sound spectral decreasing [20]. Considering that the struck pair of strings of the clavichord leaks energy to the bridge and the soundboard, the interaction between the two strings leading to the two slopes decay is retrieved by Thwaites and Fletcher's study [19]. This process was already predicted by the model elaborated by Weinreich for the piano [21].

To synthesize the clavichord sound, a simplified model elaborated by means of signal processing was applied by Välimäki *et al* [22]. The synthesis model which is suggested is based on digital wave-guide modeling of string instruments using the principle of commuted waveguide synthesis, in which the soundboard response is incorporated in the excitation signal. To enhance the realism of this synthesis, some special sampling techniques are also used. This approach was used to synthesize the sound of the acoustic guitar [23] and that of the piano [24]. Neglecting the second polarization of the string, only one commuted wave guide is used per string. Then, to model a pair of string, two digital wave guide string models are used. The coupling of two string models is taken into account, where the output of only one of the two string models is fed to the input of the other [22]. This model was modified to control the attack sharpness of the synthesized sound [22]. Recordings of clavichord tones are done to synthesize the excitation signal. The recorded signals are processed by means of sinusoidal analysis, subtracting partials, equalizing the residual, and truncating the resulting signals with the right half of a Hanning window [22]. The sound coming from the cavity is included by triggering a soundbox response sample at a low level each time any note is played. These samples are obtained by hitting the clavichord bridge with an impulse hammer at various points. Furthermore, knocks of the key are recorded to synthesize the ending of the clavichord notes. The

effect of the string quasi-static stiffening due to the contact tangent/string was not addressed by these authors. Some sound sample produced by the model by Välimäki are available[2]. Also, a Neupert clavichord was simulated by the Modartt company[3] within the framework of the KIViR (Keyboard Instrument Virtual Restoration) project.

A study conducted by Bernhard Winkler focused in measuring mechanical and acoustic aspects of three different clavichord belonging to Alfons Huber, restorer at Kunsthistorisches Museum in Vienna: a replica of the *Reiseclavichord* of Johann Andreas Stein and two medieval clavichords (one with brass strings and the other with iron strings) [25]. The mobility of the soundboard is measured by means of two techniques : by means of an interferometer and a acceleration sensor. Also, the decay time of different tones of these clavichord measured. The modes found by these two measuring technics and the measured decay time for the instruments are compared.

More recently, mechanical considerations of this instrument were studied once again by d'Alessandro [3]. By means of an experimental approach conducted on an unfretted clavichord, built in 1983 by F. Bal at A. Sidey's workshop, a theoretical approach is compared to measurements. Specifically, an experimental study of variations in the sound of clavichord notes at different dynamic levels is given. Conducting measurements playing all 51 notes of this instrument, the radiated acoustic signal, tangent velocity and two tangent string contact signals are measured. To obtain as much variation in dynamic levels as possible, more than ten repeated measurements are done for every note. A description of the tangent velocity in the time and frequency domain is given. d'Alessandro elaborated a model of the tangent-string contact point velocity, whose simulation matches with experimental data. Furthermore, three aspects of the clavichord acoustics are analysed : relationship between sound pressure level and pitch variations, spectral slope of the radiated sound, and tangent velocity. Results show a linear relationship between sound pressure level and tangent peak log velocity. Also, the sound spectral slope is almost constant with respect to tangent velocity and dynamic level. It is shown that the fundamental frequency is influenced by tangent velocity and finger pressure.

In another study by d'Alessandro, some vibro-acoustic features of this clavichord built by F. Bal are compared to those of three other clavichords : the LAM1 clavichord, a fretted clavichord built around 1985 from the popular 'King of Sweden' Zuckermann kit, and a medieval clavichord built by Peter Bavington in 1988 in London [26]. All the notes have been measured for all these four instruments, using the whole possible range of dynamic nuances. The acoustic signal, the tangent velocity signal and the string/tangent contact signal for each string in a pair are measured. This amounted to a database to give an acoustic portrait for each of these instruments, showing some acoustic differences between them.

This study of the clavichord excitation system has been deepened by the same author, tackling the issue of the paradoxical gesture when playing the clavichord [4]. Having recalled the traditional playing of the clavichord carried on by Johann Sebastian Bach, this study explains the importance of the finger motion in order to play well. In particular, the pushed gesture, characterised by a vertical trajectory,

[2] http://users.spa.aalto.fi/vpv/publications/icmc00.htm [consulated in November 16 2020]

[3] https://www.modartt.com/neupert [consulted in November 16 2020]

leads to a risk of playing out of tune with the intention of playing loudly. Indeed, playing loudly implies pressing the key with sufficient velocity. However, with a pushed gesture done by a musician, this tends to uplifting the string with too much height, creating a pitch being out of tune. As a result, in the history of clavichord performance, a pulled gesture (*Schnellen* in German) has been elaborated to avoid such a consequence, by adding a backward horizontal component to the finger trajectory. A comparison of the acoustic and vibratory consequences of the pushed and pulled gesture is also presented by [4].

1.5 A brief review of acoustic keyboard instruments

1.5.1 The piano

Most of the key questions regarding the organological evolution and the acoustics of the clavichord can be reconsidered by means of musical acoustic studies on string and keyboard instruments. The one which has been the object of in-depth vibro-acoustic studies is the piano. All the basics of its acoustic functioning and its instrument making is summarised in the five conferences gathered by Askenfelt [27]. The piano, as well as the clavichord, is an instrument whose strings are struck. It was created in 1709 by Bartoloméo Christofori in Florence. Instead of being struck by a tangent or to be plucked by a plectrum in the case of the harpsichord, the string is struck by a hammer. As opposed to the clavichord where the tangent remains in contact with the string, the hammer moves away from the string just after the excitation by means of actions. This mechanism is reinforced by the double repetition action introduced by Sébastien Érard between 1820 and 1821. The timing of the key action, that from the finger pressure on the key up to the production of the string vibration was studied and described [28]. The hammer core is made of wood and is covered by felt (it could also be leather or cork). The relaxation and the disposition of the felt depends on the excited string. Depending on this relaxation and disposition, the hammer impulse force applied on the string changes, modifying the spectral content of the produced sound. The harmonisation of the piano consists in relaxing the felt adequately depending on the sound desired for each string. The transitory part of the piano excitation was subject to a temporal and frequency analysis [29].

Physical models have been elaborated to simulate the hammer impact on the piano string [30, 31]. Other models proceed by means of waveguide methods to model the string-hammer interaction [32]. Some signal processing techniques can be used to reconstruct the hammer impulse force profile by means of measurements of the piano string velocity of vibration [33]. The measurement of the interaction between the string and the hammer was also an object of study. Specific experimental techniques have been used to observe this interaction, like contact identification, string motion, and details on the force-compression behavior and the hammer and the string [34]. Also, some studies focused on the modelling of the key action in the piano [35, 36, 37], in order to simulate the realism of the excitation dynamics [38].

Furthermore, the sound synthesis of the piano have been carried out, either by means of waveguide methods [39, 40], or by means of physical models [41]. About the piano soundboard, some vibro-acoustic studies have been done to synthesize its mobility and its acoustic radiation [42, 43]. In particular, the behaviour of the piano soundboard in mid-frequency domain was also an object of study [44, 45].

Other studies of the soundboard vibratory behaviour, that of the piano as well as that of other string instruments, consisted in elaborating procedures to identify the structure modal densities in order to characterise the specific instrument [46]. Furthermore, unlike the clavichord, their is a possibility to change the piano tone by means of the impact velocity of the hammer. So by his/her playing, the pianist can have a specific control on that timbre. Investigations have been done to study the individual pianist's control on the sound [47]. The weight applied on the key is also important when it comes to controlling the piano tone, given the existence of the double escapement action. Using more weight, the pianist presses the key to the bottom of the keyboard. Otherwise, using less weight, he plays more at the keyboard surface. A specific study investigated the influence of this weight on the control of the piano tone [48].

1.5.2 The harpsichord

When it comes to the harpsichord, some researches have been done regarding its acoustic aspects. To our knowledge, the first scientific studies on the harpsichord deal with the design as well as aspects regarding its performance practice [49]. Others studied the harpsichord soundboard and the acoustic role of the air volume in the cavity by means of experimental and analytical methods [50, 51]. The influence of the metal rose on the vibratory behaviour of the soundboard was put forward [52]. The excitation of the string is done by the plectrum plucking the string at the moment when the finger presses the key. The main part of the harmonisation of the harpsichord consists in adjusting the plectrum dimensions before laying it out on the instrument. Acoustic and perceptive studies show the influence of the harmonisation of the harpsichord sound [53, 54]. The study of the transitory part of the excitation and its consequences on the harpsichord string vibration was done [55]. Numerical and experimental studies were carried out to investigate the soundboard vibratory behaviour using finite element methods [56]. In addition to this, acoustical holographic techniques were used to highlight the acoustic radiation of the harpsichord [57].

About the strings, experimental studies were done to understand the temporal evolution of the harpsichord string partials [55]. Following this study, it led to the elaboration of a damping model valid for strings that are monofilaments [58]. Some historically informed studies were performed to understand the making process of strings in the past [59].

As for the soundboard, studies focused on the vibratory proprieties of wood [60]. Wood is a material sensitive to hygrometry, which means that its vibratory proprieties can change depending on hygrometric conditions. Furthermore, wood is an orthotropic material, meaning that its mechanical and elastic properties are different according to the vertical, horizontal and longitudinal axis. Wood proprieties vary depending on the fact that the piece of wood comes from the trunk centre or the periphery of the tree. The direction of the wood fibers indicates the axis towards which the structure can support substantial mechanical stresses without deforming itself significantly [61].

1.6 A brief review of studies of coupling in musical acoustics

In a mechanical engineer's point of view, all string instruments have a common feature : they are mechanical and vibratory coupled systems. Given the fact that the strings cannot efficiently radiate sound in the air because of their small radiating surface, these strings must transfer their vibratory energy to a soundboard. This former having a large radiating surface in contact with the air, and being quite flexible and quite stiff at the same time, it can radiate the string sound with enough sound level. When the strings transfer vibratory energy to the soundboard, it is said that the strings are coupled to the soundboard. Thus, to study the string instruments, it is necessary to study the couplings between mechanical vibratory systems.

In musical acoustics, particular models have been either elaborated or directly applied to model couplings between strings and the soundboard. One of the first models to study this coupling, especially focusing on couplings between piano strings, is the one put forward by Weinreich [21]. This analytical model has been developed to predict the shift of the frequency and that of the damping of two partials of two coupled strings when frequency coincidence occurs. Also, this model can account for the two-part slope process of the radiated sound. Another model developed by Gough puts forward the consequences of coupling between a string partial and that of the soundboard [62]. Then, Woodhouse elaborated a new coupling model by means of the modal equations of the string-soundboard coupled system [63]. He uses the term "veering" [64] to describe the shift undergone by the coupled partial frequency and damping with respect to the tuning in frequency of the string partial and that of the soundboard. Also, Woodhouse's model leads to the quantification of the string-soundboard coupling strength, namely the quantification of the perturbation amplitude at the specific coupling point when frequency coincidence arises. By the influence of partial frequency coincidence, the coupling impedance at the string coupling point decreases, which leads to enlarging the perturbation at this coupling point [27]. This strong perturbation leads to a significant veering of the coupled string partials' frequency. Generally, musical instruments are made in such a way that no strong couplings between the string and the soundboard occur. Otherwise, the instrument could not be tuned correctly. In the case of weak couplings, the assumption of small perturbations leads to the possibility to model the coupling mobility influence on the string dampings [58]. This damping modelling was used for instance to study the influence of the neck mobility on the string partials' decay in the case of the electric guitar [65].

More complete modelling of string instruments were achieved using coupled systems. The model of the piano elaborated by Chabassier and Chaigne consists in modelling the constraining forces responsible for the coupling between the string and the bridge [41, 66]. By noticing that the harp soundboard possesses a vibratory behaviour similar to that of a beam, a model based on a transfer function approach was used to model the couplings of harp strings [67]. In the case of the Portuguese guitar, a model based on a penalty formulation was elaborated [68]. This formulation consists in modelling the couplings between the string and the bridge by means of equivalent stiffness and damping coefficients. One of the most recent formulation used to model the couplings of string instruments is the Udwadia-Kalaba formula-

tion [69]. This formulation was used primarily to model the couplings of mechanical structure, such as those found in the field of robotics [70]. Then Antunes and Debut adapted this formulation to vibratory systems by introducing the modal expansion in the equations of motion [71]. Thus, this model was used to model string couplings in the case of the guitar [72]. It was also used to model the strings' couplings of Gabonese harps [73].

Sympathy refers to the indirect vibration of strings which are not excited. This indirect vibratory process is due to the vibratory energy transmission coming from the excited string transmitted by means of the coupling with the bridge. In that case, it is said that the string is set into vibration because of sympathy. Thus, it is commonly accepted that sympathy designates the process where some strings are set indirectly into vibration because of vibratory energy transmission. A string is considered to be sympathetic in so far as it undergoes this indirect vibration. In the case of the concert harp, as no string is damped by means of felt, all the strings are potentially sympathetic. It is also said that these strings are responsible for the "halo of sound" present in the radiated sound [74, 75]. In the case of the piano, if the pedal responsible for damping the strings remains pressed, then this same "halo of sound" arises by sympathetic vibrations. However, in the case of some keyboard instruments like the clavichord, this phenomenon appears because of the sympathetic part of the strings. The Blüthner piano has been conceived specifically with added strings called *aliquot*, which are not played and whose role is to contribute to the produced sound thanks to sympathetic vibration. In the case of the Steinway, the sympathetic strings are called duplex strings. An acoustic and perceptive study consisted in determining the acoustic role of these duplex strings [76]. As it is observed for the clavichord, instrument makers and theoreticians like Virdung and Adlung insisted on the essential role of the string sympathetic part to enrich the produced sound [6, 9]. As this part of the string is set into vibration indirectly by vibratory energy transfer because of couplings, it is possible to bestow to these strings the status of sympathetic strings. A study was carried out on the clavichord to determine these string acoustic input by means of impulse response [77, 78]. Once again, a "halo of sound" created by the presence of sympathetic strings is mentioned.

1.7 Objectives of this PhD

After considering this review of the literature, only the signal model elaborated by Välimäki represents an overall model of the clavichord. One way to enhance the understanding of its physical functioning is to conceive an overall physical model of the clavichord. Specific topics need to be dealt with to study the vibro-acoustics of the clavichord. This first main topic is the excitation of the clavichord string by means of the tangent. The impact of the tangent transmitting momentum to the clavichord string when exciting it has not yet been modelled. This is crucial to simulate the dynamics of the clavichord string. The second topic regards the acoustic effect of the sympathetic strings. This effect is an important aspect of the clavichord sound. To study the response of the sympathetic strings, the couplings of the strings with the bridge need to be taken into account. Therefore, specific aims of this PhD are to study the excitation system and the sympathetic strings of the clavichord by modelling them and by conducting experimental approaches. The

method used to model the instrument must be adequate to include these two main aspects.

This PhD provides a complete vibratory model of this instrument, as opposed to partial models or complete signal models. This new model is based on the Udwadia-Kalaba formulation, which considers the instrument as a mechanical system formed by the coupling of different mechanical subsystems. Simulations of this model can be done to study the miscellaneous acoustic aspects of the clavichord. The excitation system, referring to the interaction between the string and the tangent, is studied. The simulation of the excitation system gives results similar to experimental results found by specific measurements and those presented in the literature. The simulations allows a precise description of the clavichord string motion, which is specific to this instrument only. New experimental approaches were used to describe the interaction between the tangent and the string while playing the instrument, in particular using a robotic finger to program controlled finger trajectory. Specifically, the phenomenon called the paradox of the clavichord was studied with these new experimental approaches. Then, a thorough study of sympathy in the case of the clavichord is undertaken by means of simulations and experimental approaches. After distinguishing the difference between reverberation and resonance when it comes to sympathy, appropriate vibro-acoustic descriptors were used to account for these sympathetic vibratory phenomena. In the end, this PhD synthesises new results in the study of the vibro-acoustics of the clavichord.

Chapter 2 is devoted to the presentation of the Udwadia-Kalaba formulation, used to model coupled mechanical systems. This has been adapted to vibratory structures by Antunes and Debut [71] by introducing the modal representation of the system substructures in this formalism. The structures modeled in the case of the clavichord is highlighted in figure 1.3. Then, chapter 3 focuses on the simulation of the elaborated physical model of the clavichord. The measurements and the determination of the modal parameters' numerical value of each substructure is done, and the study of the simulation parameters is investigated. Part III focuses on the study of the excitation by means of experimental approaches and simulations of the model. In chapter 4, the characteristics of the excitation system, which include the motion of the key, the vibratory motion of the string following the excitation by the tangent, the quantification of the string fundamental frequency variation created by the string uplift, are investigated. Then, some aspects of the paradoxical gestures when playing the clavichord are tackled in chapter 5, studying the control of the string's pitch by controlling the key depth and the control of the loudness by controlling the key velocity. Then, Part IV focuses on the notion of sympathy when it comes to the clavichord. The distinction between reverberation and resonance is done. These two are considered by means of two different experimental approaches. The experimental study of reverberation is done in chapter 6, highlighting its definition and quantifying it by means of impulse responses study. The necessity of considering the string resonance is pointed out by observing the response of each sympathetic strings. It shows that the role of the sympathetic strings is not limited to the reverberation effect, but it also includes the string resonance understood as sympathy occurring by frequency coincidence. This kind of sympathy is investigated in chapter 7, considering an experimental approach and comparing with results obtained by means of simulations.

Part II

Modelling and simulation of the clavichord

Chapter 2

Modeling of the clavichord

2.1 Introduction

This chapter is devoted to the modelling of the clavichord by means of a formulation leading to the coupling of mechanical systems vibrating in a single polarisation of motion. After presenting the state of the art of the formulations available to couple mechanical systems in section 2.2, the decision of using the Udwadia-Kalaba (U-K) formulation is justified. Then in section 2.3, a presentation of the U-K formulation is done, as well as the introduction of the modal representation in the U-K formulation. The objective of this modal U-K formulation is to use it to model the different vibratory substructures of the clavichord in section 2.4. In this section, the modal representation of the different modeled substructures (string, bridge, key-tangent substructure, damper) are given. Finally, the way that the couplings of these different substructures are modeled is presented.

2.2 A review of coupling models in musical acoustics

Many studies have been done to model couplings in the case of flexible mechanical structures. The model developed by Weinreich is one of the first to study the effect of coupling on the strings coupled to the bridge [21]. In summary, it shows how the rate of energy transmission to the bridge as a function of time varies with respect to the bridge admittance, the piano hammers irregularities, and the tuning of the instrument. It considers a set of undamped harmonic oscillators which are coupled with each other. This coupling is modeled by means of a matrix called the dynamic matrix. Then, the system is reduced to two oscillators to come to a simplified two-string model, only considering vertical polarisation of motion. The dynamic matrix is then reduced to a two by two matrix. The two strings are considered to be coupled with the same bridge coupling point. This former is expressed in terms of the bridge admittance and the mistuning of the two strings. The eigenvalues of the dynamic matrix are determined, which are complex. Their real part and their imaginary part represent the shift of frequency and that of damping respectively of the two strings with respect to the bridge impedance properties and the string mistuning. As a result, this model leads to the prediction of the shift of the coupled partials' frequency and damping with respect to the tuning of these two partials

and the bridge coupling admittance. Furthermore, this same model accounts for the two-part slope of the sound radiated by the soundboard when frequency coincidence between two strings partials occurs.

Then, Gough put forward another model to study the coupling between the string and the bridge [62]. In particular, when frequency coincidence occurs between a string partial and that of the bridge, the phenomenon of string resonance arises. That is described and explained by means of Gough model. To introduce the model, it first considers the resonances of a lossy and flexible string coupled with rigid end-supports. The classical string equation of motion is used to derive its dynamic properties. Then, a yielding end-support is introduced to allow coupling to the resonances of the instrument body on which the string is mounted. It is done by adding a perturbation term to the expression of the string wave number. This perturbation depends on the bridge mechanical resistance and the string characteristic impedance. Both weak coupling and strong coupling are assumed. Then, the resonance responses of the string in the case of weak coupling and strong coupling are derived. Furthermore, the interaction of this string with a second, not necessarily similar, string tuned to resonate at the same frequency can be studied by means of Gough model. Like in the Weinreich model, at string resonance, the bridge impedance can be assumed to be a slowly varying function of frequency. These two strings are also coupled with the same bridge coupling point. Solving the equations related to two vibrating strings vibration and the induced bridge motion, the effect on the bridge admittance curve can be derived and results similar to that found by Weinreich are retrieved.

Also, by means of the modal equations of the string-soundboard coupled system, Woodhouse elaborated a new coupling model [63]. This approach led to the modelling of the coupling between a guitar string and its bridge. First, a modal representation of the string and of the bridge is presented, considering that the two are coupled with each other. Deriving the expression of the kinetic energy and potential energy of this vibratory coupled system, the expression of the corresponding modal mass matrix and that of the modal stiffness matrix are yielded. The expression of the damping matrix is given by assuming proportional damping for the string and for the bridge. As such, the expression of the modal response of the string-bridge coupled system is derived. Along with this, Woodhouse put into light the veering phenomenon [64] to describe the shift in frequency and damping of the tuned string partial and that of the bridge. This is a similar phenomenon to that found by Weinreich.

Then, when no frequency coincidence occurs, an approach developed by Valette and Cuesta led to the modeling of the bridge coupling admittance effect on the string dampings [58]. Similar to the Gough model, a perturbation is added to the expression of the wave number. This perturbation is small assuming that the coupling is weak. Given the continuity between the string admittance and that of the bridge at the coupling point, and assuming that the string characteristic impedance dominates the bridge impedance to ensure the reflection of the waves, it is possible to express the string wave number with respect to the bridge coupling admittance. This leads to the expression of the string perturbed frequencies and that of the string perturbed dampings. This gives the influence of the coupling admittance on the string frequencies and string dampings. In the case of the electric guitar, this model was used to predict the effect of the neck coupling admittance on the electric

guitar strings' dampings [65].

The model elaborated by Chabassier *et al* is a complete modeling of the piano taking into account the main elements that contribute to the sound production, including the constraining forces responsible for the coupling between the string and the bridge [41]. The Reissner Mindlin equations are used to model the soundboard as a bidimensional thick, orthotropic, heterogeneous, frequency dependant damped plate. The strings are modeled as a set of one dimensional damped system of equations, taking into account the transversal waves, the shear waves arising from the string stiffness, and the longitudinal waves arising from geometric nonlinearities. An initial velocity is given to the hammer, which projects it to a choir of strings before being repelled. The interaction between the string and the hammer is modeled by an interacting force, being a nonlinear function of the hammer compression. The strings are coupled to the soundboard at the bridge, forming a slight angle from the horizontal plane. This coupling is modeled by a coupling force, using Lagrange multipliers.

In the case of the concert harp, Le Carrou *et al* elaborated a transfer function approach to couple the different substructures [67]. It is considered that the soundboard represents a simple beam, with which several strings are coupled. With this assumption, it is possible to compute analytically the modes of this coupled system using the state vector formalism and the transfer matrix method. The state vector of the strings and that of the soundboard, containing the kinematic and force variables of these structures, are introduced. The bending motions of the string and that of the soundboard are described using elastic string theory and Euler-Bernoulli beam model respectively. Introducing the state equation of a subsystem, a transfer matrix is introduced to connect two state vectors at two different locations of the subsystem. To couple the strings with the soundboard, the kinematic continuity relations are assumed. That leads to the derivation of the continuity and coupling matrices of the coupled system. Then, modal properties of the modeled beam-N^{th} strings system can be obtained.

Then, the penalty formulation was used by Debut and Antunes to model the Portuguese guitar [68]. First, the dynamical string model originally derived by Morse and Ingard [79] is presented. Also, to approximate the nonlinear behaviour of musical strings, the simplified Kirchoff-Carrier model [80, 81] is used. Then, the modal formulations of the nonlinear string dynamics for the two transverse polarizations and of the soundboard are given. A model of the bridge kinematics, elaborated on the basis of simple geometrical rationale, is used to model the coupling between the strings and the soundboard at the bridge. Also, a penalty formulation is used to ensure the string-bridge coupling. It requires the calculations of the motion of the two coupled subsystems and two arbitrary coupling coefficients. These coefficients correspond to an equivalent stiffness coefficient and an equivalent damping coefficient.

Another formulation was used to proceed to the modelling of these couplings, which is the Udwadia-Kalaba formulation [69]. This is a formulation implemented in the field of robotics, in order to couple rigid mechanical systems. Then this formulation was adapted to flexible mechanical systems to model the guitar strings coupled to the bridge [71, 72].

Since the clavichord is a coupled system, one of the aforementioned models can be used to proceed to its modelling. Because of the elegance and the effectiveness of

the Udwadia-Kalaba formulation, this approach has been chosen in this work. As opposed to the transfer function approach developed by Le Carrou *et al*, which is only restricted to an instrument having a soundboard with a modal basis similar to that of a beam, the Udwadia-Kalaba formulation do not include such assumptions. It was shown that this formulation was numerically more effective than that of the penalty formulation [71]. As to the numerical approach, the modal basis of the bridge can be measured by means of experimental modal analysis [82], and then the measured parameters can be included in the model to simulate the modal behaviour of the bridge [71]. Moreover, the model based on the Udawadia-Kalaba formulation can be simulated by means of a simple finite difference scheme in time. As a result, this formulation seems adequate to model the clavichord.

2.3 U-K model

2.3.1 U-K formulation of a coupled system

The original U-K formulation is derived by Firdaus E. Udwadia and Robert E. Kalaba, using Gauss' principle of least action [69]. Then Arabyan and Wu [83], as well as Laulusa and Bauchau [84] found an original algebraic approach for deriving the U-K formulation for constrained systems from the classical formulation with Lagrange multipliers [71]. Originally, this formulation was used to model rigid constrained mechanical system [83].

Let us consider a mechanical system of M particles, with a $M \times M$ diagonal mass matrix $\mathbf{M}$, which is subjected to an external force vector $\mathbf{F}_e(t)$, including all constraint-independent forces. This system is also subjected to a set of $P = P_h + P_{nh}$ constraints composed of P_h holonomic and P_{nh} non-holonomic constraints which depend on the system displacement $\mathbf{y}(t)$ and velocity $\mathbf{v}(t)$. Denoting the dynamical solution $\mathbf{y_u}(t)$ of the unconstrained system and that $\mathbf{y}(t)$ of the constrained system, which depends on the constraining forces $\mathbf{F}_c(t)$, as it is shown in [83], one obtains the equations of motion of the constrained system proposed by Udwadia and Kalaba [69]. The $\varphi_i(\mathbf{y}, t)$ holonomic constraints and the $\psi_j(\mathbf{y}, \dot{\mathbf{y}}, t)$ non-holonomic constraints can be written in the following way :

$$\varphi_i(\mathbf{y}, t) = 0, \quad i = 1, 2, ..., P_h \tag{2.1}$$

$$\psi_j(\mathbf{y}, \dot{\mathbf{y}}, t) = 0, \quad j = P_h + 1, 2, ..., P_{nh} \tag{2.2}$$

Also, by differentiating equation 2.1 two times and equation 2.2 one time, these constraints can be formulated in the form of a constraint matrix equation in terms of acceleration [83] :

$$\mathbf{A}(\mathbf{y}, \dot{\mathbf{y}}, t)\ddot{\mathbf{y}}(t) = \mathbf{b}(\mathbf{y}, \dot{\mathbf{y}}, t). \tag{2.3}$$

Where the $P \times M$ matrix $\mathbf{A}(\mathbf{y}, \dot{\mathbf{y}}, t)$ and the $P \times 1$ vector $\mathbf{b}(\mathbf{y}, \dot{\mathbf{y}}, t)$ are functions of the motion. There is no need for the P constraints to be independent, therefore,

the rank r of matrix $\mathbf{A}$ is $r \leqslant P$. The acceleration $\ddot{\mathbf{y}}_u$ of the unconstrained system is given by Newton's second law :

$$\mathbf{M}\ddot{\mathbf{y}}_u = \mathbf{F}_e \tag{2.4}$$
$$\ddot{\mathbf{y}}_u = \mathbf{M}^{-1}\mathbf{F}_e \tag{2.5}$$

Also, as opposed to the non-constrained system, the displacement $\ddot{\mathbf{y}}$ of the constrained system depends on the constraint forces $\mathbf{F}_c$:

$$\mathbf{M}\ddot{\mathbf{y}} = \mathbf{F}_e + \mathbf{F}_c \tag{2.6}$$

By using the Lagrange multipliers λ, which is a vector, the constraint forces $\mathbf{F}_c$ can be expressed by means of the constraint matrix $\mathbf{A}$ [85] :

$$\mathbf{F}_c = -\mathbf{A}^T\lambda \tag{2.7}$$

So, out of equation 2.6, it follows :

$$\mathbf{M}\ddot{\mathbf{y}} + \mathbf{A}^T\lambda = \mathbf{F}_e \tag{2.8}$$

Equations 2.3 and 2.8 lead to the matrix equation of the constrained system motion :

$$\begin{bmatrix} \mathbf{M} & \mathbf{A}^T \\ \mathbf{A} & \mathbf{0} \end{bmatrix} \begin{pmatrix} \ddot{\mathbf{y}} \\ \lambda \end{pmatrix} = \begin{pmatrix} \mathbf{F}_e \\ \mathbf{b} \end{pmatrix} \tag{2.9}$$

Assuming that no mass within matrix $\mathbf{M}$ is equal to zero and that the constraint matrix $\mathbf{A}$ is full, then the matrix of equation 2.9 is invertible. As a result, equation 2.9 becomes :

$$\begin{pmatrix} \ddot{\mathbf{y}} \\ \lambda \end{pmatrix} = \begin{bmatrix} \mathbf{M} & \mathbf{A}^T \\ \mathbf{A} & \mathbf{0} \end{bmatrix}^{-1} \begin{pmatrix} \mathbf{F}_e \\ \mathbf{b} \end{pmatrix} \tag{2.10}$$

As it is put forward by Arabyan and Wu [83], after using some algebra, the inverse matrix can be rewritten thus :

$$\begin{bmatrix} \mathbf{M} & \mathbf{A}^T \\ \mathbf{A} & \mathbf{0} \end{bmatrix}^{-1} = \begin{bmatrix} \mathbf{M}^{-1} - \mathbf{M}^{-1}\mathbf{A}^T(\mathbf{A}\mathbf{M}^{-1}\mathbf{A}^T)^{-1}\mathbf{A}\mathbf{M}^{-1} & \mathbf{M}^{-1}\mathbf{A}^T(\mathbf{A}\mathbf{M}^{-1}\mathbf{A}^T)^{-1} \\ (\mathbf{A}\mathbf{M}^{-1}\mathbf{A}^T)^{-1}\mathbf{A}\mathbf{M}^{-1} & -(\mathbf{A}\mathbf{M}^{-1}\mathbf{A}^T)^{-1} \end{bmatrix} \tag{2.11}$$

As a result, equations 2.10 and 2.11 lead to the expression of the dynamic system acceleration :

$$\begin{aligned} \ddot{\mathbf{y}} &= (\mathbf{M}^{-1} - \mathbf{M}^{-1}\mathbf{A}^T(\mathbf{A}\mathbf{M}^{-1}\mathbf{A}^T)^{-1}\mathbf{A}\mathbf{M}^{-1})\mathbf{F}_e + \mathbf{M}^{-1}\mathbf{A}^T(\mathbf{A}\mathbf{M}\mathbf{A}^T)^{-1}\mathbf{b} \\ &= \mathbf{M}^{-1}\mathbf{F}_e + \mathbf{M}^{-1}\mathbf{A}^T(\mathbf{A}\mathbf{M}^{-1}\mathbf{A}^T)^{-1}(\mathbf{b} - \mathbf{A}\mathbf{M}^{-\mathbf{1}}\mathbf{F}_\mathbf{e}) \end{aligned} \tag{2.12}$$

Then, using equation 2.5, it leads to :

$$\ddot{\mathbf{y}} = \ddot{\mathbf{y}}_u + \mathbf{M}^{-1}\mathbf{A}^T(\mathbf{A}\mathbf{M}^{-1}\mathbf{A}^T)^{-1}(\mathbf{b} - \mathbf{A}\ddot{\mathbf{y}}_u) \tag{2.13}$$

Equation 2.13 shows that the dynamics of the constrained system is obtained by means of a correction given by the dynamics of the non-constrained system. Also, by means of equation 2.10, the expression of the Lagrange multiplier $\lambda(t)$ becomes :

$$\begin{aligned} \lambda(t) &= (\mathbf{A}\mathbf{M}^{-1}\mathbf{A}^T)^{-1}\mathbf{A}\mathbf{M}^{-1}\mathbf{F}_e - (\mathbf{A}\mathbf{M}^{-1}\mathbf{A}^T)^{-1}\mathbf{b} \\ &= -(\mathbf{A}\mathbf{M}^{-1}\mathbf{A}^T)^{-1}(\mathbf{b} - \mathbf{A}\mathbf{M}^{-1}\mathbf{F}_e) \end{aligned} \tag{2.14}$$

Then, by means of equation 2.7 and 2.14, it is possible to obtain the expression of vector $\mathbf{F}_c(t)$:

$$\mathbf{F}_c(t) = \mathbf{A}^T(\mathbf{A}\mathbf{M}^{-1}\mathbf{A}^T)^{-1}(\mathbf{b} - \mathbf{A}\mathbf{M}^{-1}\mathbf{F}_e) \tag{2.15}$$

Matrix $\mathbf{B}$ is defined as such : $\mathbf{B} = \mathbf{A}\mathbf{M}^{-1/2}$. Thus, the second term of equation 2.13 can be rewritten as such :

$$\begin{aligned} \mathbf{M}^{-1}\mathbf{A}^T(\mathbf{A}\mathbf{M}^{-1}\mathbf{A}^T)^{-1} &= \mathbf{M}^{-1/2}\mathbf{M}^{-1/2}\mathbf{A}^T(\mathbf{A}\mathbf{M}^{-1/2}\mathbf{M}^{-1/2}\mathbf{A}^T)^{-1} \\ &= \mathbf{M}^{-1/2}\mathbf{B}^T(\mathbf{B}\mathbf{B}^T)^{-1} = \mathbf{M}^{-1/2}\mathbf{B}^+ \end{aligned} \tag{2.16}$$

where $\mathbf{B}^+$ is the Moore-Penrose generalized inverse of matrix $\mathbf{B}$. Thus the dynamic equation of the constrained system given by the U-K formulation :

$$\ddot{\mathbf{y}} = \ddot{\mathbf{y}}_u + \mathbf{M}^{-1/2}\mathbf{B}^+(\mathbf{b} - \mathbf{A}\ddot{\mathbf{y}}_u). \tag{2.17}$$

Furthermore, out of equation 2.15, the following equation unfolds :

$$\mathbf{F}_c(t) = \mathbf{M}^{1/2}\mathbf{B}^+(\mathbf{b} - \mathbf{A}\ddot{\mathbf{y}}_u). \tag{2.18}$$

Then, the U-K formulation provides equations 2.17 and 2.18 describing the dynamics of constraint mechanical systems. These equations can be applied to linear or nonlinear, conservative or dissipative systems. For a given external force $\mathbf{F_e}$, it is possible to solve equation 2.17 by using a suitable time-step integration scheme. Moreover, the Moore-Penrose generalized inverse $\mathbf{B}^+$ can be rendered numerically robust, even when the constraint matrix is singular. If no constraint is applied, equation 2.12 leads back to the unconstrained formulation 2.5. The main elegance of the U-K formulation lies in the encapsulation in a single explicit equation of both the dynamical equations of the system and the applied constraints. In particular, no Lagrange multipliers or any additional variables are needed. Note that the vector $\mathbf{F_e}$ contains the non-linear forces $\mathbf{F}_{nl}$ of the system and the excitation forces $\mathbf{F}_{ext}$ exerted on the system. The relation between these forces is expressed in section 2.3.2 when considering the modal U-K formulation.

2.3.2 The modal U-K formulation

The U-K formulation can be adapted to continuous flexible systems whose dynamics is described in terms of modal coordinates. This was done by Antunes and Debut so that this formulation could be used to model string instruments such as the guitar [71]. A number of S vibrating subsystems is assumed, each one defined in terms of its unconstrained modal basis and being coupled through P kinematic constraints. Defining $\mathbf{r}$ as the coordinate vector, a modal expansion of the system dynamic response is done, leading to :

$$Y(\mathbf{r},t) = \sum_{n=0}^{N} q_n(t)\phi_n(\mathbf{r}). \tag{2.19}$$

With $Y(\mathbf{r},t)$, $q_n(t)$, $\phi_n(\mathbf{r})$ being the dynamic response in terms of displacement, the modal amplitudes and the mode shapes respectively in scalar form, and N is the string number of modes. Let $\mathbf{y}(\mathbf{r},t)$ be the dynamic response vector in terms of displacement. In matrix form, this conversion of physical coordinates to the modal space gives :

$$\mathbf{y} = \mathbf{\Phi q}, \quad \dot{\mathbf{y}} = \mathbf{\Phi}\dot{\mathbf{q}}, \quad \ddot{\mathbf{y}} = \mathbf{\Phi}\ddot{\mathbf{q}} \tag{2.20}$$

Where $\mathbf{q}$ is the modal amplitudes vector and $\mathbf{\Phi}$ is the mode shapes matrix. The physical coordinates, the modal coordinates and the mode shapes are defined as such :

$$\mathbf{y} = \begin{pmatrix} \mathbf{y}^1 \\ \mathbf{y}^2 \\ \vdots \\ \mathbf{y}^S \end{pmatrix}, \quad \mathbf{q} = \begin{pmatrix} \mathbf{q}^1 \\ \mathbf{q}^2 \\ \vdots \\ \mathbf{q}^S \end{pmatrix}, \quad \mathbf{\Phi} = \begin{bmatrix} \mathbf{\Phi}^1 & \mathbf{0} & \dots & \mathbf{0} \\ \mathbf{0} & \mathbf{\Phi}^2 & \dots & \mathbf{0} \\ \vdots & \vdots & \ddots & \vdots \\ \mathbf{0} & \mathbf{0} & \dots & \mathbf{\Phi}^S \end{bmatrix} \tag{2.21}$$

The modal basis of the vibratory subsystem s with N_s modes is defined thus :

$$\mathbf{q}^s(t) = \begin{pmatrix} q_1^s(t) \\ q_2^s(t) \\ \vdots \\ q_{N_s}^s(t) \end{pmatrix}, \quad s = 1, 2, ..., S. \tag{2.22}$$

$$\Phi^s = \begin{pmatrix} \phi_1^s(\mathbf{r}_1^s) & \phi_2^s(\mathbf{r}_1^s) & \dots & \phi_{N_s}^s(\mathbf{r}_1^s) \\ \phi_1^s(\mathbf{r}_2^s) & \phi_2^s(\mathbf{r}_2^s) & \dots & \phi_{N_s}^s(\mathbf{r}_2^s) \\ \vdots & \vdots & \ddots & \vdots \\ \phi_1^s(\mathbf{r}_{R_s}^s) & \phi_2^s(\mathbf{r}_{R_s}^s) & \dots & \phi_{N_s}^s(\mathbf{r}_{R_s}^s) \end{pmatrix}, \quad s = 1, 2, ..., S. \tag{2.23}$$

Where $R = 1, 2, \dots, R_s$ puts forward the coordinates where the mode shapes are defined. Replacing 2.20 into 2.13, it gives :

$$\mathbf{M\Phi\ddot{q}} = \mathbf{M\Phi\ddot{q}_u} + \mathbf{A}^T(\mathbf{AM}^{-1}\mathbf{A}^T)^{-1}(\mathbf{b} - \mathbf{A\Phi\ddot{q}_u}) \tag{2.24}$$

where $\ddot{\mathbf{q}}_\mathbf{u}$ are the modal accelerations of the unconstrained system. Then, the modal mass matrix $\boldsymbol{M}$ (written in italics) is defined as $\boldsymbol{M} = \mathbf{\Phi}^T\mathbf{M\Phi}$, which gives its inverse form $\mathbf{M} = \mathbf{\Phi}^{-T}\boldsymbol{M}\mathbf{\Phi}^{-1}$. By means of these definitions, equation 2.24 can be rewritten :

$$\boldsymbol{M}\ddot{\mathbf{q}} = \boldsymbol{M}\ddot{\mathbf{q}}_\mathbf{u} + \mathbf{\Phi}^T\mathbf{A}^T(\mathbf{A\Phi}\boldsymbol{M}^{-1}\mathbf{\Phi}^T\mathbf{A}^T)^{-1}(\mathbf{b} - \mathbf{A\Phi\ddot{q}_u}) \tag{2.25}$$

By introducing the modal constraint matrix $\boldsymbol{A}$ (written in italics), with $\boldsymbol{A} = \mathbf{A\Phi}$, it leads to :

$$\ddot{\mathbf{q}} = \ddot{\mathbf{q}}_\mathbf{u} + \boldsymbol{M}^{-1}\boldsymbol{A}^T(\boldsymbol{AM}^{-1}\boldsymbol{A}^T)^{-1}(\mathbf{b} - \boldsymbol{A}^T\ddot{\mathbf{q}}_u) \tag{2.26}$$

Then, by defining matrix $\boldsymbol{B} = \boldsymbol{AM}^{-1/2}$, it leads to the dynamic equation of the constrained system expressed in terms of modal coordinates :

$$\ddot{\mathbf{q}} = \ddot{\mathbf{q}}_u + \boldsymbol{M}^{1/2}\boldsymbol{B}^+(\mathbf{b} - \boldsymbol{A}\ddot{\mathbf{q}}_\mathbf{u}). \tag{2.27}$$

Let us consider the subsystem s on which an external force is applied. Its dynamics can be described as a set of modal equations, which is introduced as follows :

$$\boldsymbol{M}^s\ddot{\mathbf{q}}^s + \boldsymbol{C}^s\dot{\mathbf{q}}^s + \boldsymbol{K}^s\mathbf{q}^s + \boldsymbol{F}^s_{nl}(\mathbf{q}^s, \dot{\mathbf{q}}^s) = \boldsymbol{F}^s_{ext}, \quad s = 1, 2, \ldots, S \tag{2.28}$$

where $\mathbf{q}^s$ represents the modal amplitudes of the subsystem, $\boldsymbol{M}^s$, $\boldsymbol{C}^s$ and $\boldsymbol{K}^s$ are respectively the modal mass matrix, the modal damping matrix and the modal stiffness matrix of the subsystem, and $\boldsymbol{F}^s_{nl}$ and $\boldsymbol{F}^s_{ext}$ are modal force vectors, representing respectively the nonlinear forces and the excitation forces applied on the subsystem s. These mentioned modal forces come from the constraint-independent forces, which are obtained by the modal projection of the physical external force vector $\mathbf{F}_e$. To compute the modal acceleration $\ddot{\mathbf{q}}$ of the constrained system, as suggests equation 2.27, the modal acceleration $\ddot{\mathbf{q}}_u$ of the unconstrained system is computed by means of equation 2.5 :

$$\ddot{\mathbf{q}}^s_u = (\boldsymbol{M}^s)^{-1}\boldsymbol{F}^s \tag{2.29}$$

where vector $\boldsymbol{F}^s$ refers to all independent modal constraint forces, which include external forces $\boldsymbol{F}^s_{\boldsymbol{ext}}$, modal dissipative and modal elastic linear and nonlinear forces :

$$\boldsymbol{F}^s = \boldsymbol{F}^s_{ext} - \boldsymbol{C}^s\dot{\mathbf{q}}^s - \boldsymbol{K}^s\mathbf{q}^s - \boldsymbol{F}^s_{nl}(\mathbf{q}^s, \dot{\mathbf{q}}^s), \quad s = 1, 2, \ldots, S \tag{2.30}$$

By writing the modal equations of the S subsystems in matrix form, the modal accelerations of the unconstrained system $\ddot{\mathbf{Q}}_u = [\mathbf{q}^1_u, \mathbf{q}^2_u, \ldots, \mathbf{q}^S_u]^T$ are written as follow :

$$\ddot{\mathbf{Q}}_u = \boldsymbol{M}^{-1}[\boldsymbol{F}_{ext} - \boldsymbol{C}\dot{\mathbf{Q}} - \boldsymbol{K}\mathbf{Q} - \boldsymbol{F}_{nl}(\mathbf{Q}, \dot{\mathbf{Q}})] \tag{2.31}$$

where vectors $\mathbf{Q} = [\mathbf{q}^1, \mathbf{q}^2, \ldots, \mathbf{q}^S]^T$ and $\dot{\mathbf{Q}}$ represent the modal displacement and velocity of the S coupled subsystems. The matrices $\boldsymbol{M}$, $\boldsymbol{C}$ and $\boldsymbol{K}$ are respectively the modal mass matrix, the modal damping matrix and the modal stiffness matrix of the constrained system, which are diagonal and are constructed by means of the subsystems' modal matrices :

$$\begin{gathered}\boldsymbol{M} \equiv \begin{pmatrix} \boldsymbol{M}^1 & \mathbf{0} & \ldots & \mathbf{0} \\ \mathbf{0} & \boldsymbol{M}^2 & \ldots & \mathbf{0} \\ \vdots & \vdots & \ddots & \vdots \\ \mathbf{0} & \mathbf{0} & \ldots & \boldsymbol{M}^S \end{pmatrix}, \boldsymbol{C} \equiv \begin{pmatrix} \boldsymbol{C}^1 & \mathbf{0} & \ldots & \mathbf{0} \\ \mathbf{0} & \boldsymbol{C}^2 & \ldots & \mathbf{0} \\ \vdots & \vdots & \ddots & \vdots \\ \mathbf{0} & \mathbf{0} & \ldots & \boldsymbol{C}^S \end{pmatrix}, \\ \boldsymbol{K} \equiv \begin{pmatrix} \boldsymbol{K}^1 & \mathbf{0} & \ldots & \mathbf{0} \\ \mathbf{0} & \boldsymbol{K}^2 & \ldots & \mathbf{0} \\ \vdots & \vdots & \ddots & \vdots \\ \mathbf{0} & \mathbf{0} & \ldots & \boldsymbol{K}^S \end{pmatrix}\end{gathered} \tag{2.32}$$

where the parameters of the modal matrices of each subsystem, that is the modal masses m_n^s, the modal dampings c_n^s and the modal stiffness k_n^s are defined in the following way :

$$m_n^s = \int_{D_s} \rho(\mathbf{r}^s)[\Phi_n^s(\mathbf{r}^s)]^2 d\mathbf{r}^s, \quad c_n^s = 2m_n^s\omega_n^s\zeta_n^s, \quad k_n^s = m_n^s(\omega_n^s)^2. \tag{2.33}$$

where ω_n^s represents the modal pulsation, ζ_n^s the modal damping and $\rho(\mathbf{r}^s)$ is the mass density. To compute the modal forces $\boldsymbol{F}_{ext}^s$, the corresponding physical forces $\mathbf{F}_{ext}^s$ need to be projected on the mode shapes :

$$F_{ext,n}^s(t) = \int_{D_s} F_{ext}(\mathbf{r}^s, t)\phi_n^s(\mathbf{r}^s) d\mathbf{r}^s, \quad s = 1, 2, \ldots, S, \quad n = 1, 2, \ldots, N_s \tag{2.34}$$

With D_s the space domain of the system and with $F_{ext,n}^s$ and F_{ext} being the modal forces and the physical forces respectively in scalar form, which gives in matrix form :

$$\boldsymbol{F}_{ext}^s = (\Phi_{ext}^s)^T \mathbf{F}_{ext}^s \tag{2.35}$$

where Φ_{ext}^s is a matrix built from the mode shapes of the corresponding subsystem s at the excitation points.

The unconstrained modal accelerations $\ddot{\mathbf{Q}}_u(t)$ are computed by means of equations 2.30 and 2.29 :

$$
\begin{pmatrix} \ddot{\mathbf{q}}_u^1 \\ \ddot{\mathbf{q}}_u^2 \\ \vdots \\ \ddot{\mathbf{q}}_u^S \end{pmatrix} = \begin{pmatrix} (\boldsymbol{M}^1)^{-1} & \mathbf{0} & \dots & \mathbf{0} \\ \mathbf{0} & (\boldsymbol{M}^2)^{-1} & \dots & \mathbf{0} \\ \vdots & \vdots & \ddots & \vdots \\ \mathbf{0} & \mathbf{0} & \dots & (\boldsymbol{M}^S)^{-1} \end{pmatrix}
$$
$$
\times \left(\begin{pmatrix} \boldsymbol{F}_{ext}^1(t) \\ \boldsymbol{F}_{ext}^2(t) \\ \vdots \\ \boldsymbol{F}_{ext}^S(t) \end{pmatrix} - \begin{pmatrix} \boldsymbol{C}^1 & \mathbf{0} & \dots & \mathbf{0} \\ \mathbf{0} & \boldsymbol{C}^2 & \dots & \mathbf{0} \\ \vdots & \vdots & \ddots & \vdots \\ \mathbf{0} & \mathbf{0} & \dots & \boldsymbol{C}^S \end{pmatrix} \begin{pmatrix} \dot{\mathbf{q}}^1 \\ \dot{\mathbf{q}}^2 \\ \vdots \\ \dot{\mathbf{q}}^S \end{pmatrix} \right. \tag{2.36}
$$
$$
\left. - \begin{pmatrix} \boldsymbol{K}^1 & \mathbf{0} & \dots & \mathbf{0} \\ \mathbf{0} & \boldsymbol{K}^2 & \dots & \mathbf{0} \\ \vdots & \vdots & \ddots & \vdots \\ \mathbf{0} & \mathbf{0} & \dots & \boldsymbol{K}^S \end{pmatrix} \begin{pmatrix} \mathbf{q}^1 \\ \mathbf{q}^2 \\ \vdots \\ \mathbf{q}^S \end{pmatrix} - \begin{pmatrix} \boldsymbol{F}_{nl}^1(\mathbf{q}^1, \dot{\mathbf{q}}^1) \\ \boldsymbol{F}_{nl}^2((\mathbf{q}^2, \dot{\mathbf{q}}^2)) \\ \vdots \\ \boldsymbol{F}_{nl}^S((\mathbf{q}^S, \dot{\mathbf{q}}^S)) \end{pmatrix} \right)
$$

Moreover, the system is submitted to constraint conditions which couple the different subsystems with each other at a specific physical coordinate $\mathbf{r}_c^s$. Using equation 2.3, the coupling equations are written thus :

$$
\boldsymbol{A}(\mathbf{Q}, \dot{\mathbf{Q}}, t)\ddot{\mathbf{Q}} = \mathbf{b}(\mathbf{Q}, \dot{\mathbf{Q}}, t) \tag{2.37}
$$

with $\boldsymbol{A}(\mathbf{Q}(t), \dot{\mathbf{Q}}(t), t)$ and $\boldsymbol{b}(\mathbf{Q}(t), \dot{\mathbf{Q}}(t), t)$ defined at specific constraint locations $\mathbf{r}_c^s$ between the subsystems.

$$
\begin{bmatrix} A_1(\Phi^1(\mathbf{r}_1^1), \dots, \Phi^S(\mathbf{r}_1^S); \mathbf{q}^1, \dots, \mathbf{q}^S; \dot{\mathbf{q}}^1, \dots, \dot{\mathbf{q}}^S; t) \\ A_2(\Phi^1(\mathbf{r}_2^1), \dots, \Phi^S(\mathbf{r}_2^S); \mathbf{q}^1, \dots, \mathbf{q}^S; \dot{\mathbf{q}}^1, \dots, \dot{\mathbf{q}}^S; t) \\ \vdots \\ A_P(\Phi^1(\mathbf{r}_P^1), \dots, \Phi^S(\mathbf{r}_P^S); \mathbf{q}^1, \dots, \mathbf{q}^S; \dot{\mathbf{q}}^1, \dots, \dot{\mathbf{q}}^S; t) \end{bmatrix} \times \begin{pmatrix} \ddot{\mathbf{q}}^1 \\ \ddot{\mathbf{q}}^2 \\ \vdots \\ \ddot{\mathbf{q}}^S \end{pmatrix}
$$
$$
= \begin{pmatrix} b_1(\mathbf{q}^1, \dots, \mathbf{q}^S; \dot{\mathbf{q}}^1, \dots, \dot{\mathbf{q}}^S; t) \\ b_2(\mathbf{q}^1, \dots, \mathbf{q}^S; \dot{\mathbf{q}}^1, \dots, \dot{\mathbf{q}}^S; t) \\ \vdots \\ b_P(\mathbf{q}^1, \dots, \mathbf{q}^S; \dot{\mathbf{q}}^1, \dots, \dot{\mathbf{q}}^S; t) \end{pmatrix} \tag{2.38}
$$

The modal forces $\boldsymbol{F}_c(t)$ due to the constraints are computed from equation 2.27 by multiplying the second term of the equation, which represents the modal acceleration complement $\ddot{\mathbf{Q}}_c = \boldsymbol{M}^{-1/2}\boldsymbol{B}^+(\mathbf{b} - \boldsymbol{A}\ddot{\mathbf{Q}}_u)$, by the system modal mass matrix $\boldsymbol{M}$, hence,

$$
\boldsymbol{F}_c = \boldsymbol{M}^{1/2}\boldsymbol{B}^+(\mathbf{b} - \boldsymbol{A}\ddot{\mathbf{Q}}_u) \tag{2.39}
$$

Then, the physical constraining forces are computed by means of the following approximation [71] :

$$
\mathbf{F}_c = \left((\Phi_c)^T\right)^+ \boldsymbol{F}_c \tag{2.40}
$$

which gives :

$$\mathbf{F}_c = \left((\Phi_c)^T\right)^+ \boldsymbol{M}^{1/2}\boldsymbol{B}^+(\mathbf{b} - \boldsymbol{A}\ddot{\mathbf{Q}}_u) \tag{2.41}$$

Then it is possible to compute the constraint forces $\mathbf{F}_c$ after computing the modal amplitudes $\ddot{\mathbf{Q}}_u$. The excitation force profile $\boldsymbol{F}_{ext}$ corresponds to the input of the system. The expression of the non-linear forces $\boldsymbol{F}_{nl}$ depends on the nature of these non-linearities. When it comes to the string, the geometrical non-linear forces are modelled in section 2.4.1.

2.4 Modelling of the substructures of the clavichord

On the basis of the approach developed by Antunes and Debut, adapting the U-K formulation to model the coupled substructures of the guitar, this adapted formulation is used here to model the coupled substructures of the clavichord. The modelling of the string, the bridge, the key-tangent substructure and the damper are dealt with in this section. Along side with this, the coupling between the string and the bridge is tackled. The excitation of the string by the key-tangent substructure is modeled by means of coupling at the instant when the tangent strikes the string. Then, the coupling between the damper and the string is done in order to model the effect of the cloth damper. The way the different substructures are coupled is summarised in figure 2.1.

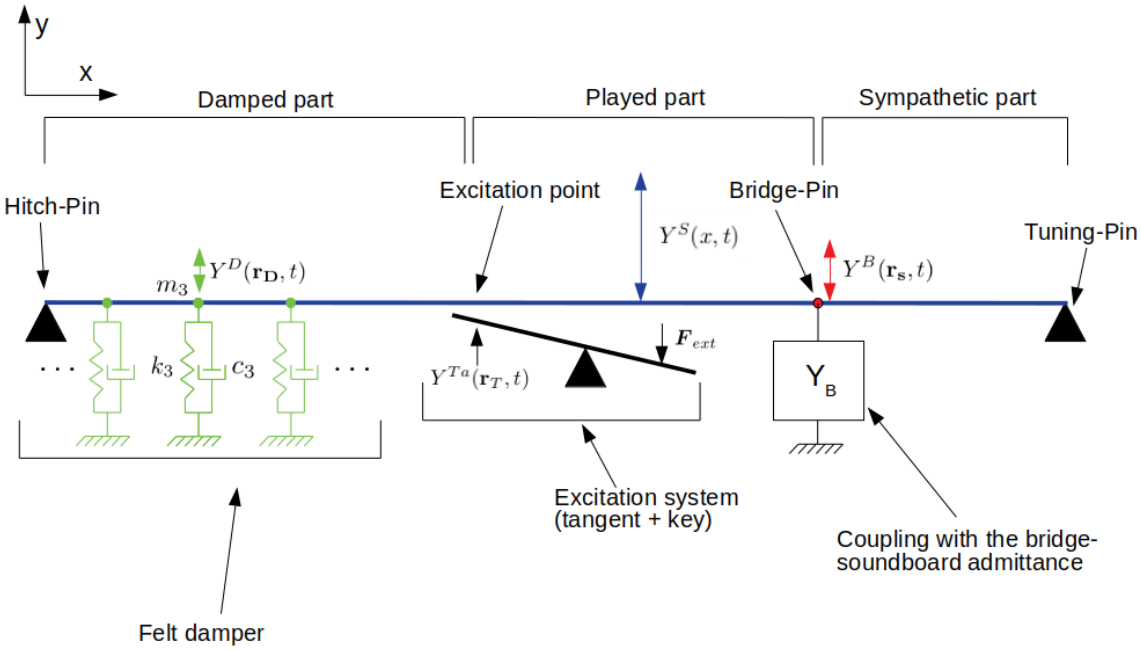

Figure 2.1: Schema of the modeled G#3 string being excited by the tangent.

2.4.1 String modelling

Linear description of the vibrating string

In this section, the modelling of the string by means of a modal representation is considered. Legitimate assumptions considered to model the string are presented. Then, the model for the stiff vibrating string is put into light. A damping model of the string is then presented. Because of the considerable static displacement of the string, a model of the geometrical non-linear force is considered to take into account the variation of the string tension.

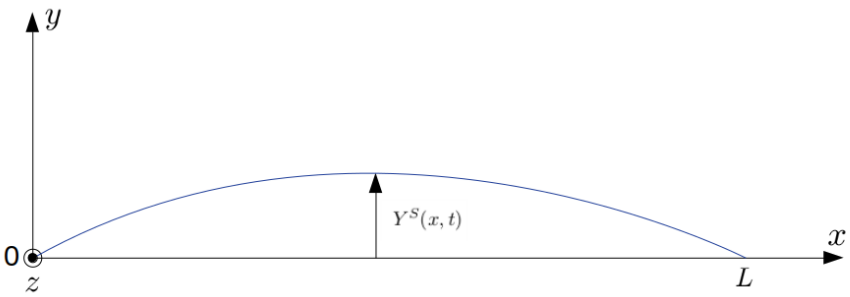

Figure 2.2: Sketch of the vibrating string moving with respect to only one polarisation of motion.

Let us consider an homogeneous string with length L, linear density μ and stretched with a tension T_0 (see figure 2.2). In reality, the string oscillates with respect to two polarisations of motion (with respect to the y axis and to the z axis). So at one point of the string, its trajectory in the (O,y,z) plane is an ellipse. In this modelling, only the polarisation with respect to the y axis is considered. It is assumed that the string vibratory displacement is small, so that the longitudinal waves are neglected. The torsional waves are also neglected. For the moment, the geometrical non-linearity is not taken into account.

By considering an elastic, thin and flexible string whose flexural stiffness is negligible, it is possible to yield a simple model of the string transverse motion (with respect to the y axis). Proceeding by means of the application of Newton second law on an infinitesimal portion of the string, and considering the small displacement assumption, it leads to the wave equation of the flexible string expressed in terms of displacement Y^S with respect to the y axis [58] :

$$\mu \frac{\partial^2 Y^S(x,t)}{\partial t^2} - T_0 \frac{\partial^2 Y^S(x,t)}{\partial x^2} = 0 \tag{2.42}$$

where μ is the linear mass density of the string. It is considered that the boundary conditions are pinned, which means that $Y^S(0,t) = Y^S(L,t) = 0$. By means of equation 2.42 and these boundary conditions, it yields the perfectly harmonic frequencies of the flexible strings $f_n = nf_0$, where n is the number of the partial and f_0 is the fundamental frequency of the string given by $f_0 = \frac{1}{2L}\sqrt{\frac{T_0}{\rho S}}$.

By considering the flexural elasticity of the string and its radius, the string bending stiffness plays a role in the string motion. Then, equation 2.42 becomes :

$$\rho S \frac{\partial^2 Y^S(x,t)}{\partial t^2} - T_0 \frac{\partial^2 Y^S(x,t)}{\partial x^2} + EI \frac{\partial^4 Y^S(x,t)}{\partial x^4} = 0 \tag{2.43}$$

where ρ is the mass density of the string and S its cross-section area so that $\mu = \rho S$, E is the Young modulus of the string material and I is the second moment of inertia of the string $I = \frac{\pi r^4}{64}$ with r the radius of the string. Considering that this stiff string is pinned at its extremity, its leads to the following boundary conditions [58] :

$$Y^S(0,t) = Y^S(L,t) = \frac{\partial^2 Y^S(x,t)}{\partial x^2}(0,t) = \frac{\partial^2 Y^S(x,t)}{\partial x^2}(L,t) = 0 \quad n = 1, 2, \ldots, N \tag{2.44}$$

It comes down to the following modal frequencies of the string :

$$f_n = n f_0 \sqrt{1 + Bn^2} = n \frac{c_0}{2L} \sqrt{1 + Bn^2} \tag{2.45}$$

where $c_0 = \sqrt{\frac{T_0}{\mu}}$ is the velocity of the transverse wave in the string, and $B = \frac{\pi^2 EI}{T_0 L^2}$ is the inharmonic coefficient of the string. As a result, one can see in equation 2.45 that the modal frequencies are changed when including the string bending stiffness. These frequencies are not absolutely harmonic anymore. The higher the rank n of the partial, the more the shift of these modal frequencies from the harmonic frequencies. Note that equation 2.43 can be rewritten with a modal representation.

Modal description of the string

To comply the string model with the modal U-K formulation, a modal representation of the string is given in this section. A modal expansion of the string displacement Y^S is done :

$$Y^S(x,t) = \sum_{n=1}^{N_s} \phi_n^S(x) q_n^S(t) \tag{2.46}$$

where ϕ_n^S are the mode shapes of the string, which are assumed to be real, q_n^S are its modal amplitudes, and N_s is the string number of modes so that $n = 1, 2, ..., N_s$. Because of the modal expansion, it is necessary to resolve the eigenvalue problem related to equation 2.43 which reads as follow :

$$-T_0 \frac{\partial^2 \phi_n^S(x)}{\partial x^2} + EI \frac{\partial^4 \phi_n^S(x)}{\partial x^4} - \rho S \omega_n^2 \phi_n^S = 0 \tag{2.47}$$

where $\omega_n = 2\pi f_n$ is the modal pulsation. When solving equation 2.47 and using the pined-pined boundary conditions given in equation 2.44, it leads to the following string mode shapes :

$$\phi_n^S(x) = \sin\left(\frac{n\pi x}{L}\right) \quad n = 1, 2, \ldots, N \tag{2.48}$$

It is possible to demonstrate that, for a uniform string, these mode shapes are orthogonal to each other, which means that taking two index $n = 1, 2, ..., N$ and $i = 1, 2, ..., N$:

$$\int_0^L \phi_n^S(x)\phi_i^S(x) = \delta_{n,i} \tag{2.49}$$

where $\delta_{n,i}$ is the Kronecker delta. Using equation 2.46, equation 2.43 as well as the orthogonal property of the string modes, it leads to the modal equations of the string (where S refers to the string) :

$$\boldsymbol{M}^S\ddot{\mathbf{q}}^S + \boldsymbol{C}^S\dot{\mathbf{q}}^S + \boldsymbol{K}^S\mathbf{q}^S = \mathbf{0} \tag{2.50}$$

where $\boldsymbol{M}^S$, $\boldsymbol{C}^S$ and $\boldsymbol{K}^S$ are the modal mass matrix, the modal damping matrix and the modal stiffness matrix of the string respectively, and $\mathbf{q}^S$ is the modal amplitude vector of the string.

If the static displacement is large enough, the geometrical non-linear force related to the string variation of tension also needs to be included. That yields the following string modal equations :

$$\boldsymbol{M}^S\ddot{\mathbf{q}}^S + \boldsymbol{C}^S\dot{\mathbf{q}}^S + \boldsymbol{K}^S\mathbf{q}^S + \boldsymbol{F}_{nl}^S(\mathbf{q}^S) = \mathbf{0} \tag{2.51}$$

It was mentioned at the end of section 2.3.2 that the excitation force corresponds to the input of the system. This force leads to a time-changing tension of the string while the tangent is pressing the string. However, the expression of the geometrical non-linear force can be expressed by means of the Kirchhoff-Carrier model, which is the topic of the next section.

String geometrical non-linearity

The variation of tension of the string created by its uplift done by the tangent causes the variation of its fundamental frequency. As this static displacement is considerable for the clavichord, inducing a substantial shift of the fundamental frequency, this variation of the string tension needs to be modeled. In fact, the string uplift is a geometrical deformation creating nonlinear forces. By modeling these nonlinear forces caused by geometrical deformation, this variation of tension causing the variation in tuning frequency can be reproduced in the simulation. This is put forward by Debut and Antunes in the case of a twelve-string Portuguese guitar, modeling the non-linear forces of the strings by using the Kirchhoff-Carrier model, for high amplitude vibrations [68, 72]. We propose here that the same formal approach can be developed for modeling the time-varying string tension (and modal frequencies) when the tangent pressure leads to quasi-steady large amplitude deformations. The Kirchhoff-Carrier model leads to geometric nonlinear terms creating the dynamic tension T_{dyn} :

$$T_{dyn} = \frac{ES}{2L} \int_0^L \left[\left(\frac{\partial Y^S(x,t)}{\partial x} \right)^2 \right] dx \tag{2.52}$$

which gives rise to the nonlinear differential equation of motion :

$$\rho S \frac{\partial^2 Y^S(x,t)}{\partial t^2} - (T_0 + T_{dyn}(t)) \frac{\partial^2 Y^S(x,t)}{\partial x^2} = 0 \tag{2.53}$$

Where ρ is the mass density and S is the string section. Thus :

$$\rho S \frac{\partial^2 Y^S(x,t)}{\partial t^2} - T_0 \frac{\partial^2 Y^S(x,t)}{\partial x^2} = T_{dyn}(t) \frac{\partial^2 Y^S(x,t)}{\partial x^2} \tag{2.54}$$

In equation 2.54, the right side can be modeled as an external force named F^{nl} applied on the string :

$$F^{nl}(x,t) = T_{dyn} \frac{\partial^2 Y^S(x,t)}{\partial x^2} \tag{2.55}$$

In terms of string modes, using equation 2.52, the dynamic tension is rewritten :

$$\begin{aligned} T_{dyn}(t) &= \frac{ES}{2L} \int_0^L \left[\left(\sum_{m=1}^{N} \frac{\partial \phi_m(x)}{\partial x} q_m(t) \right) \left(\sum_{n=1}^{N} \frac{\partial \phi_n(x)}{\partial x} q_n(t) \right) \right] dx \\ &= \frac{ES}{2L} \sum_{m=1}^{N} \sum_{n=1}^{N} \left[q_m(t) q_n(t) \int_0^L \frac{\partial \phi_m(x)}{\partial x} \frac{\partial \phi_n(x)}{\partial x} dx \right] \end{aligned} \tag{2.56}$$

Equation 2.55 becomes :

$$F^{nl}(x,t) = T_{dyn} \frac{\partial^2 \phi_n(x)}{\partial x^2} q_n(t) \tag{2.57}$$

Thereby, it yields the nonlinear modal force terms :

$$F_n^{nl}(t) = \int_0^L F^{nl}(x,t) \phi_n(x) dx = T_{dyn}(t) \sum_{n=1}^{N} q_n(t) \int_0^L \frac{\partial^2 \phi_n(x)}{\partial x^2} \phi_n(x) dx \tag{2.58}$$

When it comes to calculating the integrals in equation 2.56 :

$$\begin{aligned} \int_0^L \frac{\partial \phi_m(x)}{\partial x} \frac{\partial \phi_n(x)}{\partial x} dx &= \frac{m\pi}{L} \frac{n\pi}{L} \int_0^L \cos\left(\frac{m\pi x}{L} \right) \cos\left(\frac{n\pi x}{L} \right) dx \\ &= \begin{cases} \frac{n^2\pi^2}{2L} & m = n \\ 0 & m \neq n \end{cases} \end{aligned} \tag{2.59}$$

leading to :

$$T_{dyn}(t) = \frac{ES\pi^2}{4L^2} \sum_{n=1}^{N} n^2 \left(q_n(t)\right)^2 \tag{2.60}$$

Calculating the integral in equation 2.58 :

$$\begin{aligned} \int_0^L \frac{\partial^2 \phi_n(x)}{\partial x^2} \phi_n(x) dx &= -\left(\frac{m\pi}{L}\right)^2 \int_0^L \sin\left(\frac{m\pi x}{L}\right) \sin\left(\frac{n\pi x}{L}\right) dx \\ &= \begin{cases} -\frac{n^2\pi^2}{2L} & m = n \\ 0 & m \neq n \end{cases} \end{aligned} \tag{2.61}$$

leading to :

$$F_n^{nl}(t) = -\frac{\pi^2}{2L} n^2 q_n(t) T_{dyn}(t) = -\frac{\pi^2}{2L} n^2 q_n(t) \left[\frac{ES\pi^2}{4L^2} \sum_{m=1}^{N} m^2 \left(q_m(t)\right)^2\right] \tag{2.62}$$

Hence, the cubic modal force terms are deduced [68] :

$$F_n^{nl} = \frac{ES\pi^4}{8L^3} n^2 q_n(t) \sum_{m=1}^{N} m^2 q_m(t)^2 \tag{2.63}$$

Finally, equation 2.63 is the expression of the modal non-linear forces for the string being pinned at its two extremities. Typically, in the case of the clavichord, the equation 2.63 is used to model the physical consequences of the string static displacement. It is shown in section 4.2.1 that this nonlinear modal formulation is entirely compatible with the quasi-steady geometrical formulation.

Model of string modal dampings

One of the interesting feature of the modal approach is the possibility to bestow to each mode a proper damping coefficient. These dampings can be estimated by means of vibratory measurements of the string vibrating freely. In the case where these dampings cannot be determined experimentally, it is possible to do it by means of a model. Thus, the presentation of a physical damping model is proposed in this section.

In the case of strings, the damping of the vibratory structure is low. By means of this assumption, an imaginary part is added to the expression of the modal frequencies to take account of dissipation. Damping occurs out of many phenomena, and these have been deeply studied by Valette and Cuesta [58]. One of the sources of dissipation is the effects of friction occurring inside the string when put into motion. These frictions take place because of the visco-elasticity and thermo-elasticity of the material. This source of damping is taken into account by the quality factor $Q_{n,ve-te}$ which is expressed in the following way :

$$Q_{n,ve-te}^{-1} = \frac{4\pi^2 \mu E I}{T^2} (f_n)^2 \delta_{ve-te} \tag{2.64}$$

where E is the Young modulus of the string, I is the second moment of inertia of the string, T is the string tension, μ is the linear density of the string, and δ_{ve-te} is the imaginary part of the string Young modulus [58]. The term $\delta_{ve-te} = \delta_{ve} + \delta_{te}$ encapsulates visco-elastic effects δ_{ve} and thermo-elastic ones δ_{te}, taking the same approach as Paté [65].

Moreover, at the microscopic level, the string represents a crystalline network. In the course of the string history, irregularities are formed within this network, which forms deformations at the macroscopic level. This effect is considered by means of the term Q_{struc} which is a constant value. Also, during its vibration, the string makes frictions because of the contact with the air, producing dissipation. It is possible to model these dampings by assuming that the air flow is stationary and that the fluid is perfect [58]. This viscous friction denoted by $Q_{n,air}$ is modeled as follows :

$$Q_{n,air}^{-1} = \frac{R}{2\pi\mu} (f_n)^{-1} \tag{2.65}$$

where R designates the mechanical resistance

$$R = 2\pi\eta_{air} + 2\pi d_s \sqrt{\pi \eta_{air} \rho_{air} f_n} \tag{2.66}$$

and where ρ_{air} and η_{air} corresponds to the dynamic viscosity and the density of the air respectively, and d_s represents the string diameter. Finally, it comes down to the string damping model :

$$Q_n^{-1} = Q_{n,air}^{-1} + Q_{n,ve-te}^{-1} + Q_{struc}^{-1} = \frac{R}{2\pi\mu} (f_n)^{-1} + \frac{4\pi^2 \mu E I \delta_{ve}}{T_0^2} (f_n)^2 + Q_{struc}^{-1} \tag{2.67}$$

Notice that $\zeta_n = \frac{1}{2} Q_n^{-1}$, where ζ_n is the damping coefficient of the n^{th} mode of the string. By means of equation 2.67 and by choosing the appropriate parameters, it is possible to model the dampings of the modelled string modes. The parameters can either be found in the literature [58], or it can be obtained by means of measurements. The latter approach is chosen in section 3.1.1.

2.4.2 Bridge modelling

The motion of the bridge is modelled by its modal equations. Considering the modal expansion of the bridge displacement :

$$Y^B(\mathbf{r},t) = \sum_{n=1}^{N_B} \phi_n^B(r) q_n^B(t) \tag{2.68}$$

where $\mathbf{r}$ is the location vector, N_B is the number of bridge modes, ϕ_n^B are the mode shapes of the bridge and q_n^B are the modal amplitudes of the bridge. Then, the modal equations governing the bridge vibratory motion are :

$$\boldsymbol{M}^B\ddot{\mathbf{q}}^B + \boldsymbol{C}^B\dot{\mathbf{q}}^B + \boldsymbol{K}^B\mathbf{q}^B = \mathbf{0} \tag{2.69}$$

where $\boldsymbol{M}^B$, $\boldsymbol{C}^B$ and $\boldsymbol{K}^B$ are the modal mass matrix, the modal damping matrix and the modal stiffness matrix of the bridge respectively, and $\mathbf{q}^B$ is the modal amplitude vector of the bridge. Because of the complexity of the structure, as opposed to the string, there is no continuous model that can yield analytically the expression of the bridge modal parameters. These could be derived numerically by means of finite element method by reproducing the geometry and the material properties of the bridge, as it was done for instance in the case of the piano [41]. Experimental modal analysis of the bridge is done in section 3.1.2 to give numerical values to the bridge modal parameters.

2.4.3 Key-tangent modelling

The tangent/key subsystem can be considered as a rigid rod which tilts with respect to a pivot. When the tangent strikes the string, the elastic string reacts and the whole system oscillates. The tangent has a mass M_{Tg}, the key has a mass M_k. The length of the key is L_T. The pivot of the key (balance point) is situated at a distance L_p of the back of the key, the finger presses the key at a distance L_f of the back of the key, and the tangent is located at a distance L_{tg} of the back of the key (see figure 2.3).

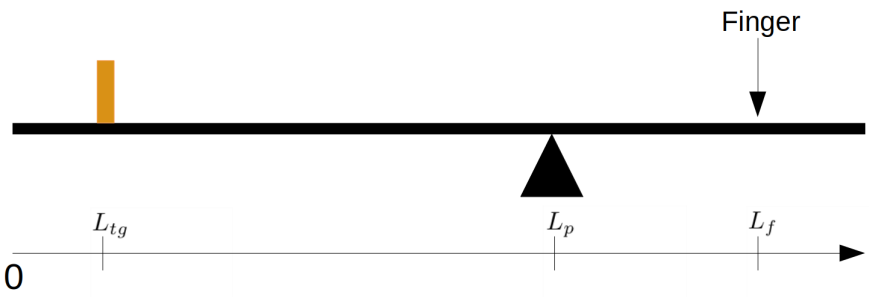

Figure 2.3: Stylised sketch of the key, indicating the distances L_{tg}, L_p and L_f.

A mode shape is associated to the key-tangent subsystem to model the tilting motion of the key. The modal representation of this system is given by the following equations :

$$Y^{Ta}(\mathbf{r},t) = \phi^{Ta}(x)q^{Ta}(t) \tag{2.70}$$

where Y^{Ta} is the displacement of the key-tangent substructure, ϕ^{Ta} is its mode shape and q^{Ta} is its modal amplitude, "Ta" standing for "tangent", and,

$$m^{Ta}\ddot{q}^{Ta}(t) + c^{Ta}\dot{q}^{Ta}(t) + k^{Ta}q^{Ta}(t) = F_{ext}(t) \tag{2.71}$$

where m^{Ta}, c^{Ta} and k^{Ta} are respectively the modal mass, modal damping and modal stiffness of the key-tangent subsystem, and F_{ext} is the modal excitation force that the musician exerts on the key. The mode shape of the tangent is reduced to a rigid-body mode corresponding to the motion of a key-lever. Thus, the mode shape ϕ^{Ta} is given in the following way :

$$\phi^{Ta}(x) = \frac{L_T - x}{L_T - L_p} - 1 \tag{2.72}$$

Considering that the linear density of the key is $\rho_k = \frac{M_k}{L_T}$, the modal mass of the key-tangent substructure m^{Ta} can be found thus :

$$m^{Ta} = M_{Tg}\phi^{Ta}(L_{tg})^2 + \int_0^{L_T} \rho_k \phi^{Ta}(x)^2 dx \tag{2.73}$$

After some calculations, it gives :

$$\begin{aligned} m^{Ta} = M_{Tg}&\left(\frac{L_T - L_{tg}}{L_T - L_p} - 1\right)^2 \\ &+ M_k \frac{3L_p^2 - 3L_pL_T + L_T^2}{3\left(L_T - L_p\right)^2} \end{aligned} \tag{2.74}$$

Contacts between the tangent and the string are, in general, intermittent. Furthermore, it is on this key-tangent substructure that the musician's excitation force is exerted, whose profile is described in section 3.1.5.

2.4.4 Damper modelling

The damper is modeled by coupling a portion of string with a number of mass-spring-dampers assuming a continuity of displacement between the dampers and the string at their contact points. All theses mass-spring-dampers are considered independent to one another. Let N_D is the chosen number of dampers D:

$$\boldsymbol{M}^D\ddot{\mathbf{q}}^D + \boldsymbol{C}^D\dot{\mathbf{q}}^D + \boldsymbol{K}^D\mathbf{q}^D = \mathbf{0} \tag{2.75}$$

Where $\mathbf{q}^D$ is the amplitude vector of the damper responses. Matrices $\mathbf{M}^D$, $\mathbf{C}^D$ and $\mathbf{K}^D$ are square diagonal with identical coefficients m^D, c^D and k^D, respectively.

All the mass-spring-dampers associated to the cloth damping device have the same mass, stiffness and damping coefficients. These mass-spring-dampers representing the cloth damper are coupled with a certain length of the string, as it is modeled in section 2.5.3.

2.5 Modelling of the couplings between the clavichord substructures

After presenting the modal representation of the different modelled substructures belonging to the clavichord, their couplings need to be tackled. After precising the coupling of all the different substructures, then it is possible to determine analytically the modal constraint matrix $\boldsymbol{A}$ and the vector $\mathbf{b}$ of the constrained system given by equation 2.37 :

$$\boldsymbol{A}\ddot{\mathbf{Q}} = \mathbf{b} \quad \text{with} \quad \boldsymbol{A} = \begin{bmatrix} \boldsymbol{A}_B \\ \boldsymbol{A}_{Ta} \\ \boldsymbol{A}_D \end{bmatrix}, \quad \mathbf{b} = \begin{bmatrix} \mathbf{b}_B \\ \mathbf{b}_{Ta} \\ \mathbf{b}_D \end{bmatrix}, \quad \ddot{\mathbf{Q}} = \begin{bmatrix} \ddot{\mathbf{q}}^S \\ \ddot{\mathbf{q}}^B \\ \ddot{\mathbf{q}}^{Ta} \\ \ddot{\mathbf{q}}^D \end{bmatrix} \tag{2.76}$$

where $\boldsymbol{A}_B$ is the matrix coupling the string with the bridge with $\mathbf{b}_B$ its associated vector, $\boldsymbol{A}_{Ta}$ is the matrix coupling the string with the key-tangent substructure with $\mathbf{b}_{Ta}$ its associated vector, and $\boldsymbol{A}_D$ is the matrix coupling the string with the damper with $\mathbf{b}_D$ its associated vector. Note that $\boldsymbol{A}_{Ta}$ is time-dependent, being nil when there is no contact between the tangent and the string. By giving the continuity conditions related to all these couplings, these matrices and vectors are determined in sections 2.5.1, 2.5.2 and 2.5.3.

2.5.1 String-Bridge coupling

The interaction of the string with the bridge is modeled by means of coupling. It is assumed that the displacement of the string is continuous with that of the bridge at the coupling location. Therefore, one can express the necessary coupling conditions to model the constraints of the system. This continuity implies that the string displacement $Y^S(x_B, t)$ must be the same as that of the bridge $Y^B(\mathbf{r}_B, t)$, "S" standing for "string" and "B" standing for "bridge", x_B is the location of the coupling point on the string and $\mathbf{r_B}$ is the vector of location of the coupling point on the bridge. Thus :

$$Y^S(x_B, t) - Y^B(\mathbf{r_B}, t) = 0 \tag{2.77}$$

with modal coordinates, it leads to :

$$[\Phi^S(x_B)]^T \mathbf{q}^S(t) - [\Phi^B(\mathbf{r_B})]^T \mathbf{q}^B(t) = 0 \tag{2.78}$$

with the mode shape vectors :

$$\begin{aligned} \Phi^S(x_B) &= [\phi_1^S(x_B)\phi_2^S(x_B)\dots\phi_{N_S}^S(x_B)]^T, \\ \Phi^B(\mathbf{r_B}) &= [\phi_1^B(\mathbf{r_B})\phi_2^B(\mathbf{r_B})\dots\phi_{N_B}^B(\mathbf{r_B})]^T \end{aligned} \tag{2.79}$$

where N_B is the number of bridge modes, N_S is the number of string modes. As a result, defining N_c as the number of strings of the system, equation 2.78 leads to the following matrix $\boldsymbol{A}_B$ and vector $\mathbf{b}_B$:

$$\boldsymbol{A}_B = \begin{bmatrix} [\Phi^{S_1}(x_B)]^T & \mathbf{0} & \dots & \mathbf{0} & -[\Phi^B(\mathbf{r_{B_1}})]^T & \mathbf{0} \\ \mathbf{0} & [\Phi^{S_2}(x_B)]^T & \dots & \mathbf{0} & -[\Phi^B(\mathbf{r_{B_2}})]^T & \mathbf{0} \\ \vdots & \vdots & \ddots & \vdots & \vdots & \vdots \\ \mathbf{0} & \mathbf{0} & \dots & [\Phi^{N_c}(x_B)]^T & -[\Phi^B(\mathbf{r_{B_{N_c}}})]^T & \mathbf{0} \end{bmatrix}, \quad \mathbf{b}_B = \begin{pmatrix} 0 \\ \vdots \\ 0 \end{pmatrix} \tag{2.80}$$

Equation 2.80 shows the coupling matrix $\boldsymbol{A}_B$ and the associated vector $\mathbf{b}_B$ used to couple the strings with the bridge.

2.5.2 String and key-tangent substructure coupling

To model the contact between the tangent and the string, the approach developed by Antunes et al [86] for modelling intermittent contacts in the framework of the U-K formulation is adopted. This contact is considered to be a coupling between the tangent and the string at the moment when the tangent touches the string. At the contact location, assuming a continuity of displacement between the two subsystems, this yields the following coupling condition :

$$Y^S(x_{ext}, t) - Y^{Ta}(\mathbf{r}_T, t) = 0 \tag{2.81}$$

which leads to :

$$[\mathbf{\Phi}^S(x_{ext})]^T \mathbf{q}^S(t) - [\mathbf{\Phi}^{Ta}(\mathbf{r}_T)]^T \mathbf{q}^{Ta}(t) = 0 \tag{2.82}$$

where Y^{Ta} is the displacement of the tangent, x_{ext} is the position where the string is excited, $\mathbf{r}_T$ is the location of contact on the tangent. The tangent is initially located below the string with respect to axis y. The whole string is initially at rest at altitude $y = 0$. At the moment when the tangent reaches altitude $y = 0$, $\boldsymbol{A}_{Ta}$ can be modified to couple the two subsystems. The contact is thus modeled by this coupling written within matrix $\boldsymbol{A}$ at this moment in time. Then, the conditions for this coupling are written as follow :

$$\begin{cases} Y^{Ta}(\mathbf{r}_T, t) < Y^S(x_{ext}, t) & \boldsymbol{A}_{Ta} = \mathbf{0} & \mathbf{b}_{Ta} = 0 \\ Y^{Ta}(\mathbf{r}_T, t) = Y^S(x_{ext}, t) & \boldsymbol{A}_{Ta} = \begin{bmatrix} [\mathbf{\Phi}^S(x_{ext})]^T & 0 \dots 0 & -[\mathbf{\Phi}^{Ta}(\mathbf{r}_T)]^T & 0 \dots 0 \end{bmatrix} & \mathbf{b}_{Ta} = 0 \end{cases} \tag{2.83}$$

where $\mathbf{\Phi_c^S}$ and $\mathbf{\Phi_c^{Ta}}$ represent respectively the string mode shape vector and that of the key-tangent substructure at the coupling point. Also, the U-K formulation apply constraints on the system acceleration. It means that, when simulating the model, the constraints on the system acceleration are met. However, respecting these constraints does not imply respecting the constraints on the system displacement and on the system velocity. Without the implementation of stabilization techniques, numerical drifts take place during the simulation, because of the constraint violation in terms of displacement and velocity. The technique elaborated by Yoon *et al* [87] can be used to eliminate the aforementioned violations. It is based on a geometric

projection approach applied after each time step. The displacement constraint violations are eliminated by reinforcing the constrained system displacement through local linearisation :

$$\mathbf{y}_c = \mathbf{y} + \Delta\mathbf{y} \quad \Rightarrow \quad \mathbf{y}_c = \mathbf{y} - \mathbf{A}\boldsymbol{\varphi}_{\boldsymbol{p}}(\mathbf{y}, t) \quad \Rightarrow \quad \mathbf{q}_c = \mathbf{q} - \boldsymbol{A}\boldsymbol{\varphi}_{\boldsymbol{p}}(\mathbf{q}, t) \tag{2.84}$$

Then, the same procedure is done when it comes to the velocity constraint violations :

$$\dot{\mathbf{y}}_c = \dot{\mathbf{y}} + \Delta\dot{\mathbf{y}} \quad \Rightarrow \quad \dot{\mathbf{y}}_c = \dot{\mathbf{y}} - \mathbf{A}\boldsymbol{\Psi}_{\boldsymbol{p}}(\mathbf{y}, \dot{\mathbf{y}}, t) \quad \Rightarrow \quad \dot{\mathbf{q}}_c = \dot{\mathbf{q}} - \boldsymbol{A}\boldsymbol{\Psi}_{\boldsymbol{p}}(\mathbf{q}, \dot{\mathbf{q}}, t) \tag{2.85}$$

where $\mathbf{y}_c$ and $\dot{\mathbf{y}}_c$ represent respectively the corrected displacements and velocity, $\Delta\mathbf{y}$ and $\Delta\dot{\mathbf{y}}$ represent respectively the correction of the displacement and that of the velocity, $\boldsymbol{\varphi}_{\boldsymbol{p}}(\mathbf{y}, t)$ and $\boldsymbol{\Psi}_{\boldsymbol{p}}(\dot{\mathbf{y}}, t)$ are respectively the displacement and velocity constraints.

2.5.3 String-Damper coupling

Like the string-bridge coupling, the continuity of the string displacement $Y^S(x_D, t)$ with that of the damper $Y^D(\mathbf{r}_s, t)$ is assumed, "D" standing for "damper", x_D being the location of the damper on the string and r_D being the vector locating the damper. Thus :

$$Y^S(x_D, t) - Y^D(\mathbf{r_D}, t) = 0 \tag{2.86}$$

which leads to :

$$[\Phi^S(x_D)]^T \mathbf{q}^S(t) - [\Phi^D(\mathbf{r_D})]^T \mathbf{q}^D(t) = 0 \tag{2.87}$$

Then, considering N_c strings in the system, equation 2.78 leads to the following matrix $\boldsymbol{A}_D$ and vector $\mathbf{b}_D$:

$$\boldsymbol{A}_D = \begin{bmatrix}
[\Phi^{S_1}(x_{D_1})]^T & 0 & \dots & 0 & -1 & 0 & \dots & 0 \\
[\Phi^{S_1}(x_{D_2})]^T & 0 & \dots & 0 & 0 & -1 & \dots & 0 \\
\vdots & \vdots & \vdots & \vdots & \vdots & \vdots & \ddots & \vdots \\
[\Phi^{S_1}(x_{D_{N_D}})]^T & 0 & \dots & 0 & 0 & 0 & \dots & -1 \\
[\Phi^{S_2}(x_{D_1})]^T & 0 & \dots & 0 & -1 & 0 & \dots & 0 \\
[\Phi^{S_2}(x_{D_2})]^T & 0 & \dots & 0 & 0 & -1 & \dots & 0 \\
\vdots & \vdots & \vdots & \vdots & \vdots & \vdots & \ddots & \vdots \\
[\Phi^{S_2}(x_{D_{N_D}})]^T & 0 & \dots & 0 & 0 & 0 & \dots & -1 \\
\vdots & \vdots & \vdots & \vdots & \vdots & \vdots & \vdots & \vdots \\
[\Phi^{S_{N_c}}(x_{D_1})]^T & 0 & \dots & 0 & -1 & 0 & \dots & 0 \\
[\Phi^{S_{N_c}}(x_{D_2})]^T & 0 & \dots & 0 & 0 & -1 & \dots & 0 \\
\vdots & \vdots & \vdots & \vdots & \vdots & \vdots & \ddots & \vdots \\
[\Phi^{S_{N_c}}(x_{D_{N_D}})]^T & 0 & \dots & 0 & 0 & 0 & \dots & -1
\end{bmatrix}, \quad \mathbf{b}_D = \begin{pmatrix} 0 \\ \vdots \\ 0 \end{pmatrix} \tag{2.88}$$

where $\Phi^{S_n}(\mathbf{r_{D_j}})$ is the mode shape of the n^{th} string coupled with the j^{th} damper at the $\mathbf{r_{D_j}}$ location.

2.6 Conclusion

The U-K formulation, which is used to model coupled mechanical systems, was presented. It was reformulated by introducing the modal representation of mechanical structures in order to apply this formulation to vibratory systems. The elegance of this formulation lies in the fact that all the couplings are modeled by means of a single constraint matrix equation. It comes in handy to model the vibratory coupled system, and also to model the excitation system by means of coupling. Then, this modal U-K formulation was used to model the clavichord, considering its vibratory substructures (string, bridge, key-tangent substructure, damper). After presenting the modal representation of each of these substructures, continuity conditions were given in order to find the expression of the system constraint matrix. In this context, an original nonlinear approach is introduced for modelling the dynamical string tension (and modal changes) due to the dynamic interaction between the tangent and the string. This approach is able to stipulate frequency glidings due to such interaction, as well as "vibrato" phenomena due to "aftertouch" interactions by the player. Finally, an effective approach was implemented for modelling the intermittent interaction between the tangent and the string. In chapter 3, This model of the clavichord is simulated by estimating numerical values of each substructure modal parameter, and testing the stability and convergence of the used numerical method.

Chapter 3

Simulation of the clavichord model

This chapter focuses on the elaboration of the simulation based on the model put forward in chapter 2. In section 3.1, the modal parameters for the different substructures are estimated : measurements of the strings' damping is done, complying the damping model presented in section 2.4.1 with the experimental results ; then, using experimental modal analysis, the modal parameters of the bridge at three specific locations are estimated. The values given to the key-tangent substructure modal parameters and that of the damper are *ad hoc*, so that the solution given by the simulation remains coherent. After defining a standard force profile applied to the key-tangent substructure in section 3.1.5, the stability and the convergence of the simulation is studied in section 3.3.

3.1 Parameters of the simulation

3.1.1 String modal dampings

It is possible to compute the string modal masses and modal stiffness analytically knowing the string mode shapes (using equation 2.33). String dampings, being part of the linear characteristics of the string, are obtained by means of the measurements of the string vibration without the influence of its coupling with the body. One of the hardships in the determination of strings' dampings is the elimination of the influence of the coupling with the body on them. To deal with this, the string is placed on a string bench with the same geometrical dimensions (see figure 3.1). This bench is a device which reduces the influence of coupling on the string vibration. Having tuned the string at the right frequency with the right length, the vibratory displacement of the string is measured at its other extremity by means of optical forks [88]. The excitation is controlled by means of a thin string of copper rolled up around the string diameter and whose break down always occurs at the same level of string uplift. To obtain the maximum of modes with a satisfactory signal-to-noise ratio, the string is plucked nearby one of its extremity and with respect to the vertical polarisation. As it is not possible to proceed to the measurement of all the strings of the clavichord, only a few of them have been chosen (the sympathetic part of the $G\#_3$ string, the sympathetic part of the $G\#_4$ string, the sympathetic part of the $C\#_5$ string). For each string, the vibratory measurement on the string bench is repeated 10 times. Then, here comes the question of the frequency band which is possible to analyse for each string set up on the bench. With respect to

the string length and its tuning frequency, its vibration is more or less damped, causing the high frequencies' energy to be too low for the analysis. In this case of study, for the sympathetic part of the C#$_5$ string (L = 23.6 cm, d_s = 0.28 mm, f_0 = 489.3 Hz), 9 partials are analysed, which gives a frequency band going from 489.3 Hz to 4431 Hz. For the sympathetic part of the G#$_4$ string (L = 24.8 cm, d_s = 0.30 mm, f_0 = 489.2 Hz), 11 partials are analysed, which gives a frequency band going from 489.2 Hz to 5434 Hz. Then, for the sympathetic part of the G#$_3$ string (L = 31.7 cm, d_s = 0.33 mm, f_0 = 396.9 Hz), 23 partials are analysed, which gives a frequency band going from 396.9 Hz to 9354 Hz. In fact, the larger the string length and the tuning frequency, the larger the frequency band. The strings used to extract these dampings are those made by Vogel (see figure 3.1).

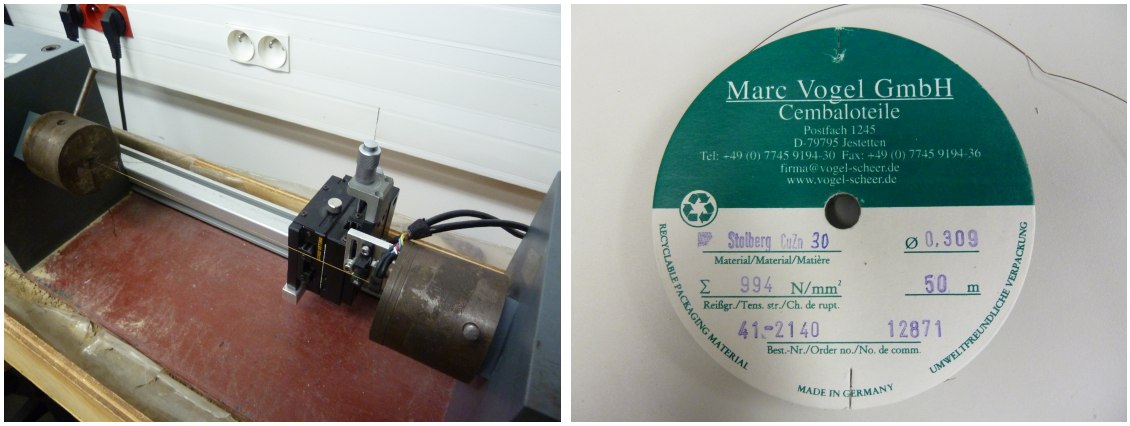

Figure 3.1: String bench used to measure the damping of the studied strings by means of optical forks (left), String made of copper and zinc by Vogel used to study the damping of the studied strings (right)

The measurements are analysed by means of a high-resolution algorithm called ESPRIT [89]. The portion of the signal processed starts at 0.5 s, so that the signal is analysed beyond the transitory phase. A duration of 2 s is taken for the analysis in order to avoid a low signal-to-noise ratio. To analyse with precision the dampings, all string modes are processed individually with respect to the following procedure [74, 65] : for all considered string modes, the algorithm centers its corresponding frequency to 0 Hz. Then, the signal is processed by a FIR (Finite Impulse Response) filtering centered at the same frequency before being decimated to reduce the time of the computation. Finally, an estimation of the number of components is done before applying the ESPRIT algorithm [74]. The analysis results give many frequencies instead of just yielding the mode frequency of interest. To select the right component, the proximity to the desired frequency and the highest level of energy of identified partials are chosen as means of criteria.

By using the Valette and Cuesta model (see section 2.4.1) with the same damping parameters, this model is matched with the measured dampings of the three strings. To do this, the following parameters are chosen for the model (see Table 3.2) :

where the value of E and ρ are consistent values for strings made of brass, and the value of η_{air} and ρ_{air} are taken from the literature [90]. The results are presented in figure 3.2. The maximum relative error that can be found between the measurements and the model is around 1.5 % for the G#$_4$ string. This relative error is lower for the two other strings. As for the dampings, in overall, the curve representative of the

ρ (kg.m^{-3})	E (Pa)	δ_{ve-te}	Q_{struc}	η_{air} (kg.m^{-1}.s^{-1})	ρ_{air} (kg.m^{-3})
7000	62×10^9	$1{,}5 \times 10^{-4}$	5×10^4	$1{,}8 \times 10^{-5}$	1,2

Table 3.1: String parameters used to simulate the string damping coefficients

model fit with the measured data, taking into account the computed error bars. The upper value of the computed relative error in terms of damping for the G#$_3$ string is 0.3 %, except for three values that go up to 0.55 %. As for the two other strings, the relative errors are below 0.3 %. The order of magnitude of the computed relative errors in terms of damping is similar to that found by Issanchou when measuring the dampings of an electric guitar string [91]. The quality factors found by Valette and Cuesta studying the dampings of harpsichord strings [58], which are similar to clavichord strings in terms of dimensions and materials, go from 2000 in low frequency up to 6000 in high frequency around 3000-4000 Hz. These values are similar to the quality factors found in figure 3.2. This shows the coherency of the measured damping in this study. This satisfying match between the model and the measurements leads to the possibility of transposing the value of the dampings for all the other strings of the clavichord. Furthermore, the damping model can be implemented to compute the mode dampings for other strings, those that have not been identified by the experimental approach.

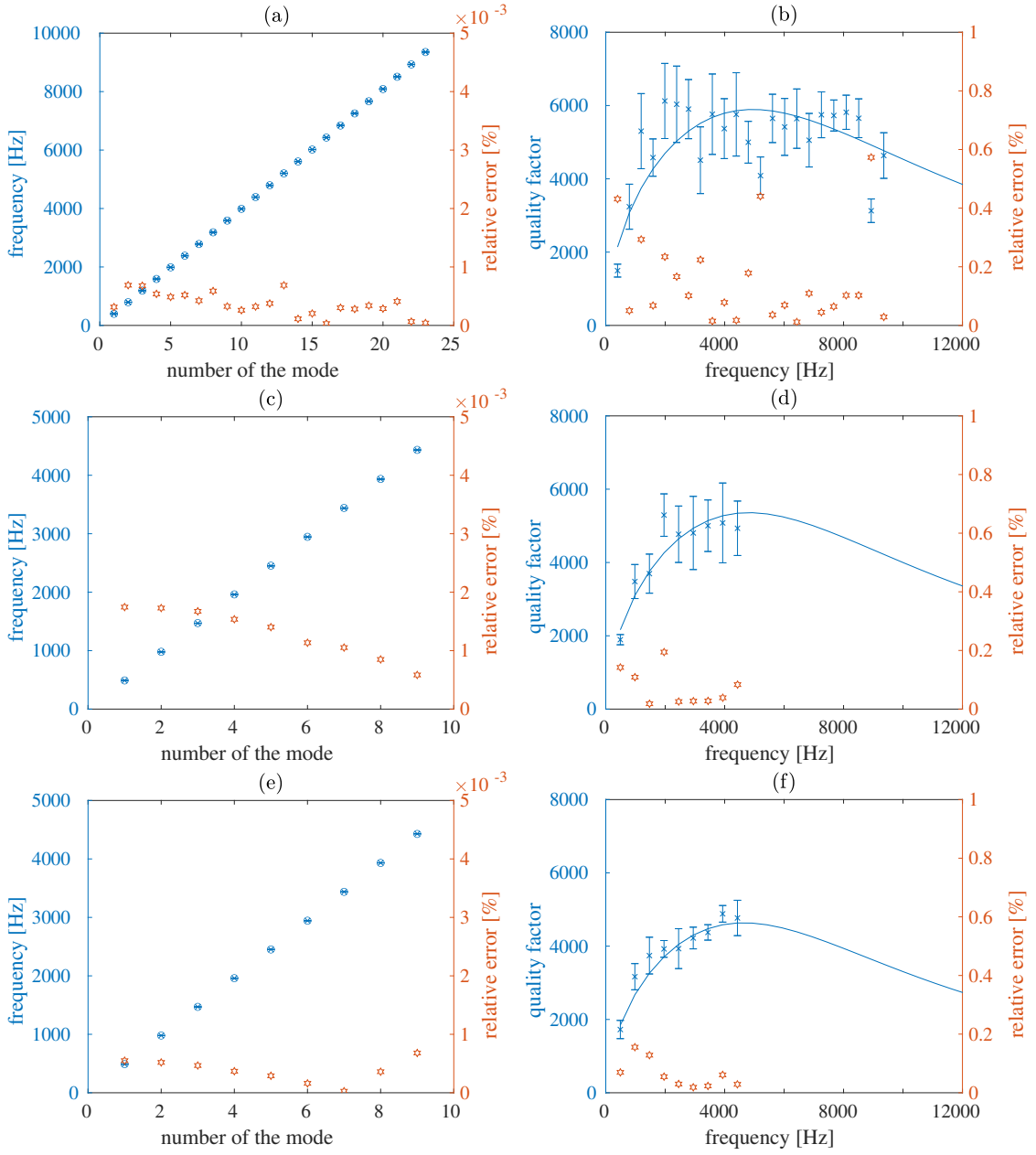

Figure 3.2: Sympathetic part of the isolated G#$_3$ string (a)-(b), sympathetic part of the isolated G#$_4$ string (c)-(d), sympathetic part of the isolated C#$_5$ string (e)-(f). Experimental (blue cross) and theoretical (blue circle) eigen frequencies, f_{exp} and f_{th} respectively, incertitude to 95 % on ten measurements (blue bar) and relative error $\epsilon_f = \frac{|f_{exp}-f_{th}|}{f_{exp}}$ (red star) (a, c and e), Experimental (blue cross) and theoretical (blue line) quality factor, Q_{exp} and Q_{th} respectively, incertitude to 95 % on ten measures (blue bar) and relative error $\epsilon_Q = \frac{|Q_{exp}-Q_{th}|}{Q_{exp}}$ (red star) (b, d and f).

3.1.2 Bridge modal parameters

To simulate the vibratory motion of the bridge, the modal parameters (mass matrix, stiffness matrix, damping matrix, mode shapes) of this subsystem need to be known. As no classical continuous model (like the beam) has a similar modal basis as that of the bridge, these modal parameters need to be extracted out of modal analysis. This could be done by means of finite element method, by reproducing numerically the modal behaviour of the bridge. However, to obtain modal parameters reproducing accurately the measured bridge FRF's (Frequency Response Function), the experimental modal analysis approach is chosen. It means that the FRF's at the interested coupling points are measured in order to identify by means of modal analysis algorithms the associated modes. Only the interested coupling points are considered in this experiment, even though the modal analysis of the whole bridge was done in another experiment (see annex C). In figure 3.3, the experimental setup for this measurement is presented. Measurements are done with an acquisition system with a sample rate of 51.2 kHz and a 24 bit depth. Impulses are given by an automatic impact hammer equipped with a force sensor PCB 086E80. It gives impacts beside the measurement point on the bridge. Three positions, denoted (1) (2) and (3), of the bridge are chosen : the coupling point between the bridge and the $G\#_3$ string (2), that of the F_3 string (3) and that of the D_4 string (1) (see figure 3.3 (a)). An accelerometer PCB M352C65 is used to measure the vibratory response of the bridge at these coupling points. It is placed on the hitch-pin that holds the string. It is assumed that the vertical vibration of the hitch-pin is the same as that of the bridge at this location in space, and the accelerometer measures the vertical acceleration of the hitch-pin. The number bestowed to each coupling point in this experimental modal analysis is pointed in figure 3.3. To measure only the FRF of the bridge at these different points, all the strings are damped by means of added felt damper.

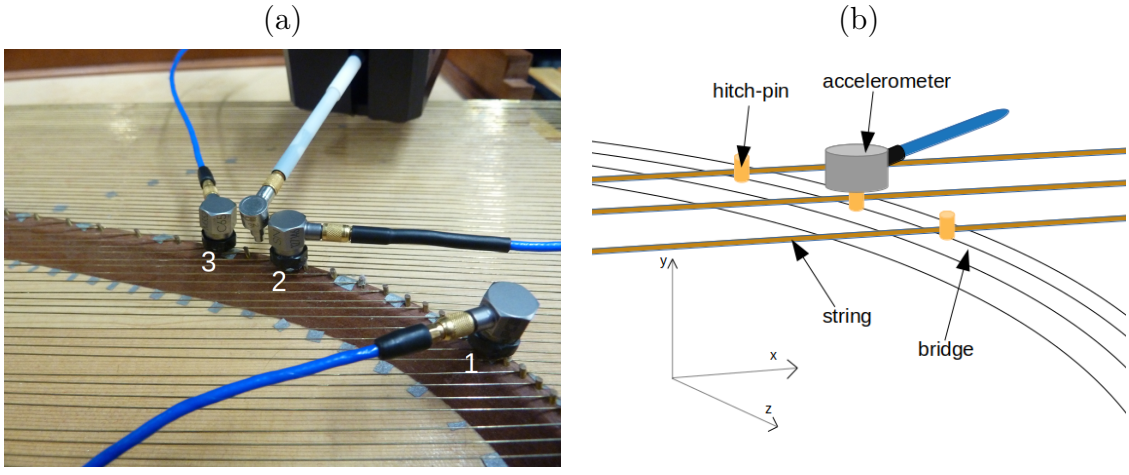

Figure 3.3: Experimental set up of the impulse response measurements at three coupling point with the bridge, the driving point (point n°2) located at the $G\#_3$ string-bridge coupling point, and the number of the measured point (a), diagram of the accelerometer put on the hitch-pin of the bridge with respect to the y axis (b).

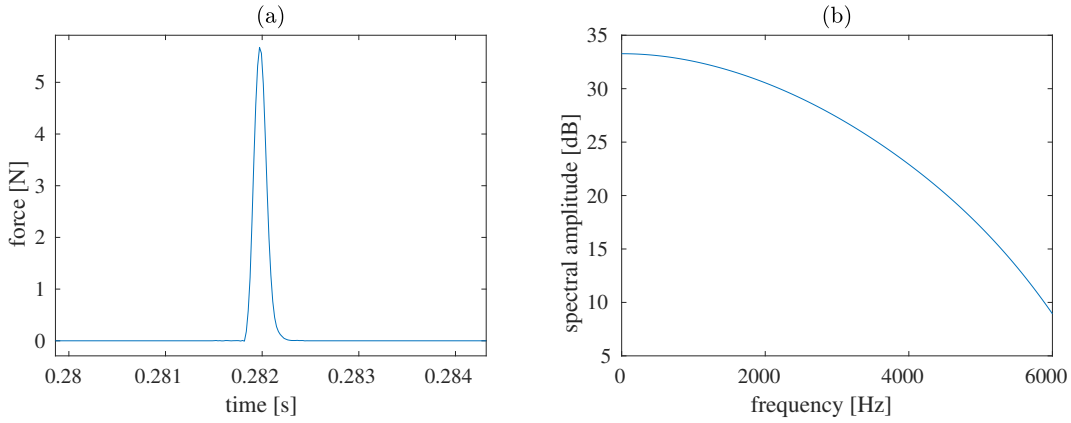

Figure 3.4: Temporal (a) and spectral signal (b) of the impulse force related to the driving point measurement of the FRF (ref 1dB : 1m.s^{-2}).

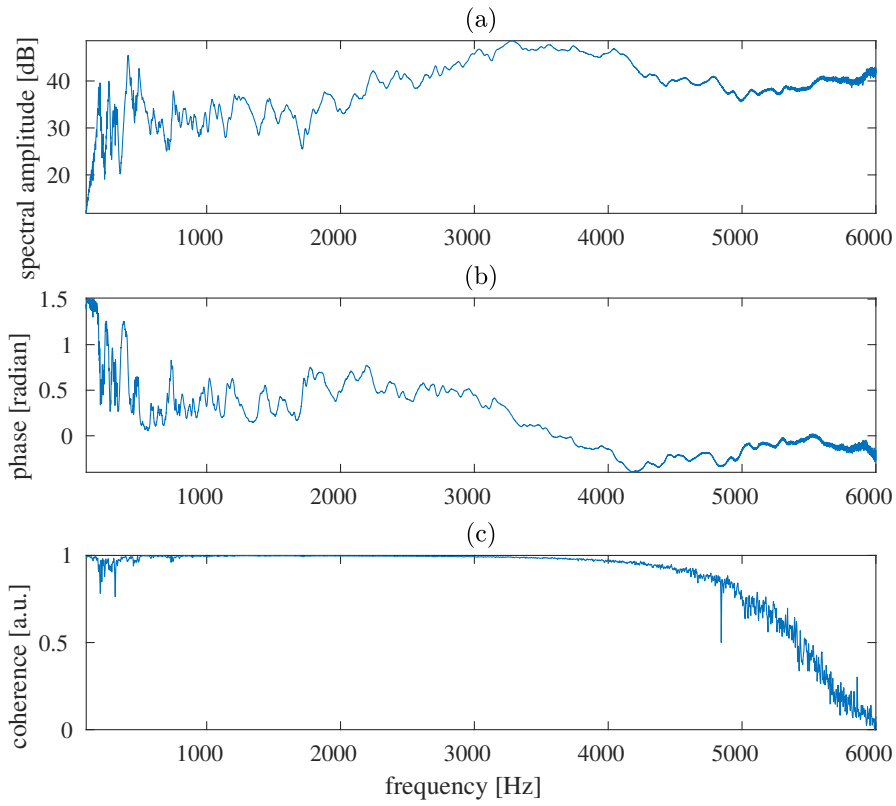

Figure 3.5: Driving point measurement of the FRF in terms of acceleration at the coupling point n°2 between the bridge and the G#$_3$ string : Spectral amplitude (Ref 1 dB : 1 m.s^{-2}.N^{-1}) (a), Unwrapped phase (b), Coherency (c).

In figure 3.4, the temporal and spectral profile of the impulse force is presented. In figure 3.5, the corresponding FRF along with its coherency are calculated. The coherency shows that the frequency band where there is energy goes up to approximately 5000 Hz.

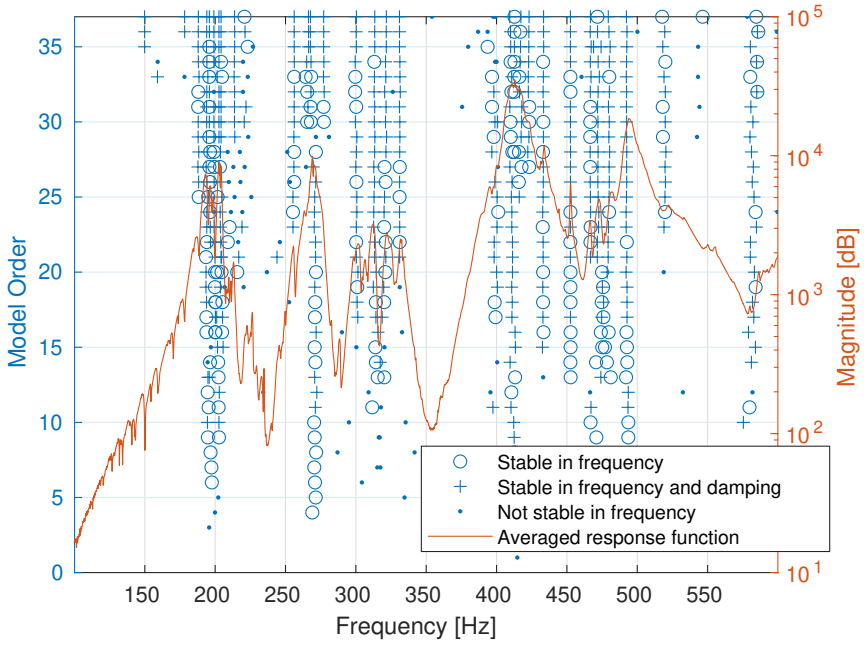

Figure 3.6: Stabilization diagram of the analysed FRF (Ref 1 dB : 1 m.s^{-2}.N^{-1}) of the G#$_3$ coupling point (point n°2).

There are two stages when it comes to proceeding with modal analysis. The first stage solution is the estimation of physical poles containing the modal frequencies and dampings of the analysed structure (see annex D). The LSRF (Least square rational function) estimation method is used, which is programmed in the Matlab signal processing toolbox [92]. To check the stability of the identified modes, a stabilization diagram is computed by means of the Matlab function *modalsd*. From this computation, only one stable pole for each modal order, that is modes having stable frequency and damping, are considered to be the physical poles of the analysed system (see figure 3.6).

The second stage solution is the estimation of residues which encapsulate the mode shapes and modal masses of the system (to see this estimation in detail, see annex D.3). The residues are assumed to be real. Therefore, the residues extracted are forced to be real using the non negative least-squares curve fitting solver described in [93] implemented in Matlab. It is decided that the modal masses are normalized as such : $m_n = 1$ kg, with the bridge mode $n = 1,2,...,N_B$. Out of this normalisation, the corresponding mode shapes are deduced from the residues. Considering that $\mathbf{B_n}$ represent the real residues :

$$\mathbf{B_n} = \frac{\phi_n \phi_n^T}{m_n} \tag{3.1}$$

With $m_n = 1$ kg, the real mode shapes are given by :

$$\phi_n = \frac{1}{\sqrt{B_{nj}}} \begin{pmatrix} B_{n1} \\ B_{n2} \\ \vdots \\ B_{nj} \\ \vdots \\ B_N \end{pmatrix} \tag{3.2}$$

In figure 3.7, the mode shapes located in the three studied coupling points are shown, and the measured FRF at the driven coupling point is compared with the reconstructed one by means of modal analysis. The mode shapes associated to the G#$_3$ string coupling point should outline the shape of its corresponding FRF's spectral amplitude, which is the case. Furthermore, the three different mode shapes indicate the difference in amplitude of the bridge mobility for the different modes between the three different coupling points. For instance, it can easily be seen that the bridge mobility at the F$_3$ string coupling point is higher than that at the D$_4$ string coupling point for the mode at 490 Hz. On the contrary, for the mode at 470 Hz, the bridge mobility at the D$_4$ string coupling point is higher than that at the F$_3$ string coupling point.

When it comes to the reconstruction of the FRF's G#$_3$ string coupling point, presented in figure 3.7, which is done by means of the extracted modal parameters, this reconstructed FRF seems satisfying. Since this satisfying reconstruction was done by means of real mode shapes, it means that the assumption that the residues are real is justified. It means that the identified modes are much more real than complex. Thus, the corresponding modal parameters can be used to simulate the dynamics of the bridge using U-K formulation. As a result, the poles and the modal masses of the system, as well as the mode shapes of the G#$_3$ string coupling point and that of the D$_4$ string and F$_3$ string, are obtained and can be used for the simulation.

Mode n	f_n (Hz)	ζ_n (%)
1	149.7	3.8
2	159.1	4.3
3	170.2	3.6
4	178.2	4.6
5	188.4	5.3
6	194.7	8.8
7	196.5	6.7
8	199.1	4.2
9	202.8	7.8
10	204.0	8.9
11	213.1	3.5
12	220.4	14.1
13	226.5	2.1
14	235.2	10.2
15	256.1	3.4
16	264.0	26.2
17	269.2	10.3
18	276.0	8.5
19	288.5	2.6
20	303.4	3.3
21	308.2	4.0
22	313.7	8.6
23	322.1	12.8
24	325.0	3.0
25	331.2	8.4
26	390.5	9.9
27	394.7	8.6
28	399.7	3.2
29	406.9	2.6
30	411.9	14.5
31	415.4	7.7
32	421.8	4.5
33	431.5	1.7
34	433.4	2.9
35	452.4	1.4
36	468.8	14.0
37	474.3	3.5
38	481.1	5.9
39	489.6	1.6
40	493.8	11.9
41	521.0	5.0
42	534.1	13.4
43	549.4	4.6
44	554.7	2.1
45	579.8	1.2
46	586.4	8.8
47	594.6	8.1

Table 3.2: String modal frequencies and modal dampings extracted by means of modal analysis

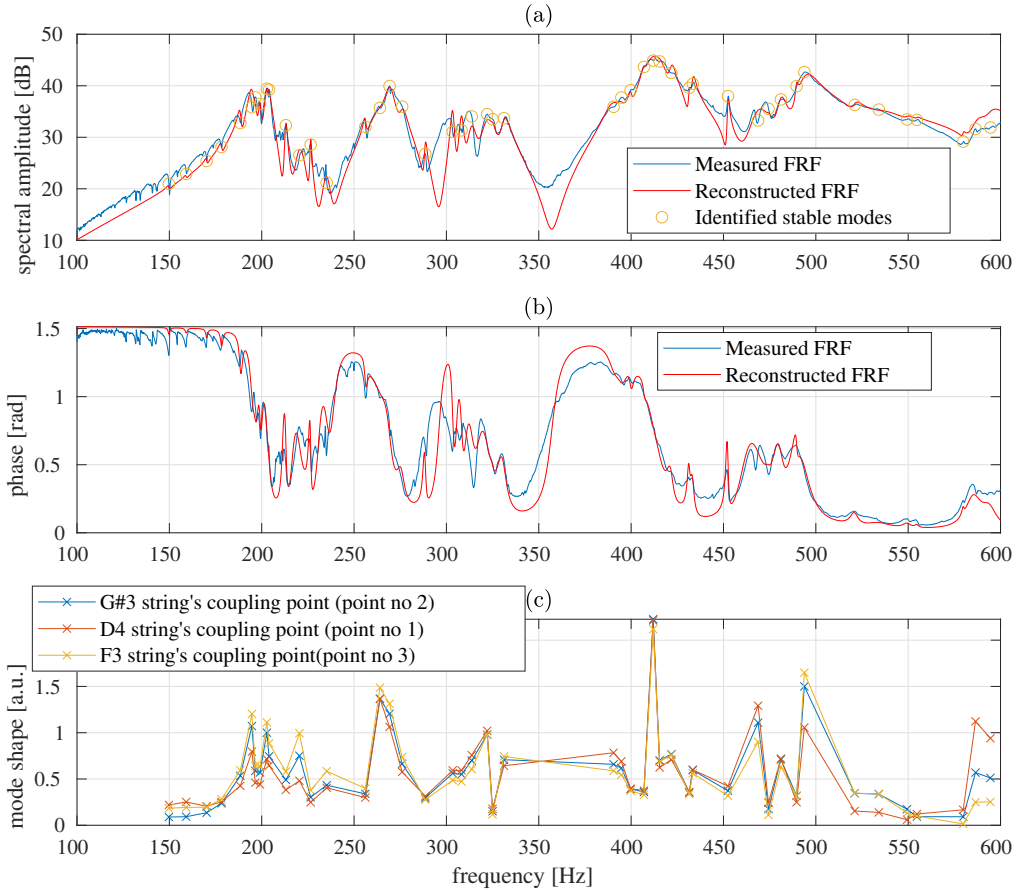

Figure 3.7: Comparison of the spectral amplitude (Ref 1 dB : 1 m.s^2.N^{-1}) of the measured FRF (blue line) with its reconstruction (red line) by means of modal analysis at the driving point (point n°2) coupling the bridge with the G#$_3$ string (a), Unwrapped phase of the measured FRF (blue line) and its reconstruction (red line) by means of modal analysis (b), Mode shapes extracted out of this modal analysis (c).

3.1.3 Modal parameters of the key-tangent substructure and the damper

To start with, the G#$_3$ string is modeled (see figure 2.1) to test the simulation and to verify the variation of tension, the stability, the modal convergence and the time convergence of the simulation. The three different parts of the string can be differentiated. First, between $x = 0$ m and $x = 0.2$ m, there lies the damped part of the string, where the damper is placed between $x = 3.4$ mm and $x = 13.7$ mm. Then, between $x = 0.2$ m and $x = 0.53$ m, this is the played part of the string. The rest of the string is its sympathetic part, which is beyond the coupling point with the bridge.

The dimensions of the key are $L_T = 28.9$ cm, $L_p = 17.2$ cm, $L_f = 27.9$ cm, $L_{tg} = 3.5$ cm, and $M_{Tg} = 5$ g, $M_k = 30$ g as for the mass of the tangent and the key respectively. The tilting mode of the G#$_3$ key equipped of its tangent is a rigid body mode. Then its frequency is $f_{Ta} = 0$ Hz. Its modal mass, determined in section

2.4.3, is $m_{Ta} = 1.17 \times 10^{-2}$ kg, its modal stiffness is $k^{Ta} = 4\pi^2 f_{Ta}^2 m^{Ta} = 0$ N.m^{-1} and its modal damping is $c^{Ta} = 2.5$ kg.s^{-1}. This damping coefficient is an *ad hoc* value chosen so that the simulation remains coherent.

The damper in the model is a series of 65 dash-pots. This number of dash-pots is chosen so that the string can be sufficiently damped when the key is released. The parameters c^D, m^D and k^D are chosen so that the damping effect exerted on the string once the key is released can be reproduced. Since the damper weighs a few grams, the value chosen for the modal mass is $m^D = 1.0 \times 10^{-2}$ kg. Considering that the mode of the damper is a body-mode, then $k^D = 0$ N.m^{-1}. Finally, to obtain sufficient damping, it is chosen that $c^D = 8.0 \times 10^2$ kg.s^{-1}.

3.1.4 Discretization of the equation of motion

To simulate the model put into light in chapter 2, a numerical scheme need to be chosen. A classical explicit scheme is used to discretize the equation of motion 2.36. It consists in discretizing the temporal derivatives of this equation. It comes down to obtaining the expression of the solution of the next time step $\mathbf{Q}^{n+1}$, with n being the time sample of the solution, with respect to that of the two preceding steps $\mathbf{Q}^n$ and $\mathbf{Q}^{n-1}$. This leads to the following discretization of the modal amplitudes' derivatives :

$$\dot{\mathbf{Q}} = \frac{\mathbf{Q}^n - \mathbf{Q}^{n-1}}{\Delta t} \tag{3.3}$$

and :

$$\ddot{\mathbf{Q}} = \frac{\mathbf{Q}^{n+1} - 2\mathbf{Q}^n + \mathbf{Q}^{n-1}}{\Delta t} \tag{3.4}$$

Where Δt is the time step of the temporal discretization. Then, the explicit scheme of equation 2.36 gives :

$$\begin{aligned}\mathbf{Q}^{n+1} &= 2\mathbf{Q}^n - \mathbf{Q}^{n-1} + \Delta t^2 \boldsymbol{M}^{-1/2}\boldsymbol{B}^+\mathbf{b} \\ &+ \Delta t^2 \left[\left(\boldsymbol{M}^{-1}\boldsymbol{M}^{-1/2}\boldsymbol{B}^+\boldsymbol{A}\boldsymbol{M}^{-1} \right) \left(-\boldsymbol{C}\frac{\mathbf{Q}^n - \mathbf{Q}^{n-1}}{\Delta t} - \boldsymbol{K}\mathbf{Q}^n + \boldsymbol{F}_{ext,n} - \boldsymbol{F}_{nl,n} \right) \right]\end{aligned} \tag{3.5}$$

To ensure the stability of the numerical scheme presented in equation 3.5, its stability condition can be derived (see annex E) [94] :

$$\Delta t \leq \frac{2}{\max(\mathrm{eig}(\boldsymbol{W}\boldsymbol{M}^{-1}\boldsymbol{K}))} \tag{3.6}$$

Then, according to equation 3.6, the time step should not be larger than a value depending on the matrices $\boldsymbol{W}$, $\boldsymbol{M}$ and $\boldsymbol{K}$. The term $\boldsymbol{M}^{-1}\boldsymbol{K}$ give the eigen pulsations. So the value of the denominator of equation 3.6 depends on the value of the largest pulsation of the vibratory coupled system. As a result, increasing the number of modes leads to reducing the time step compatible with the stability

condition. To give an example, with 100 string modes in the case of the modeled G#$_3$ string, the time step Δt cannot be larger than 2×10^{-5} s. Beyond this value, the simulation loses its stability. Even though this stability condition is respected, it does not guaranty the good quality of the solution. Indeed, a time step convergence is done in section 3.3.1 to find a reasonable time step which is not too small without affecting the convergence of the solution.

3.1.5 Force profile

To excite the G#$_3$ string, a force profile needs to be applied to the key-tangent substructure. It is decided that this profile with respect to time be in the form :

$$\begin{cases} F_{ext}(t) = \alpha t & \alpha > 0 & 0 < t < t_1 \\ F_{ext}(t) = \beta_1 & \beta_1 = t_1 \times \alpha_1 & t_1 < t < t_2 \\ F_{ext}(t) = -\alpha t + \beta_2 & \beta_2 = \frac{t_3}{t_3 - t_2}\beta_1 & t_2 < t < t_3 \\ F_{ext}(t) = 0 & & t_3 < t \end{cases} \tag{3.7}$$

This force profile is made of a steep slope at the beginning, and then it remains constant from the time t_1 up to time t_2. Note that this moment is before that the key-tangent substructure strikes the string. So the force profile remains constant when the contact between the key-tangent substructure and the tangent occurs. Then, this force decreases linearly from the time t_2 and goes to zero at time t_3. In figure 3.8, one can see a standard force profile used for the simulation, with $\alpha = 600$ N.s^{-1}, $t_1 = 0.01$ s, $t_2 = 1.0$ s, $t_3 = 1.01$ s. This force profile is similar to that used by the robotic finger as it is shown in annex F.

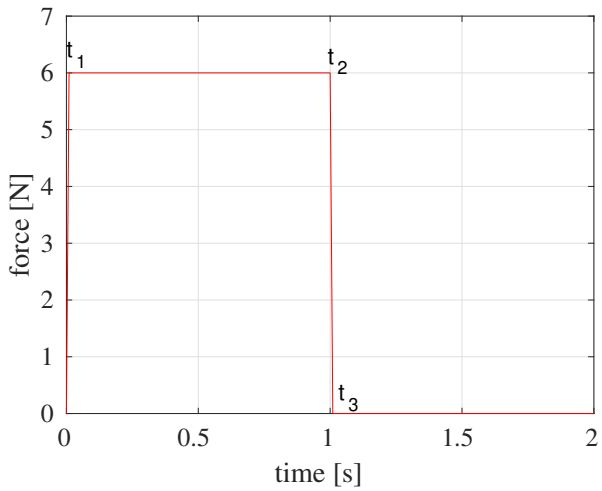

Figure 3.8: Force profile used for the simulation, with $\alpha = 600$ N.s^{-1}, $t_1 = 0.01$ s, $t_2 = 1.0$ s, $t_3 = 1.01$ s.

3.2 Observation at the contact point between the key-tangent substructure and the string

The correction of the constraint violation in terms of displacement and velocity given by equations 2.84 and 2.85 is implemented in the simulation. To verify the continuity of the displacement and the velocity at the contact point between the string and the key-tangent substructure, these are observed in figure 3.9 (a) and (b). One can see that the displacement and the velocity of the string and that of the tangent are superimposed after the impact, without observing any numerical drifts. One can see a little discontinuity of 0.02 $m.s^{-1}$ in the velocity at the moment of contact. That represents a 2.6% difference, which is quite low and it doesn't influence much the simulation. Then, the correction of these constraints are well implemented. Also, the acceleration at the contact point is observed in figure 3.9 (c). Once again, the continuity of the acceleration of the two substructures at the contact point is verified.

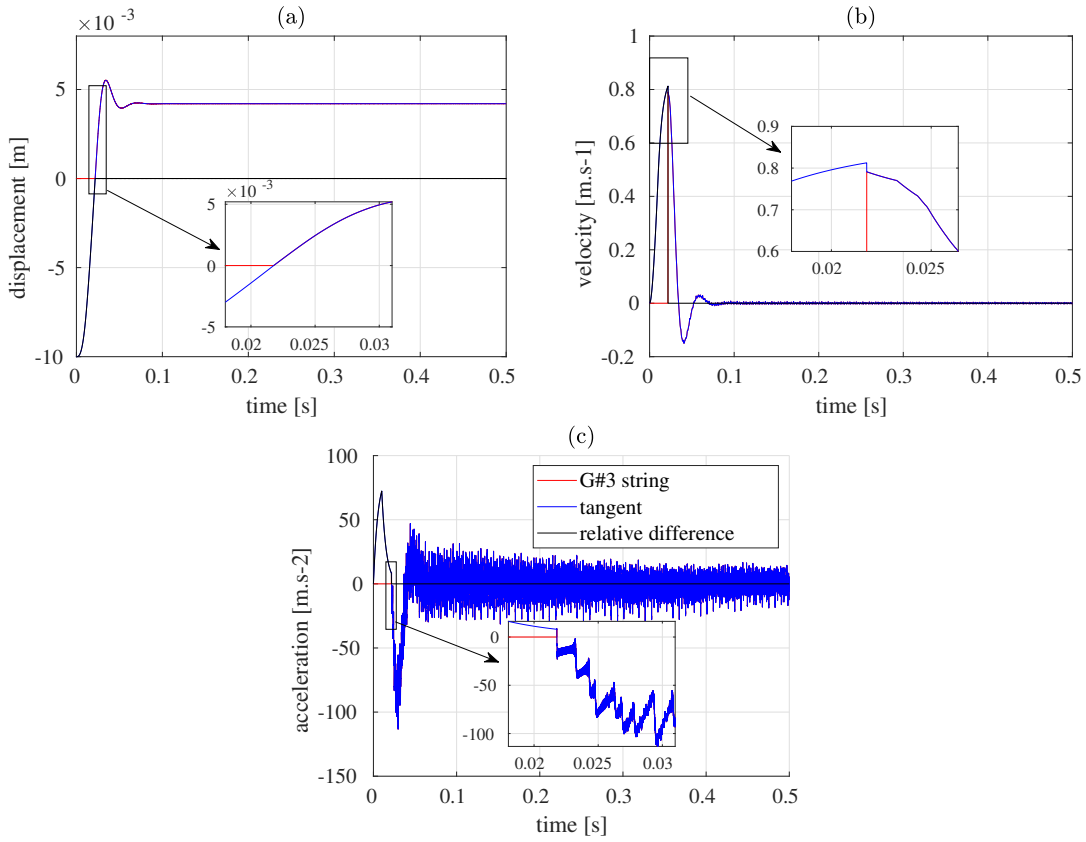

Figure 3.9: Displacement (a), velocity (b), and acceleration (c) of the tangent and of the string at the excitation point with respect to time.

Number of modes : m
10
20
30
40
50
60
70
80
90
100

Number of string modes : N_s
50
75
100
125
150
175
200

Time step : Δt (s)
$5\times\ 10^{-6}$
$4\times\ 10^{-6}$
$3.5\times\ 10^{-6}$
$3\times\ 10^{-6}$
$2\times\ 10^{-6}$
$7\times\ 10^{-7}$

Table 3.3: Tables of the variation of the different parameters chosen to proceed to the numerical study : the number of mode m related to equations 2.60 and 2.63, the number of string modes : N_s, and the time step : Δt.

3.3 Study of the simulation parameters

To verify that the simulation processed by means of the numerical method chosen in section 3.1.4 is stable and convergent, a numerical study of some of the simulation parameters needs to be done. The convergence of the series in equation 2.60 needs to be verified, by varying the number of string modes given by m from 10 to 100 modes. The influence of the string number of modes N_s on the results of the simulation is observed by varying N_s from 50 modes to 200 modes. Also, the influence of the time step Δt of the simulation is studied, by varying it from 5×10^{-6} s to 7×10^{-7} s. The different parameters chosen for this numerical study is shown in table 3.3.

3.3.1 Study of the time step

Study of the time step by means of the relative error of the string displacement and that of the contraint force

To discretize the differential equation of motion 2.27, a value for the time step Δt is chosen. First, this value is conditioned by the stability condition of the scheme, without which no solution is given by the simulation. Then, the time step gives the sampling frequency of the solution. According Shannon's sampling theorem :

$$f_{max} \leq \frac{1}{2\Delta t} \tag{3.8}$$

Where f_{max} is the frequency of the system mode having the highest frequency. If the condition given by equation 3.8 is not respected, then divergences occur. Also, the smaller the time step, the better the precision of the computation.

Let us choose $N_s = 100$ modes for the modeled string. Different time steps are taken to compute the successive relative errors of the solution in terms of string displacement and of constraint force applied to the point of contact between the string and the tangent. To compute their relative error, these solutions are resample so that they have the same sampling length. The relative error of the string

displacement is computed by means of $\epsilon_{\gamma_n}^{Y^S} = \frac{\sum_{i=0}^{N_T} |Y_{\gamma_n}^S(t_i) - Y_{\gamma_{n+1}}^S(t_i)|}{\sum_{i=0}^{N_T} |Y_{\gamma_{n+1}}^S(t_i)|}$, where $Y_{\gamma_n}^S(t_i)$ is the string displacement related to the current time step, $Y_{\gamma_{n+1}}^S(t_i)$ is the string displacement of the next time step, and $N_T = \frac{T}{\Delta t}$ with T the length of the signal. Analogically, the relative error of the constraint force at the tangent-string contact point is $\epsilon_{\gamma_n}^{F_c} = \frac{\sum_{i=0}^{N_T} |F_{c,\gamma_n}(t_i) - F_{c,\gamma_{n+1}}(t_i)|}{\sum_{i=0}^{N_T} |F_{c,\gamma_{n+1}}(t_i)|}$. For instance, in figure 3.10 (a), the data are presented in the following way : the data placed between 5×10^{-6} and 4×10^{-6} whose value is around 0.02 % is the relative error between the string displacements related to the two aforementioned times steps. The same way of reading the data is applied in figure (b) when it comes to the relative error of the constraining force F_c. Looking at figures 3.10 (a) and (b), it is shown that the solution converges with respect to the time step, whether in terms of displacement or of constraining force.

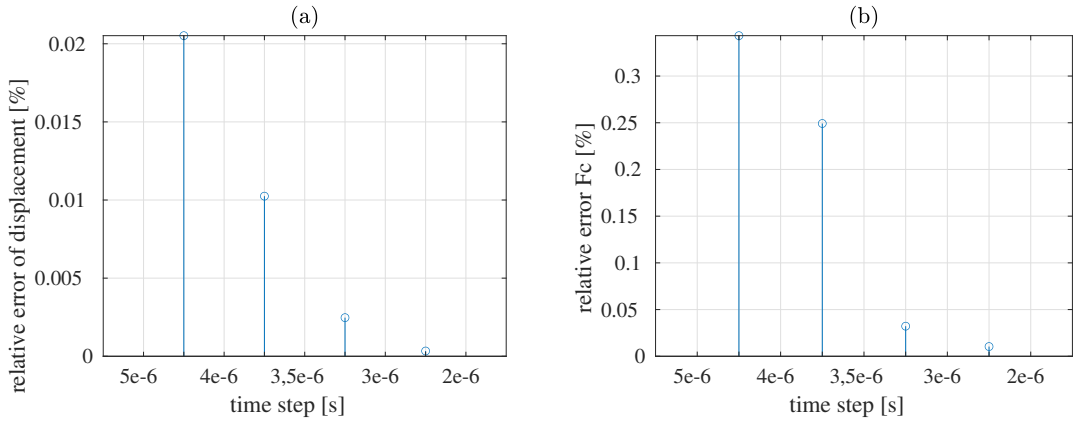

Figure 3.10: Relative error of the displacement at one point of the string and of the constraint force applied to the point of contact between the string and the tangent with respect to the time step.

Study of the time step by means of an energy analysis of the system

Also, to assure the quality of the computation, it is possible to evaluate it by means of an energy analysis. The objective here is to conduct an energy analysis of the simulation to assure that the solution provided by it (displacement, velocity and acceleration of the system and its constraining forces) is improved when decreasing the time step. By definition, the energy given to a mechanical system at rest initially must be equal to the sum of the energies of its subsystems. The energy provided to the system is the work $E_e = \sum_{n=1}^{N} E_{e,n}$ done by the tangent, with the modal work $E_{e,n}$:

$$E_{e,n}(t) = \int_0^T F_{ext,n}(\mathbf{r}_T, t) \dot{q}_n^{Ta}(t) dt \tag{3.9}$$

The sum of all modes' energy of the string, of the system tangent-key, of the damper and of the bridge gives the total energy of the modeled system (for the detail of the energy analysis and the computation, see annex G). In figure 3.11, the work done by the key-tangent substructure is computed as well as the total energy of the coupled system for different time steps. One can see that when the time step goes down, the total energy curve becomes closer to that of the key-tangent substructure work. This shows the degree of accuracy of the computation depending on the value of the time step. As a result, choosing a small time step improves the equivalence between the system mechanical energy and the work provided by the excitation system. Furthermore, the sampling frequency associated to this time step is $F_s = \frac{1}{\Delta t} = 500000$ Hz, so the associated Nyquist frequency is 250000 Hz. Since the frequency of the modeled G$\#_3$ string is 392 Hz, the frequency of the 200^{th} string mode is 78400 Hz. Then, this maximum frequency do not go beyond the Nyquist frequency which means that Shannon theorem is respected. So up to 200 string modes, there is no risk of divergence because of aliasing. As a result of the energy analysis, one can see that the quality of the simulation is improved by decreasing the time step. Thanks to this analysis, a reasonable time step can be chosen to ensure the quality of the simulation. In accordance with figure 3.11, the time step chosen for the following simulations is $\Delta t = 2 \times 10^{-6}$, which is a good compromise between the accuracy of the computation and its duration.

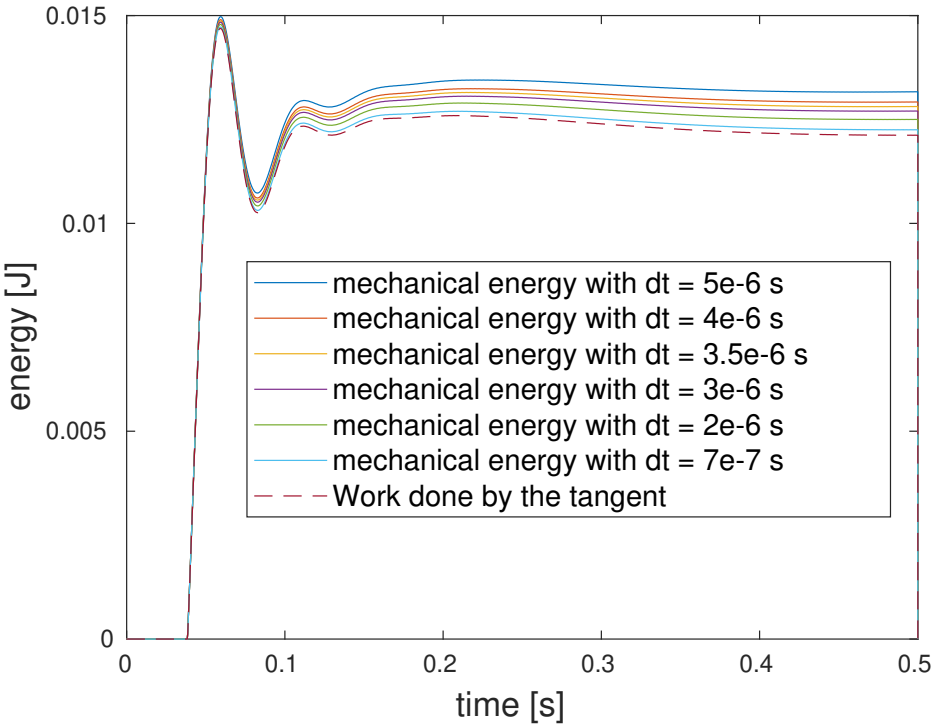

Figure 3.11: Convergence of the total mechanical energy of the system compared to the work done by the tangent.

3.3.2 Study of the number of string modes

The convergence of the solution with respect to the number of modes chosen needs to be evaluated. The relative error of the G#$_3$ string displacement is $\epsilon_n^{Y^S} = \frac{\sum_{i=0}^{N_T} |Y^S_{N_n}(t_i) - Y^S_{N_{n-1}}(t_i)|}{\sum_{i=0}^{N_T} |Y^S_{N_{n-1}}(t_i)|}$, and that of the constraint force at the tangent-string contact point is $\epsilon_n^{F_c} = \frac{\sum_{i=0}^{N_T} |F_{c,N_n}(t_i) - F_{c,N_{n-1}}(t_i)|}{\sum_{i=0}^{N_T} |F_{c,N_{n-1}}(t_i)|}$. First, the convergence of the series within equation 2.60 expressing the dynamic tension T_{dyn} can be evaluated. With $n = 100$ modes, the number of mode m is varied from 10 to 100 modes, and the impact on the string displacement and on the constraint force at string-tangent contact location is observed. Figure 3.12 shows the successive relative errors obtained for these physical terms. The relative error dwindles with respect to the number of modes m. Thereby the series within equation 2.60 converges and leads to the convergence of the solution. Next, the convergence of the solution with respect to the number of string modes N_s needs to be checked. Figure 3.13 shows that the relative error converges with respect to the number of string modes, whether it is in terms of string displacement or in terms of coupling force.

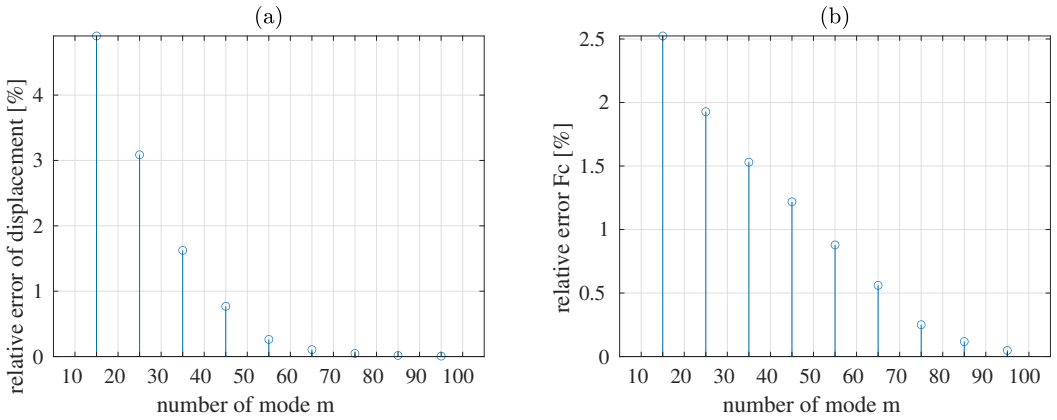

Figure 3.12: Relative error of the displacement at one point of the string (a) and of the constraint force applied to the point of contact between the string and the tangent (b) with respect to the number of modes m, with $\Delta t = 2 \times 10^{-6}$ s for all the simulations.

If the relatives errors of the string displacement and that of the coupling force at the tangent-string contact point decrease with respect to the number of string modes N_s, then increasing this number leads the solution given by the simulation to converge. Since the relative error is less than 2% for the displacement and the coupling force when $N_s = 100$ modes, this number of string modes seems reasonable to be chosen for the following simulations.

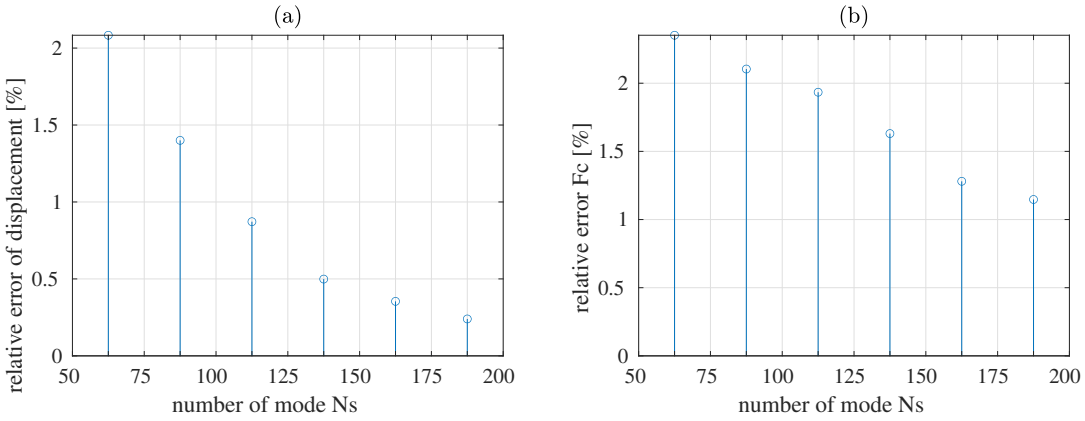

Figure 3.13: Relative error of the displacement at one point of the string (a) and of the constraint force applied to the point of contact between the string and the tangent (b) with respect to the number of string modes N_s, with $\Delta t = 2 \times 10^{-6}$ s for all the simulations.

3.4 Simulation of the model

Assessment of the model is performed in 2 steps: 1/ visualisation of string motion; 2/ visualisation of subsystems vibrations and comparison with experimental data.

3.4.1 String motion

The string motion of the clavichord is shaped by the specific excitation mechanism of the instrument. Time domain simulation of the system allows for visualisation of the string motion. Simulation of the G#$_3$ string motion is displayed in figure 3.14, in response to a 6 N excitation force. The top panel represents the initial 35 ms, i.e. the beginning of the motion. The tangent (represented by circles at $x = 0.6$ m, sampled with a period of 0.1 ms) comes in contact with the string and lifts the string to a maximum. When the tangent strikes the string, an angular point is created and propagates to the bridge. At the same time, the string is uplifted by the tangent. After the arrival of the angular point at the bridge, it is reflected back and then reflected again by the tangent. As the mechanical impedance of the bridge and that of the tangent are high compared to the string mechanical impedance, most of the wave energy is reflected. The vibratory amplitude (then the sound amplitude level) depends on the angle of the angular point, and then on the ratio of wave velocity in the string and tangent velocity, as discussed in [3], and then on the steepness of the tangent motion slope. In the middle panel of figure 3.14 the string motion history is displayed between 35 and 200 ms (sampled with a period of 1 ms). The low frequency (62.5 Hz) oscillation of the key-tangent subsystem because of the elasticity of the string is observed. Bottom panel of figure 3.14 shows vibration by sympathy of the part of string between the bridge and tuning pin, corresponding to the circle in the middle panel, between 35 and 200 ms (sampled with a period of 1 ms). Note that the sympathetic vibration is two order of magnitude lower than the played part of the string, between 10^{-5} - 10^{-6} m, and that the string motion looks rather disorganized compared to more regular motion between the tangent and bridge pin. No direct measurement of the whole string motion are available to the best of our knowledge. Comparison with high-speed videos of the string motion

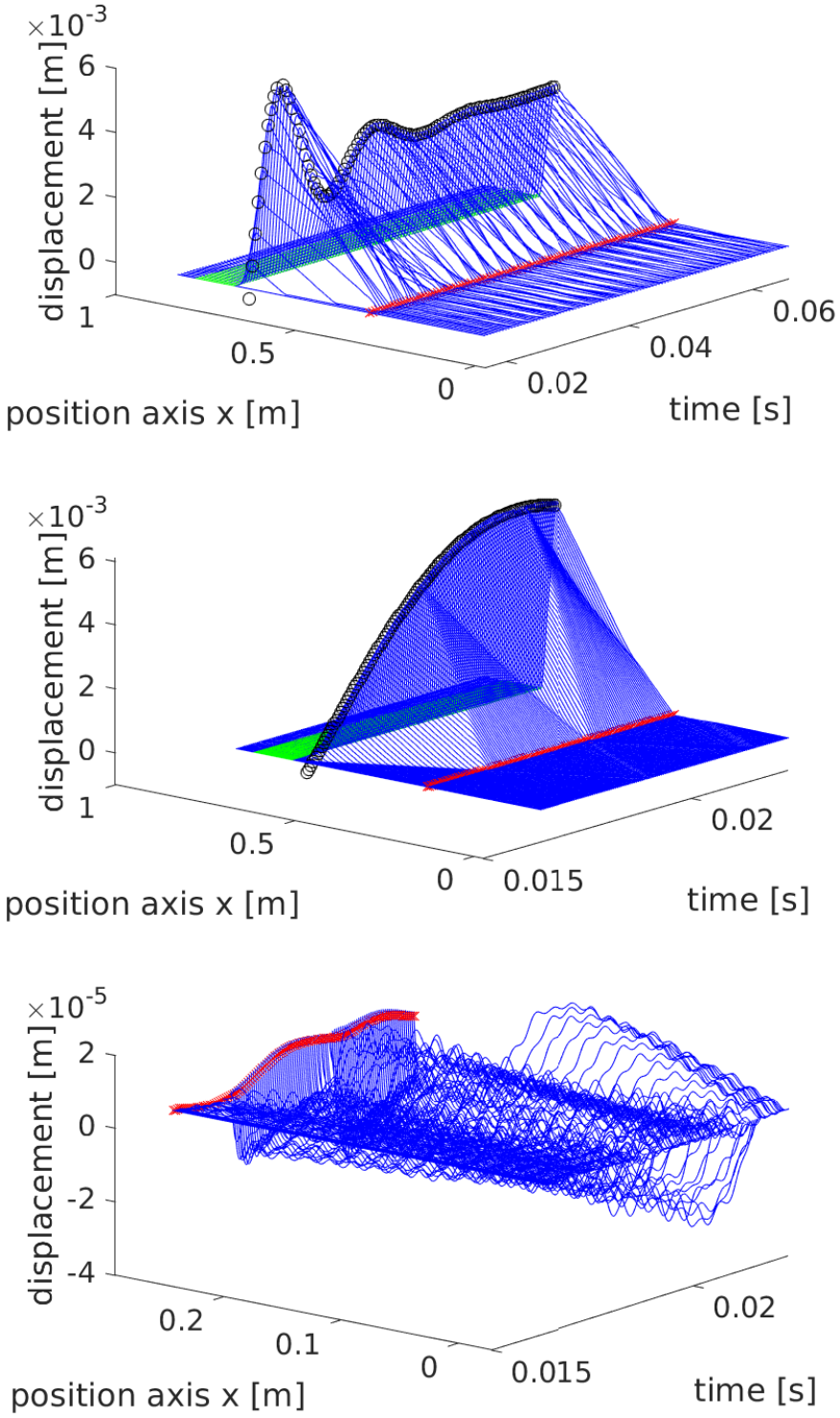

Figure 3.14: History of the transverse motion for the G#3 string.x axis: time (s); y axis : string length; z axis: transverse string motion. Top panel: full string between $t = 0.0164$ s and $t = 0.0759$ s . Middle panel: full string between $t = 0.0164$ s and $t = 0.0224$ s. bottom panel: sympathetic part alone, between $t = 0.0164$ s and $t = 0.0224$ s.

in the vicinity of the tangent[1] show good agreement with the simulation : the same "zipper" motion of the angular point on the string can be observed in high-speed videos and figure 3.14.

3.4.2 Bridge motion

The bridge is a key point in sound production, because it moves the soundboard, and then produces the sounds. For assessment of the model, simulated and measured bridge motions are compared. The acceleration at the bridge pin for the string is measured using the same PCB M352C65 accelerometer and the same acquisition system as in section 3.1.2. For this measurement, all the other strings are muffled using felt strips. Measured and simulated signals oscillograms and spectrograms are displayed in Figure 3.15. The results are on the whole comparable. The main difference between the two signals is the damping, where that of the simulated signal is too high. The damping of the simulated signal can still be improved to obtain a better result. Another difference between the two signals is in the attack transition. The real acceleration exhibits a sharper attack transient. This could be explained by the "drum noise" that is present in a real clavichord but not in the model. The drum noise is the structural noise due to the shock of the tangent on the string, that excites all the body (structure) of the instrument. This is a well known effect, not simulated here, the string being isolated from the structure. Otherwise, the essential features of simulation and measurement are very similar, and the orders of magnitude of these accelerations are the same.

The forces applied to the key and the response at the bridge are analyzed with the help of figure 3.16. A step force of 6 N is applied on the key for 1 s (see figure 3.16 (c)). The constraint force at the contact point between the tangent and strings is computed. Note that the tangent force is lower than the force applied to the key, because of the leverage ratio on the pivoting key (since $L_f - L_p$ is smaller than $L_p - L_{tg}$). Two conditions are studied in the simulation with and without damper. The middle panel shows the simulated force at the bridge. As expected, the force is lowered during the tone, because the tangent lifts the string, and then releases the string pressure on the bridge. When dampers are removed, the string appears less constrained, and the force at the bride is higher. String vibration is apparent in the force signal. The top panel shows the vibration displacement. As expected, the string is raised in response to the tangent lift, and raised higher when the dampers are withdrawn. The vibratory magnitude is surprisingly low (a maximum of about 0.015 mm). Displacement measurements were subsequently performed on the $G\#_3$ string using a Keyence (LJ-V7060) profilometer. As this device is not meant to measure vibratory signals, only the order of magnitude of the bridge motion can be evaluated. The same order of magnitude were observed : a bridge lift of 0.010-0.020 mm and a maximal vibratory amplitude of about 0.010-0.015 mm, in good agreement with the simulated motions (see figure 3.17). After the key release, the tangent loses contact with the string. The remaining vibration after the key release corresponds to the sympathetic vibration between the bridge and tuning pin, and in the non-damped situation to the vibration of all the length of the string. In this latter situation, the magnitude is larger.

[1] see https://www.musimediane.com/7dalessandro/ [Retrieved: 2021-02-11]

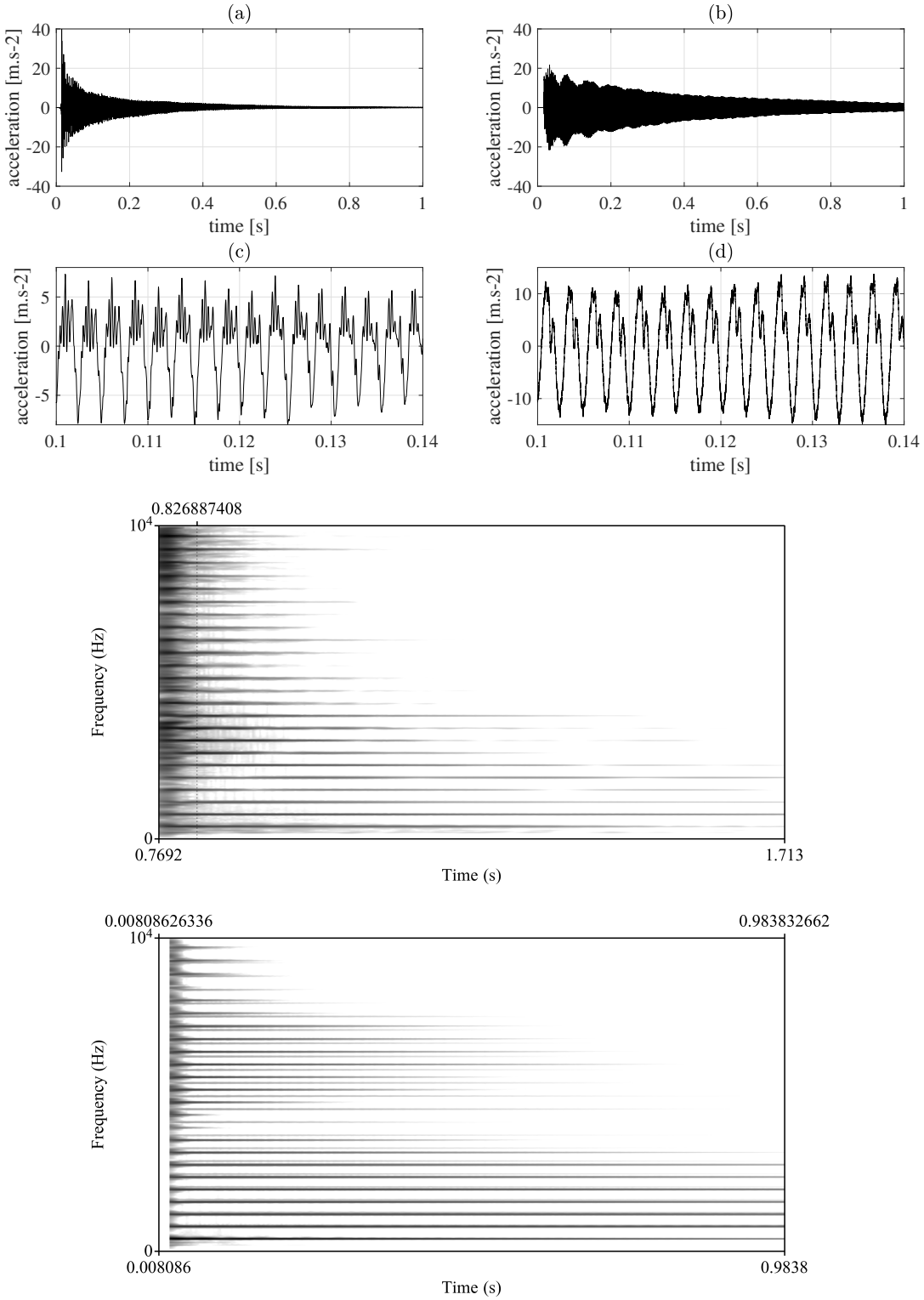

Figure 3.15: Comparison of simulated and measured acceleration at the bridge. Oscillogram for 1s of the measurement (a) and of the simulation (b). Zoom on a 40 ms section of the measurement (c) and of the simulation (d). Spectrograms of the measured signal (Top) and of the simulated signal (Bottom).

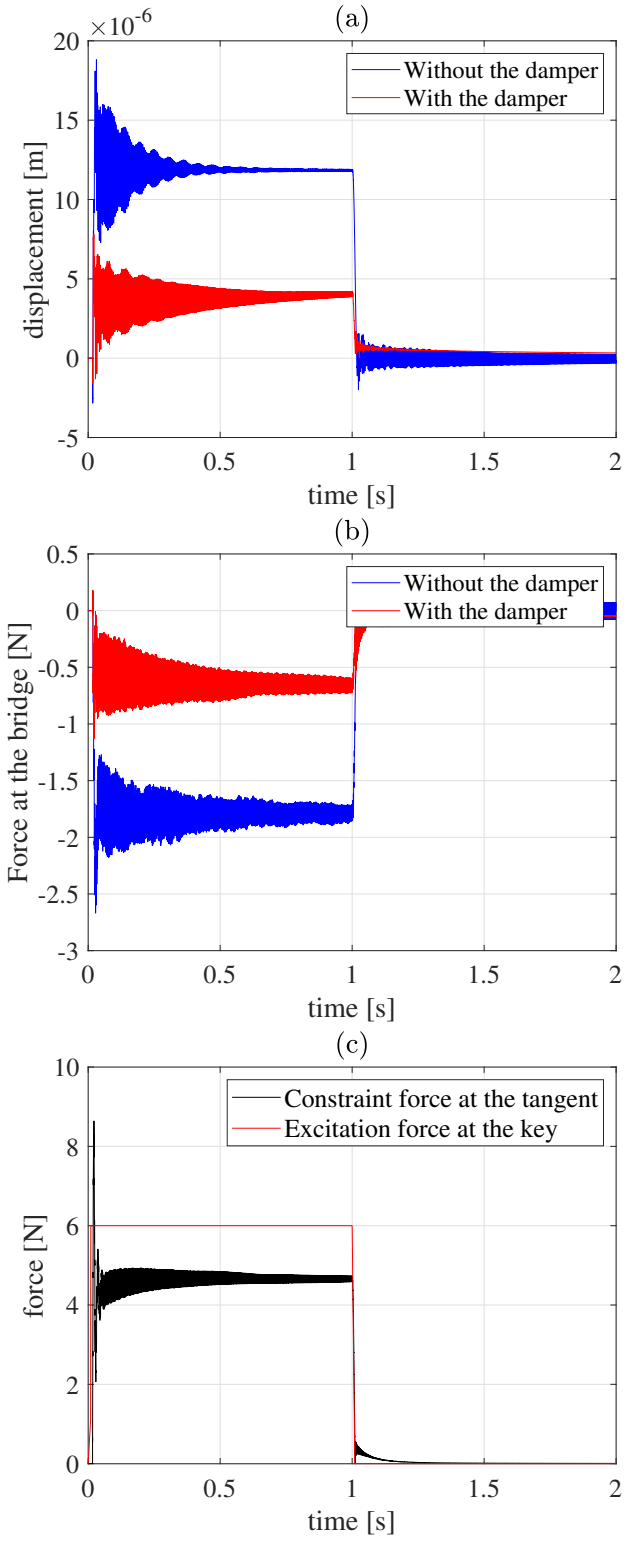

Figure 3.16: Bridge displacement with (red) and without (blue) dampers (a), Force on the bridge with (red) and without (blue) dampers (b), Force applied on the key and resulting force on the tangent (c).

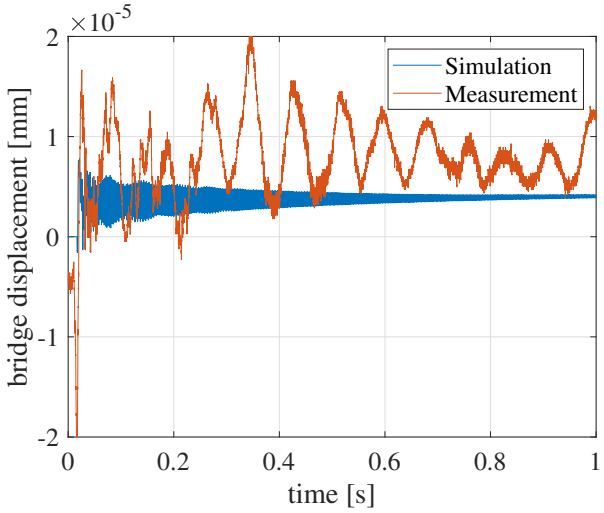

Figure 3.17: Displacement of the bridge at the G#$_3$ string coupling point, measured and simulated.

3.5 Pair of strings

In the case of the clavichord, a pair of strings are struck by the tangent to produce a note. According to Weinreich [21], because of the frequency near-coincidence of the two string fundamental frequencies and the coupling with the bridge, the resulting vibration shows the two-part slope process. This phenomenon must be retrieved by the simulation when coupling two excited strings tuned to the same frequency. Two identical G#$_3$ strings are modeled, tuned to the same frequency and coupled in the same way to the same coupling point (see figure 3.18). The tangent strikes the two strings at the same time and at the same location. The results of this simulation can be compared when simulating only the first of the two G#$_3$ strings. It is possible to verify that the constrained force is the same at the static phase whether striking one string or two strings with the same exciting force. Since the two strings are the same and their excitation is done at the same time and at the same location, an equal distribution of the constrained force between the strings and the tangent is expected once the system becomes static. Figure 3.19 shows the constrained forces between the two cases. Before time 0.5 s, this is where the dynamic phase of the system takes place, in which an oscillation of the constrained force with respect to time can be observed. One can see that the amplitude of this force oscillation is higher in the two strings' case than in the one string case. This is consistent with Bavington's study which shows that when the finger is in contact with the key, the force felt by the musician is higher in the two strings' case than in the one string case at the moment of contact [95]. From 0.5 s onward, the equality of the constrained forces between the two cases can be observed, which is approximately the moment when the static phase is reached. That result is consistent with the aforementioned expectation.

In figure 3.20, the acceleration at the G#$_3$ strings' coupling point is shown when striking the first of these strings only and when striking the two strings. By means of comparison, the two-part slope process is noticeable when striking the two strings as oppose to the case when striking only one string. This two-part slope process is the same phenomenon that is described in Weinreich study [21], when coupling two

identical piano strings to the same coupling point. Therefore, this effect observed in the simulation when coupling two identical strings to the same coupling point is plausible.

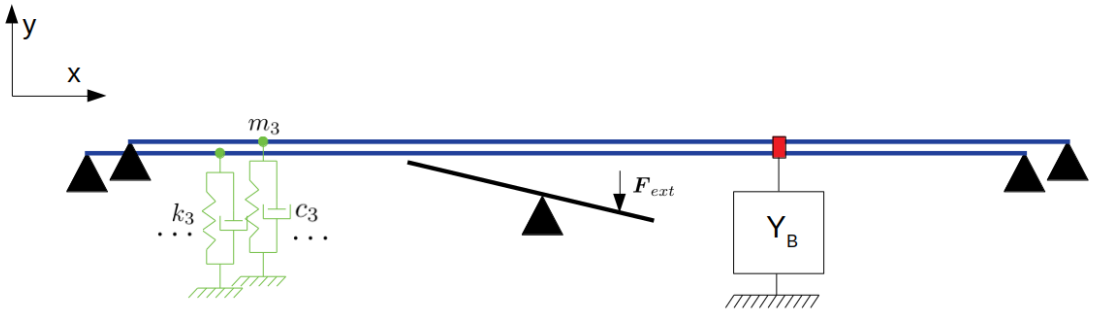

Figure 3.18: Sketch of the modelling of the pair of strings being excited by the same tangent at the same time.

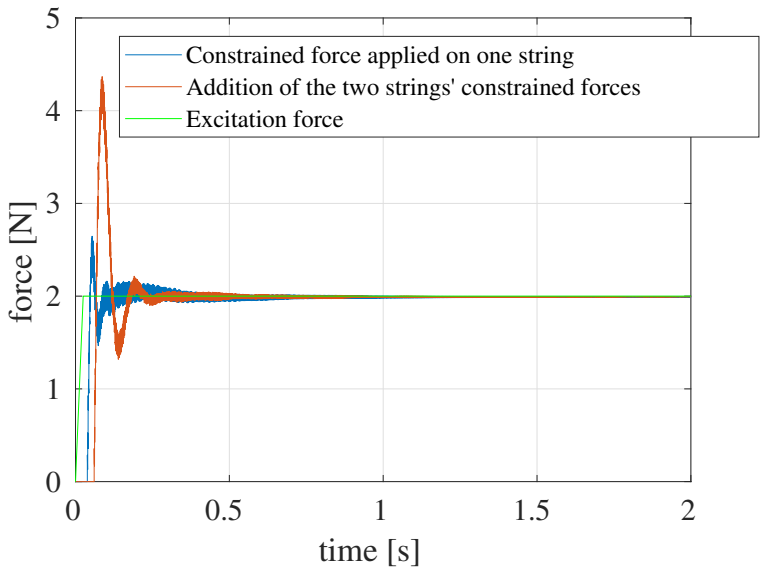

Figure 3.19: Exciting force applied on the tangent and constraining force applied on the string-tangent coupling point, when one string is struck and when two strings are struck.

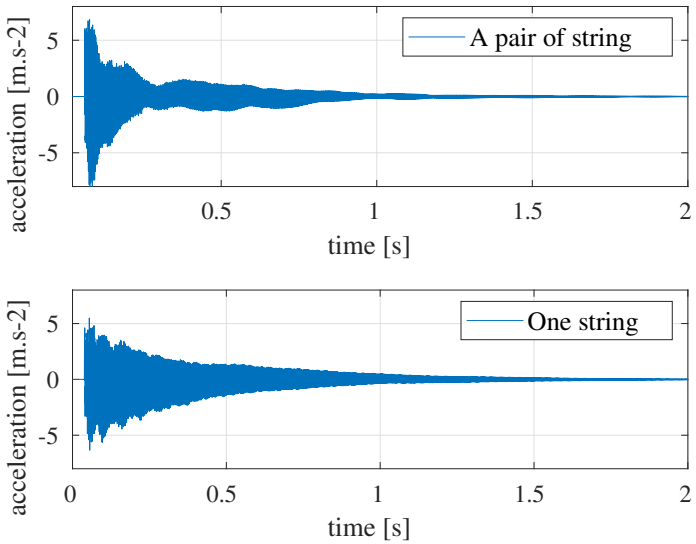

Figure 3.20: Acceleration at the G3-G#3 strings' coupling point, in the case where only the first G3-G#3 string is excited and where the two strings are excited.

3.6 Conclusion

An overall estimation of the parameters needed for the simulation was performed. The strings' dampings were found by means of measurements on three different strings on a string bench. Then, complying the model of string damping with experimental results, the dampings of all the clavichord strings could be derived. Then, using FRF's measurements and the modal representation of the bridge, experimental analysis could be done to estimate the modal parameters of the bridge at the interested locations. In view of the coherency of the simulation results, convenient and *ad hoc* values for the key-tangent substructure modal parameters and for that of the damper are given. Furthermore, tests of the simulation were done to verify its stability and its convergence. The simulation of one and two clavichord strings seems to give good results. This model is used in chapter 4 to study the relation between the impact velocity and its vibratory consequences in section 4.3, to study the variation of the string tension because of its static displacement in section 4.2, and to study the motion of the string and that of the tangent following the excitation in section 4.4. Also, this model is used in chapter 7 to study numerically the vibration of the sympathetic part of the strings.

Part III

Excitation

Chapter 4

Functional analysis of the excitation system

4.1 Introduction

When playing the clavichord, the musician finger presses the key, i.e. the tangent is uplifted. Then this tangent strikes the string with some momentum, which leads to the fact that the string is set into vibration. As long as the key is pressed by the finger, the tangent remains in contact and elevates the string. As a consequence, the tension of the string is influenced which impacts on the string fundamental frequency. Also, depending on the velocity impact of the tangent, the sound produced by the clavichord is influenced.

In this chapter, these aspects of the excitation of the clavichord string is studied. First, the simulation is used to quantify the variation of the string tension and that of its fundamental frequency in section 4.2. Next, the bridge vibratory response to the excitation is studied by means of simulations in section 4.3, in order to retrieve experimental results found by d'Alessandro [3]. Finally, the observation of the string motion given by the simulation in section 4.4 is done, giving a precise view of the specificity of the clavichord string motion and showing the interaction between the string and the key-tangent substructure. Then, the two polarisations of motion of the clavichord string are measured in section 4.5. It allows to see how the excitation impacts on the string vibration in the two polarisations of motion. Then, the legitimacy of the one polarisation assumption of the model established in chapter 2 can be verified.

4.2 String tension

Regarding the study of the clavichord string tension, two aspects need to be tackled. First, the modelling of the dynamic string tension by means of the Kirchhoff-Carrier model needs to be verified by comparing it to a static approach of modelling this tension after having proved the equivalence between these two approaches. Then, the influence of the modeled dynamic string tension on its fundamental frequency is studied.

4.2.1 Equivalence of the tensions given by the static approach and the dynamic one

In this section, the equivalence of the non-linear dynamic approach and the geometrical quasi-static one to express the string tension variation is demonstrated[1].

Static approach

As it is pointed out in [3], the string static tension T_{stat} can be expressed by a geometric approximation :

$$\Delta T_{stat} = ES\left(\frac{\sqrt{L_l^2+Y_e^2}+\sqrt{L_r^2+Y_e^2}}{L}-1\right) \tag{4.1}$$

where $L_l = x_e$, $L_r = L - x_e$ and Y_e are distances described in figure 4.2. This can be rewritten in the following way :

$$\Delta T_{stat} = ES\left(\frac{L_l}{L}\sqrt{1+\left(\frac{Y_e}{L_l}\right)^2}+\frac{L_r}{L}\sqrt{1+\left(\frac{Y_e}{L_r}\right)^2}-1\right) \tag{4.2}$$

For usual position x_e of the tangent, it can be assumed that $\frac{Y_e}{L_l} \ll 1$ and $\frac{Y_e}{L_r} \ll 1$. Simplifying equation 4.2 using a Taylor expansion, it leads to :

$$\Delta T_{stat} = ES\left[\frac{L_l}{L}\left(1+\frac{1}{2}\left(\frac{Y_e}{L_l}\right)^2\right)+\frac{L_r}{L}\left(1+\frac{1}{2}\left(\frac{Y_e}{L_r}\right)^2\right)-1\right] = Y_e^2\frac{ES}{2L_lL_r} \tag{4.3}$$

which can be written thus :

$$\Delta T_{stat} = Y_e^2\frac{ES}{2x_e(L-x_e)} \tag{4.4}$$

By the way, in quasi-static conditions, the physical displacement of the string is given by :

$$Y(x) = \begin{cases} \frac{x}{x_e}Y_e & 0 \leqslant x \leqslant x_e \\ \\ \frac{L-x}{L-x_e}Y_e & x_e \leqslant x \leqslant L \end{cases} \tag{4.5}$$

[1]This demonstration came from a personal communication given by José Antunes

Dynamic approach

The result given in equation 4.4 can be retrieved using a non-linear dynamic approach, that is by using the Kirchoff-Carrier model. The expression of the tension variation based on the aforementioned model given by equation 2.60 is recalled :

$$T_{dyn} = \frac{ES\pi^2}{4L^2} \sum_{n=1}^{N} n^2 \left(q_n\right)^2 \tag{4.6}$$

Then, the modal displacements q_n^S are computed by noticing that :

$$Y^S(x) = \sum_{n=1}^{N} \phi_n^S(x) q_n^S \Rightarrow \int_0^L Y(x)\phi_n^S(x)dx = \int_0^L \left[\phi_n^S(x)\right]^2 q_n^S dx \tag{4.7}$$

so that the modal displacements created by the string displacement field are given in the following way :

$$q_n^S = \frac{\int_0^L Y(x)\phi_n^S(x)dx}{\int_0^L \left[\phi_n^S(x)\right]^2 dx}, \quad n = 1, 2, ..., N \tag{4.8}$$

which gives :

$$q_n^S = Y_e \frac{\int_0^{x_e} \frac{x}{x_e}\phi_n^S(x)dx + \int_{x_e}^L \frac{L-x}{L-x_e}\phi_n^S(x)dx}{\int_0^L \left[\phi_n^S(x)\right]^2 dx}, \quad n = 1, 2, ..., N \tag{4.9}$$

with $\phi_n^S(x) = \sin\left(\frac{n\pi x_e}{L}\right)$. Computing the integrals in equation 4.9, one obtains :

$$q_n^S = \frac{2L^2 \sin\left(\frac{n\pi x_e}{L}\right)}{n^2\pi^2 x_e \left(L - x_e\right)} Y_e, \quad n = 1, 2, ..., N \tag{4.10}$$

Then, replacing equation 4.10 in equation 4.6 :

$$T_{dyn}(t) = \frac{ES\pi^2}{4L^2} \sum_{n=1}^{N} n^2 \left(\frac{2L^2 \sin\left(\frac{n\pi x_e}{L}\right)}{n^2\pi^2 x_e \left(L - x_e\right)} Y_e \right)^2 \tag{4.11}$$

By simplifying :

$$T_{dyn}(t) = Y_e^2 \frac{ESL^2}{\pi^2 x_e^2 \left(L - x_e\right)^2} \sum_{n=1}^{N} \left(\frac{1}{n} \sin\left(\frac{n\pi x_e}{L}\right) \right)^2 \tag{4.12}$$

Notice that when the number of modes N is large enough, then :

$$\sum_{n=1}^{N}\left(\frac{1}{n}\sin\left(\frac{n\pi x_e}{L}\right)\right)^2 \approx \sum_{n=1}^{\infty}\left(\frac{1}{n}\sin\left(\frac{n\pi x_e}{L}\right)\right)^2 \tag{4.13}$$

Then noticing that :

$$\begin{aligned}\sin(x)^2 &= \frac{1-\cos(2x)}{2}\\ \sum_{n=1}^{\infty}\frac{1}{n^2} &= \frac{\pi^2}{6}\\ \cos(x) &= \frac{\exp(jx)+\exp(-jx)}{2}\end{aligned}$$

Equation 4.13 is rewritten thus :

$$\sum_{n=1}^{\infty}\left(\frac{1}{n}\sin\left(\frac{n\pi x_e}{L}\right)\right)^2 = \frac{\left(-3\mathrm{Li}_2\left(\exp\left(\frac{2\pi j x_e}{L}\right)\right)-3\mathrm{Li}_2\left(\exp\left(\frac{-2\pi j x_e}{L}\right)\right)+\pi^2\right)}{12} \tag{4.14}$$

where Li_2 is the dilogarithmic function defined as $\mathrm{Li}_2(z)=\sum_{n=1}^{\infty}\frac{z^n}{n^2}$ with z being a complex number. Using the following property of the dilogarithmic function [96] :

$$\mathrm{Li}_2(z)+\mathrm{Li}_2\left(\frac{1}{z}\right) = -\frac{\pi^2}{6}-\ln(-z) \tag{4.15}$$

Then :

$$\mathrm{Li}_2\left(\exp\left(\frac{2\pi j x_e}{L}\right)\right)+\mathrm{Li}_2\left(\exp\left(\frac{-2\pi j x_e}{L}\right)\right) = \frac{\pi^2}{3}+2\pi^2\frac{x_e}{L}\left(\frac{x_e}{L}-1\right) \tag{4.16}$$

Using equations 4.14 and 4.16, that amounts to the following result :

$$\sum_{n=1}^{N}\left(\frac{1}{n}\sin\left(\frac{n\pi x_e}{L}\right)\right)^2 \approx \sum_{n=1}^{\infty}\left(\frac{1}{n}\sin\left(\frac{n\pi x_e}{L}\right)\right)^2 = \frac{\pi^2}{2}\frac{x_e}{L}\left(1-\frac{x_e}{L}\right) \tag{4.17}$$

Then, replacing equation 4.17 in equation 4.12

$$\Delta T_{stat} = Y_e^2\frac{ES}{2x_e(L-x_e)} \tag{4.18}$$

which is identical to equation 4.4, given by the geometrical quasi-static approach. Then, it is shown that the geometrical quasi-static approach is compatible with the non-linear dynamic one based on the Kirchhoff Carrier model.

Numerical verification of the equivalence between the dynamic and static string tension variation

In the case of the clavichord, the boundary conditions of the string are "pinned-pinned" (see figure 4.1). As a result, geometric nonlinear modal force terms are calculated by means of equation 2.63. As a means of verification, the dynamical tension computed by the simulation of equation 2.60 can be compared to the tension computed by means of a static approach. When the string is excited by the tangent, the shape of the string is assumed to be a triangle.

Figure 4.1: Photo indicating the pined nature of the boundary conditions of clavichord strings

The variation of tension $\Delta T(t)$ computed dynamically by means of equation 2.60 and statically by means of equation 4.1 are shown in figure 4.2 (b). In this simulation, the string is fixed on both ends. The dynamic approach and the static one have to give the same string tension variation. Figure 4.2 shows that ΔT and ΔT_{stat} given by these two approaches are well superimposed. As a result, the two approaches are consistent, which implies that the dynamic tension of the string is well simulated. Also, one can see that the variation of tension has a similar form to that of the string displacement at the coupling point with the tangent (see figure 3.9). If the variation of tension given by these two approaches are the same, then it means that the dynamic tension is well modelled, whether there is a coupling with the bridge or not. The same oscillation observed for the displacement can be observed at the beginning of the $\Delta T(t)$. This oscillation depends on the modal behaviour of the key-tangent substructure and that of the string.

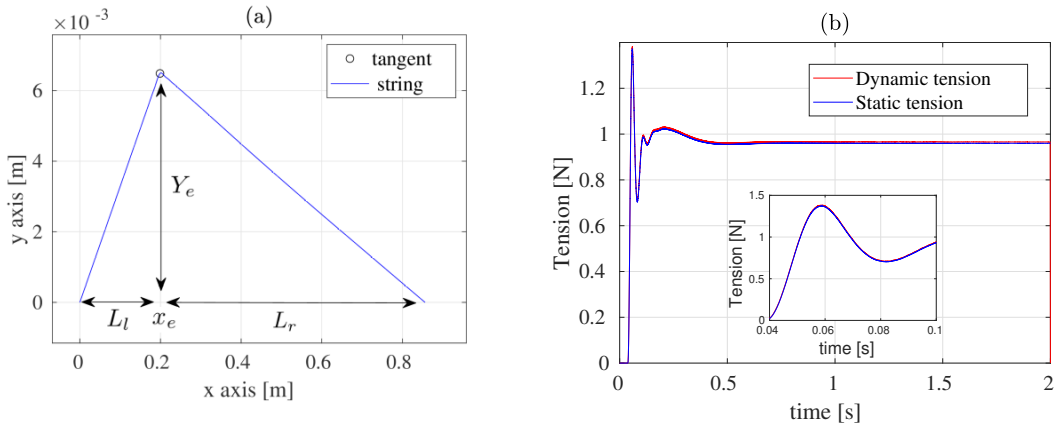

Figure 4.2: Representation of the G#$_3$ string when uplifted by the tangent, where the string is uncoupled with the bridge (left). Comparison of the dynamic tension T_{dyn} to the static tension T_{stat} in the case of this string uplifted by the key-tangent substructure (right).

4.2.2 Variation of the fundamental frequency by the dynamic tension

Let us now reconsider the case where the G#$_3$ is coupled with the bridge, like that shown in the simulation in section 3.4. To estimate the influence of this variation of tension on the string fundamental frequency f_0, it is possible to compute this frequency by means of Mersenne's law [58] :

$$f_0 = \frac{1}{2L}\sqrt{\frac{T + \Delta T}{\mu}} \tag{4.19}$$

where μ is the linear density of the string, L is the length of the string, T is the tension of the string and ΔT is the variation of tension created by the string uplift. The interest here is to estimate the variation of the string fundamental frequency Δf_0 with respect to time. Rewriting equation 4.19 :

$$f_0 = \frac{1}{2L}\sqrt{\frac{T}{\mu}}\sqrt{1 + \frac{\Delta T}{T}} = f_{0,r}\sqrt{1 + \frac{\Delta T}{T}} \tag{4.20}$$

where $f_{0,r} = \frac{1}{2L}\sqrt{\frac{T}{\mu}}$ is the fundamental frequency of the string where it is only stretched by its extremities with its tension T. The value of the tension ΔT is 0.8 N according to figure 4.3 at the static phase. The tension T (whose value is 45 N) is larger than this variation, so it is possible to expand the term $\sqrt{1 + \frac{\Delta T}{T}}$ at the first order. It yields :

$$f_0 = f_{0,r}(1 + \frac{\Delta T}{2T}) = f_{0,r} + \frac{\Delta T}{2T} f_{0,r} = f_{0,r} + \Delta f_0 \tag{4.21}$$

As a result, the variation Δf_0 is given by this relation :

$$\Delta f_0 = \frac{\Delta T}{2T} f_{0,r} \tag{4.22}$$

Let $\gamma = \frac{\Delta T}{2T}$, which is shown in figure 4.3 (a) with respect to time. It is found that γ converges toward 0.9%. This implies that the resulting frequency f_0 of the uplifted string is obtained by augmenting the frequency $f_{0,r}$ when the string was at rest by 0.9% of its value. Yin algorithm is used to measure the fundamental frequency of the simulated clavichord struck string [97] (the position taken for the string displacement signal used is $x = 34.2$ cm). This frequency is shown in figure 4.3 (b), which ends up being at 391.6 Hz after the transitory part of the excitation. This is the fundamental frequency of the string once it is uplifted. To have that of the string at rest, one has to consider $f_0 = 391.6$ Hz and $\gamma = 0.9\%$. Using equation 4.21, one obtains $f_{0,r} = 388.1$ Hz for the simulated G#$_3$ string at rest. By calculating the difference of these two frequencies in terms of cent, one obtains 16 cent. Beyond 4 cent, the difference in pitch is perceptible [98]. Therefore, the pitch shift produced by the simulation is perceptible. When playing a real clavichord, the pitch shift created by the string uplift is also perceptible. As a result, the excitation system yields plausible results in terms of tension variation and fundamental frequency variation.

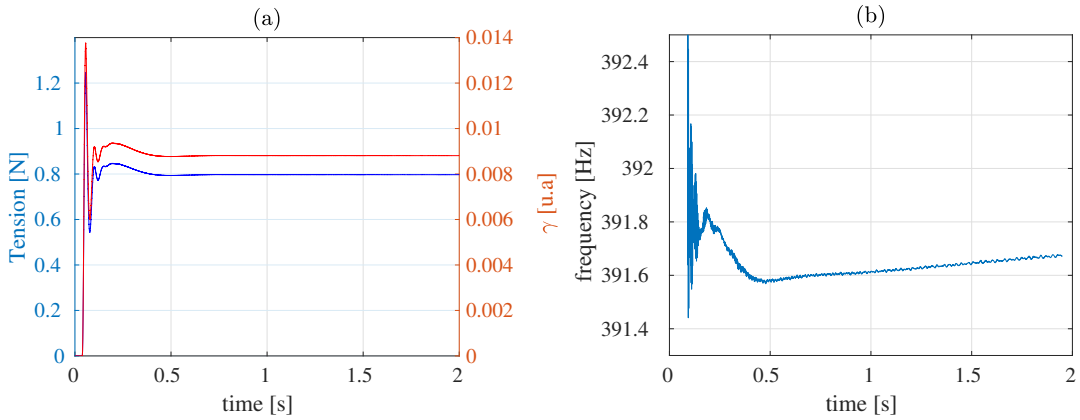

Figure 4.3: Variation of tension of the G#$_3$ string when uplifted by the tangent, where the string is coupled with the bridge, and the coefficient γ with respect to time (a), Fundamental Fundamental frequency of the simulated G#$_3$ string computed by means of yin algorithm (b).

4.3 Bridge vibration reacting to the tangent

4.3.1 Linearity between the vibratory level and the logarithm of the impact velocity

It was shown experimentally by d'Alessandro [3] that the sound level produced by the clavichord is proportional to the logarithm of the impact velocity of the tangent. A similar result can be retrieved by means of the simulation. Since the simulation only yields vibratory results, one can expect that this impact velocity may be proportional to the produced acceleration at the coupling point between the bridge and the excited string. To vary the impact velocity, the force $\boldsymbol{F}_{ext}$ applied on the key-tangent substructure is varied (see figure 4.4). For each excitation force given, the impact velocity and the average acceleration computed by the simulation are obtained. Similarly to the sound pressure level (SPL) the acceleration level is computed as the logarithm of acceleration integrated over 250 ms, starting from the impact time. In figure 4.4, the average acceleration in dB with respect to the logarithm of the velocity is plotted. The linear regression shows the approximated linearity between the two parameters, which is similar to results found by d'Alessandro measuring sound pressure level. As a result, the simulation gives a coherent result in comparison with experimental approaches.

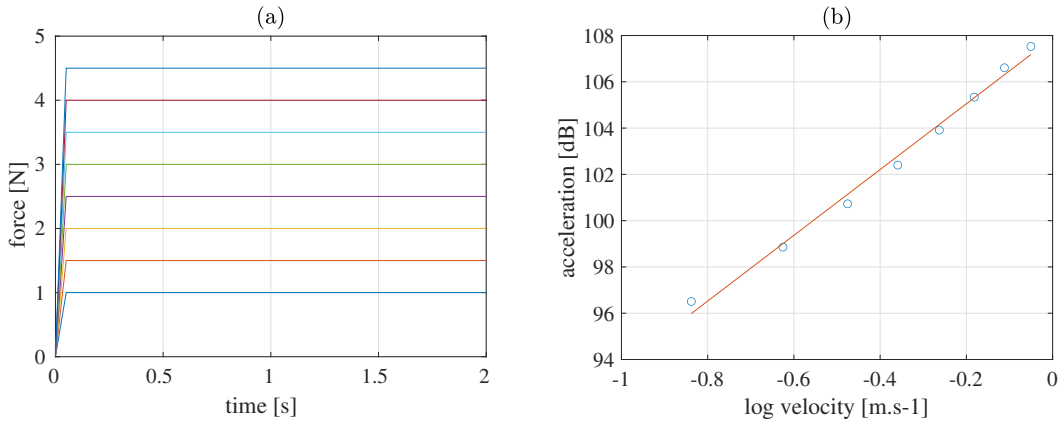

Figure 4.4: Force profiles used to obtain the simulated impact velocities and the associated bridge acceleration (a), Time average of the bridge acceleration (ref 1 dB : 1 m.s^{-2}) at the G#$_3$ string coupling point with respect to the logarithm of the tangent impact velocity (b).

4.3.2 Link between spectral slope and impact velocity

It is possible to investigate the influence of the impact velocity on the timbre of the bridge acceleration at the same coupling point. The same simulations as the previous study with forces shown in figure 4.4 (a) are used to compute the spectral slope of these different simulated accelerations. The results are presented in figure 4.5 for different impact velocities. First, one can see that the higher the impact velocity, the higher the partials' frequency of the string. In other words, the partials' frequency increase little by little by increasing the impact velocity. This impact velocity increases because of the increase in the excitation force amplitude. But

with the force profiles that are used (figure 4.4 (a)), increasing the excitation force amplitude leads to increasing the static displacement of the string, hence the increase in the string fundamental frequency. That accounts for the little shift in frequency of the partials in figure 4.5. Along with this, the first partials' spectral amplitude increase with respect to the impact velocity, which is consistent. Most importantly, one can see that the spectral slopes for the different spectra are approximately the same, which is put forward by drawing an average spectral slope for all the curves. As a result, the timbre of the simulated bridge acceleration does not change with respect to the tangent impact velocity, which is the same conclusion as the one found in the light of the experimental study by d'Alessandro [3].

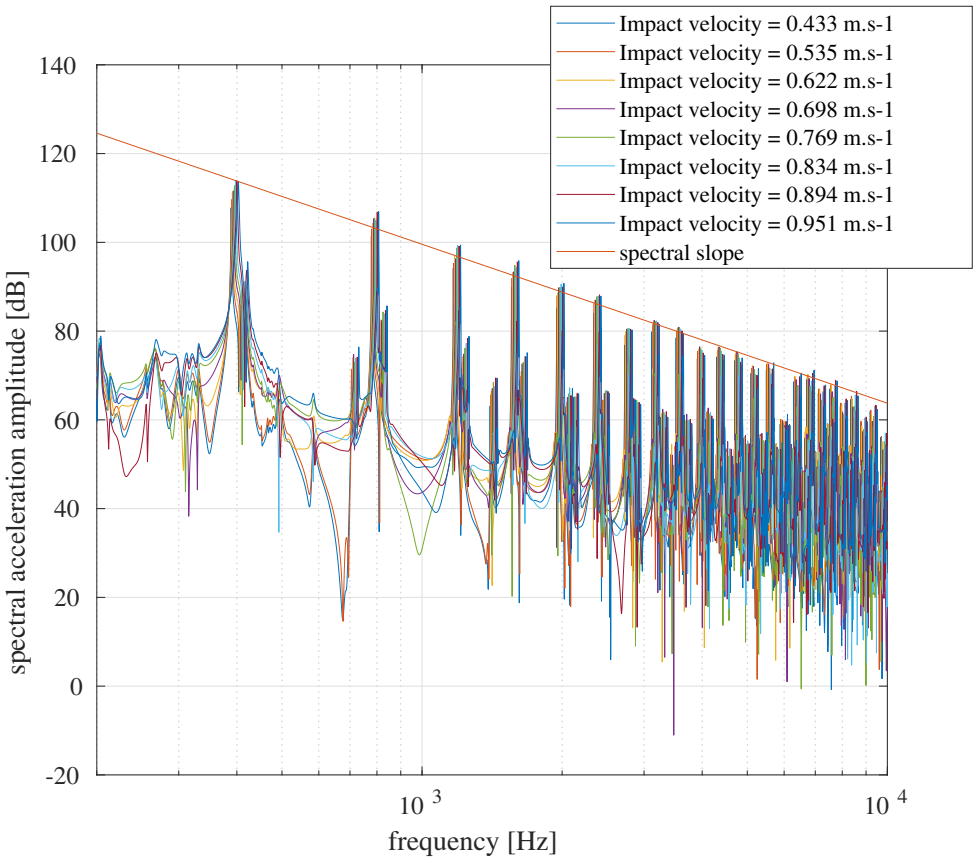

Figure 4.5: Spectral amplitude of the different bridge accelerations at the G#$_3$ string coupling point with respect to time (ref 1 dB : 1 m.s^{-2}), for different impact velocity of the key-tangent substructure, with the average spectral slope.

4.4 Motion of the struck string

4.4.1 Key-tangent motion

The objective of this section is to compare an experimental tangent velocity profile with that coming from the simulation in order to see if these profiles are comparable. To that purpose, a robotic finger is used. The DROPIC finger was conceived to program finger trajectories in order to simulate excitations for string instruments [99]. Its trajectory is programmed in terms of displacement and velocity in a 2 dimensional space (for further details, see annex F). The excitation performed by the robotic finger was done on the F_3 string (this is not the same string as the $G\#_3$ string which is simulated, but the two strings and the two corresponding keys are not so different in dimension, so they are qualitatively comparable). The velocity profile coming from the standard simulation done in section 3.4 and that derived from the key displacement measurement caused by the robotic finger trajectory in annex F are shown in figure 4.6 (a). The values chosen for the simulated velocity profile are $\alpha = 200$ N.s^{-1}, $t_1 = 0.01$ s, $t_2 = 1.0$ s, $t_3 = 1.01$ s (see section 3.1.5). The ascending slope of the measured velocity profile is similar to that of the simulation, whose value is 84.5 m.s^{-2}. The impact velocity of the experimental velocity profile is around 0.6 m.s $^{-1}$ while that of the simulated one is around 0.8 m.s^{-1}. In figure 4.6 (b), the Fourier transform of the two velocity profiles are presented. A little vibratory energy can be seen at 330 Hz on the curve associated to the robotic finger motion, which corresponds to the fundamental frequency of the F_3 string excited by the robotic finger. A similar observation can be seen for the curve associated to the simulated key-tangent substructure motion where vibratory energy is found at 391 Hz, which corresponds to the modelled $G\#_3$ string fundamental frequency. The lowest frequency of the robotic finger velocity profile where the spectral amplitude is significant is 13 Hz, while that of the simulated key-tangent substructure velocity profile is 62 Hz, which is exactly what was observed in section 3.4. In d'Alessandro's study, the low frequency motion at the contact point between the excited string and the tangent is around 30 Hz for the Sidey clavichord [3]. The order of magnitude of this frequency is consistent with that found with experimental data. The value of this low frequency varies depending on the inertia of the specific key.

Another main difference in figure 4.6 (b) between the two curves is that the lowest frequency is more damped in the robotic finger case than that in the simulated motion case. Yet, the low frequency motion of this contact point is not so largely damped in d'Alessandro's velocity profile measurements [3]. So the damping of the simulated motion low frequency remains plausible. Furthermore, the same bridge acceleration spectral amplitudes are represented in figure 4.6 (c) between 100 Hz and 10000 Hz with a logarithmic representation of the frequency axis. The spectral slope of these curves are the same and is -6 dB/octave. In d'Alessandro's study, the spectral slope of the tangent velocity is also -6 dB/octave [3]. So the spectral slope found in the simulation is consistent with that of the experimental data.

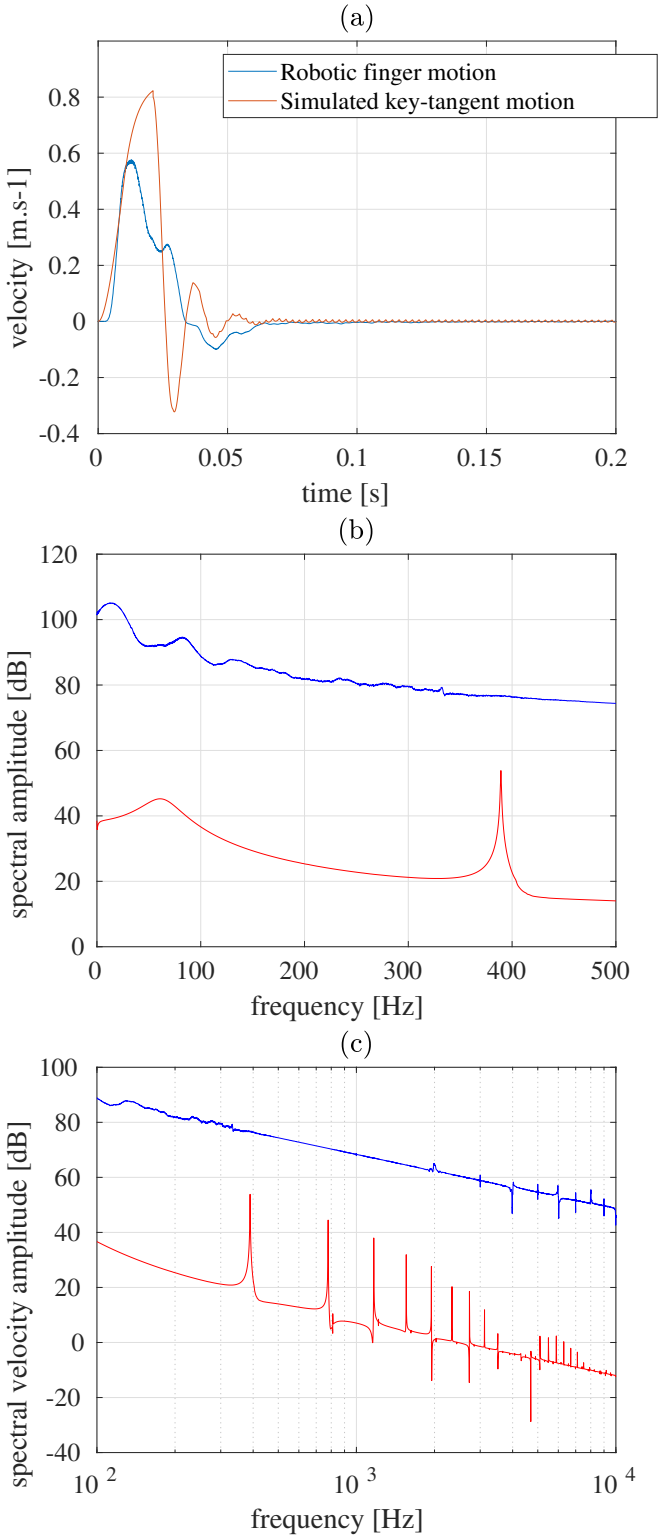

Figure 4.6: Measured velocity of the F_3 key caused by the robotic finger pressure and velocity of the simulated key-tangent substructure displacement (a), Spectral amplitude of the simulated key-tangent substructure displacement (ref 1 dB : 1 $m.s^{-1}$), marking the two first modes' frequency of this system (b), spectral amplitudes plotted between 100 Hz and 10000 Hz with a logarithmic representation of the frequency axis (c).

4.5 Two dimensional motion of a struck string

When the string is set into vibration, it is vibrating with respect to two polarizations, namely the vertical and the horizontal one. The measurement of these two polarizations of motion can be used to compare their vibratory amplitude. As such, one can observe which polarization is predominant when the clavichord string vibrates. To proceed to these measurements, pairs of optical forks (OMRON EE-SX1131) are laid out on the clavichord as it is shown in figure 4.7. Each of the two forks measure the displacement of the string with respect to a specific polarization of motion. During the string motion, the light beam of each sensor is cut creating a voltage proportional to the displacement. Since the F_3 string diameter is 0.33 mm, the radius of the photo-transistor chosen is 0.3 mm. The nearby strings need to be displaced in order to lay out properly the optical forks. Then, before doing the measurements, these forks need to be calibrated in accordance with the procedure indicated by Le Carrou [88].

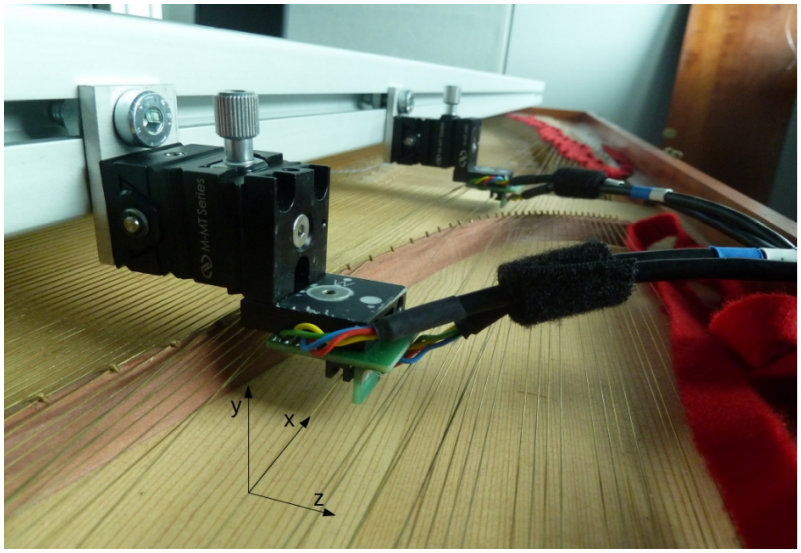

Figure 4.7: Optical forks placed at the sympathetic part and at the played part of the second F_3 string of the LAM1 clavichord.

This vibratory measurement in the two polarisations is done in the case of the F_3 string. A pair of forks is placed at the played part of the string, at 34 cm from the tangent. Another is placed at its sympathetic part, at 11.5 cm from the bridge. Then, the vibratory motion in the two polarisations of the string, in the played part and in the sympathetic part, is measured. The excitation of the F_3 string is done by the robotic finger with the same trajectory that was programmed in annex F.

In figure 4.8, the vibratory displacement of the F_3 string played part is measured in the vertical polarization (y axis) and in the horizontal one (z axis). One can notice the offset of these signals caused by the string uplift along both z and y axis. The vibrating part of the signal is centered at zero. The uplift is done in the y direction. Therefore it is consistent to observe an offset in the y axis larger than that in the z axis. Also, the vibratory displacement of the string played part in the y axis is 10 times larger than that in the z axis. So the tangent transmits more energy to the vertical vibratory displacement of the string than to the horizontal one. Given that the tangent strikes the string in the y axis, this interpretation seems

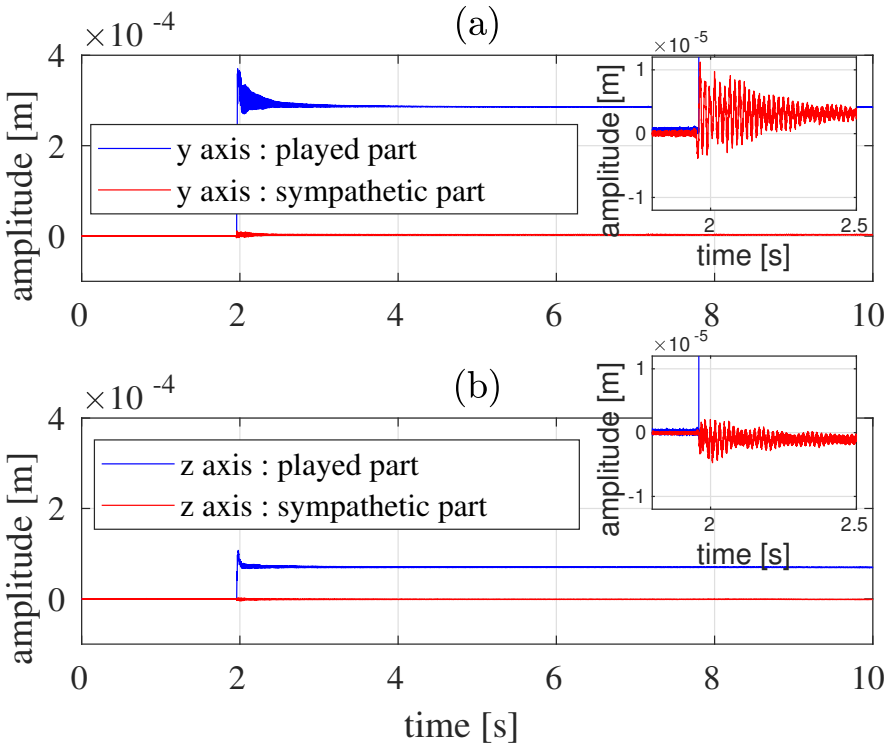

Figure 4.8: Vibratory motion of the F_3 P-string measured at 34 cm from the tangent, the dynamic range of the fork measuring the vertical polarisation is [0.16 V - 0.83 V] and that measuring the horizontal polarisation is [0.03 V - 0.19 V] (a), Vibratory motion of the F_3 S-string measured at 11.5 cm from the bridge, the dynamic range of the fork measuring the vertical polarisation is [0.04 V - 0.23 V] and that measuring the horizontal polarisation is [0.12 V - 0.54 V] (b).

consistent with the measurements. It implies that when it comes to the clavichord, the assumption that only the vertical polarization matters in the case of the excited string is reasonable. In figure 4.8, the measurement of the displacement of the sympathetic part of the F_3 string in the two polarisations is shown. A little offset can be observed in these measurements. The order of magnitude of the vibratory amplitude in the y axis is four times larger than in the z axis. So the assumption of considering only the vertical polarization in the case of the sympathetic part is still legitimate.

4.6 Conclusion

The study of the tension in section 4.2 when the string is excited showed that its uplift leads to a variation of string fundamental frequency of around 1%, which is perceptible to the human ear. Then, the excitation in the case the F_3 string showed that its vibration in the vertical polarization (y axis) is superior to that of the horizontal one for the played part and sympathetic part of the string, which is an assumption that is used for the model in chapter 2. Using simulations in section 4.3, similar results found in the experimental investigation of the clavichord by d'Alessandro were retrieved [3], such as the linearity between the logarithm of the tangent impact velocity and the amplitude of the vibratory acceleration of the bridge and the constancy of the spectral slope of the bridge vibratory acceleration with respect to the impact velocity. Finally, the simulation in section 4.4 have shown the motion of the excited string, where the combination of the static uplift movement and that of the travelling wave could be observed. Also, the interaction between the excited string and the key-tangent substructure was observed, presenting features similar to the measurements. In particular, the low frequency motion of this contact point is similar to that of the measurements done in this work or presented in the literature.

Chapter 5

The clavichord paradox

5.1 Introduction

As an introduction to this chapter, the singular aspect of clavichord performance practice called the "clavichord paradox" is presented. First, this paradox is introduced in section 5.1.1. Then, from the information taken from the works of Brauchli [1] and d'Alessandro [100], a historical account of the music practice of the clavichord is given in section 5.1.2.

5.1.1 Presentation of the clavichord paradox

As it is pointed out by Marin Mersenne [7], the clavichord is an instrument producing a weak sound level compared to other stringed keyboard instruments. To give a typical value for clavichords, the radiated sound at 30 cm above the centre of the 1784 Hubert clavichord soundboard has a maximum sound pressure level of 60 dB SPL [101]. Also, it is the only keyboard instrument allowing for pitch control. When a key is pressed, the corresponding pair of strings is impacted by a small metal blade (the tangent) placed at the end of the key. As long as the key is pressed, the tangent remains in contact with the strings. The tangent is at the same time the nut (i.e. one extremity) of the string and the string exciter (the string is then excited at a vibration node). It has been shown experimentally and numerically that the sound level of the clavichord is proportional to the tangent velocity at impact (see [3] and section 4.3.1). So the faster the key is pressed, the louder the sound becomes. However, when a key is pressed with a high velocity, the key displacement tends to be higher. The tangent raises the string, then increases its tension, and thereby increases the string fundamental frequency (see section 4.2). As a result, playing louder ends up in raising the pitch, if the key is pressed in a simple vertical motion. To control independently loudness and intonation would require a paradoxical gesture: at the tangent-string contact, the tangent should have enough velocity, but should not uplift too much the string. In other words, the key should transfer all the tangent momentum to the string, but without raising it too much, or losing contact with it. This dependence between loudness and pitch accuracy is coined "the clavichord paradox"[102, 4]. It is difficult, at least for human players, to achieve exactly such a motion. However compromises between tangent impact velocity and string displacement are possible.

5.1.2 Historical account of the music practice of the clavichord

This demanding rigour of the clavichord player music practice is a pedagogical virtue developed for the practice of keyboards. As there is no such mechanical constraint in the piano and in the harpsichord, this specific non-intuitive gesture can only be elaborated by means of the clavichord. Also, a long tradition of keyboard practice is connected to the clavichord. Since the XVth century, playing the clavichord was considered as the groundwork for the music practice of keyboard instruments. One of the first treaty to highlight this is the one by Paulus Paulirinus entitled *Liber XX Artium* (1459-1463). This same consideration is found in the *Musica getutscht* (1511) by Sebastian Virdung [6]. Once again, it is repeated in the XVIIIth century by Johann Gottfried Walther, one of the cousins of Johann Sebastian Bach, in his book *Musikalisches Lexicon* (1732) [103]. George Simon Löhlein affirmed in his treaty *Clavierischule* (1765) [104] that the clavichord should be the starting instrument for anyone who wants to start the practice of keyboard instruments. Carl Philipp Emanuel (C.P.E.) Bach's treaty *Versuch über die wahre Art, das Clavier zu spielen* (1753) [105], whose author is one of those who praised and popularised the clavichord in the XVIIIth century, puts forward the fact that in order to become a good keyboard player, one has to practise the clavichord[1].

By means of this music practice, the clavichord musical qualities were valued, to the point of being highly appreciated in the XVIIIth century Germany. At that period, as the sophistication of the instrument making of the clavichord reached its zenith in this country, the expressive style connected to this instrument was associated to the musical motion entiteld *Empfindsamkeit*, whose leader is C.P.E. Bach. The XVIIIth musical historiographer Charles Burney witnessed the expressive character of this instrument in one of his comments (*Present State Germany, Netherlands, Vol.1, pp. 108* [106]) on Daniel Schubart's playing when practising the clavichord, who was organist at the Stadtkirche of Ludwigdburg. Also, the clavichord was considered at that time as a symbol of sensibility and intimacy, as it is witnessed by the philosopher and poet Johann Gottfried Herder in 1800 in his book *Kalligone*[2] [107]. This expressive aesthetics of the clavichord came into light by playing techniques only possible with this instrument. Among these techniques, there is the *Bebung* which is a kind of vibrato done by varying quickly the finger pressure on the key. Also, the *Tragen der Töne* consists in a single variation of this pressure done on a series of notes after each attack. This frequency variation of the string gives a singing aspect to the produced sound.

On the other hand, this expressivity is also connected to a way of placing the hand at the keyboard. One of the first treaties dealing with this topic is that of

[1] Bach, Carl Phillipp Emanuel, *Versuch über die wahre Art, das Clavier zu spielen* (1753), §15 : "*Man muss also das Clavicord zur Erlernung des guten Vortrags und den Flügel, um die gehörige Kraft in die Finger zu kriegen, brauchen. [...] Man kan sogar mit der Zeit, wenn man bloß auf einem Clavicorde spielt, die Stärcke aus den Fingern verliehren, die man vorhero hatte* (One must therefore use the clavichord to learn good performance and the harpsichord to get the proper strength in the fingers. [...] One can even lose the strength in the fingers that one had before, if one only plays on a clavichord).

[2] "Music plays in us a clavichord which is our innermost nature (*Die Musik spielt in uns ein Clavichord, das unsre eigene innigste Natur ist*)", Herder, *Kalligone*, 1800,: *Sämtliche Werke XXII, 68* [107], from Brauschli, Bernard, *The clavichord*, *op. cit.* [1]

Tomàs de Santa Maria entitled *Libro Llamado Arte de Tañer Fantasía* (1565). The first treaties do not make a difference between the fingering at the organ, at the harpsichord or at the clavichord. One of the most important feature mentioned by Tomàs de Santa Maria is the fact of playing with the balls of the finger. This allows to ensure a good contact with the keys and to avoid attacks of the notes which are too percussive. In 1593, an important treaty entitled *Il Transilvano* written by Girolamo Diruta is published. This author is the first to insist on the hand and arm relaxation when playing, as well as on the suppleness and lightness of the hand. For this, Diruta gives indications on the recommended hand shape : it should have a cupped position, with the fingers slightly arched. Furthermore, the wrist should supply the hand so as to form a straight line with the arm. With this configuration, the author affirms that it is possible to play with agility and velocity. If these indications put forward by Diruta may seem logical today, they represented at that time an important evolution in the understanding of the technical playing at the clavichord. This author is critical towards Santa Maria's hand shape, where the wrist is below the hand with arched fingers. With such a posture, Diruta affirms that it is impossible to play well at the keyboard without getting tired. This archaic posture of Santa Maria's hand shape was abandoned at the profit of that of Diruta, where the importance is given to relaxation and lightness. Regarding the hand shape, later treaties give advises essentially on the height of the wrist and the degree of finger bending.

It is interesting to linger on German treaties of the XVIIIth century. As it is a period corresponding to the golden age of the clavichord, a lot of considerations are focused on the clavichord player's finger motion. In particular, one of the playing style that kept the attention of the theoreticians and of the musicians is that of Johann Sebastian Bach [100]. This performance practice was said to be "Every Players first Grammatica" to quote J.G. Walther (1732) (see [103], page 169). The treaty on the flute by Johann Joachim Quantz dating back to 1752 (*Versuch einer Anweisung die Flöte traversiere zu spielen* [108]) is one of the first to describe this playing. According to Quantz, it is possible to make an important distinction between two main gestures : a "pushed" gesture and a "pulled" one. The pushed gesture corresponds to a finger motion which would be strictly vertical. On the other hand, the pulled gesture corresponds to a motion possessing a vertical and a horizontal components. Quantz describes this gesture as a rotating motion, where the finger is pulled back just after its contact with the key. The vertical component is responsible for the downward displacement of the key, while the horizontal one aims at pulling back the finger in order to avoid a too important key depth. The French name given to this gesture is "*tire*", which according to Quantz is the equivalent of the German term "*Schneller*" [109]. The aforementioned treaty by C.P.E. Bach (*Versuch über die wahre Art, das Clavier zu Spielen*) also refers to this same kind of gesture when it comes to the clavichord. In this text, this digital motion is called by the verb *schnellen*. A more precise description of this gesture is given by Ernst Wilhem Wolf in the preface of his 1785 sonata collection (*Eine Sonatine, Vier affectvolle Sonaten und Ein dreyzehnmal variirtes Thema, welches sich mit einer kurzen und freien Fantasie anfängt und endigst. Fürs Klavier*). It is said in the following extract (Preface, p. IV, see [110]) :

> The best way of playing this type of melodic figure at the clavichord, one which sufficiently differentiates the détaché from the normal style of

> articulation, and one which produces the best tone, is this: one strikes the key with a stiff finger (as when playing a syncopation), and then immediately draws the finger back towards the player so that it slides off the front, and the key quickly springs back up. The tone, when thus struck on good clavichords sounds rather as if the consonants "t'nt!" were sounding along with it: this "t'nt!" has a better effect than the "t't" one gets when the finger releases the key without the slide-off.

Wolf refers to the continuous control of the possible sound quality when playing the clavichord. This mentioned pulling back motion of the player is a way to avoid an undesired large increase of the string tension in order to keep the right pitch. This paradoxical gesture was highlighted explicitly by Nicolas-Joseph Hülmandel in 1791 in an article entitled "Clavecin" in *l'Encyclopédie méthodique. Musique* (Hüllmandel 1791, p. 285-286) [111] :

> The advantage of this languet [the clavichord tangent] is to increase and to soften the sound by pressing the finger more or less strongly on the key, and its disadvantage is to elevate or to lower the sound at the same time[3].

5.1.3 Objectives

In a preceding work [102], the effect of vertical finger motion ("pushing motion") and sliding finger motion ("pulling") on loudness and pitch of clavichord tones have been studied. It has been shown that the pulling gesture is a better compromise for dealing with the clavichord paradox: loudness and pitch are controlled more independently with pulled than with pushed motions. The aim of this chapter is to study the clavichord paradox with the help of new measurement techniques and robotic simulation: 1/ to measure accurately finger trajectories and their consequences on vibration and sound patterns (see section 5.2); 2/ to reproduce these trajectories using a robotic finger, in order to study the limits of the clavichord paradox, and then the "optimal" trajectories, decoupling key velocity at impact and string displacement (see section 5.3).

5.2 Experimental approach with a musician

5.2.1 Experimental setup

The objective is to measure the vibration of the excited string resulting from the motion of the musician's finger. The musician involved in this experiment is well trained in clavichord playing. In preceding works [3, 100], measurements were performed with the help of an accelerometer near the tangent, a string-tangent contact signal and a measurement microphone. It appeared necessary to measure directly the finger motion and the string motion, using non-invasive measurement devices.

[3] "*L'avantage de cette languette [la tangente du clavicorde] est d'augmenter et d'adoucir le son en appuyant du doigt plus ou moins fort sur la touche, et son inconvénient est de le hausser ou de le baisser en même temps.*", in d'Alessandro, Christophe. "Le paradoxe du clavicorde et la technique de Bach au clavier." Revue musicale OICRM 6.1 (2019): 87-112. [100] [Personal translation]

Finger motions are filmed by a high-speed camera (Phantom Miro M 120) with a 2000 frame per second rate. Several marks are placed on the finger. Trajectories of these marks are estimated thanks to image processing detailed in section 5.2.2.

String vibrations are measured with the help of calibrated opto-switch sensors [88], as previously detailed in section 4.5. These sensors are optical forks, positioned around the string. The string motion in one direction is measured with accuracy and without contact. Only the vertical displacement of the string is considered here (although the horizontal displacement can also be significant, see section 4.5). The string chosen for our measurements is the G_2 string (length is 70 cm, fundamental frequency 185 Hz). The sensor is placed at 2 cm from the extremity of the string, near the bridge in order to ensure that the string displacement is within the sensor measurement range. Sound pressure is measured with the help of an omnidirectional DPA 4006-TL microphone placed at 30 cm above the soundboard. A set of 8 trajectories are recorded, using index and middle fingers, pulled and pushed motions for long and short notes.

5.2.2 Image processing : trajectory identification

To extract the trajectory corresponding to the motion of the finger, an image processing algorithm needs to be elaborated. One way to deal with this trajectory extraction is to take advantage of contrast in the picture. An image is represented by a matrix containing pixels. So each value in the matrix corresponds to the brightness degree of the pixel. The musician's finger is marked by means of felt-tipped pen. In such a way, it is possible to create a contrast between the mark on the finger and its vicinity. Once the motion of the finger is filmed, the pictures are processed by means of an analysis window centred on the mark and including also its vicinity. By means of the first picture of the filming, the trajectory point of origin is placed at the centre of location of the finger mark. Also, a threshold is defined. If the pixels' value is under this threshold, then these values go to zero. Between the two successive pictures, the mark undergoes a displacement because of the finger motion. The window analysis is large enough so that the mark still remains within the window in the second picture after the small displacement. After applying the aforementioned threshold to the second picture, the maximum value of the contrast within the analysis window corresponds to the centre of the mark. So the location of this maximum value corresponds to the trajectory next point. Then, it is possible to identify the displacement vector of the mark between the point of origin of the first picture and its next location in the second picture. This next location is saved and the analysis window is displaced by means of the same displacement vector, so that it becomes centred on the finger mark in the second picture. Thus, this algorithm is repeated for the following pictures so that the trajectory successive points of the finger mark are measured.

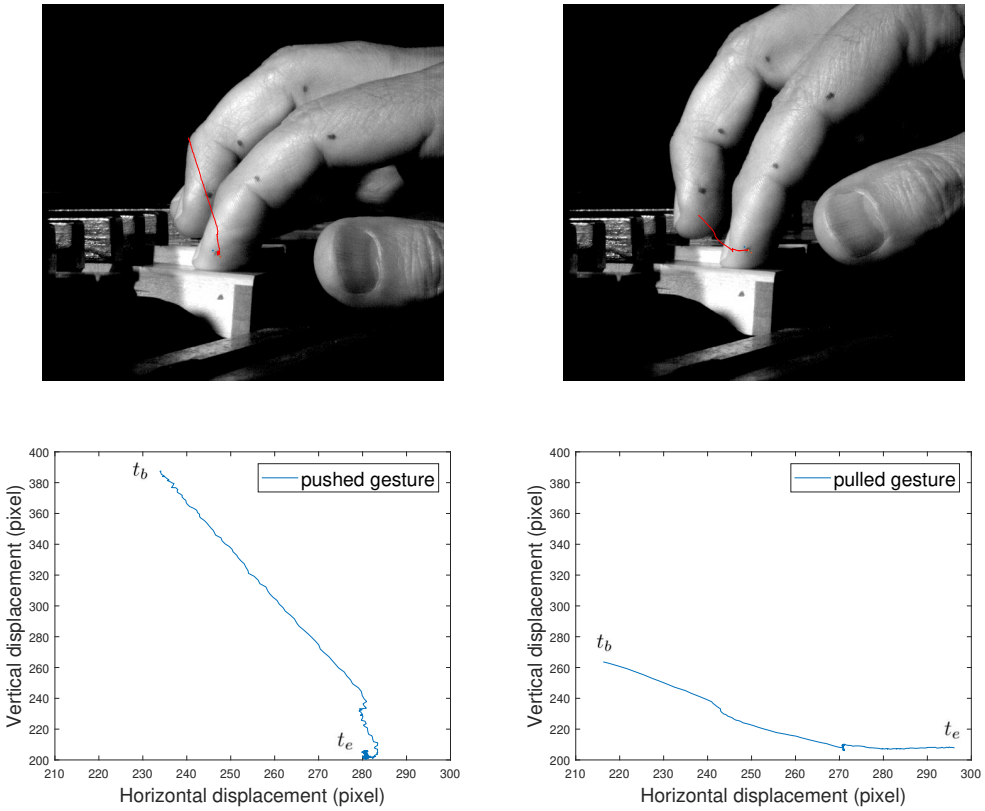

Figure 5.1: (Top) Images of the pushed (left-hand side) and the pulled gesture (right-hand side) performed by the index finger. (Bottom) Trajectories of the pushed (left-hand side) and the pulled gesture (right-hand side) performed by the index finger (with t_b the beginning time and t_e the ending time).

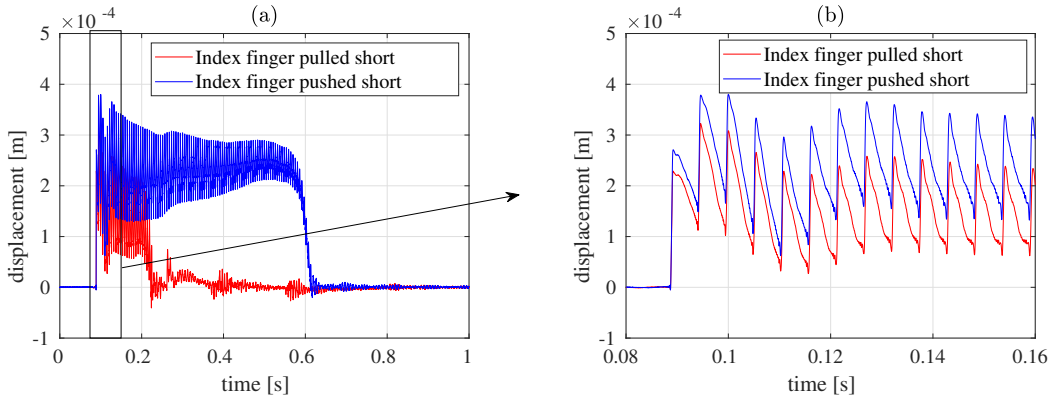

Figure 5.2: Vibratory signal of the G_2 string excited by means of the two different trajectories done by the index finger with a short length (a), with a zoom at the beginning of the signals (b).

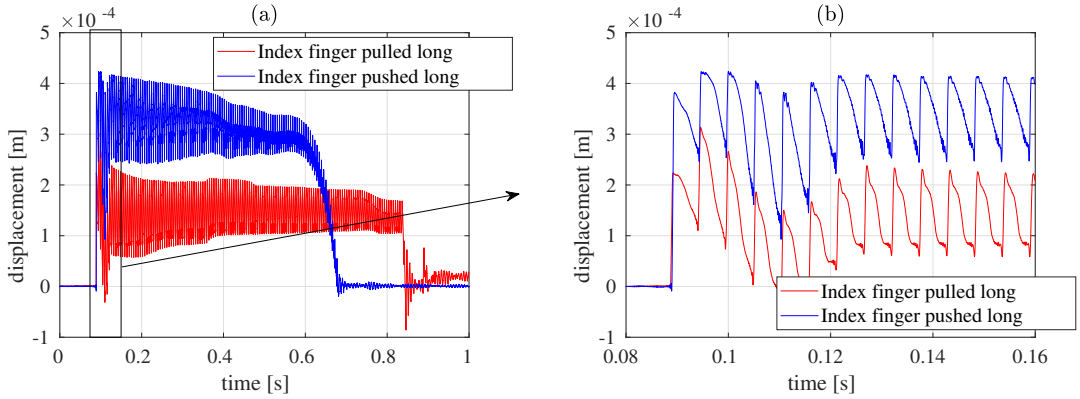

Figure 5.3: Vibratory signal of the G_2 string excited by means of the two different trajectories done by the index finger with a long length (left), with a zoom at the beginning of the signals (right).

5.2.3 Results

In figure 5.1, we used the videos to extract the trajectories representative of the two distinct motions : the pushed and pulled gestures. The pushed motion refers to a vertical trajectory, with the finger going mostly downward. The pulled motion corresponds to a vertical and horizontal trajectory, with the finger sliding on the key and going downward at the same time. Figure 5.1 displays a selection of extracted trajectories. Note that the key depression is shallower in the second case.

Example of string vibration pattern are displayed in figure 5.2 and 5.3 for the pushed and pulled gestures by the index finger. As the sensor is placed near the bridge, the vibratory motion is of small amplitude, about 0.2 mm. The string height is also small at this position, about 0.2-0.3 mm. It is much larger at the tangent position. The string is much more elevated in the case of the pushed gesture than in the case of the pulled one (see figure 5.2 and 5.3). Because of this difference in string height, the string tension and then the sound fundamental frequency is higher for the pushed gesture. Note that the vibration amplitude is also larger in the case of the pushed gesture, resulting in a louder tone. The string fundamental

frequency is measured on the sound and vibration signals using the Yin algorithm [97] implemented in Matlab. The G_2 string fundamental frequency with respect to time is displayed in figure 5.4 (a). The fundamental frequency produced by the pushed gesture of the index finger is around 185.5 Hz, whereas that produced by the pulled gesture of the index finger is around 184.75 Hz. As expected, the fundamental frequency is higher for the pushed gesture compared to the pulled gesture. The difference between the fundamental frequencies of the pushed and the pulled gesture is more than 4 cents. Such a difference is perceptually noticeable [112]. This feature was also observed when studying the excitation system by means of the simulation (see section 4.2). Fundamental frequency gives information about the way the musician deals with the contact between the tangent and the string with respect to time. In figure 5.4 (a), one can observe that the fundamental frequency for the pushed gesture decreases with respect to time, whereas that of the pulled gesture remains around the same fundamental frequency although with some little hills. This shows that the key control differs for both gestures. These variations of finger depth after the string-tangent contact are certainly perceived in terms of quality of touch.

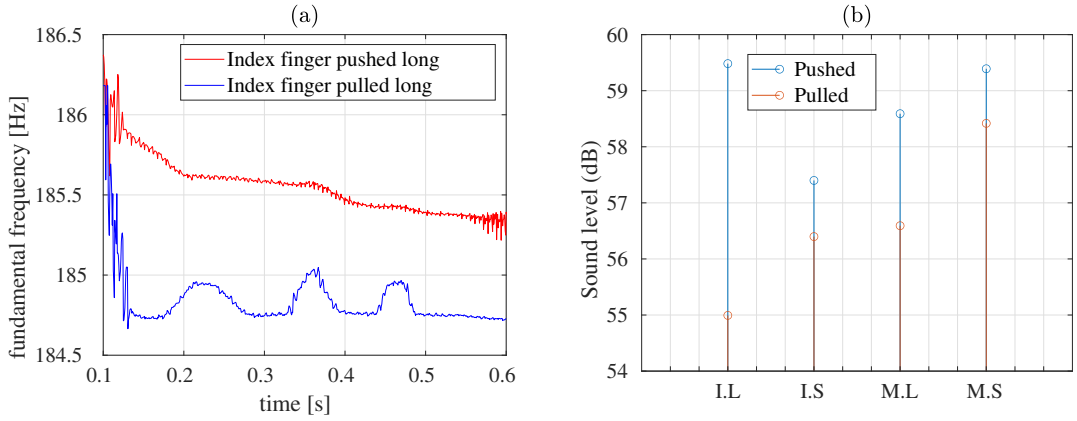

Figure 5.4: Fundamental frequency of the signals in the case of the pushed and pulled gesture done by the middle finger and the index finger (left-hand side). Sound level of the different exciting configurations (right-hand side) (I : Index finger, M : Middle finger, S : Short, L : Long).

The sound level in dB for the different microphone signals $p(t)$ are computed for the index finger and the middle finger thus :

$$L_{eq} = 10 \log_{10} \left(\frac{1}{T} \int_{t_0}^{t_0+T} \frac{p(t)^2}{p_{ref}^2} dt \right) \tag{5.1}$$

where T is the integration time, t_0 is the time at which the computation begins and $p_{ref} = 20 \times 10^{-5}$ Pa. The results are displayed in figure 5.4 (b) (the integration time is 250 ms). For the pushed gesture and the pulled gesture respectively, the long gesture produces a sound level of 59.5 dB and 55.0 dB for the index finger, and 58.6 dB and 56.6 dB for the middle finger. In the case of the short gesture, For the pushed gesture and the pulled gesture respectively, the sound level is 57.3 dB and 56.3 dB for the index finger, and 59.3 dB and 58.4 dB for the middle finger. It

Figure 5.5: DRoPiCrobotic finger for key trajectory control.

seems that the difference in sound level between pushed and pulled gesture is lower for short excitation than for long excitation. Because of a lack of repeatability, this observation cannot be stated for sure. However, in any case, pushed gestures produce higher sound levels than pulled gestures. This has already been observed on the signal amplitude in figure 5.2 and 5.3.

In summary, different gestures, corresponding to different finger trajectories, are producing different vibratory patterns of the string, and then different sounds. In the small set of recordings obtained, the pushed motions always produce a larger string displacement : the string is always raised higher, and the amplitude of vibration is larger. A larger amplitude of vibration results in a louder sound. A higher string height results in a higher fundamental frequency. For the same reasons, the finger motion in the case of pulled gestures gives lower fundamental frequencies and also weaker sounds. Note that in previous studies it has been shown that pulled motions, to some extent, allows for independent loudness and pitch control, a result that cannot be observed here, because no sample have similar loudness. These measurements are the first direct measurements of string height, and are in good agreement with the theory developed in [3].

5.3 Experimental approach with the robotic finger

Measurements of finger motion show the dependence between string height, radiated sound and fundamental frequency. As predicted by the clavichord paradox, it seems difficult to control simultaneously the key (then tangent, then string) velocity and displacement. The pulled motion provides a better control and a better management of the clavichord paradox, because the finger trajectory is more complex: pressure on the string can be released after the tangent-string impact. It is interesting to study the clavichord paradox with the help of controlled and reproducible key trajectories. For this purpose, the DROPIC robotic finger is used [99] (see figure 5.7).

5.3.1 Experimental setup

For a given starting trajectory, two parameters are considered and modified: downward displacement (resulting in string height) and its maximal velocity (corresponding to loudness). The A_2 string (length is 59.1 cm, fundamental frequency tuned at 205 Hz) is studied. The initial position of the robotic finger above the key is set

before modifying either the velocity or the displacement. A joint measurement of the string vibration by means of calibrated opto-switch sensors is performed. Taking a specific robotic finger trajectory as a reference, this can be modified to program three different velocities with the same displacement, and three different downward displacements with the same velocity (these displacements and velocities are not measured in this experiment). The displacement of the key corresponding to a referent trajectory performed by the robotic finger is the one programmed in annex F. The trajectory has a typical shape with a notch followed by a plateau. It is possible to adjust independently the depth of the notch and the height of the plateau, that correspond roughly to the key velocity at contact and to the string height.

5.3.2 Trajectories simulation and sound results

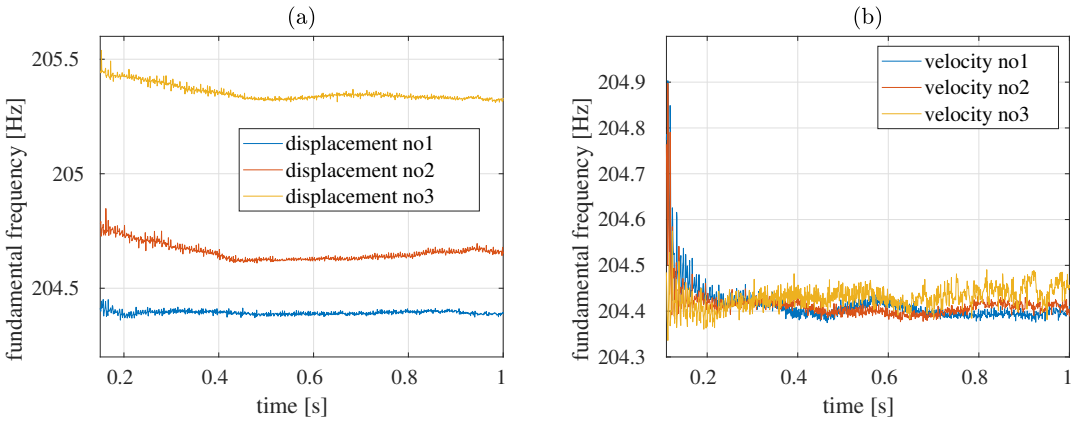

Figure 5.6: Tracking of the fundamental frequencies of the signals in the case where we modify the displacement of the key (left-hand side) and in the case where we modify its velocity (right-hand side).

Systematic variations of displacement and velocity are performed. Displacement n° 1 is the largest one done in the vertical axis (y axis) by the robotic finger, displacement n° 3 is the smallest one, and displacement n° 2 is in between. Velocity n° 1 is the fastest one performed by the robotic finger, velocity n° 3 is the smallest one, and velocity n° 2 is in between. Note that in this second experiment, the note studied is A_2 instead of G_2 studied in Section 5.2. These two notes are close enough to be compared.

In figure 5.7 (a), the key velocity is varying but the key depth is constant. The key depth is about 5-6 mm in this case (it is the same key depth as the trajectory performed in annex F). Figure 5.6 (b) displays the fundamental frequency of the different string displacement signals measured when the key is pressed with the robotic finger with different velocities and the same key depth. The resulting fundamental frequency does not change, while the amplitude of the signal increases. This shows that the finger displacement is well repeated by the robot no matter the change in velocity. Moreover, it demonstrates that the clavichord paradox can be managed with appropriate trajectories. These results also confirm that the displacement of the key is directly linked to the string fundamental frequency. Conversely, as it is shown in figure 5.6 (a), changing the displacement of the key while maintaining the same velocity produces changes in fundamental frequency. However, fundamental

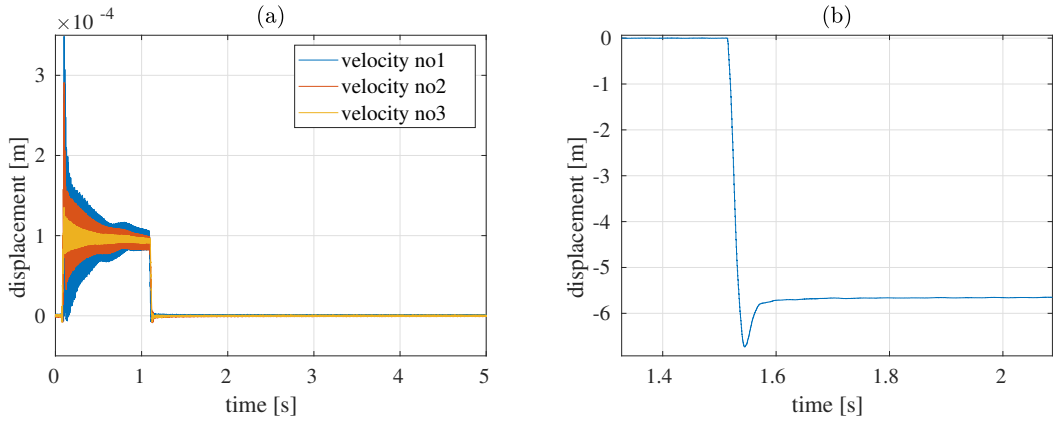

Figure 5.7: Temporal signals of the A2 string produced by the different velocities of the key (a). Displacement of the key (at the extremity of the finger) in the case of the referent trajectory performed by the robotic finger (b).

frequency is very stable in the case of the robotic finger compared to a musician's finger (compare figures 5.6 (a) and 5.4 (a)).

These results demonstrate that a robotic control is able to manage the clavichord paradox. Whether human and robotic control are comparable is questionable. In the present experiment, the robotic finger has no haptic or sound feedback: the trajectories are optimized directly, without any perceptual loop. On the contrary, human control relies much on audio and haptic feedback. The musicians tend to control the contact between the tangent and the string after the excitation by modifying the key position according to the perceived effect of their initial motion. This variation in time of the key position is probably an essential feature of the specific style of a musical performance. Another difference between the robotic finger and human finger is their mechanical and dynamical properties. Human fingers have a much limited range of velocity and acceleration than the robotic ones. Oscillations of the key-string-finger system that are observed in human control [3] seem negligible in the case of the robotic finger (see the displacement of the key in figure 5.7 (a)).

5.4 Conclusion

This chapter presented two experiments addressing the clavichord paradox, i.e. simultaneous control of velocity and displacement of the string and tangent when playing the instrument. In the first part, new measurements using a new methodology is used. Two types of finger trajectories have been used for performing two different motions : the pushed and the pulled gesture. This experiment confirms the dependence of displacement and velocity, and the possibility to modulate this dependence with appropriate gestures. In the second experiment, a robotic finger is used to further optimize the key trajectory, by modifying in terms of velocity and downward displacement a referent trajectory. In this case it seems possible to manage the clavichord paradox, and to control independently velocity and displacement, i.e. intonation and loudness of the instrument. Whether a musician would be able to effectively perform this type of movement remains an open question.

Part IV

Sympathy in the clavichord

Foreword

In the case of the clavichord, there is a part of the strings which is never excited called sympathetic strings. Because of the vibratory energy transmission by means of the coupling with the bridge, all the strings vibrate when exciting one of those strings. The played part of the strings do not vibrate that much because of the cloth damper. Given that the bass strings are less damped than the others, their sympathetic vibration is audible when listening to the sound. This contribution of the bass strings' sympathetic vibration is commonly called the "drum effect". Most importantly, the sympathetic part of the strings vibrate sympathetically following the excitation of one of the played strings. Their vibration contribute to the sound of the clavichord, and their effect have been notified by clavichord makers as it is shown by some historical treaties. This effect was first notified by Sebastian Virdung in 1511 in one of his musical treaty [6], where he talks about a *resonance* coming from the sympathetic strings. In 1768, Jakob Adlung used the expression *cum sympathia* to denote the sympathetic strings' effect [9].

Contrary to the square piano, these strings are not damped because their vibratory contribution leads to a reinforcement of the sound. This is opposed to the case of the square piano whereby all strings are damped, in order to get rid of the hazing sound effect resulting from the contribution of all these strings. This acoustic reality of the piano led to the creation of the forte pedal by Clementi in the 1830's. In the case of the clavichord, this reinforcement is desirable because of its low sound level production, which is one of the reasons why it was named "épinette sourde"[4] in the XVIIth century by Marin Mersenne [1]. The sound level measured 30 cm above the center of the soundboard is 60 dB SPL at maximum as to our studied instrument, which is a typical value for other clavichords [101].

It is possible to find studies tackling the phenomenon of the "halo of sound" in string instruments. Besnainou and Castellango highlight that this halo created by sympathetic strings influences the duration of the instrument sound [113], a similar conclusion by d'Alessandro's studying the clavichord [78]. Nevertheless, these authors consider this phenomenon as though it was similar to a "resonance". In a study focused on the influence in terms of timbre of sympathetic strings on the Indian instruments' sound, the term "resonance" is used once again [114]. By the way, this is the same term used by Virdung (*Resonanz*) referring to the sympathetic vibration causing the halo of sound. Yet, Gough uses the term "resonance" to designate something else in his study [62]. According to him, resonance refers to the string vibratory behaviour when one of its partials is coincided with one of the soundboard partials in terms of frequency. This resonant phenomenon mentioned by Gough does not refer to the production of the halo of sound coming from sympathetic vibrations.

[4] muffled spinet

Then, there is a difference between these two vibro-acoustic effects (halo of sound and resonance) produced by sympathetic vibration which needs to be clarified. In reality, many distinct acoustic and vibratory phenomena take place in this indirect vibration of strings by couplings, which is not precised in preceding studies on sympathy.

Distinction between reverberation and resonance

Two physical phenomena are present when it comes to sympathetic vibration : reverberation effect and the string resonance because of frequency coincidence. These two phenomena are conditioned by the soundboard which conditions the coupling as well as the vibratory amplitude of the string partials.

Soundboard

The coupled system strings-bridge-soundboard can be considered as a linear vibratory system, depending on the vibratory amplitude of the coupled system. Therefore, the relation connecting the excitation force at one location of the system with the resulting vibration at another location is given by a transfer function, also called Green function [115]. This transfer function characterises the system mobility. Each string is coupled to a specific location of the soundboard. Depending on the excited string, an excitation force is exerted on the bridge at this string coupling point. Then, depending on the excited string among all the strings played on the instrument, the vibratory response of the soundboard changes. In addition to this, depending on the fact that the coupling points are located near an anti-node or a node of vibration, the soundboard mobility favours or not the vibration of the sympathetic strings.

Reverberation effect

If the clavichord strings are not damped, then their contribution to the radiated sound can be shown. This contribution results in a halo of sound, in other words in a reverberation effect. This acoustic effect arises because of the overall sum of frequencies of the vibrating sympathetic strings, including their fundamental frequencies as well their first partials. Then, a large frequency range is involved in this reverberation effect. This large band effect in the frequency domain is created by the short term transitory phase of the excitation applied on the played string. As this transitory phase of the excitation is close to an impulse, this excitation is then large band in the Fourier domain. When it comes to the reverberation effect, the couplings between the strings and the bridge-soundboard are weak. In other words, there is no need of frequency coincidence between the strings' partials and that of the soundboard, then no pole (frequencies and dampings) of the coupled system modal basis is modified by means of resonance. However, depending on the location of the excited string coupling point, the amplitude and damping of the sympathetic string partials may vary.

Resonance : coupling by frequency coincidence

When a frequency coincidence occurs between the string partials and that of the soundboard, another coupling phenomenon takes place. If a string partial coincides with one of the excited string partials, then this partial amplitude increases and the vibratory amplitude of the sympathetic string increases. Regarding the radiated sound, this process results in a whistling corresponding to the partial frequency in question. Also, this frequency coincidence creates a change in frequency and damping associated to the partial in question. This consists in a veering of the modal basis' eigen values of the coupled system. This is what Gough refers to when mentioning the string resonance [62], regarding the frequency coincidence between a string partial and a body partial. This is what Weinreich referred to when it comes to the frequency coincidence of two string partials coupled to the same bridge [21]. It is said that these specific couplings between vibratory structures are stronger than those when there is no frequency coincidence between partials. To obtain these strong couplings, this frequency coincidence must be very precise, and the strength of this coupling is given by the veering indicator [63]. This kind of coupling is a short band phenomenon in the frequency domain, and it is associated to the long term of the permanent phase of the exciting signal. The amplitude of this sympathetic vibration by means of resonance may be varied because of the soundboard mobility, as it was shown between the F_3 S-string case and that of the D_4 S-string case in the study of the LAM1 clavichord.

The question is to determine by a vibro-acoustic study how is the sound of the clavichord modified by the sympathetic vibration of the sympathetic strings. To tackle this issue, there are two approaches that can be considered. First, the reverberation effect of the LAM1 clavichord, which corresponds to the overall effect of its sympathetic strings' vibration, can be studied. Instead of considering the individual vibratory response of a single sympathetic string, the sum effect of all these strings given by the soundboard vibration and the radiated sound is considered. On the other hand, the effect of a single sympathetic string on the sound when resonating is another topic. When the excited string fundamental frequency coincides with that of a sympathetic string, the latter vibratory response changes the clavichord radiated sound in a different way than the reverberation effect. As a result, two different effects can be used by means of the sympathetic strings to modify the radiated sound. The differences between these two effects are summarised in table 5.1. The first effect refers to the reverberation of the instrument and is tackled in chapter 6, whereas the second effect referring to the string resonance when frequency coincidence occurs is considered in chapter 7.

Reverberation effect	Resonance by frequency coincidence
Large band excitation	Short band excitation
Short term excitation	Long term excitation
Weaker couplings	Stronger couplings
Sum of all sympathetic string vibratory contribution	Increase of amplitude of the sympathetic string coupled partial
No change in frequency and damping	Veering of frequencies and dampings
Halo of sound	Whistling of the sympathetic string

Table 5.1: Features distinguishing the reverberation effect from the string resonance.

Chapter 6

Study of reverberation

6.1 Introduction

This chapter is devoted to the effect of all sympathetic strings' vibration on the clavichord sound. The purpose is to study how this overall vibratory effect influences the sound of the clavichord. To proceed, an experimental study is conducted, where the impulse response of the studied clavichord at one driven point of the bridge is studied. Measuring impulse responses at a driving point leads to a simplification of the vibrating system to a single vibrating point. This is practical when it comes to deconvoluting the impulse responses afterwards. The influence of the played part of the strings and that of the sympathetic part on the clavichord impulse response is considered by damping these strings by means of cloth damper. After presenting the experimental protocol in section 6.3.1, the impulse responses are analysed in different ways in section 6.3.2. As such, the influence of the sympathetic strings' vibration on the duration of the sound, its sound level and its spectral centroid are determined experimentally. These features could have been studied by means of the simulation. However, it requires to simulate the 74 strings of the LAM1 clavichord. This leads to computational difficulties, given the size of the computed matrices and the associated computational time. As a result, only an experimental approach is considered to study this effect. The results show that the overall contribution of the sympathetic strings' vibration, also called reverberation effect, can be characterised by means of the sympathetic strings' impulse response. It increases the duration of the clavichord sound as well as the instrument sound level. The spectral centroid is also changed by the sympathetic string vibration. This effect is associated to the reverberation of the instrument, whose effect is similar to that found in room acoustics. Then the sympathetic strings can be considered as a reverberator, which is a linear system convoluted to the signal of the excited string.

To facilitate the references to the different parts of the clavichord and to the specified phenomena, a specific terminology which is in accordance with figure 6.1 is proposed. The played portion of the strings (P-string) is the part bounded between the tangent and the bridge. This part of the string is excited by the tangent, and oscillates until the key is released. The motion of the played string leads to a force applied on its boundary condition, which moves the bridge and the soundboard. The damped portion of the strings, also called muffle part (M-string) is limited between the hitch-pin and the bridge, which is damped by the damper although sometimes weakly, particularly for bass tones. Then, the sympathetic portion of the string

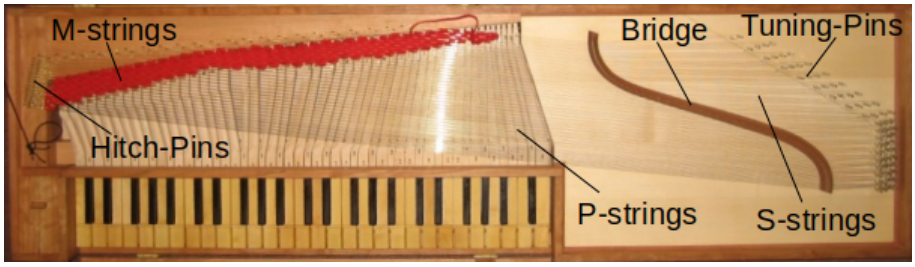

Figure 6.1: A view from above of the LAM1 clavichord with indications as to the substructures.

(S-string) is bounded between the bridge and the tuning pin. This section of the string is not excited directly, but indirectly by the motion of the bridge, induced by the P-strings.

6.2 Features of the clavichord

Organological features of the clavichord, and specifically of the LAM1 clavichord, were presented in sections 1.1 and 1.3. In this present section, some acoustic features of this instrument among which the frequency range of the sympathetic strings and a description of the clavichord excitation signal are given.

Sympathetic strings (S-strings)

To characterize the studied instrument, a determination of the fundamental frequency of all the strings has to be done. To do this, the vibration of each string is measured with a vibrometer, exciting the string with a finger. Then, to obtain the frequency of the string with precision, the signal is analysed with a high-resolution method [74].

In figure 6.2, the fundamental frequency of each played and sympathetic string of the LAM1 clavichord are represented, along with their three first partials, with respect to the note of the according string. In such a way, it gives a characterization of the frequencies involved in the effect produced by the sympathetic strings. Frequency relations can also be noticed in this figure. Notice that the fundamental frequencies of the sympathetic strings go between 350 Hz to 1200 Hz. It gives a lower limit as to the acoustic influence of the sympathetic strings in the clavichord sound. Given the partials of each strings, the higher limit depends on the partials' amplitude and damping. This is given by impulse response measurements.

Acoustics of the clavichord: transient and oscillatory responses

Different substructures of the clavichord are involved in the radiated sound. Among these, one can note the shock produced by the impact between the tangent and the string and the structural noise induced coming mainly from the case and the lid. Also there are the vibrations of the different parts of the strings : played strings and sympathetic strings. Their vibrations are radiated by the soundboard by means of the coupling with the bridge. Some reflections of the sound radiated occur because of the lid. Then, the key drop induces some structural noise coming from the case and the lid (see figure 1.3).

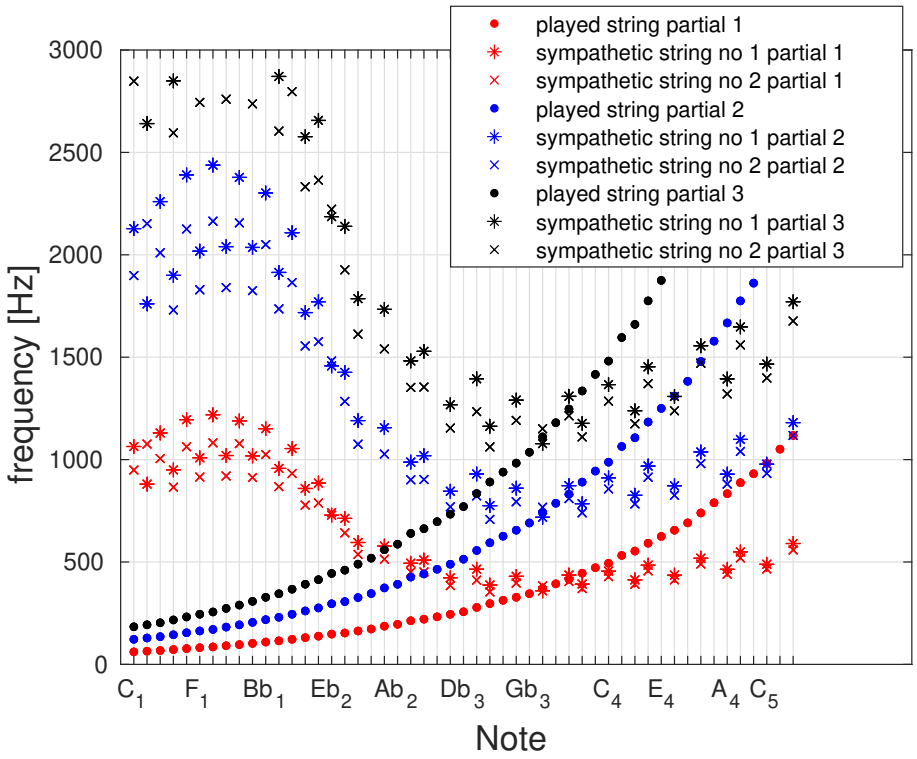

Figure 6.2: Fundamental frequencies of the sympathetic part and the played part of the strings with respect to the according notes.

The sound for a note is in three temporal phases : the first phase is the attack corresponding to the moment of the tangent-string impact. The second phase is the sustain where the string oscillates. Then the last one is the release, where the played string is being damped and the key drop noise is produced.

The attack phase is short, and the transient part of the attack is close to a Heaviside step in displacement (integral of a Dirac impulse, see figure 6.3 (c)). Then the acoustic response of the transient can be conveniently studied using impulse response analysis (i.e. response to a broadband excitation). This transient phase of the signal can give rise to body-induced partials, which has be shown to be an important feature in guitar tones [116]. The oscillatory phase is longer. The excited played string frequencies can "lock" to the S-strings' frequencies and exchange energy through sympathetic vibration. This is typically a narrow band responses (tuned response). The release phase is somehow close to the attack phase, but of weaker amplitude. Then both wide band analysis and narrow band locking or tuning (a few selected string sympathy) are expected. Sympathetic strings are not the only source of sympathetic vibration: some weakly damped string low frequencies are also likely to produce some sympathetic vibration. It should be noted that the excited signal has a double slop, separated at 100 ms after the excitation (see figure 6.3 (a)). As it was pointed out, this studied clavichord is fretted, meaning that a bundle of two strings are stroke for one note. It has been demonstrated that this coupling between the two stroke strings is responsible for the double slop phenomenon in the case of the piano [21].

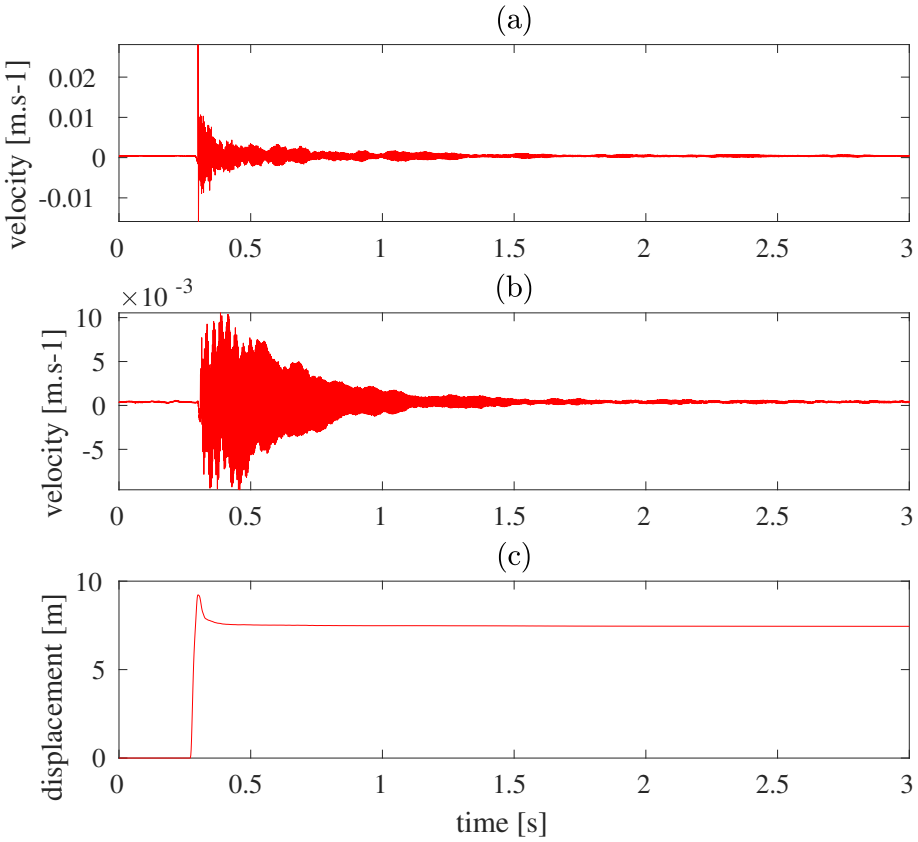

Figure 6.3: Temporal signal of a played string vibration (a), of a sympathetic string vibration (b), and of the tangent displacement (c).

6.3 Reverberation : experimental approach

6.3.1 Experimental set-up

Vibratory and acoustic impulse responses of the LAM1 clavichord are measured in order to study the effect of its sympathetic strings. Let us consider the following damping protocol with four different situations. First, all the strings are free, without being damped. Then, the P-strings only are damped. Next, the S-strings only are damped. Finally, all the strings are damped. The purpose of this protocol is to identify the vibratory effect of each part in order to evaluate the effect of the S-strings. All measurements are repeated three times, so that mean values and standard deviations for the different descriptors in section 6.3.2 can be computed. Measurements are done with an acquisition system with a sample rate of 51.2 kHz and a 24 bit depth. Impulses are given by an automatic impact hammer PCB 086E80. It gives impacts beside the measurement point on the bridge. One position of the bridge is chosen, which is the coupling point between the bridge and the $G\#_3$ P-strings. An accelerometer PCB M352C65 is used to measure the vibratory response of the soundboard at this location. A DPA 4006-TL microphone, connected to a PSP-2 amplifier, is disposed at 30 cm above the soundboard to measure its acoustic response. This experimental set up is shown in figure 6.4 and a simplified sketch of this experiment is shown in figure 6.5.

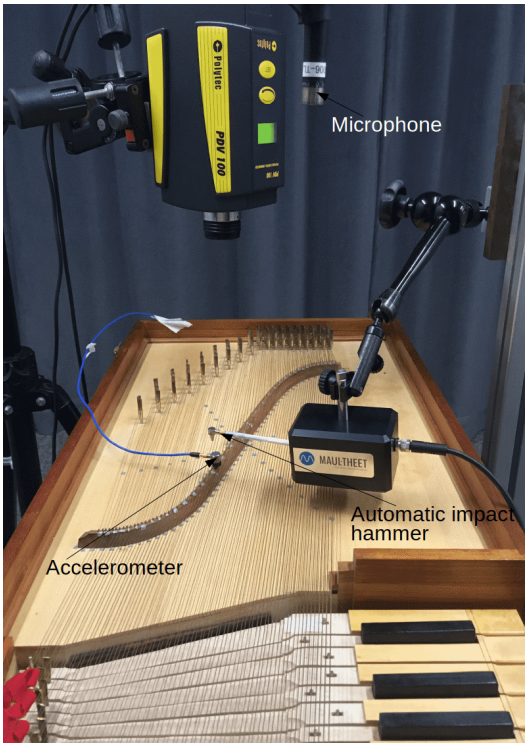

Figure 6.4: The overall experimental setup used for the impulse response measurements.

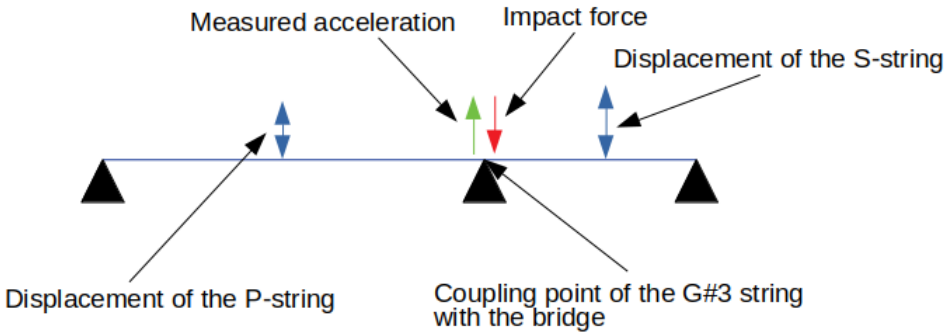

Figure 6.5: Sketch of the strings' profile where the acceleration of the bridge driven point created by the impact force of the hammer is measured.

6.3.2 Impulse response analysis

To start with, the different vibratory responses of the soundboard following the hammer impact are presented. In figure 6.6, an example of an impulse response measurement is given by presenting the measured force signal of the impact, the acceleration signal measured by the accelerometer and the sound pressure signal measured by the microphone. The spectrograms of the signals measured by the accelerometer created by the impact for each damping condition are presented in figures 6.7. One can see that the signal-to-noise ratio of the impulse responses become large from 5000-6000 Hz onward. This is caused by the bandwidth of the impact hammer, where its cutoff frequency is around 5000-6000 Hz. Then at this cutoff frequency, the signal-to-noise ratio increases. This bandwidth is similar to

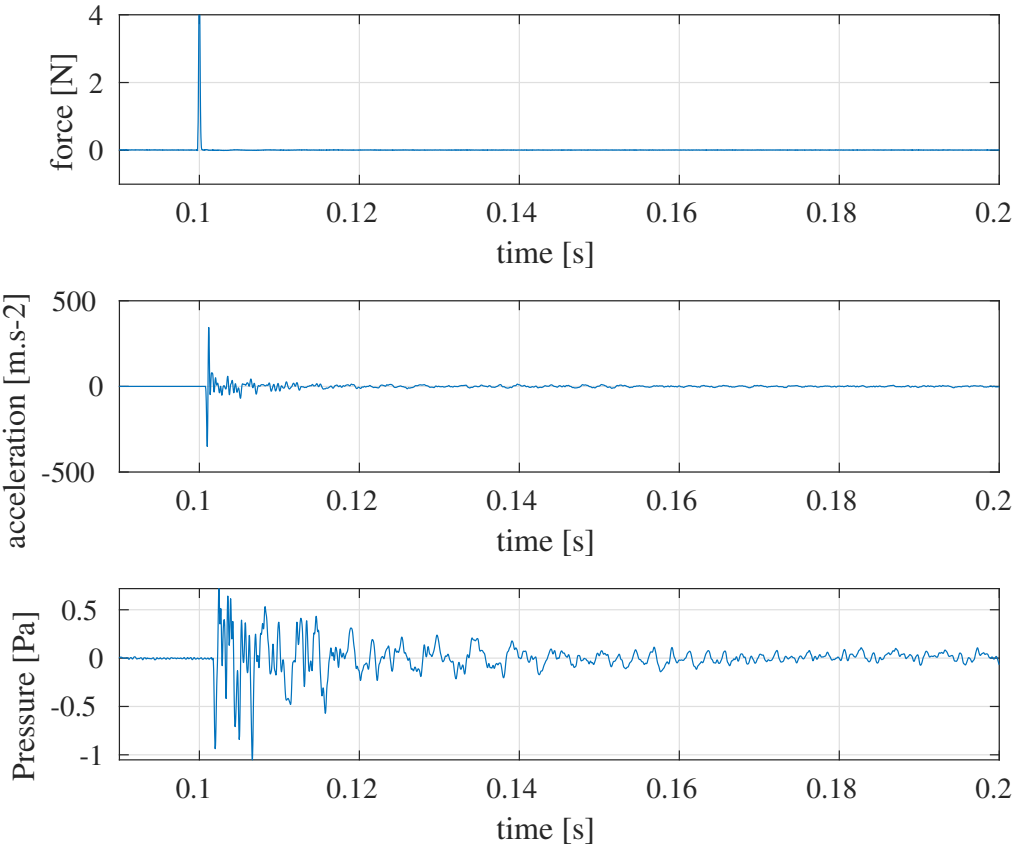

Figure 6.6: temporal signals of an hammer impact (upper graph), of the soundboard vibration at the measurement point (middle graph), and of the acoustic pressure at 30 cm above the soundboard (lower graph).

that observed with the impulse response measurements done in section 3.1.2.

Comparing spectrograms (a) and (b) in figure 6.7, one can see that much energy has been lost at very low frequency by damping the P-strings, mostly below 350 Hz. This comes from the drum effect. It refers to the contribution of the low P-strings which are weakly damped and that of the clavichord structural noise to the radiated sound. The P-strings having low fundamental frequencies are responsible for this energy provided to the signal. Comparing spectrograms (a) and (c), notice that the duration of the high frequency components (from around 1000 to 6000 Hz) of the signal have decreased by damping the S-strings. This is consistent, since these strings contribute to the energy of the signal at high frequencies. Figure 6.2 shows that the fundamental frequency of the S-strings go from around 350 Hz to 1200 Hz. Their first harmonics may well provide vibratory energy up to 6000 Hz. Then, spectrogram (d) shows that damping all the strings result in deleting almost all the high frequency energy, since only the modes of the soundboard contribute to the energy of the signal. Qualitatively, we would find similar observations with acoustic impulse responses, with nonetheless a low pass filtering due to radiation. To circumscribe the influence of the S-strings, it is possible to deconvolute the impulse response where the S-strings are free by the one where they are damped. To do

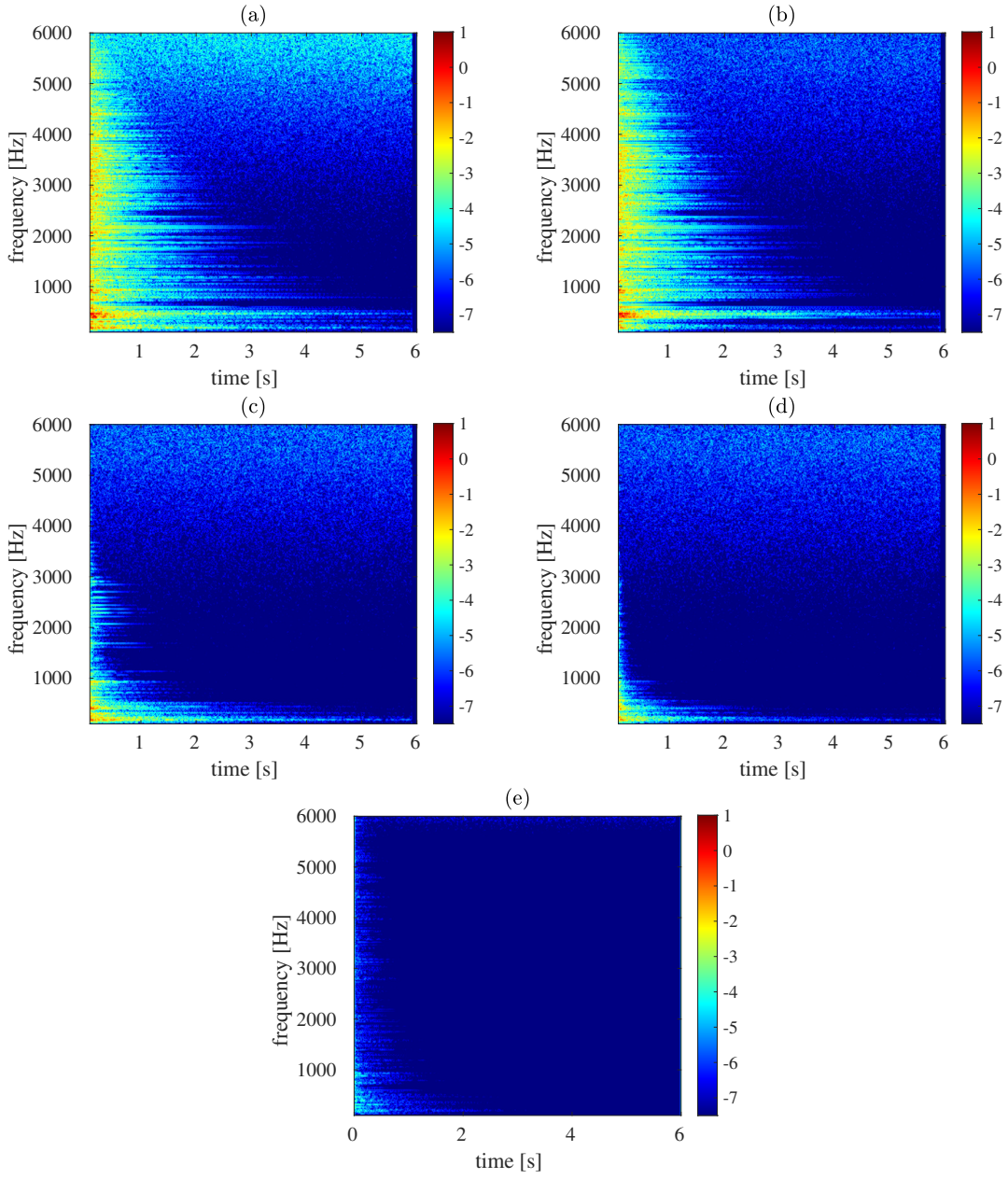

Figure 6.7: Spectrograms of the vibratory impulse response of the soundboard following the impact of the hammer where all the strings are free (a), where the P-strings are damped (b), where the S-strings are damped (c) and where the all the strings are damped (d), and spectrogram of the vibratory impulse response of the S-strings obtained by deconvolution (e) (ref 1 dB : 1 $\mathrm{m.s^{-2}.N^{-1}}$)

this, the first signal is divided by the second in the Fourier domain. Let $H_1(\omega)$ and $H_2(\omega)$ be the Fourier transform of the impulse response where the S-strings are free and where they are damped respectively. Then, the deconvolution is proceeded in the following way :

$$H_d(\omega) = \frac{H_1(\omega)}{H_2(\omega)} \tag{6.1}$$

where H_d is the FRF of the S-strings obtained by means of deconvolution. As a result, it gives the impulse response of the S-strings only, presented in spectrogram (e). Once again, the S-strings' influence is localized mostly between 350 Hz and 6000 Hz. Notice that there is almost no noise at 5000-6000 Hz in the deconvolted impulse response, since the noise of the two signals used for the deconvolution canceled.

Reverberation time of the impulse response

One way to describe the influence of the S-strings on the resulting sound is to measure the length of the signal and its intensity. To compute the decay of the signal, the Schroeder integration is implemented [117] which read as follow :

$$EDC(t) = \int_t^T h^2(\tau) d\tau \tag{6.2}$$

where EDC refers to the energy decay curve of the signal h, T is the total length of the signal and t is the starting time of the integration. Then, a linear regression of our decay curves could be done to compute the reverberating time $T60$ and $T20$, which are the times for the sound level of the signal to decrease by 60 dB and by 20 dB respectively [65]. Observing the EDC's in figures 6.8 and 6.9, some of these curves do no decrease linearly. This is mostly the case for the curves related to the 250 Hz, 500 Hz and 1000 Hz octave bands. In these cases, the reverberation time computed by means of a linear regression cannot be considered as a good indicator. The decay of our impulse responses are computed within the different octave bands to have a look at the influence of the S-strings on different frequency ranges (see figure 6.9).

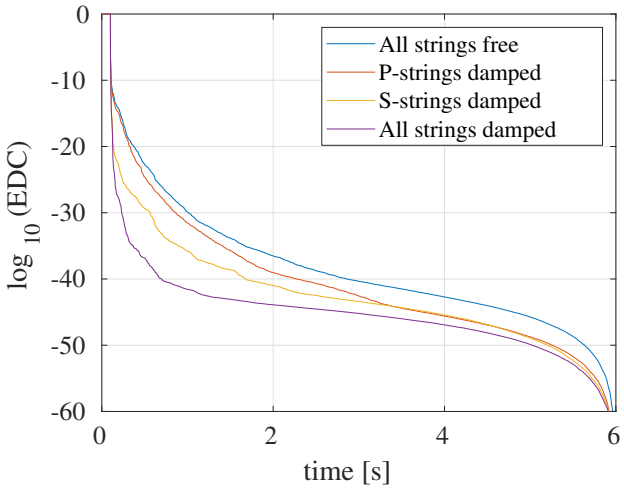

Figure 6.8: Energy decay Curves (EDC) of the different impulse responses with respect to the different damping conditions.

No matter the damping condition, the EDC is lower with respect to frequency, which is witnessing the fact that there is more energy in low frequencies than in high frequencies. Furthermore, in the 250 Hz octave band, the EDC is higher with the damped S-strings condition than the damped P-strings condition. Once again, the P-strings are responsible for the drum effect, which contributes mostly for the

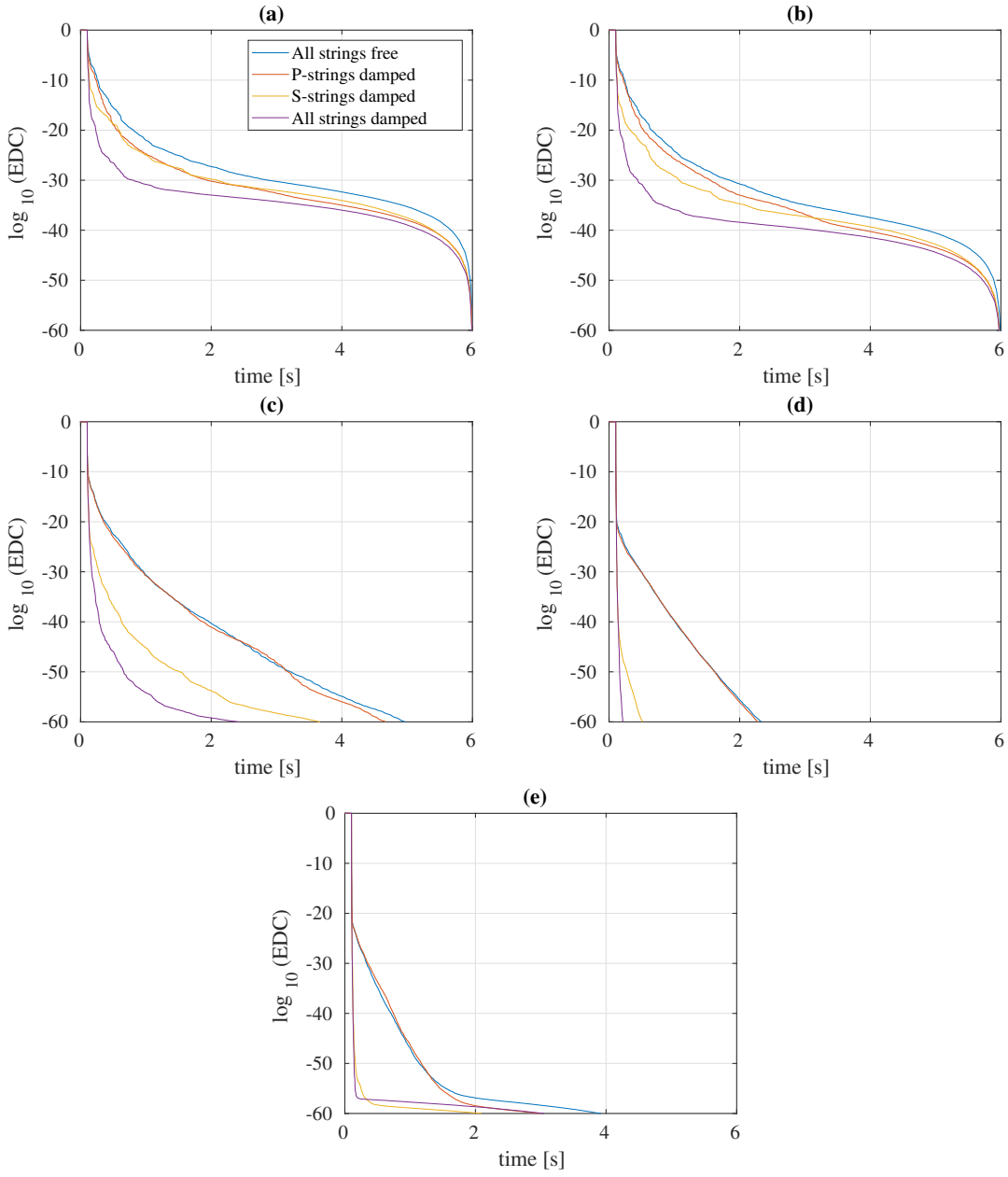

Figure 6.9: Energy decay Curves (EDC) of the different impulse responses with respect to the different damping conditions : (a) at the 250 Hz octave band, (b) at the 500 Hz octave band, (c) at the 1000 Hz octave band, (d) at the 2000 Hz octave band, (e) at the 4000 Hz octave band.

low frequency energy of the impulse response. The S-strings, limited to 350 Hz, do not provide energy to the low frequencies. It accounts for the fact that the EDC is higher at the 250 Hz octave band when damping the S-strings than when damping the P-strings. Yet, at higher octave bands, damping the S-strings ends up decreasing much more the EDC than by damping the P-strings. At the 500 Hz octave band, the EDC is higher when damping the P-strings than when damping the S-strings, suggesting that the S-strings provide more vibratory energy at that octave band than the P-strings. It seems consistent, since the drum effect created by the P-strings only regards very low frequencies, as it was seen in spectrograms

6.7 (a) and (b). So The P-strings do not effect the high frequency components of the signal as much as the S-strings. It also shows the importance of the S-strings' contribution in terms of the signal length. Also, there is no difference between the free strings condition and the damped S-strings condition in the 2000 and 4000 Hz octave bands in terms of EDC. So the limits in terms of frequency of the S-strings' contribution to the signal length can be noticed. These results show good consistency with similar measurements conducted done by d'Alessandro for another clavichord [78]. In a nutshell, figure 6.8 shows that the influence of the sympathetic strings' vibration is significant to the EDC of the clavichord sound.

Sound level of the impulse response

Then, a comparison of the different acoustic impulse responses in terms of sound pressure level is done. To do this, the sound level L_{eq} is computed in dB and in dBA, to take account of the human sensibility. Since the hammer impacts' amplitude associated to the different acoustic responses are not the same, this sound level is computed on the impulse responses given by the spectral division of the acoustic response and the hammer impact. As such, the different responses are normalised by their associated hammer impact, so that their sound levels are comparable. Given the acoustic impulse response $h(t)$, its associated equivalent sound level L_{eq} :

$$L_{eq} = 10 \log_{10} \left(\frac{1}{T} \int_{t_0}^{t_0+T} \frac{h(t)^2}{p_{ref}^2} dt \right) \tag{6.3}$$

where T is the integration time, t_0 is the time at which the computation begins and $p_{ref} = 20 \times 10^{-5}$ Pa. The computation of the sound pressure level of the different responses is done by beginning this computation after the excitation. The computation of the L_{eq} is computed 100 ms after the hammer impact. In such a way, the impact at the beginning is not taken into account and only the effect of the P-strings and the S-strings are considered. All L_{eq}'s are computed within a span of T = 1 s, which corresponds to a standard value when it comes to computing a L_{eq} with a slow weighting. The same parameters are chosen for the computation of the sound pressure level in dB and dBA. The computation in dBA is the same as that in dB (see equation 6.3), except that the A-weighting accounting for the relative loudness perceived by the human ear is applied on the pressure signal.

In figure 6.10, the different L_{eq} for each acoustic impulse response are presented. The sound pressure level decreases with respect to the succeeding damping conditions. In the free strings' case, the sound level is 18 dB, and it is almost the same in dBA. However, when damping the P-strings, the sound level is 17.5 dB and 15.8 dBA. Since the L_{eq} computation in dBA mainly considers the high frequencies' influence, the damping of the P-strings do not affect much the value of the sound level in dBA. Since this computation in dB considers the low frequencies' influence, then the L_{eq} in dB decreases when damping the P-strings. By the way, that also accounts for the difference of their standard deviations. The filtering of the low frequencies in the dBA computation leads to considerate the signal with a smaller band width, which decreases the incertitude. When damping the S-strings, the value of the L_{eq} goes down to 15.1 dB and down to 9.0 dBA. Inversely, since the S-strings contribute to providing vibratory energy to the high frequencies, the damping of the S-strings

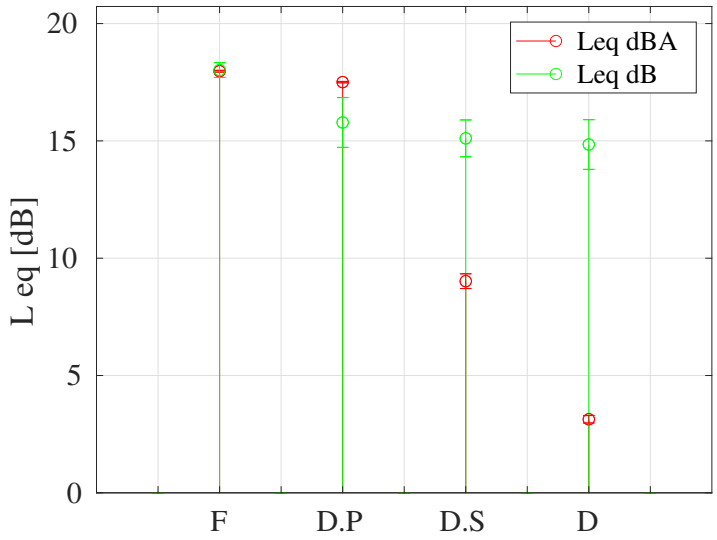

Figure 6.10: Sound level of the different impulse responses of the clavichord in dB SPL and dBA (ref 1 dB : 20 $\times 10^{-5}$ Pa.N^{-1}) with respect to the different string damping configurations (F: free strings, D.P: damped P-strings, D.S: damped S-strings, D: damped strings), where the some computations start at the excitation and others 150ms after the excitation (duration 1s).

affects more the L_{eq} computation in dBA than that in dB. Damping all the strings leads to sound level in dBA to dwindle down to 3.1 dB. The sound level in dB seems to have decreased down to 14.8 dB. Yet, given this small decreasing in dB compared to the standard deviation in the damped S-strings case and in the all damped strings case, this last observation cannot be confirmed. Any way, the difference of the L_{eq} between the case where the S-strings are damped and that where all strings are damped is not so significant. Finally, observing generally that the sound level decreases by damping the strings, it puts forward the fact that the sympathetic vibration of the strings contribute to some extant to the clavichord sound level.

Spectral centroid of the impulse responses

The spectral centroid (SC), which represents the centre of gravity of the spectrum, is introduced and defined as [118] :

$$SC = \frac{\sum_{k=1}^{N} f_k a_k}{\sum_{k=1}^{N} a_k} \tag{6.4}$$

It is computed from the discrete spectrum of the impulse response signal. The terms f_k and a_k are the frequency and amplitude respectively in bin k. The spectral centroid are computed for the different acoustic responses measured by the microphone, where the computation is limited to the spectral bandwidth given by the hammer impact which is between 0 and 6000 Hz. The mean value and the standard deviation of the computed spectral centroids obtained for the different string damping configurations are presented in figure 6.11. The spectral centroid when all the strings are free is placed at 646.5 Hz whereas that when the P-strings are damped

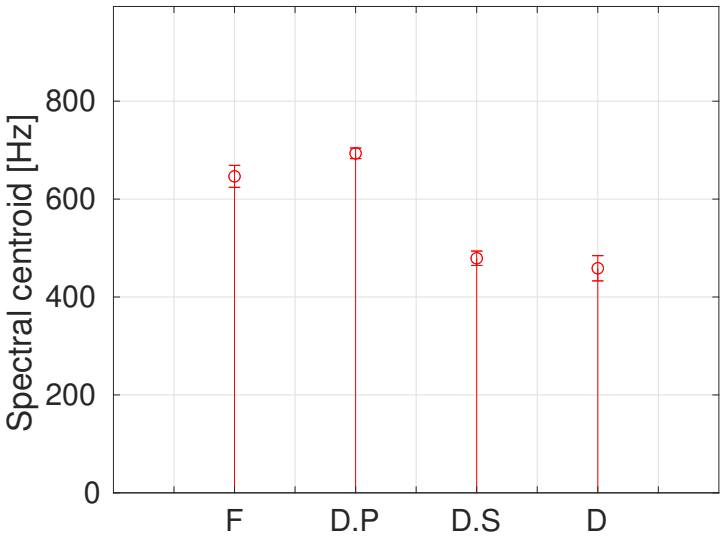

Figure 6.11: Spectral centroids of the acoustic responses measured by the microphone with respect to the different string damping configurations (F: free strings, D.P: damped strings, D.S: damped strings, D: damped strings).

is placed at 693.5 Hz. Since the P-strings are related to the drum effect responsible for providing low frequency energy to the clavichord sound, damping these strings leads to cancelling this low frequency energy. Given the fact that the S-strings are still present, there is still energy at high frequencies. As a result, this lack of this P-string low frequency leads the clavichord spectral centroid to go up. When damping the S-strings, the spectral centroid goes down to 479.1 Hz. Diminishing the high frequency energy of the sound by damping the S-strings, this leads the spectral centroid to decrease. Finally, damping all the strings, there is a little decrease of the spectral centroid down to 458.7 Hz. This can be explained by the cancelling of the few high frequency energy provided by the P-strings, which is very little. Only the soundboard modes are present when all the strings are damped. Although there seems to be a small decrease, this observation can be criticized by means of the corresponding standard deviation, which overlaps the spectral centroid value when S-strings are damped. As a result, the spectral centroid indicates a specific change in the clavichord timbre by means of the strings vibrating sympathetically.

6.4 Response of each sympathetic string

Studying the overall effect of the S-string vibration resulting in a reverberation effect gives one consequence of the sympathetic vibration. However, this does not give information to the individual response of each string. The objective of this section is to observe the response of each individual string of the instrument when exciting a particular P-string.

A vibrometer (Polytech PDV 100) is used to measure the vibratory velocity in the vertical polarization of each S-string in response to the excitation of the $G\#_3$ string (see figure 6.12). For each excitation, the velocity of vibration of one the 74 S-strings of the LAM1 clavichord is measured at 2 cm from the bridge. Given the repeatability of the robotic finger, each of these vibratory measurements are done by means of the same excitation. As a result, the individual S-strings responses to the same string excitation are measured in such a way.

In figure 6.13, the measured velocity signals are shown. Then, figure 6.13 shows the temporal energy of each of the 74 strings given by the same $G\#_3$ string excitation. Much of the strings have a vibratory velocity amplitude reaching a maximum value of around 0.01 $m.s^{-1}$. Yet, two of the S-strings receive more energy than the other, reaching an velocity energy amplitude of around 0.025-0.03 $m.s^{-1}$.

Remember that the signal of the excited $G\#_3$ string has a transitory part. This transitory part has a similar effect with that of an impulse response. This part is short term, so the frequency band input is large. As a result, vibratory energy is still given to all substructures in a large band configuration because of the excitation transitory part. This transitory part is responsible for the reverberation occurring in the clavichord. Furthermore, the permanent phase of the excitation is long term and periodic, so the frequency band input becomes narrow, centered on the excited string fundamental frequency and its harmonics. So energy is transmitted to all substructures at these specific frequencies because of the excitation signal permanent part. The great majority of the S-strings have an amount of vibratory energy approximately similar among them. This comes from the energy transmission created by both the transitory part and the permanent part of the excitation signal. However, the two strings having higher vibratory amplitudes compared to the other strings is explained by frequency coincidence. These strings are the sympathetic part of the first excited $G\#_3$ string and that of the first B_3 string respectively. The former fundamental frequency is 387.7 Hz and that of the latter is 390.4 Hz. In this experiment, the excited $G\#_3$ string is tuned at 389 Hz. Because these two strings have a fundamental frequency close to that of the excited string, these strings resonate and therefore their amplitudes become higher. The frequency coincidence between these strings' first partials is responsible for this increase of vibratory amplitude. The closer these partial frequencies, the larger these partial amplitudes. This connection between frequency coincidence and high partial amplitude can be seen in figure 6.14. The two partials located at the $G\#_3$ and B_3 strings have higher energy than all other partials. Yet, these two partials' frequencies are the closest to that of the excited string. Then the relation between frequency coincidence and partial high amplitude is noticeable. As a result, the permanent part of the excitation signal is responsible for these large amplitudes. Then, independently of reverberation, the sympathetic vibration of the strings becomes different because of frequency coincidence between their partials. This was put forward by Gough, where he explained with his model

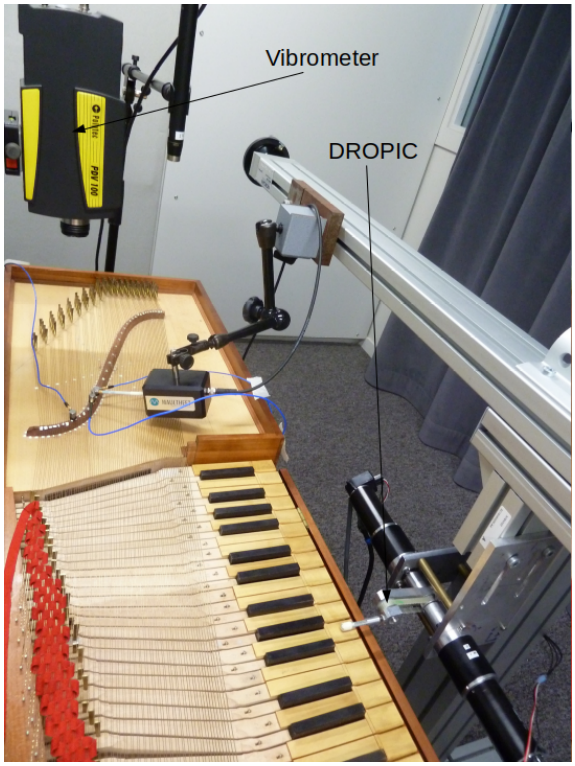

Figure 6.12: Measurement with the vibrometer of each sympathetic to the G#$_3$ string excitation by the robotic finger.

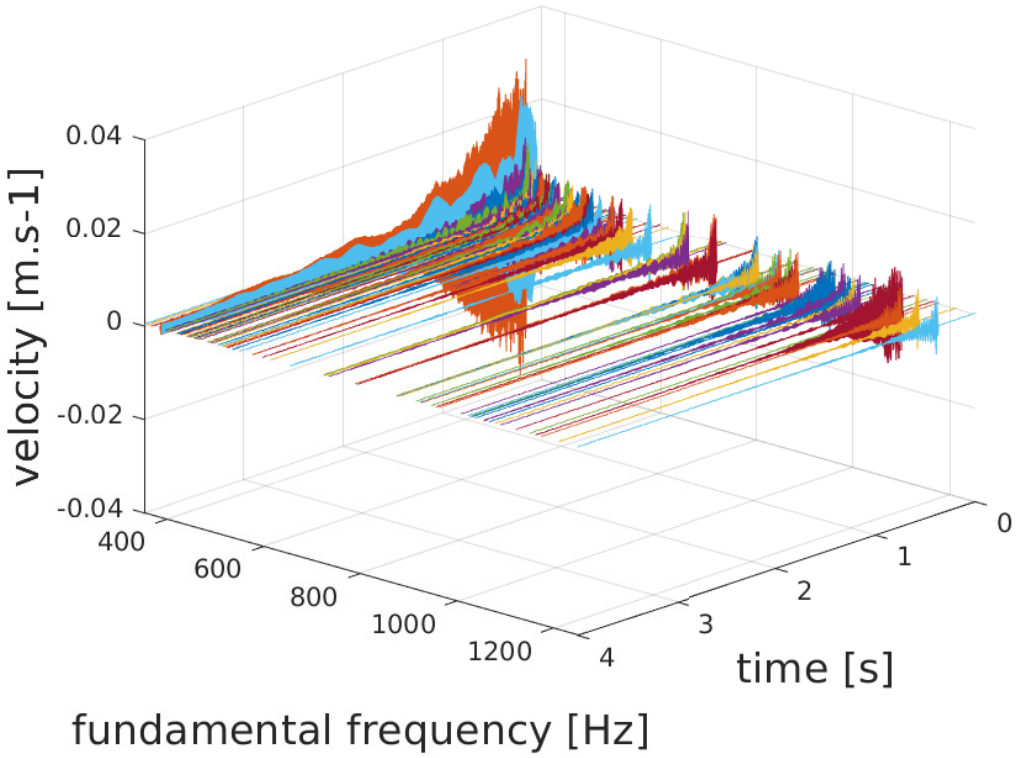

Figure 6.13: velocity signal of each sympathetic string in response to the G#$_3$ string excitation, each measured at 2 centimeter from the bridge.

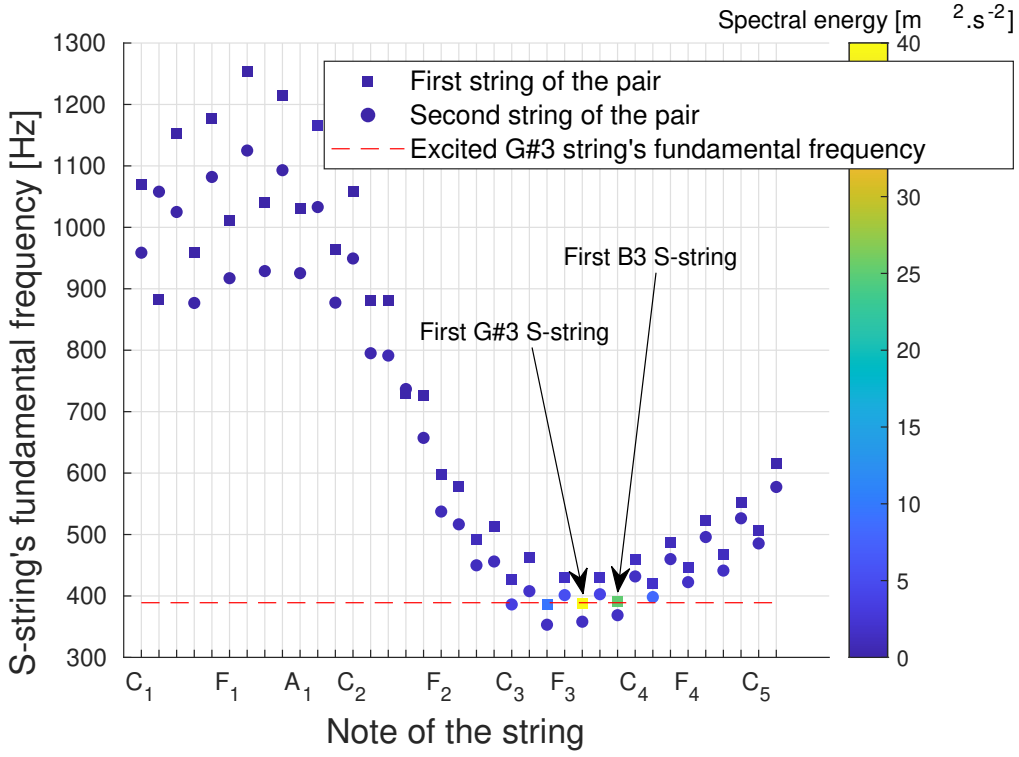

Figure 6.14: Velocity spectral energy of the S-string first partial in response of the G#$_3$ string excitation tuned at 389 Hz, with the G#$_3$ S-string tuned at 387.7 Hz and the B$_3$ S-string tuned at 390.4 Hz.

that the string resonance occurs by means of this frequency coincidence, which leads to this increase in the coincided partial amplitude [62].

An interesting difference between the sympathetic vibration of the first G#$_3$ and first B$_3$ S-strings can be observed in figure 6.15. The temporal shape of the B$_3$ S-string vibratory velocity signal is increasing in a span of time of 0.2 s. In contrast, that of the G#$_3$ S-string is already at its maximum amplitude in 1 ms after the excitation. Because the G#$_3$ S-string is the sympathetic part of the excited string, there is an added vibratory effect given to this S-string. The corresponding bridge hitch-pin being the only thing separating the played part and the sympathetic part of the G#$_3$ string, a specific effect coming from the transitory part of the excitation is transmitted to this S-string. Adding the frequency coincidence between these two strings, a specific sympathetic vibration in the case of the G#$_3$ S-string is then created.

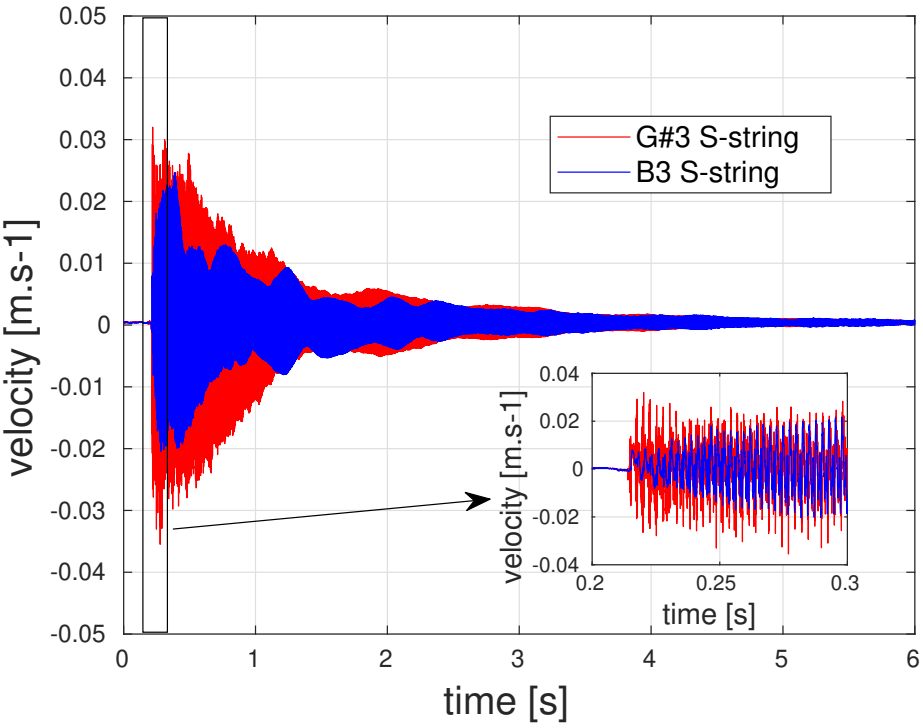

Figure 6.15: Comparison of the first G#$_3$ S-string velocity of vibration and that of the first B$_3$ S-string, measured at two centimeter from the bridge, after the G#$_3$ P-string excitation

6.5 Conclusion

The reverberation effect of the LAM1 clavichord was studied in this chapter. This effect comes from the overall contribution of all the strings vibrating sympathetically following the excitation of one clavichord played string. The impulse response approach was taken in section 6.3 to study this specific effect. After presenting the experimental protocol in section 6.3.1, an analysis of the measured vibratory and acoustic impulse responses was done in section 6.3.2. The reverberation was characterised by means of energy decay curves, sound pressure level and spectral centroid. In general, damping the S-strings lead to decreasing all these parameters of the clavichord sound. The specific role of the P-strings, responsible for the drum effect, was identified by means of this approach. Then, the results show the extant in which the sympathetic strings contribute to the clavichord sound, creating the reverberation of the instrument. By means of the observation of each singular S-string vibratory response to the same excited string in section 6.4, it was shown that reverberation is not the only vibro-acoustic consequence of the S-string vibration. There is another one related to the string resonance, a topic which is tackled in the next chapter.

Chapter 7

Study of resonance

7.1 Introduction

A different kind of coupling occurs when frequency coincidences between string modes take place in a coupled system. In this respect, different cases need to be distinguished to study the sympathetic phenomenon in terms of coupling between modes. In the first case, it is about a frequency coincidence between an excited string and a sympathetic string, without a coincidence with a mode of the soundboard. Then, the coupling between the soundboard and the two strings is weak. However, the coupling between the two strings yields a change in the coupled partials' frequency and damping. This change in frequency and damping depends on the precision of the superimposition of the two partials' frequency. This precision in frequency coincidence also influences the beats, the amplitude and the velocity of growth of the sympathetic string vibratory signal. Moreover, the vibratory amplitude of this string can vary with respect to the amplitude of the bridge mobility at the coupling point. Nearby an anti-node, the string coupling point moves with more amplitude, whereas nearby a node, it moves with less amplitude. The amplitude of motion of the coupling point can affect that of the whole string. Thereby, if the coupling point is located near an anti-node, the vibratory amplitude of the string will be larger. On the other hand, nearby a node, this amplitude will be smaller. These specific situations is a phenomenon that has been studied in the case of string sympathetic vibration of a concert harp [74]. The change in frequency and damping caused by the frequency coincidence between two modes has been explained by means of Weinreich coupling model [21]. In the second case, the influence of coupling between the bridge and the string on the string vibration is considered. With respect to the proximity of the frequencies' string modes and that of the bridge, the modal basis can favor the string vibration. This study of string/body coupling modes is dealt with by Le Carrou in the study of the concert harp [67]. Like the coupling between two strings, the string/bridge coupling yields a change in the partial frequency and damping. This change of these modal parameters varies depending on the fact that the coupling is strong or weak. To determine the strong or weak nature of this coupling, the veering indicator is used [63]. Veering corresponds to the phenomenon where the eigen values of a vibratory system are deviated after modes superimposition. This veering phenomenon is found in other fields : molecular physics, vibration of membrane, and the study of cable vibration [64]. Then, these different cases can be studied either with an experimental approach or with

simulations of a model. The objective is to study the influence of tuning and of the bridge coupling admittance on the sympathetic string vibration.

In section 7.2, theoretical considerations given in the literature regarding the coupling of a string with a bridge are presented. Then, section 7.3 deals with the experimental approach used to measure the impulse response of the LAM1 clavichord bridge and the response of two studied sympathetic strings to an excited string with different tuning configurations. The data processing of these measurements is presented as well. In section 7.4, an analysis of the influence of the LAM1 clavichord bridge coupling admittance on the amplitude and the damping of the studied sympathetic strings partial is given. Next, measurements and simulations of the clavichord model are used in section 7.5 to analyse the partial parameters of the studied sympathetic strings and their resonant responses with respect to tuning and the bridge coupling admittance.

7.2 Theoretical considerations

To study string resonance in the clavichord and the way it is influenced by the coupling with the bridge, some models elaborated in the literature need to be recalled. In section 7.2.1, the veering indicator is presented and used in the case of the LAM1 clavichord to evaluate if a string-bridge coupling is strong or weak. Then, the Weinreich model regarding piano string coupling is presented in section 7.2.2. A simulation of this model is compared with that of the model based on the U-K formulation in section 7.5.2 to evaluate the effect of resonance produced by the second model. Finally, in the case of weak couplings, the Valette and Cuesta model is presented in section 7.2.3. It is used to study the impact of the bridge mobility in the string dampings in section 7.4.

7.2.1 Veering indicator

To find an adequate indicator to study the weak or strong nature of the coupling between the string and the bridge, Woodhouse's approach, rewritten by Paté, is considered [63, 90]. The modal basis of a single string and that of a bridge are presented. Then, coupling the two substructures leads to the analytical determination of the modal mass matrix and stiffness matrix associated to this constraint system. Then, the constrained system modal basis is reduced to one string mode and one bridge mode, since only the coincidence of these two modes are necessary. That leads to reducing the order of the modal matrices. Postulating the Basile hypothesis [119], the modal damping matrix of the constraint system can be written. By determining the eigen values of the modal equations associated to this constraint system and supposing a frequency coincidence between these two modes, the veering indicator can be derived :

$$\alpha = \frac{2\rho SL}{n^2\pi^2(m_k + \frac{\rho SL}{3})} - (\xi_n - \xi_k)^2 \tag{7.1}$$

Where ρ is the density of the string, L is the string length, S is its section, n is the number of the mode, m_k is the modal mass associated to the bridge mode, ξ_n is the damping of the string mode, and ξ_k is the damping of the bridge mode. In

any case, if there is no frequency coincidence between the string modes and that of the bridge, then the coupling between the two structures is weak. Strong couplings take place only when frequency coincidence between their partials occurs and if the veering indicator α is positive. If α is positive, then the coupling between the string and the bridge is strong and the change in modal parameters occurs mainly in terms of frequency. On the other hand, if α is negative, then the coupling is weak and the change occurs mainly in terms of damping. Assuming that the Basil hypothesis is valid, which assumes that the real modal basis of the system yields a diagonal matrix, the formulation of the mobility $Y(\omega)$ of the structure in the case of a driven point is :

$$Y(\omega) = \sum_{n=1}^{N_b} \frac{j\omega\phi_k^2}{m_k(\omega_k^2 + 2j\omega\omega_k\xi_k - \omega^2)} \tag{7.2}$$

where N_b is the number of bridge mode, ω is the pulsation and ω_k is the modal pulsation of the bridge. With respect to this formulation, the mode shapes ϕ_k and modal masses m_k are normalised in a specific way [63] :

$$m_k = \frac{1}{\phi_k^2} \tag{7.3}$$

Assuming that the residues A_k are real, its expression at the driven point is :

$$A_k = \frac{\phi_k^2}{m_k} \tag{7.4}$$

Thus, the normalised mode shapes are deduced :

$$\phi_k = A_k^{1/4} \tag{7.5}$$

Then, after computing the poles of the mobility $Y(\omega)$ by means of the LSRF (Least Square Rational Function) and then deriving its real residues as it was done in section 3.1.2, the damping ξ_k and m_k are known and ξ_n is extracted from the study of the string dampings (see section 3.1.1). These are the parameters that are used to compute the veering indicator α.

In figure 7.1, the veering indicator is calculated for each n and k and for the three considered strings : G#$_3$ P-string, D$_4$ S-string and F$_3$ S-string. For the positive values, if there is a frequency coincidence between the specific string and the bridge, then the coupling becomes strong. In our case, D$_4$ S-string is tuned around the target frequency 371 Hz. Since there is no bridge modes around this frequency, the coupling with this string is then weak. When it comes to the G#$_3$ excited string and the F$_3$ S-string, the target frequency is around 392 Hz. There is a bridge mode located at 409 Hz (see the bridge modal basis extracted in section 3.1.2 presented in figure 3.7). So by moving upward the F$_3$ S-string frequency, it is possible for this string mode to coincide with this bridge mode. At 409 Hz, the indicator α is negative. So the coupling between the bridge and the string at 409 Hz is still weak.

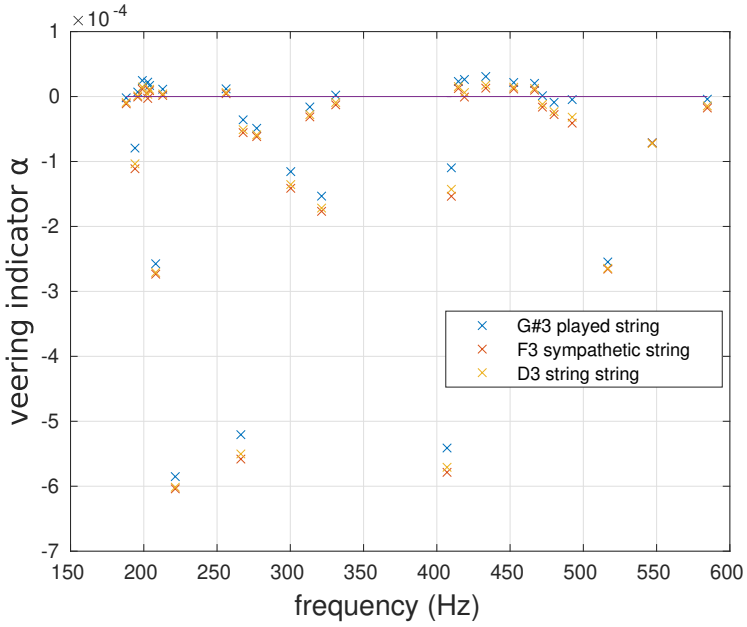

Figure 7.1: Computation of the veering indicator α for the three considered strings.

7.2.2 Weinreich string coupling model

The assumption of this model is that the two strings are attached to the same coupling point, so their related coupling admittance is the same. A dynamical matrix Ω for the simplified two-string model was derived in this study :

$$\Omega = \begin{pmatrix} 2\epsilon + \zeta & \zeta \\ \zeta & \zeta \end{pmatrix} \tag{7.6}$$

this matrix being used to couple the modal equations of the two strings. In the dynamical matrix, the mistuning ϵ and a term ζ including the admittance Y of the bridge, the string modal pulsation ω_0 and the characteristic impedance Z_0 of the string are introduced :

$$\zeta = j\omega_0 Z_0 \frac{Y}{\pi}, \quad \epsilon = f - f_0 \tag{7.7}$$

where f is mistuned frequency of the first string and f_0 is the frequency of the second string. Noticing that ζ is complex, it is possible to write $\zeta = \xi + j\eta$. The real part ξ can be positive or negative, where a positive value leads to a masslike support and a negative value leads to a springlike support. The imaginary part η is a measure of dissipation at the support ant its value must be positive. Looking for the eigen values of the dynamical matrix, the two corresponding eigen values $\beta_\pm$ are derived [21] :

$$\beta_\pm = \epsilon + j\eta \pm \sqrt{\epsilon^2 + \xi^2 - \eta^2 + 2j\xi\eta} \tag{7.8}$$

$\beta_\pm$ is complex. The real part of it gives the frequency deviation of the two strings with respect to the mistuning ϵ and its imaginary part gives the damping deviation of these two strings with respect to ϵ.

7.2.3 Weak coupling

If the coupling is weak, then the moving string extremity can be described as a small perturbation to the string wave number [58] :

$$k_n = k_{0,n} + \delta_n \tag{7.9}$$

where $k_{0,n}$ is the string wave number without perturbation, δ_n is the perturbation of the string provoked by the moving extremity, and k_n is the string wave number resulted from this perturbation. Then, it is possible to determine the expression of the string dampings with respect to the mobility of the bridge at the coupling point. Let Q_n be the total quality factor of the string, $Q_{0,n}$ the quality factor of the string without the influence of the coupling with the structure, c the velocity of the wave propagation in the string, $Y_c(L, \omega_n)$ the mobility of the bridge expressed at the coupling point and at modal pulsation ω_n, ρ_l the linear density of the string, and f_n the modal frequency of the string. Coming back to the approach developed by Valette and Cuesta [58, 65], the following expression can be established :

$$Q_n^{-1} = Q_{0,n}^{-1} + \frac{c^2 \rho_L}{\pi L} Re[Y_c(L, \omega_n)] \frac{1}{f_n} \tag{7.10}$$

Also, the mobility of the string $Y_c(x, \omega)$ at a driven point can be written like this :

$$Y_c(x, \omega) = \sum_{n=1}^{N_c} \frac{j\omega \phi_n(x, \omega)^2}{m_n(\omega_n^2 + 2j\omega\omega_n\xi_n - \omega^2)} \tag{7.11}$$

where N_c is the number of string modes, m_n the string modal masses and $\phi_n(x)$ the string mode shapes. At a frequency coincidence, $\omega = \omega_n$ and that yields :

$$|Y_c(x, \omega_n)| = \frac{\phi_n(x, \omega)^2 Q_n}{2 m_n \omega_n} \tag{7.12}$$

where $Q_n = \frac{1}{2\xi_n}$. Equation 7.12 shows that the amplitude of the partial given by $|Y_c(x, \omega_n)|$ is proportional to its quality factor. As a result, if the damping of the sympathetic string partial becomes smaller, then its amplitude becomes larger. Also, when $\omega = \omega_n$, $|Y_c(x, \omega_n)|$ reaches a maximum of amplitude, which is expected when it comes to sympathy created by frequency coincidence. After presenting these preliminary theoretical considerations, an experimental approach is conducted in the next section to study the string sympathetic response with respect to tuning and with respect to the bridge coupling admittance.

7.3 Experimental approach

7.3.1 Experimental protocol

The LAM1 clavichord is placed in an acoustic isolated room (see figure 7.2). The robotised finger DROPIC [120] is used in order to repeat the same trajectory for the excitation. In this experience, the finger presses only the G_3 key of the instrument. Since the clavichord is fretted, the considered excited string can be called G_3 or $G\#_3$ indifferently. One of the two $G\#_3$ strings is damped to simplify the study of coupling. Three accelerometers (PCB M352C65) are laid out on the bridge at three precise positions : at the $G\#_3$ excited string coupling point, at the F_3 S-string coupling point and that of the D_4 S-string. An automatic hammer impact (PCB 086E80) is placed at the $G\#_3$ string coupling point, so that it becomes a driven point. A laser vibrometer (Polytech PDV 100) is used to measure the velocity of vibration at one point of the studied sympathetic strings. As for the F_3 S-string, the vibrometer measures its vibration at 3.2 cm away from the tuning pin. As for the D_4 S-string, it is measured at 4.5 cm away from the tuning hitch-pin. A microphone (DPA 4006-TL) is placed at 30 cm above the soundboard to measure the radiated sound. The different tunings of the considered strings are presented in table 7.1. Studying the case of the F_3 string, the excited string is tuned at 392 Hz. In the case of the D_4 string, the excited string is tuned at 371 Hz. With respect to $A_3 = 415$ Hz tuning, the frequency 371 Hz corresponds to the G_3 pitch, and 392 Hz corresponds to the $G\#_3$ pitch. So the tuning of the excited string is done in a musical context. After this tuning, for each case, the studied sympathetic string is being tuned around the target frequency of the excited string. For each of the 9 tunings of each of these strings, a vibratory measurement is done. The impulse response measurements are done in two situations : with all strings free and with all strings being damped. For measurements pressing the $G\#_3$ key with the robotic finger, only the case where all strings are free is considered.

One of the hardships of this experimental approach is to conduct these measurements in a reduced time span. Indeed, the hygrometry and the temperature of the room where the clavichord is placed change with respect to time. These two parameters influence the vibratory properties of the instrument. For the hypothesis of the invariance of the system vibratory properties with respect to time to remain true as much as possible, all the measurements were done in a single day. That is the reason why a small number of tunings between the strings around the target frequency, namely 9, is decided. The target frequency corresponds to the excited string frequency. For each tuning, 5 successive measurements are done for the computation of incertitudes.

String	Length (m)	diameter (mm)	Frequency of excitation (Hz)	Material
$G\#_3$ P-string n^{o}1	31,8	0,33	371 - 392	Brass
F_3 S-string n^{o}2	30,1	0,30	-	Brass
D_4 S-string n^{o}1	29,9	0,27	-	Brass

String	Tuning frequency of the S-string (Hz)
F_3 S-string n^{o}2	386.4 | 388.3 | 392.6 | 393.4 | 393.9 | 395.8 | 395.9 | 399.0 | 401.0
D_4 S-string n^{o}1	363.3 | 367.7 | 369.5 | 370.9 | 371.6 | 372.9 | 375.9 | 377.0 | 380.0

Table 7.1: Table summarising the strings' parameters for the experimental protocol

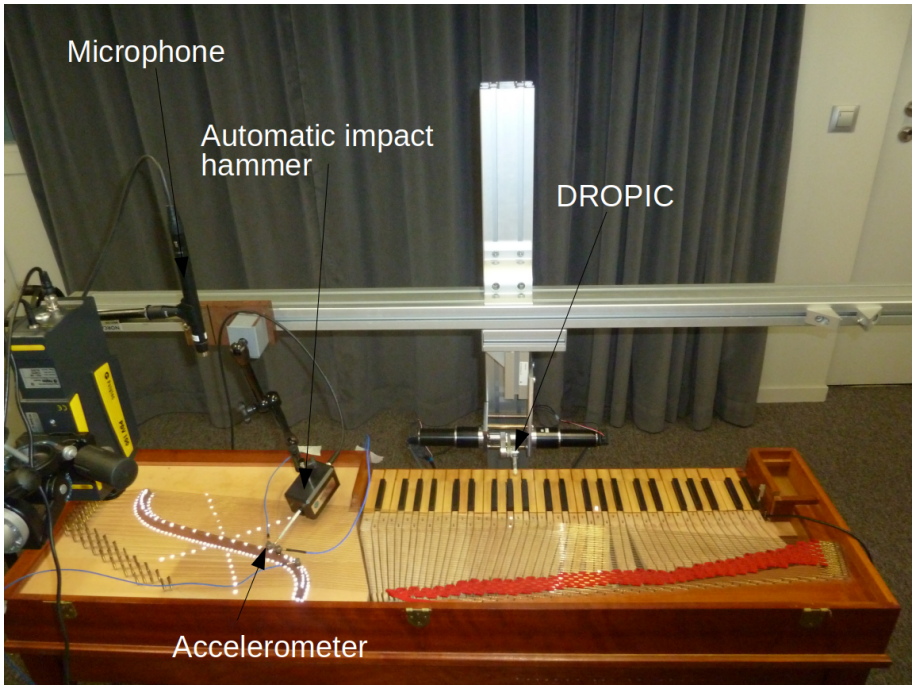

Figure 7.2: Experimental set-up used to measure the LAM1 clavichord response to impulse responses and to the $G\#_3$ string excitation, varying the tuning of the D_4 S-string and that of the F_3 S-string.

7.3.2 Data processing

Once these measurements are done, the modal properties of the first mode of the studied sympathetic strings are extracted for each tuning. They are extracted out of the impulse responses and out of the response signal following the $G\#_3$ string excitation measured by the accelerometer placed at the $G\#_3$ string coupling point. To proceed to this extraction, the measured signals are processed by means of the ESPRIT algorithm [89] to identify all the components present located around the frequency of the string excitation, which is the target frequency, 371 Hz for the D_4 S-string, 392 Hz for the F_3 S-string. For all vibratory responses following the $G\#_3$ string excitation measured, the signal is analysed 0.5 s after the excitation to get rid of the effects of its transitory phase. It is analysed within a 2 s time

span, so that a large enough SNR (signal to noise ratio) remains for the analysis. Then the signal is filtered by a FIR (Finite Impulse Response) filter centered at the fundamental frequency of the studied sympathetic string after this frequency being displaced to 0 Hz. The filter transitory phase corresponding to the first samples of the signal is brushed aside of the ESPRIT analysis. Before the analysis, the studied signal is decimated to reduce the computation time. This procedure is the same as the one done in section 3.1.1. After the analysis, the partial corresponding to the fundamental frequency of the studied sympathetic string is identified. Thus, an evolution of the properties of this partial with respect to the different tunings of the sympathetic strings can be observed. Note that these properties are expressed in terms of the ESM (Exponential Sinusoidal Model) used in the ESPRIT method.

7.4 Strings' partials parameters extracted out of the impulse responses

To denote the different mobilities, figure 7.3 shows the points of reference of the different FRF : H_{21} is the mobility relating the D_4 S-string point number 1 with that of the $G\#_3$ string number 2, H_{22} is the mobility measured at the driven point located at the $G\#_3$ string coupling point number 2, H_{23} is the mobility relating the F3 S-string coupling point number 3 to that of the $G\#_3$ string number 2. Figure 7.4 show the different measured mobilities with all strings being damped. The spectral amplitude of the H_{23} mobility shows that the target frequency of the F_3 S-string (392 Hz) is located nearby a bridge mode. On the other hand, the target frequency of the D_4 S-string (371 Hz) is located nearby a minimum of spectral amplitude of the H_{21} mobility. As a result, it is expected that the F_3 S-string vibrates with more amplitude when excited by an impulse response compared to the D_4 S-string. Also, the conductances of the H_{23} mobility is higher at the target frequency of the F_3 S-string (392 Hz) than that of the H_{21} at the target frequency of the D_4 S-string (371 Hz).

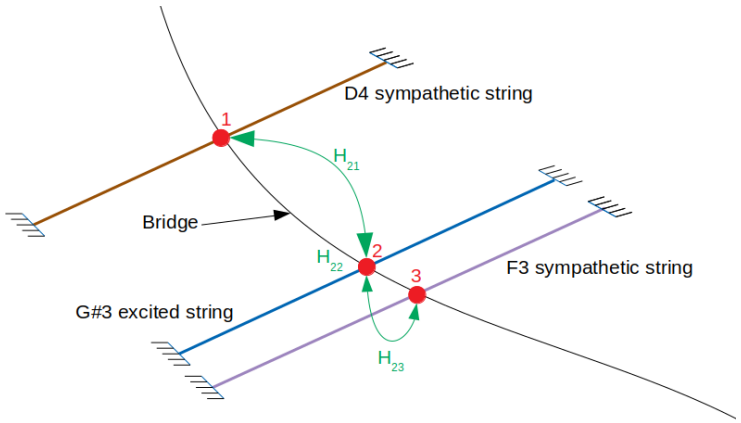

Figure 7.3: Scheme, with a stylised bridge, of the considered system to study couplings, indicating the points of reference for the different measured FRF's.

In figure 7.5 (a), the spectral amplitude of H_{21} and H_{23} are shown along with the amplitude of the D_4 S-string first partials and that of the F_3 S-string. Among the 9 different tunings in the study of the D_4 S-string, some first partials could not be found in the ESPRIT analysis because they lacked energy. Only those that could be well identified are kept. This lack of energy can be explained because of the H_{21} mobility of the bridge at these tuning frequencies. As it was pointed out, the target frequency of the D_4 S-string is located nearby a minimum of mobility spectral amplitude, far from any bridge mode. Therefore, it seems coherent that some partials analysed for the D_4 S-string may lack vibratory energy. Moreover, the partials that are well identified show that the D_4 S-string fundamental frequency does not change in terms of amplitude. It remains constant around an order of magnitude of 10^{-4} m.s^{-2}. Indeed, there is little changes in spectral amplitude when it comes to the H_{21} mobility between 360 and 380 Hz. On the contrary, all the F_3 S-string first partials are well identified, not lacking vibratory energy in any case. When the tuning frequency of the F_3 S-string increases, the amplitude of its first partial evolves considerably around an order of magnitude of 10^{-2} m.s^{-2}. The H_{23} mobility accounts for this considerable evolution, because its spectral amplitude goes higher around these frequencies. Then the bridge transmits more energy to the F_3 S-string first partial than to that of the D_4 S-string. The modal basis of the system favors the vibratory amplitude of the F_3 S-string more than that of the D_4 S-string.

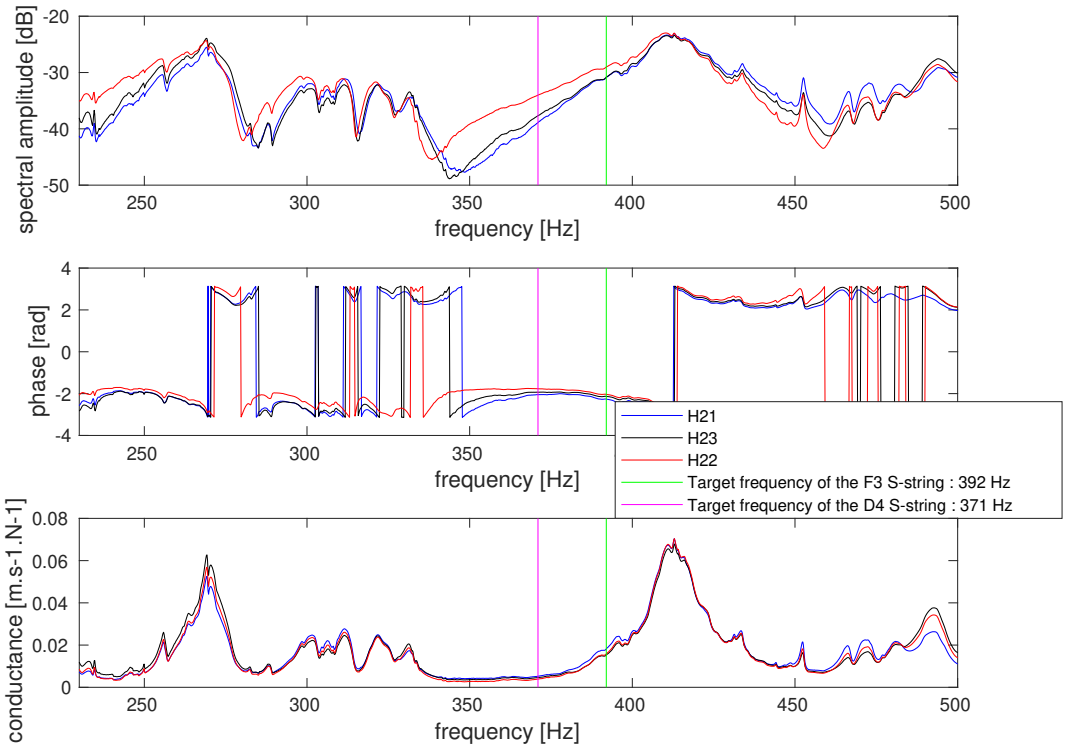

Figure 7.4: Spectral amplitudes, Phases, and conductance of the H_{12}, H_{22} and H_{23} mobilities.

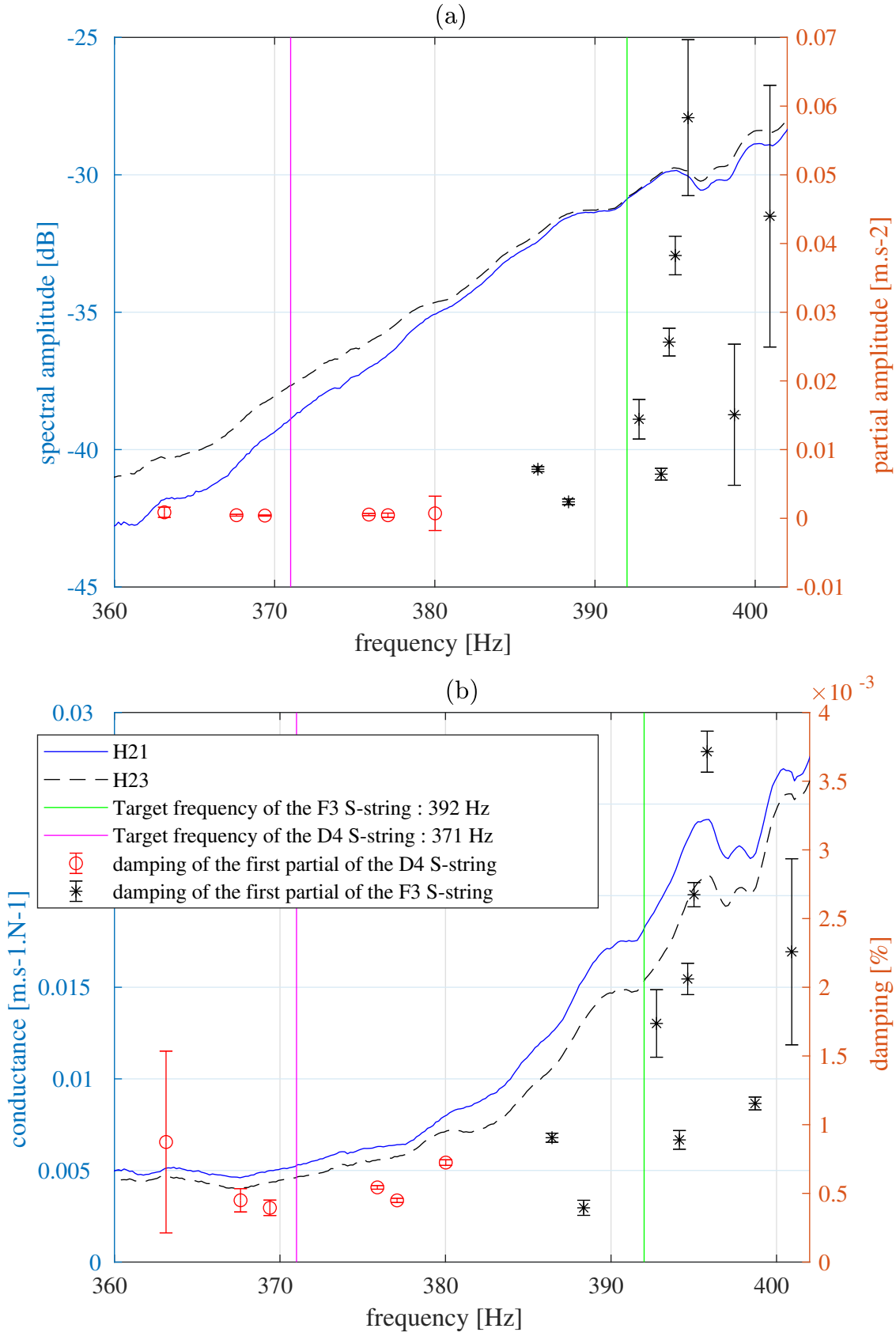

Figure 7.5: Spectral amplitude (a) and conductance (b) of the H_{12} and H_{22} mobilities with the amplitudes of the D_4 S-string first partials and that of the F_3 S-string.

In figure 7.5 (b), the conductance of H_{21} and H_{23} along with the dampings of the D4 S-string first partials and that of the F_3 S-string are also presented. Analogically to the analysis of the amplitude, the damping of the D_4 S-string first partial presents little variations whereas that of the F_3 S-string evolves considerably. One can notice a similar tendency of evolution between the amplitude and the damping of the same partial. Considering that the coupling in this context is weak, this observation can be accounted for by means of equation 7.10. The damping of the string is proportional to the conductance of the bridge mobility at its coupling point. When the mobility amplitude is higher, then the starting amplitude given to the string becomes larger. Yet, an increase in mobility amplitude leads also its conductance to be higher. When this conductance increases, then according to equation 7.10, the damping of the string partial increases too. That justifies this similar tendency between the amplitude and the damping of the partial influenced by the effect of the bridge mobility at the coupling point. As a result, the modelling of coupling by Valette and Cuesta [58] given by equation 7.10 under the assumption of weak coupling does account for the variation of amplitude and damping of the measured partials. It shows that by placing the string coupling points in different locations of the soundboard, the partials' amplitude and damping of the strings vary with the same tendency. In a location that increases the string partial amplitude, it increases also its damping. Since this is the case, the layout of the strings' coupling points influences the partials' damping and the amplitude of the clavichord sound halo given by the reverberation effect. Also, this is the reason why that when placing the string coupling points, a compromise between amplitude and damping should be found to find the best sound quality when playing the instrument.

7.5 Strings' partials parameters at frequency coincidence

The string modal parameters are influenced by the coupling mobility of the bridge, as it is shown in section 7.4. Adding to this, these modal parameters can also be influenced by the frequency coincidence between two strings' partial. Measurements conducted in section 7.3.1 with the string excitation when using the robotic finger can be used to study this influence. Also, a simplified model of the studied system can be elaborated by means of the formulation developed in chapter 2. Simulating this model, a comparison between experimental and simulated data is done in section 7.5.2.

7.5.1 Modelling of the sympathetic strings

Among the 74 strings of the LAM1 clavichord, only three strings have been considered in the experimental approach to study the string resonance when frequency coincidence occurs. Ideally, to model the whole clavichord, the 74 strings and the 74 coupling points of the bridge should be considered. However, this system can be simplified in view of the study of specific physical phenomena. For instance, to study the sympathetic vibrations with the model, since the reverberation effect resulting from the vibration of the 74 sympathetic strings is not here at stake, a few strings is only needed to investigate the string resonance. As such, the simplification of the

system only considers the needed vibratory subsystems to facilitate the investigation of the studied physical phenomena.

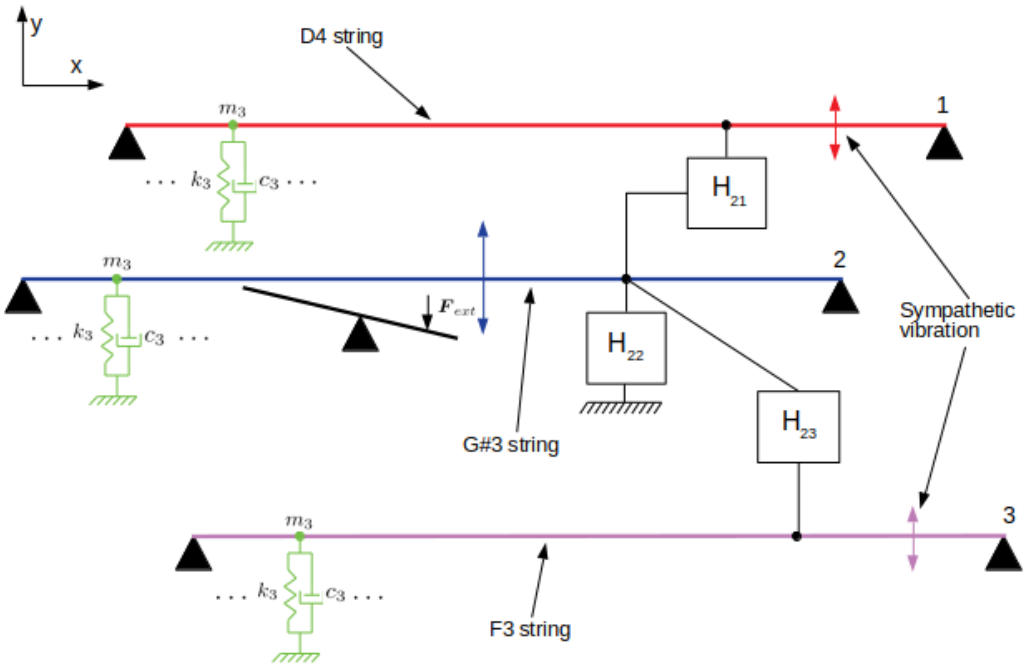

Figure 7.6: Sketch of the modelling of the G#$_3$ string, F$_3$ string and D$_4$ string coupled to the bridge.

The G#$_3$ string is still considered as the excited string in the model. Then the F$_3$ string and the D$_4$ string are considered as well. These two strings are not excited. The response of their sympathetic part to the excited string is the object of this study. This model is used in section 7.5.2 to compare simulation results with experimental data. The modelling of these strings is summarised in figure 7.6. To denote the different bridge coupling mobilities, like in figure 7.3, the different coupling FRF's are shown : H_{21} is the mobility relating the D$_4$ S-string point with that of the G#$_3$ string, H_{22} is the mobility measured at the driven point located at the G#$_3$ string coupling point, H_{23} is the mobility relating the F$_3$ S-string coupling point to that of the G#$_3$ string. As a result, the bridge is modeled by means of these three coupling points.

Simulating this model (see figure 7.7 and 7.8), a similar procedure is conducted as in the experimental approach in section 7.3.1. In the first case, the excited string is tuned at 392 Hz, and the F$_3$ S-string tuning is varied around this target frequency. In the second case, the excited string is tuned at 371 Hz, and the D$_4$ S-string tuning is varied around this other target frequency. Exciting the G#$_3$ string with these different tuning configurations, the bridge acceleration signal at the G#$_3$ string coupling point (point n°2) is analysed by means of the ESPRIT method. The same protocol as in section 7.3.2 is conducted to extract the strings' modal parameters.

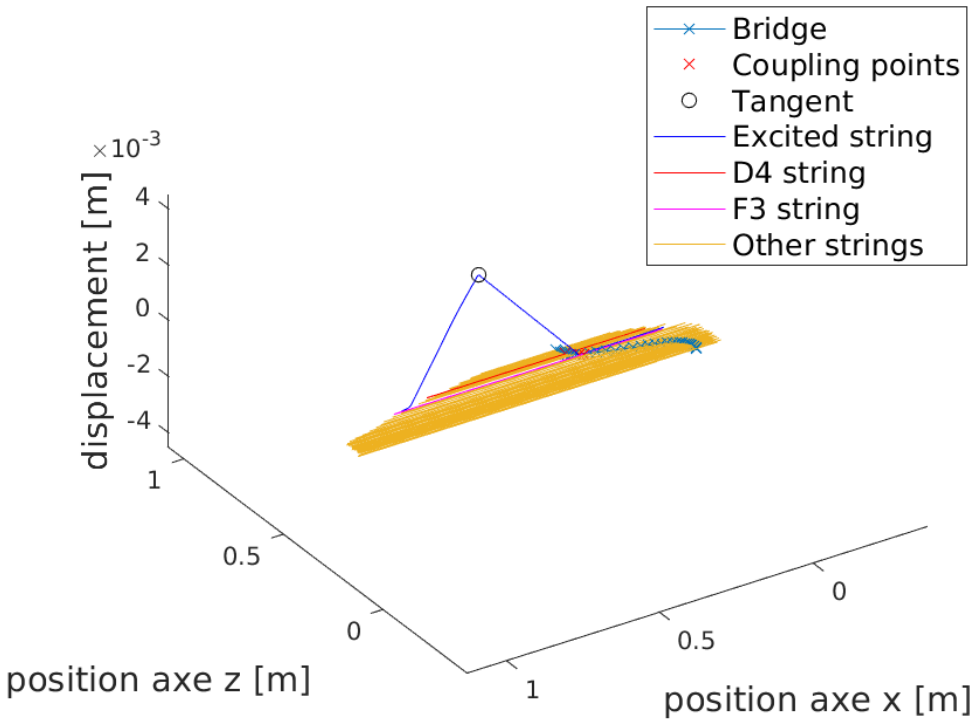

Figure 7.7: Picture of the modeled strings among those of the LAM1 clavichord : the excited G#$_3$ string, the F$_3$ string and the D$_4$ string. The axes of the picture are isomorphic

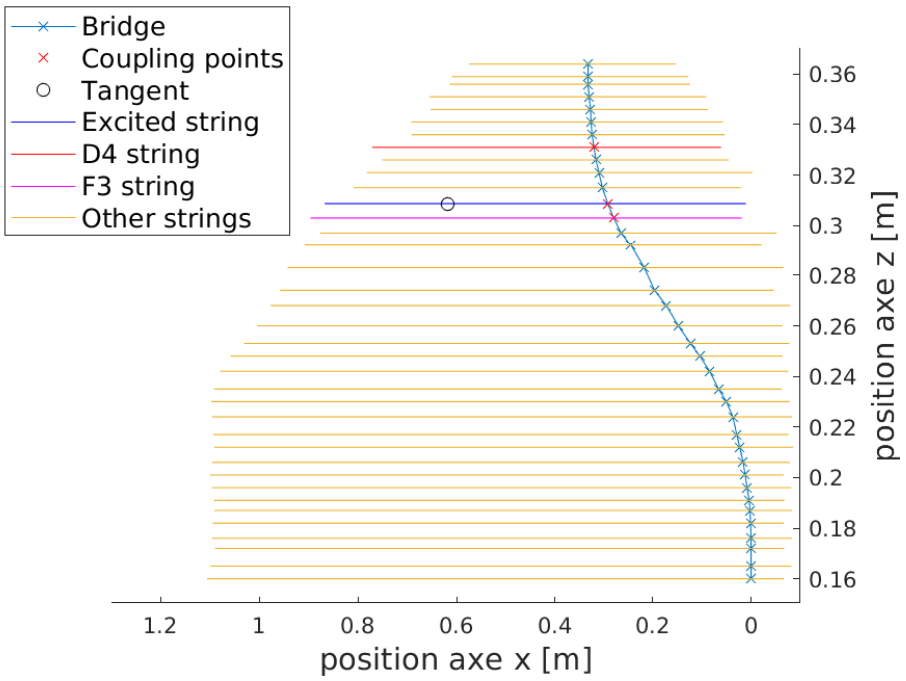

Figure 7.8: Picture of the modeled strings among those of the LAM1 clavichord seen from above. The axes of the picture are anisomorphic

7.5.2 Variation of the modal parameters of the coupled partials

Comparison between the experimental data and the simulated data

Regarding the variation of the strings' modal parameters with respect to the sympathetic string tuning compared to that of the excited string, the results obtained by measurements and simulations are presented in figure 7.9. In this figure, the F_3 S-string case as well as that of the D_4 S-string are shown. In figures 7.9 (a) and (b), the tuning frequency corresponds to the tuning of the studied S-string in each case. The resulting frequency is the frequency measured after exciting the played string. The frequencies of the excited string first partial and that of the studied S-string obtained in the simulation are presented. Also, the measured first partial frequency of the excited string with respect to that of the measured S-string is presented. Experimentally, the tuning of the studied S-string before the excitation is not known.

In figure 7.9 (a), which regards the F_3 S-string case, the measured frequency of the $G\#_3$ string first partial varies between around 390 and 395 Hz, with a maximum incertitude of 1.2 Hz. This is larger than the frequency obtained with the simulation, where this frequency varies between 392.1 and 391.7 Hz. In figure (b), which regards the D_4 S-string case, the measured frequency is subjected to a variation which goes between 372.4 and 372.3 Hz and with a maximum incertitude of 0.06 Hz, which is way smaller than the measured F_3 S-string frequencies. Also, the simulated data shows a very small variation of the first partial frequency of the D_4 S-string as well, with a 0.2 Hz of variation at maximum. With the simulated data, the shift of frequency noticed in the F_3 S-string case is a bit larger than that noticed in the D_4 S-string case. However, with the measured data, the frequency variation of the studied partials is way larger in the F_3 S-string case than in the D_4 S-string case. In the two figures (a) and (b), the shapes of the simulated curves are the same. When the tuning frequency of the S-string approaches the excited string frequency from below, the latter increases a little and the former decreases also. Once the S-string tuning frequency becomes larger than that of the excited string, then the latter decreases suddenly and the former augments also all of a sudden. It is as though the frequencies of the two strings were exchanged.

In figure 7.10 (a) and (b), the amplitude of the strings' first partial in the two case studies are shown. In the F_3 S-string case shown in figure (a), the measured modal amplitudes of the S-string go from 0.045 to 0.86 $m.s^{-2}$ among the different tunings, with a maximum incertitude of 0.37 $m.s^{-2}$. That of the excited string go from 0.12 to 0.83 $m.s^{-2}$, with a maximum incertitude of 0.23 $m.s^{-2}$. The simulated curves show that the damping of the two strings vary from 0.29 to 1.1 $m.s^{-2}$ for the excited string and from 0.069 to 0.44 $m.s^{-2}$ for the F_3 S-string. In the D_4 S-string case shown in figure (b), the measured modal amplitudes of the S-string go from 0.019 to 0.55 $m.s^{-2}$ among the different tunings, with a maximum incertitude of 0.20 $m.s^{-2}$. That of the excited string go from 0.15 to 0.32 $m.s^{-2}$, with a maximum incertitude of 0.095 $m.s^{-2}$. The simulated curves show that the amplitude of the two strings partial vary from 0.34 to 0.63 $m.s^{-2}$ for the excited string and from 0.023 to 0.21 $m.s^{-2}$ for the D_4 S-string. There is no particular conclusion to be drawn out of the simulated curves. However, it is interesting to notice that the measured S-string amplitude in figures (a) and (b) end up forming a resonance curve, where

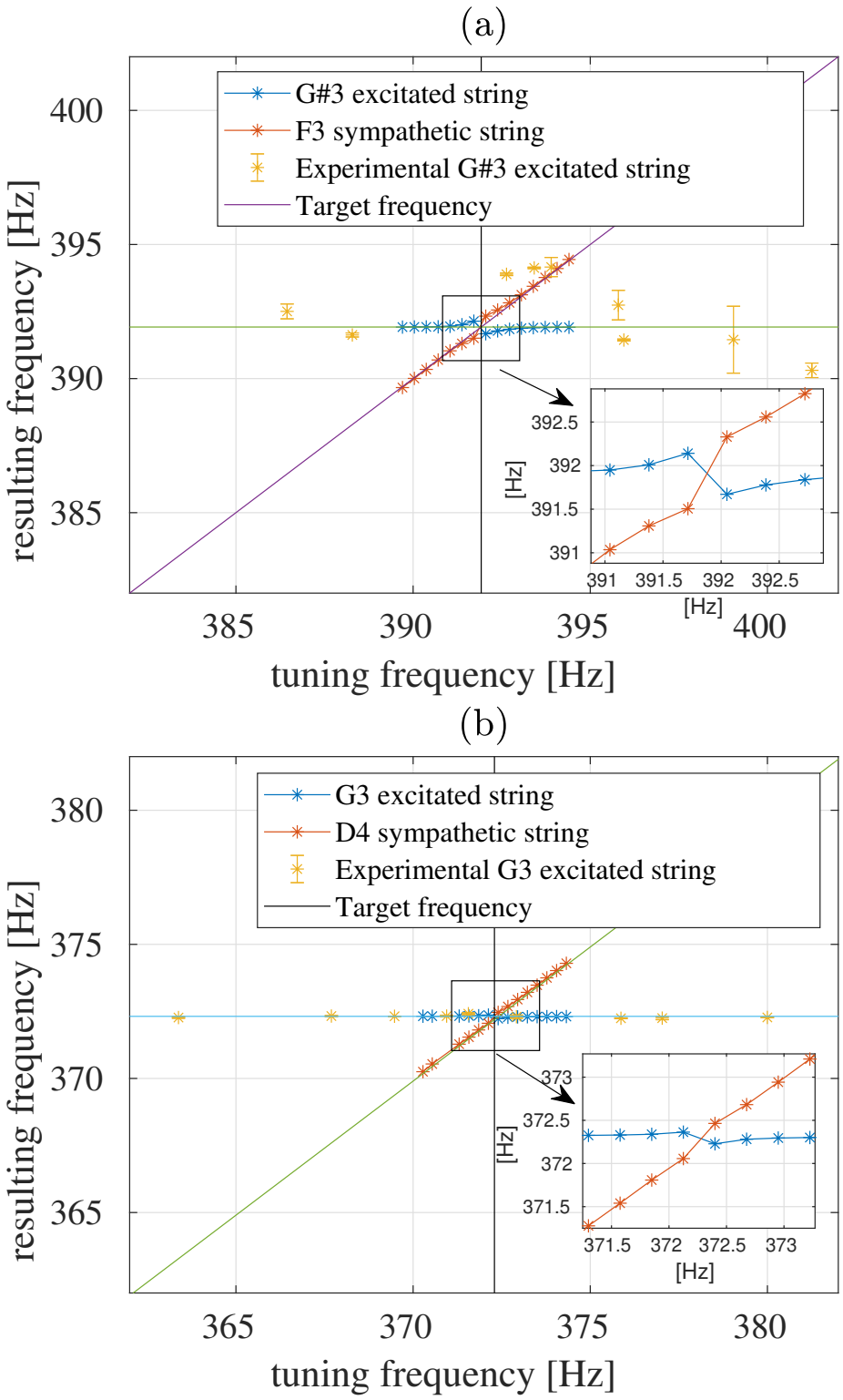

Figure 7.9: Resulting frequency of the sympathetic string coupled partial and that of the excited string with respect to the tuning frequency in the case of the F3 S-string (a) and that of the D4 S-string (b) given by the simulation, and resulting frequency of the excited string with respect to the resulting frequency of the sympathetic string given by the measurements.

this amplitude is highest when the frequency of the S-string' partial coincides the most with that of the excited string partial. Also, the amplitudes of the F_3 S-string are larger than that of the D_4 S-string, whether at frequency coincidence or not. This is to be related to figure 7.13 discussed below. The reason that the simulated curves do not reproduce these experimental curves is not known. More simulations nearby frequency coincidence would be necessary.

In figure 7.11 (a) and (b), the damping of the strings' first partial in the two case studies are shown. In the F_3 S-string case shown in figure (a), the measured dampings of the S-string go from 1 to 4.6% among the different tunings, with a maximum incertitude of 1.7%. That of the excited string go from 1.04 to 6.25%, with a maximum incertitude of 2.65%. The simulated curves show that the damping of the two strings vary from 0.96% to 4.84% for the excited string and from 1.13 to 5.24% for the F_3 S-string, which is close to the variation of the measured dampings. In the D_4 S-string case shown in figure (b), the measured modal dampings of the S-string go from 0.69 to 1.48% among the different tunings, with a maximum incertitude of 0.56%. That of the excited string go from 1.01 to 1.61%, with a maximum incertitude of 0.21%. The simulated curves show that the damping of the two strings vary from 1.01 to 1.38% for the excited string and from 0.96 to 1.37% for the D_4 S-string, which are also comparable to the values of the measured dampings. In overall, the variations of damping in the F_3 S-string case are larger that in the D_4 S-string case. Similar to the observation done for the frequency variation, the simulated damping curves in figures (a) and (b) show that the excited string partial and that of the S-string exchange there modal damping once the S-string tuning frequency becomes larger than that of the excited string.

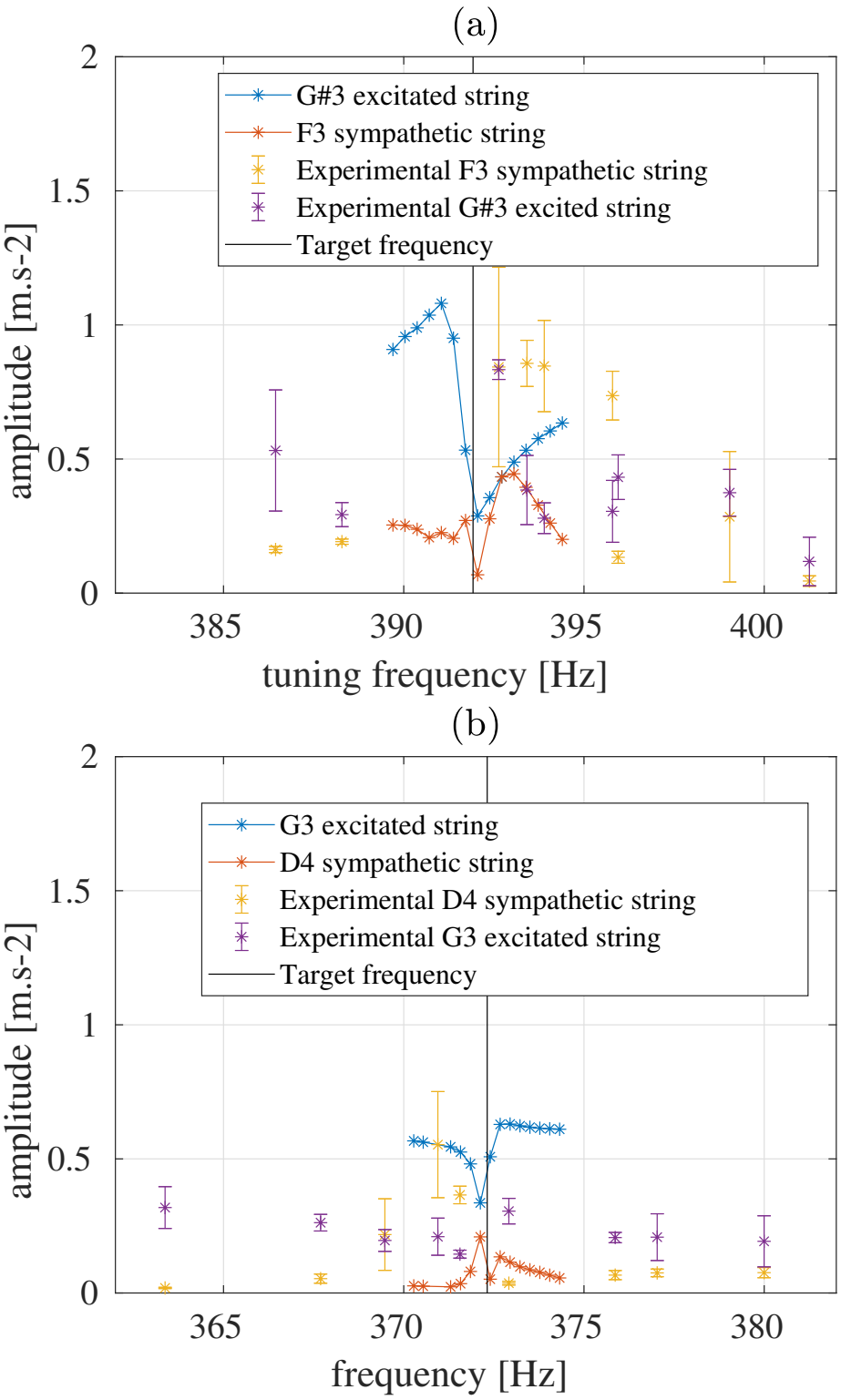

Figure 7.10: Amplitude of the sympathetic string coupled partial and that of the excited string with respect to the tuning frequency in the case of the F_3 S-string (a) and that of the D_4 S-string (b) given by the simulation, and amplitude of the excited string with respect to the resulting frequency of the sympathetic string given by the measurements.

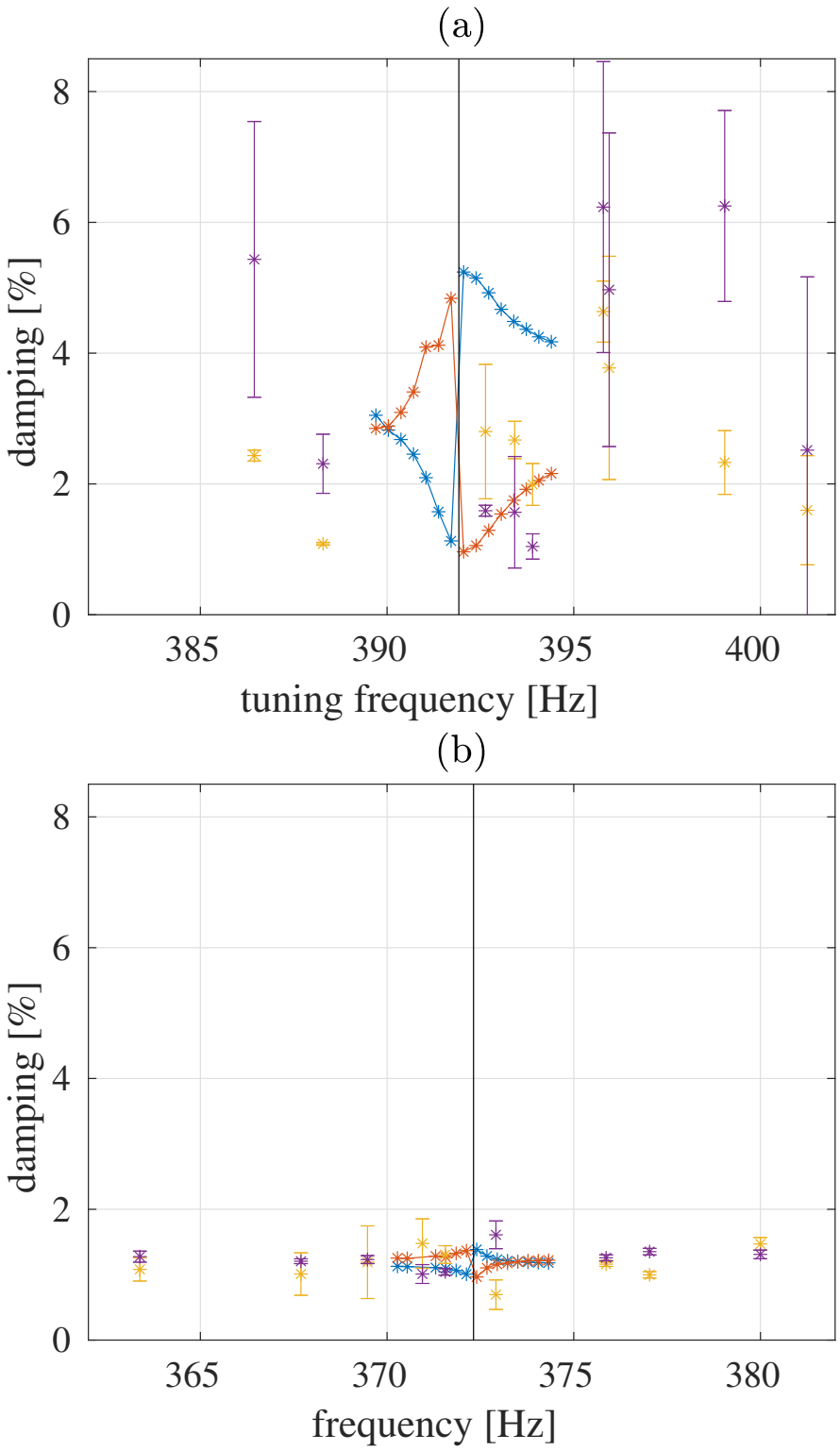

Figure 7.11: Damping of the sympathetic string coupled partial and that of the excited string with respect to the tuning frequency in the case of the F_3 S-string (a) and that of the D_4 S-string (b) given by the simulation, and damping of the excited string with respect to the resulting frequency of the sympathetic string given by the measurements.

Comparison between the simulated data provided by the model and that provided by Weinreich model

The simulated frequency and damping curves in figure 7.9 and 7.11 can be compared with another model regarding string coupling. It is possible to compare them to the values given by the model elaborated by Weinreich applied on piano strings [21] (see section 7.2.2). The simulated frequencies obtained by means of the model are transposed in terms of frequency deviation to compare them to the values given by equation 7.8 yielded by the model by Weinreich. The values chosen for the simulated Weinreich model is $\xi = 0.3$ and $\eta = 0.35$ in the F_3 S-string case, $\xi = 0.12$ and $\eta = 0.12$ in the D_4 S-string case. The comparison is shown in figures 7.12. The values in frequency in figures (a) and (b) given by the simulation of the U-K model and that of the Weinreich model give very similar results. in figures (c) and (d), the variation of damping given by the two curves have the same shape. Even though they are close, the amplitude of the damping deviation is not perfectly the same. Since the frequency deviation curve given by the Weinreich model match with the simulated frequencies given by the U-K model, the values of ξ and η should not be changed. So the associated damping deviation curves should not be modified. As opposed to the model based on the U-K formulation, the Weinreich model is based on the assumption that the excited string and the sympathetic string are coupled with the bridge at the same coupling point. Since it is not the case in our study, these strings should not be subjected to the same bridge coupling admittance. In view of this difference between the two models regarding this assumption, it may well account for the dissimilarities in damping between the Weinreich model and that based on the U-K formulation.

This satisfactory match with the Weinreich model can be useful to put forward the difference between the sympathetic vibration of F_3 S-string and that of the D_4 S-string reacting to the same excited string. The influence of the bridge coupling admittance on these two S-strings is not perfectly the same. Therefore, the deviation in frequency and in damping between these two S-strings are not the same. Namely, this deviation is larger in the F_3 S-string case than in the D_4 S-string case. As such, it can be considered that the coupling between the excited $G\#_3$ string and the F_3 S-string is stronger than that between the same excited string and the D_4 S-string.

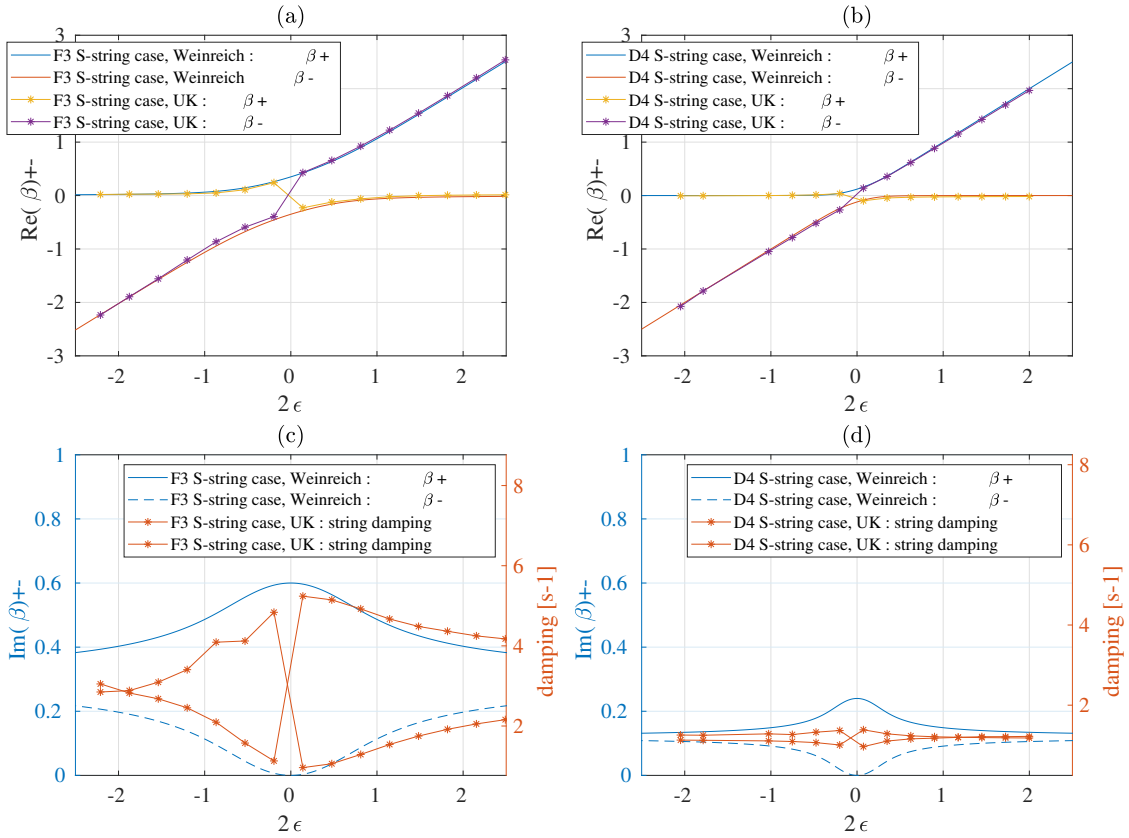

Figure 7.12: Comparison between the frequency deviation given by the simulation of the U-K model and that given the Weinreich model in the F_3 S-string case (a) and in the D_4 S-string case (b), and comparison between the damping deviation given by Weinreich model and the dampings given by the simulation of the U-K model, in the F_3 S-string case (c) and in the D_4 S-string (d).

7.5.3 Vibratory and acoustic signals of the S-strings and the soundboard

In figures 7.13, the velocity signals measured at one point of the F_3 S-string (3.2 cm away from the tuning hitch-pin) and of the D_4 S-string (4.5 cm away from the tuning hitch-pin) by the vibrometer for each tuning are presented, as well as the measured acceleration signals at the G#$_3$ coupling point (point n°2) when the S-string fundamental frequency coincides with that of the excited string in the F_3 S-string case and in the D_4 S-string case. It can be seen that the more the tuning frequency coincides with that of the S-string, the more the vibratory amplitude of the S-string increases. In particular, beats can be seen in these velocity signals. The cause of their presence is the frequency distance between the excited string frequency and the S-string frequency. In other words, The beats' frequency is equal to this frequency difference. The larger the difference between these two frequencies, the higher the frequency of the beats. As a result, when the frequency of the S-string approaches that of the excited string, the beats' frequency decreases and the vibratory amplitude increases. This increase in the vibratory amplitude is consistent with the measured modal amplitudes extracted from the acceleration signal at the G#$_3$ coupling point shown in figure 7.10. In other words, the S-string resonates

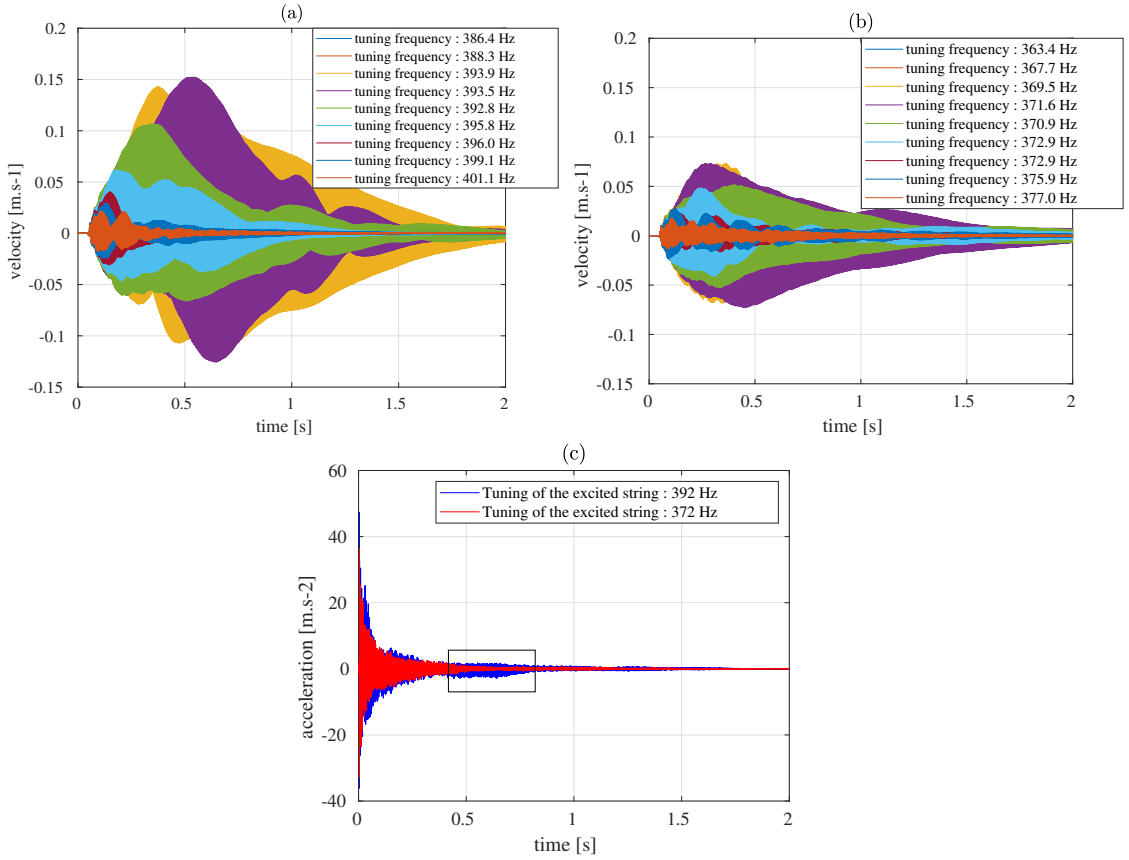

Figure 7.13: Measured velocity vibratory signals of the F3 S-string responding to the G3 string excitation (target frequency : 392 Hz), with different tunings of the F3 S-string (measured point localised at 3.2 cm away from the tuning hitch-pin) (a), That of the D4 S-string responding to the G3 string excitation (target frequency : 371 Hz), with different tunings the D4 S-string (measured point localised at 4.5 cm away from the tuning hitch-pin) (b), Acceleration of the bridge at the G#3 string coupling point which results from the excitation of this string tuned at 372 Hz and at 392 Hz, coinciding with the D4 S-string first partial and that of the F3 S-string respectively (c).

more when approaching frequency coincidence. This is accounted for by the study of string resonance made by Gough [62]. It is showed that this frequency coincidence creates a resonance at that coincided frequency in the bridge admittance. As a result, a perturbation at the S-string coupling point occurs, leading to this increase in vibratory amplitude.

As it was pointed out, the measured amplitude at resonance in figure 7.10 (a) in the F_3 S-string case is larger than that shown in figure 7.10 (b) in the D_4 S-string case. This can be verified by the acceleration signals measured at the $G\#_3$ coupling point presented in figure 7.13. The initial vibratory amplitude of the acceleration signal in blue is 47 $m.s^{-2}$ and that of the red one is 36 $m.s^{-2}$. The former is measured when the excited string is tuned at the F_3 S-string frequency (392 Hz) and the latter is measured when the same excited string is tuned at the D_4 S-string frequency (372 Hz). So the amplitude of this acceleration in the F_3 S-string case is larger than that in the D_4 S-string case. Moreover, the amplitude of the blue acceleration signal increases at 0.5 ms and decreases at 0.7 ms. Such a thing is not observed in the red

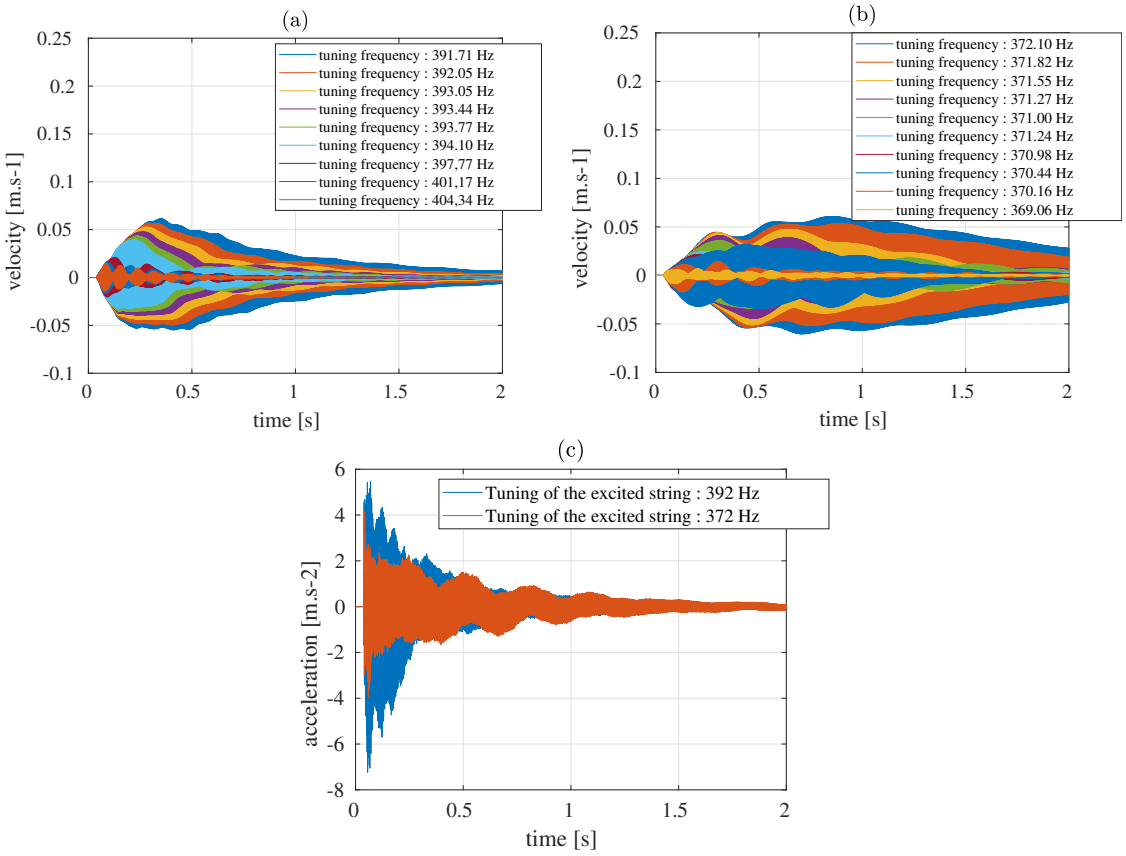

Figure 7.14: Simulated velocity vibratory signals of the F3 S-string responding to the G3 string excitation (target frequency : 392 Hz), with respect to the tuning frequency of F3 string (measured point localised at 3.2 cm away from the tuning hitch-pin) (a), That of the D4 S-string responding to the G3 string excitation (target frequency : 371 Hz), with respect to the tuning frequency of D4 string (measured point localised at 4.5 cm away from the tuning hitch-pin) (b), Acceleration of the bridge at the G#3 string coupling point which results from the excitation of this string tuned at 372 Hz and at 392 Hz, coinciding with the D4 S-string first partial and that of the F3 S-string respectively (c)

acceleration signal.

In figure 7.14, the simulated velocity signals measured at one point of the F_3 S-string and of the D_4 S-string for each tuning are presented, as well as the simulated acceleration signals at the $G\#_3$ coupling point (point n°2) when the S-string fundamental frequency coincides with that of the excited string in the F_3 S-string case and in the D_4 S-string case. The same tendencies observed in the experimental signals can be noticed in the simulated ones. The more the tuning frequency coincides with that of the S-string, the more the vibratory amplitude of the S-string increases. Also, the simulated acceleration signals indicate a similar tendency. Considering the frequency coincidence in the F_3 S-string case and that in the D_4 S-string case, the initial amplitude of the acceleration signal related to the former case, around 5 $m.s^{-2}$, is higher than that related to the latter case, around 4 $m.s^{-2}$. This can be explained by the results found in section 7.4. Given the fact that spectral amplitude of the corresponding coupling admittances is higher at 392 Hz than at 371 Hz, more amplitude is given initially to the bridge acceleration when the excited string

is tuned at 392 Hz than tuned at 371 Hz. Also, noticing that the conductance of these coupling admittances is higher at 392 Hz than in 371 Hz (see figure 7.4), more damping is given to the bridge acceleration when the excited string is tuned at 392 Hz than tuned at 371 Hz. This is the reason why the acceleration signal related to the D4 S-string case lasts longer than the one related to the F_3 S-string case.

Notwithstanding these similar tendencies between the measured signals and the simulated ones, the order of magnitude of these signals are not always the same comparing figures 7.13 and 7.14. That of the amplitude of the D_4 S-string velocity signals between the measurements and the simulation is comparable. However, that is less the case for the F_3 S-string velocity, where the simulated signals do not increase enough when frequency coincidence occurs. The maximum value reached in the measured signals is 0.15 m.s^{-1}, instead of 0.06 m.s^{-1} for the simulated signals. Also, the simulated acceleration signals are inferior to the measured ones by a factor of 10. To correct this, one could increase the amplitude of the simulating excitation force so that the vibratory amplitude of the bridge between the experiment and the simulation may be comparable. Moreover, the resonating effect found in the measured acceleration signal in the F_3 S-string case is not retrieved in the simulated

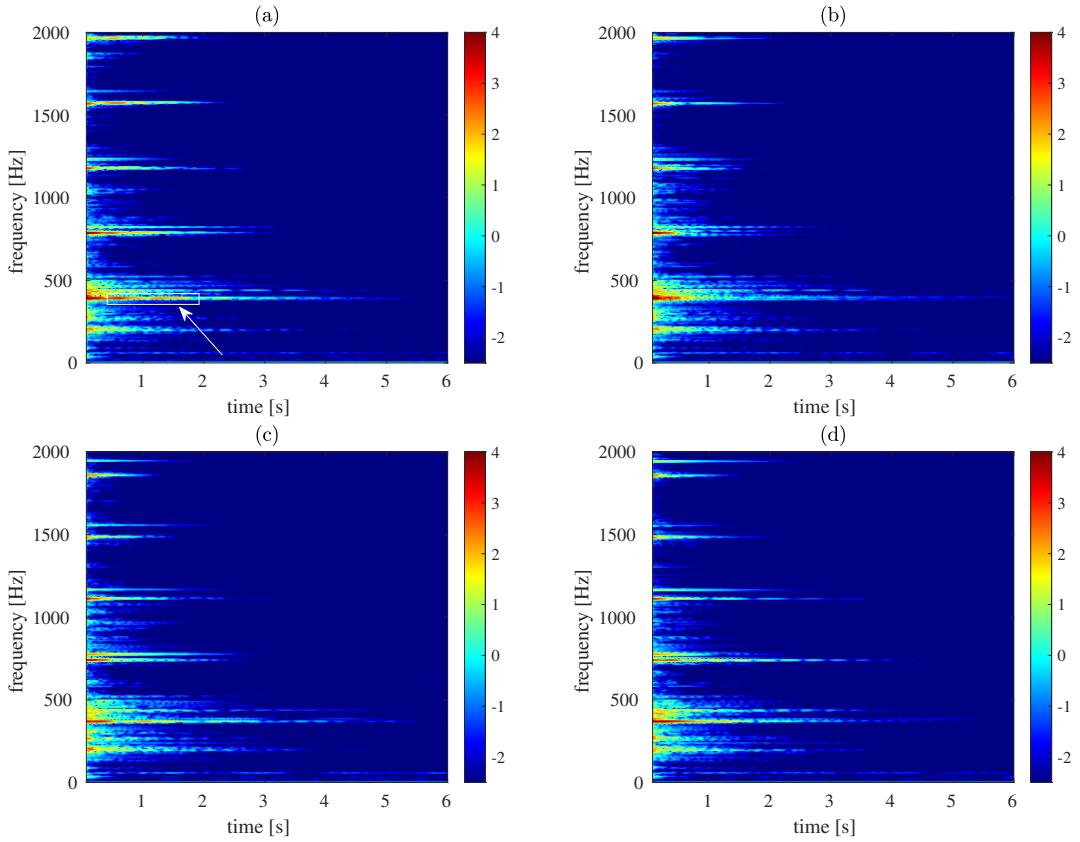

Figure 7.15: Spectrograms of the acceleration signal (Ref 1 dB : 1 m.s^{-2}) measured at the G#$_3$ string coupling point in the F_3 S-string case (a) and (b), and in the D_4 S-string case (c) and (d). In spectrograms (a) and (c), the corresponding S-strings are tuned with the excited string (392 Hz for the F_3 S-string and 372 Hz for the D_4 S-string), whereas in spectrograms (b) and (c) these sames S-strings are mistuned with respect to this same excited string (401 Hz for the F_3 S-string and 380 Hz for the D_4 S-string).

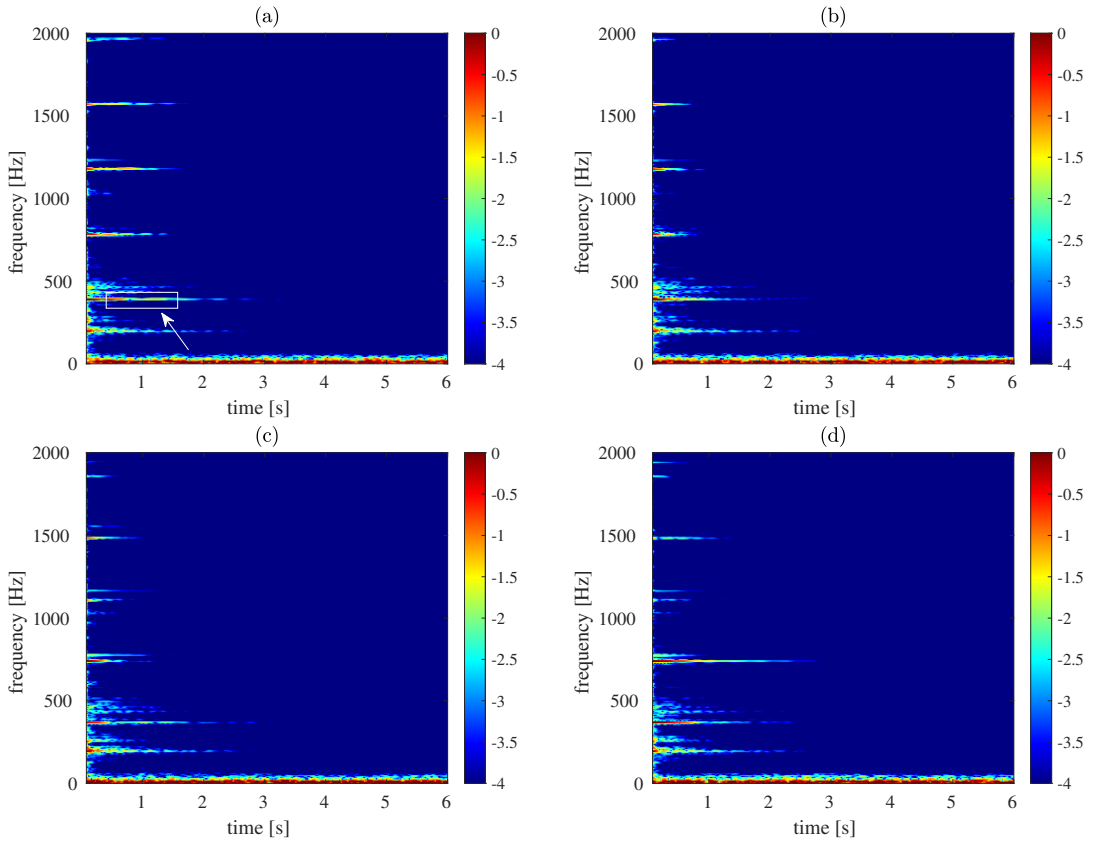

Figure 7.16: Spectrograms of the pressure signal (Ref 1 dB : 1 Pa) measured at 30 cm above the center of the soundboard in the F_3 S-string case (a) and (b), and in the D_4 S-string case (c) and (d). In spectrograms (a) and (c), the corresponding S-strings are tuned with the excited string (392 Hz for the F_3 S-string and 372 Hz for the D_4 S-string), whereas in spectrograms (b) and (c) these sames S-strings are mistuned with respect to this same excited string (401 Hz for the F_3 S-string and 380 Hz for the D_4 S-string).

signals. These main differences ought to be explained by the limitation of the model used for the simulations.

Furthermore, this difference can be seen in the spectrogram of these vibratory signals in figures 7.15. In spectrogram (a), where the frequency of the F_3 S-string first partial coincides with that of the excited string fundamental frequency, it can be seen that the partial at 392 Hz have a stronger amplitude between 0.5 and 2 s than in spectrogram (b), where there is no frequency coincidence. This partial sounds as if it was resonating, meaning that it gains slowly some amplitude at the beginning of the signal. This effect is not retrieve in the D_4 S-string, comparing spectrograms 7.15 (c) and (d). This resonance in the F_3 S-string case is shown in the sound looking at figures 7.16, where the spectrograms represent the experimental signals measured by the microphone. In spectrogram (a), the same resonating partial can be seen, which once again does not resonate in spectrogram (b). Surprisingly, in the D_4 S-string case, the partial duration at 744 Hz in spectrogram (d) is longer than in spectrogram (c). Yet, there is no frequency coincidence occurring in spectrogram (d). So this duration has nothing to do with the frequency coincidence between the excited string partial and that of the D_4 S-string.

7.6 Conclusion

With this investigation, it is possible to put forward the effect of resonance in the sound produced by the clavichord. it was found that the S-string partial at frequency coincidence in the F_3 S-string case is prominent in terms of amplitude in the soundboard vibratory signal as well in the clavichord radiated sound, which is not the case in the D_4 S-string case. The explanation of this whistling sound is the difference of the influence of the bridge coupling admittance in these two cases. It was put forward that the coupling between the excited $G\#_3$ string and the F_3 S-string is stronger than that between the same excited string and the D_4 S-string. Given this fact, the perturbation of the bridge coupling point with the F_3 S-string is larger than in the D_4 S-string case. That leads to giving more vibratory energy to the F_3 S-string coupled partial, leading to the observed whistling sound. As a result, the presence of this whistling sound coming from the string resonance is conditioned by the bridge coupling admittance. Only in the case of a sufficiently strong coupling does the whistling sound of the sympathetic vibration of the S-string appears when frequency coincidence with the excited string occurs.

Part V

Conclusion

Chapter 8

Conclusion and perspectives

Preceding studies on the clavichord either modeled only partially the instrument, or modeled it by means of signal processing methods. Experimental results on the vibro-acoustics of this instrument were found in the literature, and some were verified by means of simple vibratory models. The vibro-acoustic study of the clavichord aimed in part II at giving a first complete physical modelling of clavichord strings which would account for experimental results found in our work and in the literature by means of simulations. In a mechanical engineering point of view, the clavichord can be considered as a constraint system which is made of vibratory substructures coupled to each other. The string, the key-tangent, the bridge and the damper can be considered as individual substructures, where their couplings end up forming the instrument. Given that these substructures are modeled by means of their modal representation, experimental modal analysis was considered to find appropriate numerical values for the substructures' modal parameters. Then, a simulation study of this model was done to verify the stability and the convergence of the implemented numerical scheme. After this modelling and this simulation study, an overall study of the clavichord excitation system in part III and of sympathy in the clavichord in part IV were made, using experimental approaches and using simulations.

8.1 Results

In chapter 2, the Udwadia-Kalaba (U-K) formulation was used as a means to model the couplings of the different substructures. This formulation was found to be practical in view of this modelling. The constraint system can be easily modelled by means of the equation of motion of the system and of a constraint equation, where the couplings are considered in a single coupling matrix. This formulation is compatible with a modal representation of the system, which paves the way to the modelling of coupled vibratory substructures. The modal representation of the string, bridge, key-tangent substructure and that of the damper were presented. Given the fact that this formulation is derived from the Gauss principle, there is no issue when it comes to including non-conservative or nonlinear forces in the model. Considering that the clavichord string is uplifted with a static displacement when excited, geometrical nonlinear forces needed to be taken into account by means of the Kirchoff-Carrier model to include the variation of string tension, hence to include the variation of the excited string fundamental frequency. Then, the assumption of the continuity in displacement between each substructure was considered to derive the coupling ma-

trix of the constraint system. In particular, the excitation of the string is modelled by coupling the key-tangent substructure and the string at the moment of contact. That leads to the creation of a constraint force whose amplitude is similar to the excitation force applied at the key-tangent substructure at the moment when the mechanical system becomes static. This constraint force uplifts the string and sets the string played part into vibration. In the coupling between the string and the key-tangent substructure, given that the two substructures are not exactly in the same position at the contact moment, stabilization techniques were implemented to correct the displacement and the velocity of the system because of constraint violations.

In chapter 3, the numerical values of all modal parameters were investigated as well as the stabilization and convergence of the model simulation. The string dampings were considered by means of the study of three different clavichord strings placed at a string bench. Vibratory measurements of these isolated strings led to the using of a high resolution method to determine their dampings. Given the modal representation of the string presented in chapter 2, the string modal dampings' model was used to match these string dampings' measurements, out of which the numerical values of the damping model parameters could be found. As a result, the damping model can be applied for all clavichord strings. Given the bridge modal representation, an experimental modal analysis approach was used to determine the bridge modal parameters at three different locations : at the $G\#_3$ coupling point, that of the F_3 string and that of the D_4 string. The modal parameters of the key-tangent substructure and the damper are chosen by means of *ad hoc* values, where the consistency of these results is evaluated in view of the coherency of the simulation results. Then, a study of the implemented numerical scheme is done to find the stability condition of the simulation in terms of time step. Also, the stability is secured by respecting Shannon's sampling theorem, which imposes a limited number of string modes with respect to the chosen time step. Simulating the $G\#_3$ string, a study of the time step, in particular by means of an energy analysis, showed that the simulation converges when diminishing the time step. Also, a study of the number of string modes showed that the solution converges when increasing this number of modes. A standard simulation was finally done to present the consistency of the numerical results. The damper needs to be reconsidered to avoid exaggerated influence on the string static displacement while conserving the same damping effect. Finally, the simulation of two similar excited strings gives a bridge vibratory response similar to that found by Weinreich when considering coupled piano strings [21].

In chapter 4, the excitation system of the clavichord was investigated. The robotic finger was used to repeat the same programmed trajectory leading to the key motion. The key-depth was measured by means of a profilometer, measuring the motion in terms of distance. The vibratory displacement in the two polarisations of the string were measured to evaluate the model assumption of the one polarisation of motion of the string. This assumption is well justified for the excited string, yet debatable for the sympathetic strings. Then, the linearity of the bridge acceleration in dB with the logarithm of the impact velocity of the key-tangent substructure was verified by simulating the $G\#_3$ string excited with different impact velocities. Out of these simulations, the spectral slope of the bridge acceleration spectrum remaining constant with respect to the impact velocity was also verified. Furthermore, the

measured velocity of the key pressed by the robotic finger was compared to the simulated key-tangent substructure velocity. A similar shape with similar amplitudes and having similar low frequency motion could be observed, although the increasing slopes of the two velocities are different. This difference can be corrected by investigating the force profile exerted on the simulated key-tangent substructure. Finally, the motion of the $G\#_3$ string was simulated to observe with precision the motion of the string at the beginning of its excitation. The low frequency at the contact point between the string and the key-tangent substructure was observed. Also, the combination of the wave propagation and the string uplift forms the specificity of the clavichord string motion that was observed in the simulation.

Chapter 5 was devoted to the study of the paradoxical gesture needed to play the clavichord, also referred to as the clavichord paradox. The legacy coming from the history of the clavichord performance points out the importance of this topic. Some musical treaties mentioned the problem of the finger pushed gesture, characterised by a vertical motion which causes a lack of balance between the obtained loudness and the resulting pitch. Hence, a pulled gesture (called *Schnellen*), which add a backward horizontal component to the finger motion, was introduced to reach this compromise between pitch and loudness in the produced clavichord sound. In line with preceding studies on this topic, measurements were conducted on the LAM1 clavichord by adding new kinds of measurements : the measurement of the string vibratory displacement by means of optical forks and the filming of the finger gesture by means of a high speed camera. Measurements conducted with a musician led to retrieve qualitatively the same results found in the literature by means of these new measurements, giving another representation of this clavichord paradox. Furthermore, the robotic finger programmed trajectory was used and modified to study this phenomenon with a trajectory whose velocity and displacement are controlled. The same tendencies as that found in the case of the measurements done with a musician can be observed. Namely, increasing the key velocity leads the clavichord sound level to increase. And increasing the key depth leads the clavichord pitch to increase. Therefore, the features characterising the clavichord paradox could be objectified by means of the robotic finger.

In chapter 6, indicating the presence of two vibro-acoustic effects when it comes to the sympathetic strings' vibration, that is the reverberation effect and the string resonance, the reverberation effect was investigated. This consists in an overall acoustic effect provided by the vibration of all the sympathetic strings, an effect similar to that found in room acoustics. This was studied by means of an experimental approach based on impulse response measurements with different string damping configurations. The frequency region influencing the studied clavichord sound is between 350 Hz and 6000 Hz regarding the S-strings, and that of the P-strings is below 350 Hz which creates the drum effect. The computation of the reverberation time of the clavichord sound highlighted the fact that the sympathetic strings contribute to the duration of the signal. Computing the sound level of the impulse responses, letting free the sympathetic strings' vibration enables the sound to be louder. Also, computing the spectral centroid led to a representation of the change in the timbre of the sound when damping the sympathetic strings. All these three indicators revealed the significance of the sympathetic strings in influencing the sound of the clavichord, where this influence can be considered as a reverberation effect. Since the impulse response approach assumes the fact that the studied system is linear, the

sympathetic strings can be considered as a linear system, namely as a reverberator. Its impulse response is obtained by means of a deconvolution done with the measured signals. Afterwards, the individual vibratory response of each of the S-string to the same excited string was measured. In such a way, the amplitude of these different vibratory responses could be compared. For some S-strings, this amplitude becomes larger than for all the other S-strings. This is not to be explained by the reverberation effect. Hence, another vibro-acoustic effect also related to sympathy which is resonance needs to be investigated.

In chapter 7, the resonance of the S-string when reaching frequency coincidence is studied. Preceding works on string-bridge coupling led to the difference between strong coupling and weak coupling, highlighted by the veering indicator [63]. The strength of this coupling depends on the modal basis of the string and that of the bridge. An experimental approach was conducted to study the coupling of the F_3 S-string and that of the D_4 S-string responding to the excited $G\#_3$ S-string. The corresponding coupling admittances were measured by means of impulse response measurements. In the F_3 S-string case and that of the D_4 S-string, the S-string tuning is changed 9 times around the excited string fundamental frequency which is the target frequency. For each of these tunings, impulses responses and vibro-acoustic responses to the same excited string are measured. The partials' parameters of the excited string and of the S-strings were extracted by means of a high-resolution analysis. Impulse response measurements show a correlation between the amplitudes of the considered partials and that of the corresponding coupling admittances, as well as another correlation between their dampings and the conductance of these coupling admittances. Namely the higher the spectral amplitude of the coupling admittance, the higher the amplitude of the S-string partial. And the higher the conductance of the coupling admittance, the higher the damping of the S-string partial. The partial of the F_3 S-string have a higher amplitude and a higher damping compared to the D_4 S-string, because the coupling admittance spectral amplitude and conductance of the former is higher than that of the latter. These considerations give the influence of the bridge mobility on the sympathetic vibration of the string. In particular, since the reverberation effect results from the amplitude and the damping of all the sympathetic strings' partials, this approach shows how the bridge mobility influences the clavichord reverberation effect. Then, the excited string approach was considered. Adding to the measurements, a simplified model of the studied clavichord reproducing the same experimental instructions was simulated. The considered partial frequency, amplitude and damping given by the measurements and by the simulated data were compared in the two cases, namely the F_3 S-string case and that of the D_4 S-string. In the two cases, the order of magnitude of the change in the frequency, damping and amplitude between the measured data and the simulated ones are consistent. This variation is due to the resonance of the S-string, when a frequency coincidence between its partial and that of the excited string occurs. The lower the mistuning of the two strings, the higher the change in the partial frequency, amplitude and damping. Comparing the data given by the simulated model based on the U-K formulation with that provided by the Weinreich model, the consistency of the two models have been noticed. Also, this comparison showed that the coupling between the F_3 S-string and the bridge is stronger than that of the D_4 S-string when exciting the $G\#_3$ string. This accounted for the resonating sound of the clavichord when coinciding the excited string fundamental frequency with

that of the F_3 S-string, which is not present when tuning the same excited string to the D_4 S-string fundamental frequency. This comes from the resonating response of the F_3 S-string which is favored by its corresponding coupling admittance. The same circumstance is not found in the D_4 S-string case.

8.2 Perspectives

Some perspectives to this work are proposed in this section. These perspectives are presented starting from short term investigation aiming at improving some aspects of the elaborated clavichord model, up to long term investigations to go toward a complete model of the clavichord, studying experimentally mores clavichords and studying deeply musical performance in the case of the clavichord.

The modelling of the clavichord

Simulating the model of an instrument gives a picture of our understanding of its vibro-acoustics. The more the sound synthesis of the modeled instrument is close to that of the real one, the more the physical phenomena involved in the instrument acoustic functioning are well theorised. Although the sound synthesis of this modeled clavichord seems satisfactory, it does not reproduce exactly the radiated sound of the real LAM1 clavichord. This modelling was done in view of studying selected aspects of the clavichord, namely the excitation system and the sympathetic string vibration, reducing the number of vibratory substructures. Either this model can be used for further explorations, requiring only minor modifications of the modelling. Or this model can be enhanced to account for other vibro-acoustic aspects of the clavichord, leading to a betterment of the clavichord sound synthesis.

Further amendments and uses of the present clavichord model

Regarding the modeling of the damper, it was observed that the proposed model can be improved in view of the simulated results. The damped part of the string in the simulation still vibrates considerably after the excitation. Naturally, one would increase the damping coefficients of the damper to increase the damping of the string damped part. However, increasing these damping coefficients leads to the slow-down of the static displacement of the excited string, which can become unrealistic. Therefore, with this way of modeling the damper, it is not possible to increase the damping of this string part without influencing the static motion of the string. Another model of the damper should be elaborated to come to a sufficiently damped string vibration.

Only one form of simulated force profile was used to produce the simulated vibratory signals, which is a simplified profile compared to that produced by musicians. In reality, this force varies in subtle ways after the moment of the key-tangent contact. This is essential to reproduce some musical effects like the vibrato called *Bebung* or the quick variation of the fundamental frequency called *Tragen*. Furthermore, this force profile variation is important to study numerically the clavichord paradox which demands a control of both the excitation force and the impact velocity.

The key-tangent substructure was modeled by considering the rotation of a rigid bar produced by the finger pressure. In that regards, measurement of the key mo-

ment of inertia was done in annex H. The musician finger could be modeled by means of a set of spring-mass systems, with appropriate masses, stiffness and damping coefficients equivalent to that of a human finger. As such, the excitation force would be the constrained force created by the coupling of the finger with the key.

The coupling have been modelled by means of the extracted bridge modal parameters, and its effect on the clavichord sympathetic string vibration was observed. A parametric study investigating the influence of the variation of some specific bridge modal parameters on the clavichord sound could be considered. Varying individually the modal masses and the dampings of the bridge, the influence on the clavichord string vibration could be observed. Also, varying these parameters influences the value of the veering indicator. For instance, it would be interesting to simulate a very strong coupling to observe a large deviation of the sympathetic string frequency when resonating. Furthermore, when simulating the 74 strings of the LAM1 clavichord, the influence of the modal parameters on the reverberation effect would also be a subject of interest. So a parametric study of the bridge modal behaviour influence on the clavichord sound could be of help when understanding the effect of coupling in musical instruments.

Enhancements of the clavichord modelling

The two polarisations of motion of the string could be taken into account. In that case, measurement of the clavichord bridge impulse responses in the two polarisations need to be done. Preliminary measurements of these impulse responses have been done to come up with an operational experimental setup. In particular, measurement techniques to measure the bridge FRF, which is then used to verify the equivalence of cross admittances of the bridge, have been tested in annex I.

To complete the model proposed in chapter 2, the radiation of the clavichord sound should be included. Regarding the Udwadia-Kalaba formulation, no specific analytical elaboration has been done so far to include the sound radiation with this formulation. The soundboard could be modeled like a two dimensional thick orthotropic plate coupled with the strings. Then the radiation can be modeled by means of vibro-acoustic equations, coupling the plate equations of motion with that of the propagation of sound in the air.

A much easier way to take account of the sound radiation in the model is to include the measured acoustic and vibratory impulse responses of the clavichord at one point in space. The simulated vibration of the bridge-soundboard can be convoluted with a transfer function obtained by means of the aforementioned measured impulse responses. As such, this convolution leads to obtaining the radiation sound of the studied clavichord.

Ideally, the 74 strings of the LAM1 clavichord should be considered to model the whole instrument. However, as it was pointed out, the computational time of the simulation becomes too large considering the numerical explicit scheme used to discretize the equation of motion associated to the modeled constrained system yielded by the U-K formulation. To shorten this computational time, a numerical investigation needs to be tackled.

As it was indicated in the introduction, other modelling of the clavichord have been done, like the one elaborated by Välimäki by means of signal processing methods. To have a better idea of the sound quality obtained by means of the simulated model in this PhD, it should be compared to that obtained by preceding models.

A comparison of the clavichord A_3 note simulated by the model by Välimäki with that produced by the simulated model based on the Udwadia-Kalaba formulation could be done. Also, it would be interesting to compare the sound quality of the simulated Neupert clavichord modelled by the Modartt company compared to that produced by the simulated U-K model.

Performance studies on the clavichord

Regarding the experimental study of the finger gesture of the clavichord player, the investigation could be carried on by reproducing the same experiment and adding the tracking of the key displacement by the profilometer. A deep analysis of the measured key displacement in accordance with the finger trajectory filmed by the high-speed camera could be done. More repeatability of each measurement associated to the same instruction given to the musician should be considered. A musical context could be taken into account to analyse the clavichord paradox in a playing situation. Despite this paradox, it does not imply that all clavichord players adopt the same playing strategies to deal with it. There may not be only one kind of playing, but different ways of playing that would amount to a satisfactory musical result. Is there only one way to deal with the clavichord paradox, or is there a diversity of possible playing strategies ? Then, more musicians should be taken into account in this experiment with a comparative approach in order to deepen this investigation.

Furthermore, to underline the specificity of the playing in the clavichord, the measurements of this playing could be compared to that found in the case of the harpsichord and of the piano. Historically, the clavichord was considered as a fundamental means to practice keyboard instruments in general. Because the influence of the keyboard constraints on the fingers shape the motion of the player fingers, the clavichord player performance should be specific. These constraints are not the same when it comes to playing the piano and the harpsichord. Then, the question is how much does the mechanical constraints of the clavichord influences the playing of the musician. Comparing the finger motion of a pianist, a harpsichordist and a clavichord player on a same clavichord could be useful to deepen these investigations. The measured key depths and measured sound level could be compared to identify the principal differences in the musical results of these different musicians.

Considering more instruments

Finally, only the LAM1 clavichord was investigated in this work. Yet one clavichord cannot summarise the features belonging to the diversity of clavichords. Changing the dimension of the clavichord leads to changing the length of the stringing and its number of strings. Then the reverberation effect is different from one clavichord to another. Also, by changing the strings length, the stringing tension changes also. As a result, the hardness of touch created by the tangent-string contact can change from one clavichord to another. This means that the clavichord features analysed in this work can vary by means of instrument-making choices. Thus, one possible investigation is to study different clavichords and comparing there vibro-acoustic features to understand how different instrument-making parameters change these features. As a result, some experimental approaches should be reproduced on several clavichords. Comparing them by means of the indicators used in this work can lead

to a comparative study of the reverberation in the clavichord. Also, conducting the study of the clavichord paradox on different instruments could highlight the influences of the mechanical constraints on the playing.

Contributions

This work gave rise to a preprint of a journal paper, proceedings and presentations. The mentioned publications are showed in part VII.

Journal papers

Most of the work presented in chapter 2, 3 and 4 in this manuscript was submitted to publication in February 2021 in the *Journal of the Acoustical Society of America*.

Proceedings in national and international conferences

The conducted studies on clavichord sympathetic strings were presented at the *Congrès Français d'Acoustique* CFA in 2018 [121] and at the *International Modal Analysis Conference* (IMAC) conference in 2019 [122]. The work in chapter 5 was presented at the *International Symposium on Music Acoustics* (ISMA) conference in 2019 [123].

Presentations

Presentations of parts of this work were given by means of posters at the *Journée Jeunes Chercheurs en vibration, Acoustique et Bruit* (JJCAB) in 2017 and at the *Journées Jeunes Chercheurs en Acoustique, Audition et Signal* (JJCAAS) in 2019.

Bibliography

[1] Bernard Brauchli. *The clavichord*. Cambridge University Press, 1998.

[2] Edwin M Ripin. *Keyboard Instruments: Studies in Keyboard Organology, 1500-1800*. Dover Publications, 1977.

[3] Christophe d'Alessandro. On the dynamics of the clavichord: From tangent motion to sound. *The Journal of the Acoustical Society of America*, 128(4):2173–2181, 2010.

[4] Christophe d'Alessandro. Le paradoxe du clavicorde et la technique de Bach au clavier. *Revue musicale OICRM*, 6(1):87–112, 2019.

[5] Coin Christophe. *Amour et Sympathie*. Ensemble baroque de Limoge, 1995.

[6] Sebastian Virdung and Virdung Sebastian. *Musica Getutscht: a Treatise on Musical Instruments (1511) by Sebastian Virdung*. Cambridge University Press, 1993.

[7] M Mersenne. Harmonie universelle (1636), éditions du cnrs, 1965.

[8] Jakob Adlung. *M. Jacob Adlungs... Anleitung zu der musikalischen Gelahrtheit: theils vor alle Gelehrte, so das Band aller Wissenschaften einsehen: theils vor die Liebhaber der edlen Tonkunst überhaupt: theils und sonderlich vor die, so das Clavier vorzüglich lieben: theils vor die Orgel-und Instrumentmacher*. Jungnicol, 1758.

[9] Jakob Adlung. *Musica mechanica organoedi. Das ist: Gründlicher Unterricht von der Struktur, Gebrauch und Erhaltung, &c. der Orgeln, Clavicymbel, Clavichordien und anderer Instrumente, in so fern einem Organisten von solchen Sachen etwas zu wissen nöhtig ist*, volume 1. FW Birnstiel, 1768.

[10] Daniel Gottlob Turk and Siegbert Rampe. *Klavierschule, oder Anweisung zum Klavierspielen fur Lehrer und Lernende*. Barenreiter, 1789.

[11] Alfred James Hipkins. *A description and history of the pianoforte and of the older keyboard stringed instruments*, volume 52. London; New York: Novello, Ewer, 1896.

[12] Carl Engel. Some account of the clavichord with historical notices. *The Musical Times and Singing Class Circular*, 20(437):356–359, 411–415, 468–472, 1879.

[13] Jenny Nex and Lance Whitehead. The six early clavichords of arnold dolmetsch: their construction and inspiration. *The Galpin Society Journal*, 53:274–300, 2000.

[14] Wolfgang Strack. Christian gottlob hubert and his instruments. *The Galpin Society Journal*, pages 38–58, 1979.

[15] Koen Vermeij. *The Hubert Clavichord Data Book: A Description of All Extant Clavichords by Christian Gottlob Hubert, 1714-1793*. Clavichord International Press, 2000.

[16] Ferdinand Trendelenburg, E. Franz, and Erich Thienhaus. *Zur Klangwirkung von Klavichord, Cembalo und Flügel*. 1940.

[17] R.A. Hands. A scientific approach to the clavichord. *The Galpin Society Journal*, pages 89–98, 1967.

[18] Ralph W. Burhans. Clavichord amplification. *Journal of the Audio Engineering Society*, 21(6):460–463, 1973.

[19] Suszanne Thwaites and Neville H. Fletcher. Some notes on the clavichord. *The Journal of the Acoustical Society of America*, 69(5):1476–1483, 1981.

[20] Donald E Hall. String excitation: piano, harpsichord and clavichord. In *Proceedings of the 1993 Stockholm Music Acoustics Conference*, pages 309–314, 1993.

[21] Gabriel Weinreich. Coupled piano strings. *The Journal of the Acoustical Society of America*, 62(6):1474–1484, 1977.

[22] Vesa Välimäki and Cumhur Erkut. Commuted waveguide synthesis of the clavichord. *Computer Music Journal*, 27(1):71–82, 2003.

[23] Vesa Välimäki, Jyri Huopaniemi, Matti Karjalainen, and Zoltán Jánosy. Physical modeling of plucked string instruments with application to real-time sound synthesis. In *Audio Engineering Society Convention 98*. Audio Engineering Society, 1995.

[24] Julius O. Smith III and Scott A. Van Duyne. Commuted piano synthesis. In *ICMC*, 1995.

[25] Bernhard Winkler. Physical and acoustical properties of the clavichord: Experiment on selected instruments. In Bernard Brauchli et al, editor, *De Clavicordio VIII*. Musica Antica a Magnano, 2011.

[26] Christophe d'Alessandro, Charles Besnainou, and Luc Ginieis. Acoustic portraits of four clavichords: Tangent velocities, loudness, and decay time. In Bernard Brauchli et al, editor, *De Clavicordio VIII*. Musica Antica a Magnano, 2008.

[27] Anders Askenfelt. *Five Lectures on the Acoustics of the Piano*. Number 64. Royal Swedish Academy of Music Stockholm, Sweden, 1990.

[28] Anders Askenfelt and Erik V. Jansson. From touch to string vibrations. i: Timing in the grand piano action. *The Journal of the Acoustical Society of America*, 88(1):52–63, 1990.

[29] R.D. Weyer. Time-frequency-structures in the attack transients of piano and harpsichord sounds–i. *Acta Acustica united with Acustica*, 35(4):232–252, 1976.

[30] Antoine Chaigne and Anders Askenfelt. Numerical simulations of piano strings. i. a physical model for a struck string using finite difference methods. *The Journal of the Acoustical Society of America*, 95(2):1112–1118, 1994.

[31] Antoine Chaigne and Anders Askenfelt. Numerical simulations of piano strings. ii. comparisons with measurements and systematic exploration of some hammer-string parameters. *The Journal of the Acoustical Society of America*, 95(3):1631–1640, 1994.

[32] Julien Bensa, Frederic Gibaudan, Kristoffer Jensen, and Richard Kronland-Martinet. Note and hammer velocity dependence of a piano string model based on coupled digital waveguides. In *ICMC*, 2001.

[33] Antoine Chaigne. Reconstruction of piano hammer force from string velocity. *The Journal of the Acoustical Society of America*, 140(5):3504–3517, 2016.

[34] Stephen Birkett. Experimental investigation of the piano hammer-string interaction. *The Journal of the Acoustical Society of America*, 133(4):2467–2478, 2013.

[35] Chandrika P. Vyasarayani, Stephen Birkett, and John McPhee. Modeling the dynamics of a compliant piano action mechanism impacting an elastic stiff string. *The Journal of the Acoustical Society of America*, 125(6):4034–4042, 2009.

[36] Anders Thorin, Xavier Boutillon, and José Lozada. Modelling the dynamics of the piano action: is apparent success real? *Acta Acustica united with Acustica*, 100(6):1162–1171, 2014.

[37] Ramin Masoudi, Stephen Birkett, and John McPhee. A mechanistic multibody model for simulating the dynamics of a vertical piano action. *Journal of Computational and Nonlinear Dynamics*, 9(3):031014, 2014.

[38] Ramin Masoudi and Stephen Birkett. Experimental validation of a mechanistic multibody model of a vertical piano action. *Journal of Computational and Nonlinear Dynamics*, 10(6):061004, 2015.

[39] Julien Bensa, Stefan Bilbao, Richard Kronland-Martinet, and Julius O. Smith III. From the physics of piano strings to digital waveguides. In *ICMC*, 2002.

[40] Julien Bensa. *Analyse et synthèse de sons de piano par modèles physiques et de signaux*. PhD thesis, Aix-Marseille II, 2003.

[41] Juliette Chabassier. *Modélisation et simulation numérique d'un piano par modèles physiques*. PhD thesis, École polytechnique, 2012.

[42] Xavier Boutillon and Kerem Ege. Vibroacoustics of the piano soundboard: Reduced models, mobility synthesis, and acoustical radiation regime. *Journal of Sound and Vibration*, 332(18):4261–4279, 2013.

[43] Gautier Lefebvre, Marcel Filoche, and Xavier Boutillon. Localization in the piano soundboard. *The Journal of the Acoustical Society of America*, 140(4):3255–3255, 2016.

[44] Kerem Ege. *La table d'harmonie du piano-Études modales en basses et moyennes fréquences*. PhD thesis, École polytechnique, 2009.

[45] Kerem Ege, Xavier Boutillon, and Marc Rébillat. Vibroacoustics of the piano soundboard: (non) linearity and modal properties in the low-and mid-frequency ranges. *Journal of Sound and Vibration*, 332(5):1288–1305, 2013.

[46] Benjamin Elie. *Caractérisation vibratoire et acoustique des instruments à cordes-Application à l'aide à la facture instrumentale*. PhD thesis, Université du Mans, 2012.

[47] Michel Bernays and Caroline Traube. Investigating pianists' individuality in the performance of five timbral nuances through patterns of articulation, touch, dynamics, and pedaling. *Frontiers in Psychology*, 5:157, 2014.

[48] Caroline Traube. Piano tone control through variation of "weight" applied on the keys. *The Journal of the Acoustical Society of America*, 141(5):3874–3874, 2017.

[49] Neville H Fletcher. Analysis of the design and performance of harpsichords. *Acta Acustica united with Acustica*, 37(3):139–147, 1977.

[50] William R. Savage, Edward L. Kottick, Thomas J. Hendrickson, and Kenneth D. Marshall. Air and structural modes of a harpsichord. *The Journal of the Acoustical Society of America*, 91(4):2180–2189, 1992.

[51] P.J. Bryanston-Cross and J.W. Gardner. Application of holographic interferometry to the vibrational analysis of the harpsichord. *Optics & Laser Technology*, 20(4):199–204, 1988.

[52] Hidetoshi Arakawa. The acoustical effect of a metal rose in a harpsichord: Part i. In *Proceeding of the International Symposium on Musical Acoustics*. Citeseer, 2004.

[53] Arthur Pate, Arthur Givois, Jean-Loïc Le Carrou, Michele Castellengo, Sandie Le Conte, and Stephane Vaiedelich. Investigating multimodal perception during the musical performance: The case of harpsichord voicing. *The Journal of the Acoustical Society of America*, 141(5):3874–3874, 2017.

[54] Arthur Paté, Jean-Loïc Le Carrou, Arthur Givois, and Alexandre Roy. Influence of plectrum shape and jack velocity on the sound of the harpsichord: an experimental study. *The Journal of the Acoustical Society of America*, 141(3):1523–1534, 2017.

[55] Christian Cuesta and Claude Valette. Le transitoire d'attaque des cordes de clavecin. *Acta Acustica united with Acustica*, 68(2):112–122, 1989.

[56] Sylvie Le Moyne, Sandie Le Conte, François Ollivier, Joël Frelat, Jean-Claude Battault, and Stéphane Vaiedelich. Restoration of a 17th-century harpsichord to playable condition: A numerical and experimental study. *The Journal of the Acoustical Society of America*, 131(1):888–896, 2012.

[57] Sylvie Le Moyne, Sandie Le Conte, and François Ollivier. Couchet harpsichord soundboard vibroacoustics behaviour: An application of the impact nearfield acoustical holography (ipnah). *Journal of the Acoustical Society of America*, 123(5):3445–3445, 2008.

[58] Christian Cuesta and Claude Valette. Mécanique de la corde vibrante. *Paris: Hermes*, 520, 1993.

[59] Stephen Birkett and Paul Poletti. Reproduction of authentic historical soft iron wire for musical instruments. *Actes Rencontres Harmoniques Lausanne*, pages 259–279, 2002.

[60] Romain Viala. *Towards a model-based decision support tool for stringed musical instruments making: Outil d'aide à la décision pour la facture d'instruments de musique à cordes*. PhD thesis, Bourgogne Franche-Comté, 2018.

[61] Matt Borland. *The characterisation of piano soundboard materials with respect to their vibrational and psychoacoustical properties for evaluation purposes*. PhD thesis, University of Waterloo, 2009.

[62] Colin E. Gough. The theory of string resonances on musical instruments. *Acta Acustica united with Acustica*, 49(2):124–141, 1981.

[63] Jim Woodhouse. On the synthesis of guitar plucks. *Acta Acustica united with Acustica*, 90(5):928–944, 2004.

[64] N.C. Perkins and C.D. Mote Jr. Comments on curve veering in eigenvalue problems. *Journal of Sound and Vibration*, 106(3):451–463, 1986.

[65] Arthur Paté, Jean-Loïc Le Carrou, and Benoît Fabre. Predicting the decay time of solid body electric guitar tones. *The Journal of the Acoustical Society of America*, 135(5):3045–3055, 2014.

[66] Antoine Chaigne. Modélisation du piano et couplage cordes-chevalet. *Proceedings of 12ème Congrès Français d'Acoustique*, pages 1085–1091, 2014.

[67] Jean-Loïc Le Carrou, Francois Gautier, Nicolas Dauchez, and Joël Gilbert. Modelling of sympathetic string vibrations. *Acta Acustica united with Acustica*, 91(2):277–288, 2005.

[68] V. Debut, J. Antunes, M. Marques, and M. Carvalho. Physics-based modeling techniques of a twelve-string portuguese guitar: A non-linear time-domain computational approach for the multiple-strings/bridge/soundboard coupled dynamics. *Applied Acoustics*, 108:3–18, 2016.

[69] Firdaus E. Udwadia and Robert E. Kalaba. On the foundations of analytical dynamics. *International Journal of non-linear mechanics*, 37(6):1079–1090, 2002.

[70] Hao Sun, Han Zhao, Shengchao Zhen, Kang Huang, Fumin Zhao, Xianmin Chen, and Ye-Hwa Chen. Application of the udwadia–kalaba approach to tracking control of mobile robots. *Nonlinear Dynamics*, 83(1-2):389–400, 2016.

[71] Jose Antunes and Vincent Debut. Dynamical computation of constrained flexible systems using a modal udwadia-kalaba formulation: Application to musical instruments. *The Journal of the Acoustical Society of America*, 141(2):764–778, 2017.

[72] Vincent Debut and Jose Antunes. Physical synthesis of six-string guitar plucks using the udwadia-kalaba modal formulation. *The Journal of the Acoustical Society of America*, 148(2):575–587, 2020.

[73] Antoine Caillon, Jean-Loïc Le Carrou, Baptiste Chomette, and Sylvie Le Bomin. Modelling of gabonese harps. In *Proceedings of the International Symposium on Musical Acoustics ISMA '19*, 2020.

[74] Jean-Loïc Le Carrou, François Gautier, and Roland Badeau. Sympathetic string modes in the concert harp. *Acta Acustica united with Acustica*, 95(4):744–752, 2009.

[75] Jean-Loïc Le Carrou. *Vibro-acoustique de la harpe de concert*. PhD thesis, Université du Maine, 2006.

[76] Fredrik Öberg and Anders Askenfelt. Acoustical and perceptual influence of duplex stringing in grand pianos. *The Journal of the Acoustical Society of America*, 131(1):856–871, 2012.

[77] Christophe d'Alessandro, Brian FG Katz, and François Boudet. On the acoustics of the clavichord. In Bernard Brauchli et al, editor, *De Clavicordio VII*. Musica Antica a Magnano, 2005.

[78] Christophe d'Alessandro and Brian F.G. Katz. Tonal quality of the clavichord: The effect of sympathetic strings. In *Proceedings of the International Symposium on Musical Acoustics ISMA '04*, pages 21–24, 2004.

[79] Philip M. Morse and K. Uno Ingard. Theoretical acoustics. *Princeton University Press*, 1968.

[80] Gustav Kirchhoff. *Vorlesungen Uber Mechanik*. BG Teubner, 1883.

[81] GF Carrier. On the non-linear vibration problem of the elastic string. *Quarterly of Applied Mathematics*, 3(2):157–165, 1945.

[82] David J. Ewins. *Modal testing: theory and practice*, volume 15. Research studies press Letchworth, 1984.

[83] Ara Arabyan and Fei Wu. An improved formulation for constrained mechanical systems. *Multibody System Dynamics*, 2(1):49–69, 1998.

[84] Olivier A. Bauchau and André Laulusa. Review of contemporary approaches for constraint enforcement in multibody systems. *Journal of Computational and Nonlinear Dynamics*, 3(1):01 1004, 2008.

[85] Ahmed A. Shabana. *Computational dynamics*. John Wiley & Sons, 2009.

[86] Jose Antunes, Vincent Debut, Laurent Borsoi, Xavier Delaune, and Philippe Piteau. A modal udwadia-kalaba formulation for vibro-impact modelling of continuous flexible systems with intermittent contacts. *Procedia engineering*, 199:322–329, 2017.

[87] S. Yoon, R.M. Howe, and D.T. Greenwood. Geometric elimination of constraint violations in numerical simulation of lagrangian equations. 116(4):1058–1064, 1994.

[88] Jean-Loïc Le Carrou, Delphine Chadefaux, Léonard Seydoux, and Benoit Fabre. A low-cost high-precision measurement method of string motion. *Journal of Sound and Vibration*, 333(17):3881–3888, 2014.

[89] Richard Roy and Thomas Kailath. Esprit-estimation of signal parameters via rotational invariance techniques. *IEEE Transactions on acoustics, speech, and signal processing*, 37(7):984–995, 1989.

[90] Arthur Paté. *Lutherie de la guitare électrique solid body: aspects mécaniques et perceptifs*. PhD thesis, Paris 6, 2014.

[91] Clara Issanchou. *Vibrations non linéaires de cordes avec contact unilatéral. Application aux instruments de musique*. PhD thesis, Paris 6, 2017.

[92] Ahmet Arda Ozdemir and Suat Gumussoy. Transfer function estimation in system identification toolbox via vector fitting. *IFAC-PapersOnLine*, 50(1):6232–6237, 2017.

[93] Charles L. Lawson and Richard J. Hanson. *Solving least squares problems*. Upper Saddle River, NJ: Prentice Hall, 1974.

[94] Stefan Bilbao. *Numerical sound synthesis: finite difference schemes and simulation in musical acoustics*. John Wiley & Sons, 2009.

[95] Peter Bavington. Keylever, tangent and string—a preliminary analysis of clavichord touch and action. In *De Clavicordio III*, pages 61–99, 1998.

[96] Pierre E Cartier, Bernard Julia, Pierre Moussa, and Pierre Vanhove. *Frontiers in number theory, physics, and geometry II: on conformal field theories, discrete groups and renormalization*, volume 2. Springer Science & Business Media, 2007.

[97] Alain De Cheveigné and Hideki Kawahara. Yin, a fundamental frequency estimator for speech and music. *The Journal of the Acoustical Society of America*, 111(4):1917–1930, 2002.

[98] Bharat Bhargava. *Digital libraries and multimedia*. Springer Science & Business Media, 2007.

[99] Jean-Loïc Le Carrou, Delphine Chadefaux, Marie-Aude Vitrani, Sylvère Billout, and Laurent Quartier. Dropic: A tool for the study of string instruments in playing conditions. In *Acoustics 2012*, 2012.

[100] Christophe d'Alessandro. Le paradoxe du clavicorde et la technique de bach au clavier. *Revue musicale OICRM*, 6(1):87–112, 2019.

[101] Anders Askenfelt, C. Beebe, G. Bissinger, E. Bynum, G. Caldersmith, M. Campbell, P. Campbell, D.J. Cohen, J. Curtin, N.H. Fletcher, et al. *The science of string instruments*. Springer New York, 2010.

[102] Christophe d'Alessandro. Le paradoxe du clavicorde. In *Congrès Français d'Acoustique (CFA 2016)*, pages 2263–2269. Société Française d'Acoustique, 2016.

[103] Johann Gotfried Walther. *Musicalisches Lexicon oder Musicalische Bibliothec*. Wolfgang Deer, 1732.

[104] Georg Simon Löhlein. *Clavier-Schule, oder kurze und gründliche Anweisung zur Melodie und Harmonie: durchgehends mit practischen Beyspielen erkläret.(Klavier.)*, volume 75. Waisenhaus-und Frommannische Buchhandlung, 1773.

[105] Carl Philipp Emanuel Bach. Versuch über die wahre art, das clavier zu spielen, 2 teile. *Berlin: Henning/Winter*, 1753.

[106] Charles Burney. *The Present State of Music in Germany, the Netherlands and United Provinces Or The Journal of a Tour Through Those Countries, Undertaken to Collect Materials for a General History of Music: In Two Volumes*, volume 1. Becket, 1775.

[107] Johann Gottfried Herder. *Kalligone*. Hartknoch, 1800.

[108] Johann Joachim Quantz. *Versuch einer Anweisung die Flöte traversiere zu spielen*, volume 1. Voß, 1752.

[109] Menno Van Delft. Schnellen. a quintessential articulation technique in eighteenth-century keyboard playing. *The Keyboard in Baroque Europe*, Christopher Hogwood (dir.)(1):187–197, 2003.

[110] Christopher Hogwood. A supplement to cpe bach's versuch: Ew wolf's anleitung of 1785. In Stephen Clark, editor, *C. P. E. Bach Studies*. Clarendon Press, Oxford, 1988.

[111] Nicolas-Joseph Hülmandel. Clavecin. In Nicolas Étienne Framery et al, editor, *Encyclopédie méthodique, 1ère éd., tome 1, [A-Gym]*. Panckoucke, Paris.

[112] Sylvie Vangenot. L'oreille absolue: une oreille plus "fine"? *Musicae Scientiae*, 4(1):3–29, 2000.

[113] Charles Besnainou et Michèle Castellengo. De la résonance, une étude acoustique du phénomène sympathique. In Christophe Coin, editor, *Amour et sympathie*. Tenu á Limoge les 28 et 29 novembre 1992 (p. 53-61). L'ensemble baroque de Limoge.

[114] Stephanie Weisser and Matthias Demoucron. Shaping the resonance. sympathetic strings in hindustani classical instruments. In *Proceedings of Meetings on Acoustics 163ASA*, volume 15, page 035006. ASA, 2012.

[115] Antoine Chaigne and Jean Kergomard. *Acoustique des instruments de musique (2e édition revue et augmentée)*. Belin, 2013.

[116] Vincent Fréour, François Gautier, Bertrand David, and Marthe Curtit. Extraction and analysis of body-induced partials of guitar tones. *The Journal of the Acoustical Society of America*, 138(6):3930–3940, 2015.

[117] Manfred R. Schroeder. Response to "comments on 'new method of measuring reverberation time'"[pw smith, jr., j. acoust. soc. am. 38, 359 (l)(1965)]. *The Journal of the Acoustical Society of America*, 38(2):359–361, 1965.

[118] Geoffroy Peeters, Bruno L. Giordano, Patrick Susini, Nicolas Misdariis, and Stephen McAdams. The timbre toolbox: Extracting audio descriptors from musical signals. *The Journal of the Acoustical Society of America*, 130(5):2902–2916, 2011.

[119] Jean Piranda. Analyse modale expérimentale. *Techniques de l'ingénieur. Bruit et vibrations*, (R6180), 2001.

[120] Alexandre Roy. *Développement d'une plate-forme robotisée pour l'étude des instruments de musique à cordes pincées*. PhD thesis, Paris 6, 2015.

[121] Jean-Théo Jiolat, Christophe d'Alessandro, and Jean-Loïc Le Carrou. L'effet acoustique des cordes mortes du clavicorde. In *Congrès Français d'Acoustique, CFA 2018*, pages 233–239, 2018.

[122] Jean-Théo Jiolat, Jean-Loïc Le Carrou, and Christophe d'Alessandro. A parametric study of finger motions when playing the clavichord: towards characterization of expressive control. In *ISMA 2019-International Symposium on Music Acoustics*, pages 167–174, 2019.

[123] Jean-Théo Jiolat, Jean-Loïc Le Carrou, Jose Antunes, and Christophe D'Alessandro. Modelling of sympathetic string vibrations in the clavichord using a modal Udwadia-Kalaba formulation. In SEM, editor, *Proceedings of the 37th IMAC, A Conference and Exposition on Structural Dynamics 2019*, volume 3 of *Model Validation and Uncertainty Quantification*, pages 277–280. Springer, 2019.

[124] Anders Brandt. *Noise and vibration analysis: signal analysis and experimental procedures*. John Wiley & Sons, 2011.

[125] Jose Antunes, Vincent Debut, Pilippe Piteau, Xavier Delaune, and Laurent Borsoi. On using the hilbert transform for blind identification of complex modes: a practical approach. *Journal of Sound and Vibration*, 412:222–241, 2018.

[126] Delphine Chadefaux, Jean-Loïc Le Carrou, and Benoît Fabre. A model of harp plucking. *The Journal of the Acoustical Society of America*, 133(4):2444–2455, 2013.

[127] José Lozada. *Modélisation, contrôle haptique et nouvelles réalisations de claviers musicaux*. PhD thesis, Ecole polytechnique, 2007.

Part VI

Annexes

A Overall characteristics of the LAM1 clavichord

PACKING LIST

Unless otherwise noted, all dimensions are stated in mm with length, width and depth, and can vary slightly from those given here because the parts are cut to fit each other.

Quantities for hardware and action parts are approximate, as are lengths for the cloths.

The Hubert Clavichord is packed in a single box measuring 134 x 54 x 16cm (0.116m3) and weighing approximately 26kg.

Case parts

Bottom	1248 x 334 x 25	*spruce*	Bottom stiffener	19 x 32 x 482	*spruce*
Spine	1270 x 110 x 11	*cherry*	Casefront rail	19 x 22 x 679	"
Casefront	1270 x 110 x 11 with cutout		Box back	11 x 36 x 6	*cherry*
Case ends (2)	11 x 110 x 334		Box lid	11 x 6 x 121	"
Cheeks (2 different)	11 x 110 x 126		Box lid supports (2)	7 x 1 x 6	*lime* or *poplar*
Fallboard	11 x 52 x 683		Soundboard	3 x 333 x 51	*spruce*
Nameboard	11 x 36 x 705		Cutoff bar	8 x 15 x 492	*spruce*
Wrestplank	43 x 54 x 334	*oak*	Soundboard rib	5 x 1 x 538	"
Wrestplank dogleg	28 x 46 x 373	"	Bridge	curved and s-shaped	*pear*
Bass hitchpin block	38 x 54 x 334	"	Bottom mouldings (2)	8 x 19 x 130	*cherry*
Treble hitchpin block	55 x 92 x 673	*poplar*		8 x 19 x 42	"
Bass hitchpinrail cap	11 x 38 x 213	*cherry*	Soundboard mouldings (3)	5 x 5 x 80	*pear*
Treble hitchpinrail cap	11 x 92 x 673	"	Lid	11 x 365 x 1278	*cherry*
Bellyrail	25 x 55 x 342	*beech*	Case rim clamping blocks (8)	13 x 19 x 102	*lime* or *poplar*
Front liner	13 x 55 x 427	*lime*	Soundboard clamping cauls (6)	1 x 28 x various	"
Rear liner	13 x 55 x 477	"			

The Packing List continues on the following page with the Action Parts

Figure 8.1: Dimensions of the LAM1 clavichord components of the case part made by Dancet and Ducornet (copyright E. Dancet and M. Ducornet, The Paris Workshop).

Action parts

Keyboard & Accessories
Balance rail — 29 x 41 x 714 — *beech*
Backrail — 25 x 32 x 68 — "
Keyboard, 51 keys, C–d'''
Accidentals (21) — *cherry*

Hardware Bag (quantities approximate)
Balance rail & backrail screws 1¼" x #10 (4)
Cut nails 1¼" (±48)
Drill bits (3) — ø 3.3mm for tuning pins
ø 1mm for bridge pins
ø 1.6mm for hitchpins
Lid hinges (3) & screws — *brass*
Fallboard hinges (2) & screws
Screweyes (2) & lid cord

Various
Clavichord tuning hammer
Tuning mute — *rubber*
Tangents (55) — *brass*

Pin Bag
Hitchpins (±76)
Bridgepins (±76)
Balance pins ø 2.3mm x 32mm (53)
Guide pins ø 2.3mm x 38mm (53)
Tuning pins, with hole, ø 3.5mm (±76)
Marking tool handle and stringing hook

Action Cloths Bag
Backrail cloth (1.7m)
Cloth balance punchings (53)
Listing cloth

Separately
Bag of strings, sample loop & stringing schedule
Titebond glue
Construction manual
Drawing — *paper*

The Hubert Clavichord I, page 13

Figure 8.2: Dimensions of the LAM1 clavichord components of the action part made by Dancet and Ducornet (copyright E. Dancet and M. Ducornet, The Paris Workshop).

Figure 8.3: Building of the LAM1 clavichord box.

Figure 8.4: Gluing of the soundboard with the bridge of the LAM1 clavichord designed by Dancet and Ducornet during its construction.

Figure 8.5: Box of the LAM1 clavichord designed by Dancet and Ducornet during its construction.

B Stringing of the LAM1 clavichord

B.1 Played part of the strings

Number	Note	Frequency (Hz)	Total length (cm)	Played length (cm)	Diameter (mm)
1	C_1	61,69	110.5	108.7	0.64
2	C_1	61,69	111.0	109.2	0.64
3	$C\#_1$	65,36	109.8	108.0	0.64
4	$C\#_1$	65,36	109.8	108.0	0.64
5	D_1	69,25	108.9	106.5	0.56
6	D_1	69,25	109.9	106.5	0.56
7	$D\#_1$	73,36	109.5	105.0	0.56
8	$D\#_1$	73,36	110.0	105.0	0.56
9	E_1	77,72	109.2	103.8	0.51
10	E_1	77,72	110.0	103.7	0.51
11	F_1	82,35	108.8	102.2	0.51
12	F_1	82,35	109.7	102.3	0.51
13	$F\#_1$	87,24	108.7	100.4	0.51
14	$F\#_1$	87,24	109.6	100.2	0.51
15	G_1	92,43	108.6	99.0	0.46
16	G_1	92,43	109.9	98.8	0.46
17	$G\#_1$	97,93	108.7	97.2	0.46
18	$G\#_1$	97,93	109.1	97.0	0.46
19	A_1	103.8	107.8	95.6	0.46
20	A_1	103.8	108.2	95.2	0.46
21	$A\#_1$	109,9	106.7	93.4	0.41
22	$A\#_1$	109,9	107.5	93.1	0.41
23	B_1	116,5	106.3	91.1	0.41
24	B_1	116,5	106.5	91.0	0.41
25	C_2	123,4	105.7	89.1	0.41
26	C_2	123,4	105.6	88.6	0.41
27	$C\#_2$	130,7	104.6	86.5	0.41
28	$C\#_2$	130,7	104.5	85.9	0.41
29	D_2	138,5	102.4	83.5	0.36
30	D_2	138,5	102.9	82.7	0.36
31	$D\#_2$	146,7	99.4	80.6	0.36
32	$D\#_2$	146,7	99.8	79.6	0.36
33	E_2	155,4	95.4	77.3	0.36

Continued on next page

Number	Note	Frequency (Hz)	Total length (cm)	Played length (cm)	Diameter (mm)
34	E_2	155,4	95.6	76.3	0.36
35	F_2 - $F\#_2$	164,7 - 174,5	90.7	74.0 - 70.2	0.36
36	F_2 - $F\#_2$	164,7 - 174,5	90.7	72.8 - 68.9	0.36
37	G_2 - $G\#_2$	184,9 - 195,9	85.5	67.0 - 63.5	0.36
38	G_2 - $G\#_2$	184,9 - 195,9	85.2	65.6 - 62.3	0.36
39	A_2	207,5	80.4	60.1	0.36
40	A_2	207,5	80.5	59.0	0.36
41	$A\#_2$ - B_2	219,8 - 232,9	76.0	56.7 - 53.9	0.36
42	$A\#_2$ - B_2	219,8 - 232,9	76.1	55.5 - 52.7	0.36
43	C_3 - $C\#_3$	246,8 - 261,4	71.4	50.7 - 48.0	0.33
44	C_3 - $C\#_3$	246,8 - 261,4	70.7	49.5 - 46.9	0.33
45	D_3	277,0	66.3	44.7	0.33
46	D_3	277,0	66.3	43.5	0.33
47	$D\#_3$ - E_3	293,4 - 310,9	61.2	41.6 - 39.4	0.33
48	$D\#_3$ - E_3	293,4 - 310,9	61.0	40.8 - 38.6	0.33
49	F_3 - $F\#_3$	329,4 - 349,0	57.2	37.1 - 35.2	0.33
50	F_3 - $F\#_3$	329,4 - 349,0	57.6	36.5 - 34.6	0.33
51	G_3 - $G\#_3$	369,7 - 391,7	53.5	33.6 - 31.8	0.33
52	G_3 - $G\#_3$	369,7 - 391,7	54.2	32.9 - 31.1	0.33
53	A_3	415,0	50.6	29.7	0.33
54	A_3	415,0	51.1	29.3	0.33
55	$A\#_3$ - B_3	439,7 - 465,8	47.2	28.0 - 26.4	0.33
56	$A\#_3$ - B_3	439,7 - 465,8	47.6	27.7 - 26.1	0.33
57	C_4 - $C\#_4$	493.5 - 522,9	43.5	25 - 23.9	0.30
58	C_4 - $C\#_4$	493.5 - 522,9	44.7	24.7 - 23.6	0.30
59	D_4	554,0	41.1	22.4	0.30
60	D_4	554,0	42.8	22.2	0.30
61	$D\#_4$ - E_4	586,7 - 621,8	38.2	21.3 - 20	0.30
62	$D\#_4$ - E_4	586,7 - 621,8	39.1	20.9 - 19.7	0.30
63	F_4 - $F\#_4$	658,8 - 697,9	35.4	19 - 18	0.30
64	F_4 - $F\#_4$	658,8 - 697,9	36.3	18.9 - 17.9	0.30
65	G_4 - $G\#_4$	739,4 - 783,4	33.0	16.7 - 15.9	0.30
66	G_4 - $G\#_4$	739,4 - 783,4	33.5	16.6 - 15.8	0.30
67	A_4	830	30.2	14.7	0.28
68	A_4	830	30.7	14.6	0.28
69	$A\#_4$ - B_4	879,4 - 931,6	27.3	13.6 - 12.4	0.28

Continued on next page

Number	Note	Frequency (Hz)	Total length (cm)	Played length (cm)	Diameter (mm)
70	$A\#_4$ - B_4	879,4 - 931,6	29.0	13.6 - 12.4	0.28
71	C_5 - $C\#_5$	987,0 - 1046	24.6	11.9 - 11.9	0.28
72	C_5 - $C\#_5$	987,0 - 1046	25.5	11.8 - 11.0	0.28
73	D_5	1108	22.9	10.3	0.28
74	D_5	1108	23.4	10.3	0.28

B.2 Sympathetic part of the strings

Number	Note	Frequency (Hz)	Length (cm)	Diameter (mm)
1	C_1	938.4	6,8	0.64
2	C_1	1068	7,5	0.64
3	$C\#_1$	1080	8,3	0.64
4	$C\#_1$	893,0	8,9	0.64
5	D_1	1023	6,8	0.56
6	D_1	1147	7,6	0.56
7	$D\#_1$	876,3	8,4	0.56
8	$D\#_1$	958,8	9,1	0.56
9	E_1	1077	6,9	0.51
10	E_1	1214	7,7	0.51
11	F_1	925,4	8,6	0.51
12	F_1	1018	9,5	0.51
13	$F\#_1$	1119	7,3	0.51
14	$F\#_1$	1258	8,2	0.51
15	G_1	932,4	9,1	0.46
16	G_1	1056	10	0.46
17	$G\#_1$	1102	7,9	0.46
18	$G\#_1$	1222	8,9	0.46
19	A_1	935,2	9,7	0.46
20	A_1	1048	8,8	0.46
21	$A\#_1$	1046	11	0.41
22	$A\#_1$	1179	10,4	0.41
23	B_1	880,4	10,7	0.41
24	B_1	977,8	10	0.41
25	C_2	952.2	12,2	0.41
26	C_2	1070	11,7	0.41
27	$C\#_2$	788,0	13	0.41
28	$C\#_2$	875,2	14,4	0.41
29	D_2	802	13	0.36
30	D_2	901,3	14,5	0.36
31	$D\#_2$	756,9	16,1	0.36
32	$D\#_2$	744,2	17,9	0.36
33	E_2	655,1	16,8	0.36
34	E_2	728,2	18,3	0.36

Continued on next page

Number	Note	Frequency (Hz)	Length (cm)	Diameter (mm)
35	F_2 - $F\#_2$	542,4	20,2	0.36
36	F_2 - $F\#_2$	595,3	22,2	0.36
37	G_2 - $G\#_2$	520,8	21,3	0.36
38	G_2 - $G\#_2$	584,5	23,3	0.36
39	A_2	458,3	25,3	0.36
40	A_2	500,4	27,2	0.36
41	$A\#_2$ - B_2	461,5	24,4	0.36
42	$A\#_2$ - B_2	518,8	26,9	0.36
43	C_3 - $C\#_3$	389,2	29,4	0.33
44	C_3 - $C\#_3$	429,8	31,6	0.33
45	D_3	414,7	26,6	0.33
46	D_3	470,6	29,2	0.33
47	$D\#_3$ - E_3	529,4	31,7	0.33
48	$D\#_3$ - E_3	588,4	33,7	0.33
49	F_3 - $F\#_3$	402,4	28,3	0.33
50	F_3 - $F\#_3$	347,0	30,1	0.33
51	G_3 - $G\#_3$	360,4	32,1	0.33
52	G_3 - $G\#_3$	384,5	33,8	0.33
53	A_3	405,3	28,2	0.33
54	A_3	437,0	29,8	0.33
55	$A\#_3$ - B_3	367,7	31,3	0.33
56	$A\#_3$ - B_3	392,2	32,9	0.33
57	C_4 - $C\#_4$	434,1	27	0.30
58	C_4 - $C\#_4$	460,8	28,4	0.30
59	D_4	396	29,9	0.30
60	D_4	418	31,2	0.30
61	$D\#_4$ - E_4	458,0	25,6	0.30
62	$D\#_4$ - E_4	484,2	26.7	0.30
63	F_4 - $F\#_4$	420,4	28,1	0.30
64	F_4 - $F\#_4$	441,7	29,4	0.30
65	G_4 - $G\#_4$	495,7	23,5	0.30
66	G_4 - $G\#_4$	525,7	24,8	0.30
67	A_4	443,8	26,1	0.28
68	A_4	468,8	27,3	0.28
69	$A\#_4$ - B_4	530,2	21,7	0.28
70	$A\#_4$ - B_4	560,4	22,7	0.28

Continued on next page

Number	Note	Frequency (Hz)	Length (cm)	Diameter (mm)
71	C_5 - $C\#_5$	477,4	23,6	0.28
72	C_5 - $C\#_5$	461,1	24,7	0.28
73	C_5	571,1	19,3	0.28
74	C_5	603,9	20,2	0.28

C Modal analysis of the bridge

In the prospect of modeling the 74 strings of the LAM1 clavichord, a modal analysis of the bridge with a complete discretization of this structure is necessary. Given the proximity of the strings in the case of the clavichord, one point of discretization for each pair of strings is decided, which amounts to 37 points (see figure 8.6). First, a driven point must be chosen to proceed to the modal analysis of the bridge. Because of the geometry of the bridge, it is difficult to get a proper impulse signal by the impact hammer. Once a proper layout of the hammer is found, it should not be moved anymore to secure the good quality of the impulse. Thus, the hammer remains at the considered driven point during the experiment. All the strings are damped by means of felts. The 14^{th} point is considered as the driven point, because this place is one of the most adequate to give to the bridge an impact at the vertical axis.

Figure 8.6: Experimental setup for the modal analysis of the bridge, with the designation measurement point number, with the z axis.

Then, the sensor measuring the response of the bridge is moved to each discretized point, so that the expected 37 FRF's needed for the bridge modal analysis are measured. The decided sensor is a vibrometer (Polytech PDV 100), which measures the vibratory velocity response of the structure. Its low-pass analogical filter is placed at 22 kHz so that it doesn't affect the measurements. Also, the delay of the measured signal inherent to the vibrometer laser functioning is taken into account. The clavichord is placed in a muted chamber for this experiment.

Since the vibrometer measures the velocity response of the bridge, the obtained FRF's are mobilities. In figures 8.7 (a), (b) and (c), the spectral amplitude, conductance, and susceptance of the mobility respectively of each measured point are shown. The spectral amplitudes give an idea of the operational deformation of the structure. As it is explained in section 7.2, the conductance (the real part of the mobility) indicates how the coupling mobility can influence the damping of the coupled string at a specific coupling point. Also, the susceptance (the imaginary part of the mobility) encapsulates the information regarding the bridge mode shapes.

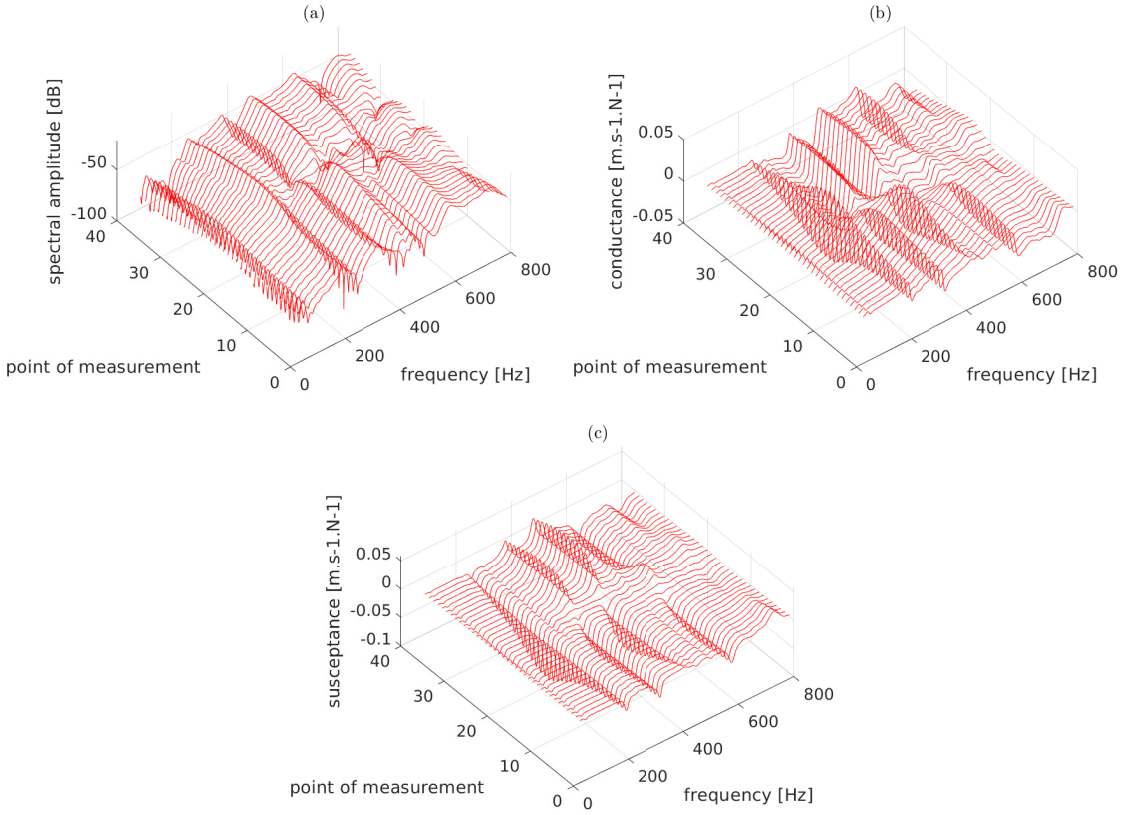

Figure 8.7: Spectral amplitude (a), conductance (b), and susceptance (c) of the 37 measurement points' FRF of the bridge.

Then, with these measurements, the bridge modal analysis is performed. A frequency range going from 40 to 800 Hz is done. A number of 12 modes are extracted. The poles are computed by means of the LSRF (Least Square Rational Functions) method [92]. As to normalisation, the modal masses are normalised as such : $m_n = 1$. Then, by means of the residues, the according real mode shapes are deduced with respect to this normalisation (see annex D). In figure 8.8, the measured FRF, that of the 14^{th} measurement (driving point) and the 26^{th} measurement point, and the corresponding ones reconstructed by means of modal analysis are shown, assuring the good quality of the extracted modal parameters. The according bridge mode shapes of some of the extracted modes are shown in figures 8.9 and 8.10. Ideally, these modal parameters could be used to model the coupling of the 37 pairs of strings.

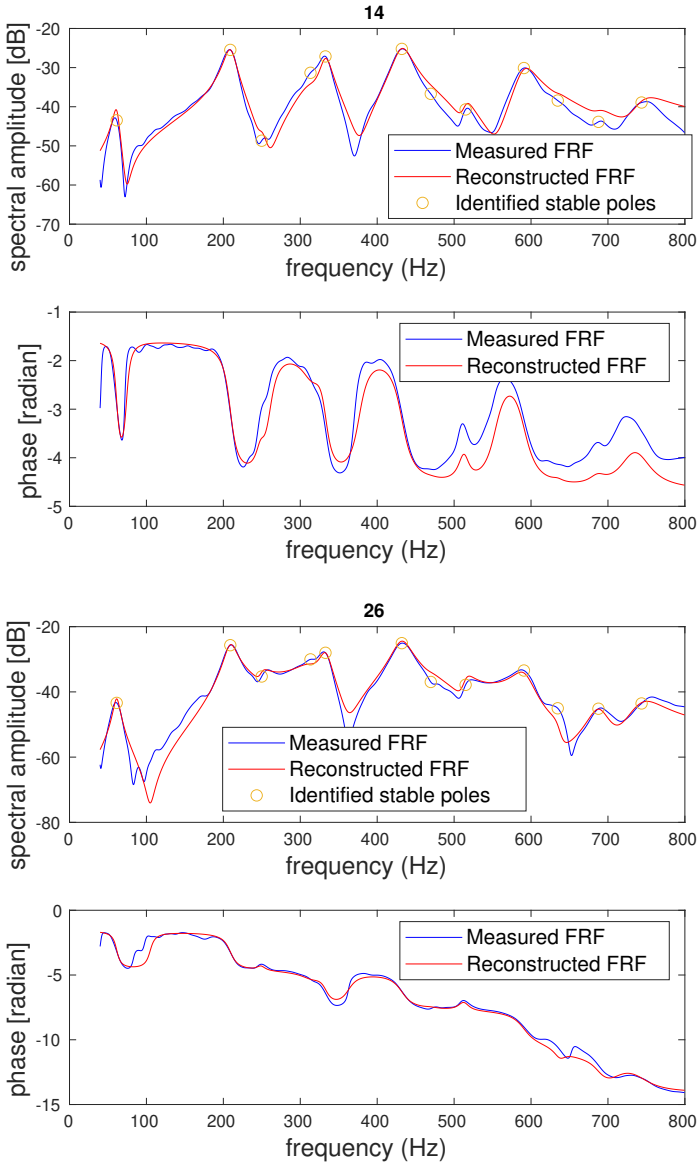

Figure 8.8: Measured FRF and reconstructed FRF by means of modal analysis of the 14^{th} point (driven point) and the 26^{th} point.

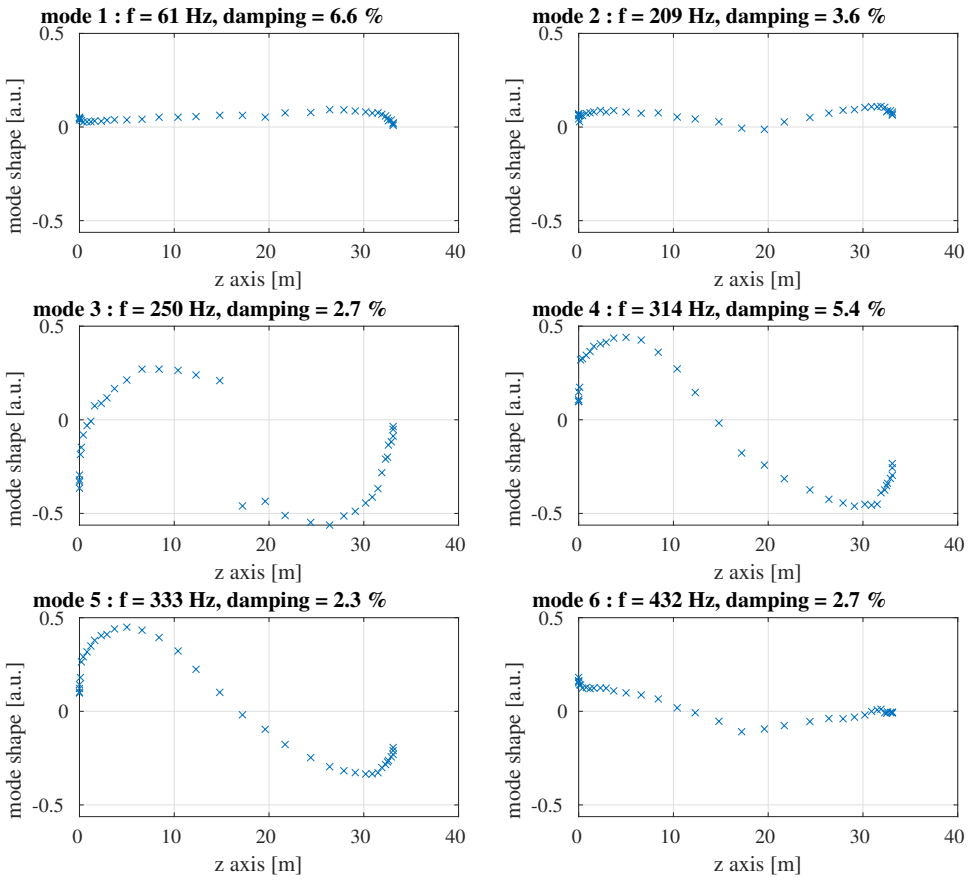

Figure 8.9: Mode shapes extracted from the 37 measurement points' FRF of the bridge, from the 1$^{\text{th}}$ mode to the 6$^{\text{th}}$ mode.

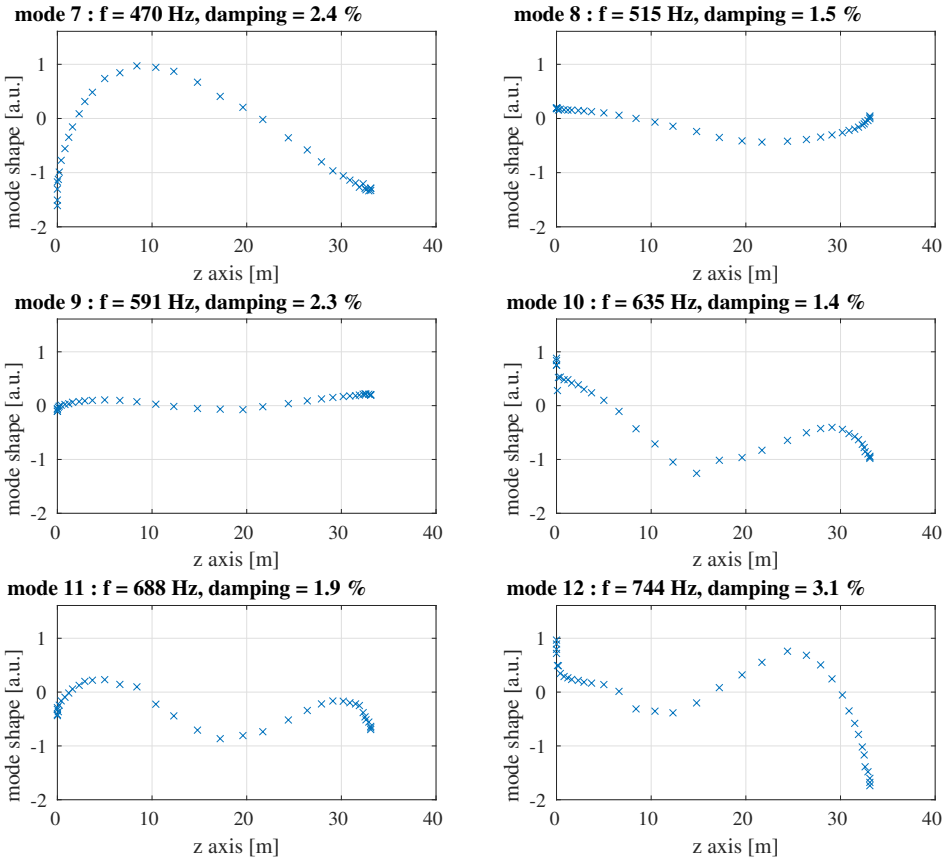

Figure 8.10: Mode shapes along the z axis extracted from the 37 measurement points' FRF of the bridge, from the 7^{th} mode to the 12^{th} mode.

D Modal analysis theory

D.1 Complex and real formulation of the frequency response function

Assuming the linearity of the vibratory system, the FRF (Frequency Response Function) $H_k(\omega)$ of the k^{th} measurement point can be written thus [124] :

$$H_k(\omega) = \sum_{n=1}^{N} \frac{A_{nk}}{j\omega - \lambda_n} + \sum_{n=1}^{N} \frac{\overline{A_{nk}}}{j\omega - \overline{\lambda_n}} \tag{8.1}$$

where λ_n represent the pole of the vibratory system of the n^{th} mode :

$$\lambda_n = -\omega_n \zeta_n + j\omega_n \sqrt{1 - \zeta_n^2} \tag{8.2}$$

where ω_n and ζ_n are the modal pulsation and the modal damping respectively. The A_{nk} refers to the system complex residues of the k^{th} measurement point :

$$A_{nk} = \frac{\Psi_{nk}\Psi_{nj}^T}{2j\omega_n m_n^c} \tag{8.3}$$

where j represents the driven point, Ψ_{nk} and m_n^c are the complex mode shapes and the modal masses of the vibratory system, $\overline{A_{nk}}$ and $\overline{\lambda_n}$ are the complex conjugate of the residues and that of the poles respectively. By applying the inverse Fourier transform to equation 8.1, one obtains the expression of the impulse response $h_k(t)$:

$$h_k(t) = \sum_{n=1}^{N} A_{nk} e^{\lambda_n t} + \sum_{n=1}^{N} \overline{A_{nk}} e^{\overline{\lambda_n} t} \tag{8.4}$$

Considering that the mode shapes are real, with Φ_n being the real mode shapes, then the real formulation of the FRF $H_k(\omega)$ and that of the impulse response $h_k(t)$ can be obtained [125] :

$$H_k(\omega) = \sum_{n=1}^{N} \frac{B_{nk}}{\omega_n^2 - \omega^2 + 2j\omega\omega_n\zeta_n} \tag{8.5}$$

$$h_k(t) = \sum_{n=1}^{N} B_{nk} \frac{e^{-\omega_n\zeta_n t}}{\omega_n\sqrt{1-\zeta_n^2}} \sin(\omega_n\sqrt{1-\zeta_n^2}t) \tag{8.6}$$

That leads to defining the real residues B_{nk} expressed thus :

$$B_{nk} = \frac{\Phi_{nk}\Phi_{nj}}{m_n^r} \tag{8.7}$$

with m_n^r the real modal masses.

D.2 Determination of the modal frequencies and modal dampings

When physical poles of the transfer function are determined, then the associated modal frequencies and modal dampings can be extracted :

$$f_n = \frac{1}{|\lambda_n|} \tag{8.8}$$

$$\zeta_n = \frac{-\Re(\lambda_n)}{\omega_n} \tag{8.9}$$

D.3 Determination of the residues and the mode shapes

Determination of the real residues by means of the frequency method

The objective is to extract the studied vibratory system real residues. It is possible to rewrite equation 8.5 in a matrix form :

$$\begin{pmatrix} H(\omega_1) \\ H(\omega_2) \\ \vdots \\ H(\omega_F) \end{pmatrix} = \left[\begin{pmatrix} \frac{1}{\omega_1^2-\omega_1^2+2j\omega_1\omega_1\zeta_1} \\ \frac{1}{\omega_1^2-\omega_2^2+2j\omega_2\omega_1\zeta_1} \\ \vdots \\ \frac{1}{\omega_1^2-\omega_F^2+2j\omega_F\omega_1\zeta_1} \end{pmatrix} \begin{pmatrix} \frac{1}{\omega_2^2-\omega_1^2+2j\omega_1\omega_2\zeta_2} \\ \frac{1}{\omega_2^2-\omega_2^2+2j\omega_2\omega_2\zeta_2} \\ \vdots \\ \frac{1}{\omega_2^2-\omega_F^2+2j\omega_F\omega_2\zeta_2} \end{pmatrix} \cdots \begin{pmatrix} \frac{1}{\omega_N^2-\omega_1^2+2j\omega_1\omega_N\zeta_N} \\ \frac{1}{\omega_N^2-\omega_2^2+2j\omega_2\omega_N\zeta_N} \\ \vdots \\ \frac{1}{\omega_N^2-\omega_F^2+2j\omega_F\omega_N\zeta_N} \end{pmatrix} \right] \begin{pmatrix} \mathbf{B_1} \\ \mathbf{B_2} \\ \vdots \\ \mathbf{B_N} \end{pmatrix} \tag{8.10}$$

by inverting equation 8.10, ones obtains :

$$\begin{pmatrix} \mathbf{B_1} \\ \mathbf{B_2} \\ \vdots \\ \mathbf{B_N} \end{pmatrix} = \left[\begin{pmatrix} \frac{1}{\omega_1^2-\omega_1^2+2j\omega_1\omega_1\zeta_1} \\ \frac{1}{\omega_1^2-\omega_2^2+2j\omega_2\omega_1\zeta_1} \\ \vdots \\ \frac{1}{\omega_1^2-\omega_F^2+2j\omega_F\omega_1\zeta_1} \end{pmatrix} \begin{pmatrix} \frac{1}{\omega_2^2-\omega_1^2+2j\omega_1\omega_2\zeta_2} \\ \frac{1}{\omega_2^2-\omega_2^2+2j\omega_2\omega_2\zeta_2} \\ \vdots \\ \frac{1}{\omega_2^2-\omega_F^2+2j\omega_F\omega_2\zeta_2} \end{pmatrix} \cdots \begin{pmatrix} \frac{1}{\omega_N^2-\omega_1^2+2j\omega_1\omega_N\zeta_N} \\ \frac{1}{\omega_N^2-\omega_2^2+2j\omega_2\omega_N\zeta_N} \\ \vdots \\ \frac{1}{\omega_N^2-\omega_F^2+2j\omega_F\omega_N\zeta_N} \end{pmatrix} \right]^+ \begin{pmatrix} H(\omega_1) \\ H(\omega_2) \\ \vdots \\ H(\omega_F) \end{pmatrix} \tag{8.11}$$

where $[\mathbf{M}]^+$ refers to the Moore-Penrose generalised inverse of matrix $\mathbf{M}$:

$$[\mathbf{M}]^+ = ([\mathbf{M}]^H[\mathbf{M}])^{-1}[\mathbf{M}]^H \tag{8.12}$$

where $[[\mathbf{M}]^H$ is the Hermitian transpose of the complex matrix $[\mathbf{M}]$

In equation 8.11, the FRF's H must correspond to receptances to obtain the right residues. In the case of admittances, the terms of the inverse matrix of equation 8.11 must be $\frac{j\omega}{\omega^2-\omega_n^2+2j\omega\omega_n\zeta_1}$. In the case of accelerances, these terms must be $-\frac{\omega^2}{\omega^2-\omega_n^2+2j\omega\omega_n\zeta_1}$.

Also, the residues given by equation 8.11 can be forced to be real by using the non negative least-squares curve fitting solver described in [93]. It consists in finding

the residues $\mathbf{B_n}$, assuming that $\mathbf{B_n} \geq \mathbf{0}$, by minimizing a norm. Let $\mathbf{T}$ be the matrix present in equation 8.10 and let :

$$\mathbf{H} = \begin{pmatrix} H(\omega_1) \\ H(\omega_2) \\ \vdots \\ H(\omega_F) \end{pmatrix}, \quad \mathbf{B} = \left(\mathbf{B_1}, \mathbf{B_2}, \ldots, \mathbf{B_N}\right) \tag{8.13}$$

with $n = 1, ..., N$. Then to determine the positive residues, the following norm must be minimized :

$$\underset{\mathbf{B}}{min} \|\mathbf{TB} - \mathbf{H}\|_2^2 \tag{8.14}$$

Then, this problem is solved by using an appropriate solver, like the Matlab function *lsqnonneg* [93].

Determination of the real residues by means of the temporal method

Also, the same reasoning can be done when it comes to the vibratory system impulse response by rewriting equation 8.6 in the following matrix form :

$$\begin{pmatrix} h(t_1) \\ h(t_2) \\ \vdots \\ h(t_T) \end{pmatrix} = \begin{bmatrix} \begin{pmatrix} \frac{e^{-\omega_1\zeta_1 t_1}}{\omega_1\sqrt{1-\zeta_1^2}}\sin(\omega_1\sqrt{1-\zeta_1^2}t_1) \\ \frac{e^{-\omega_1\zeta_1 t_2}}{\omega_1\sqrt{1-\zeta_1^2}}\sin(\omega_1\sqrt{1-\zeta_1^2}t_2) \\ \vdots \\ \frac{e^{-\omega_1\zeta_1 t_T}}{\omega_1\sqrt{1-\zeta_1^2}}\sin(\omega_1\sqrt{1-\zeta_1^2}t_T) \end{pmatrix} & \begin{pmatrix} \frac{e^{-\omega_2\zeta_2 t_1}}{\omega_2\sqrt{1-\zeta_2^2}}\sin(\omega_2\sqrt{1-\zeta_2^2}t_1) \\ \frac{e^{-\omega_2\zeta_2 t_2}}{\omega_2\sqrt{1-\zeta_2^2}}\sin(\omega_2\sqrt{1-\zeta_2^2}t_2) \\ \vdots \\ \frac{e^{-\omega_2\zeta_2 t_T}}{\omega_2\sqrt{1-\zeta_2^2}}\sin(\omega_2\sqrt{1-\zeta_2^2}t_T) \end{pmatrix} \\ \cdots & \begin{pmatrix} \frac{e^{-\omega_N\zeta_n t_1}}{\omega_N\sqrt{1-\zeta_N^2}}\sin(\omega_N\sqrt{1-\zeta_N^2}t_1) \\ \frac{e^{-\omega_N\zeta_n t_2}}{\omega_N\sqrt{1-\zeta_N^2}}\sin(\omega_N\sqrt{1-\zeta_N^2}t_2) \\ \vdots \\ \frac{e^{-\omega_N\zeta_n t_T}}{\omega_N\sqrt{1-\zeta_N^2}}\sin(\omega_N\sqrt{1-\zeta_N^2}t_T) \end{pmatrix} \end{bmatrix} \begin{pmatrix} \mathbf{B_1} \\ \mathbf{B_2} \\ \vdots \\ \mathbf{B_N} \end{pmatrix} \tag{8.15}$$

By inverting equation 8.15, one obtains :

$$\begin{pmatrix} \mathbf{B_1} \\ \mathbf{B_2} \\ \vdots \\ \mathbf{B_N} \end{pmatrix} = \begin{bmatrix} \begin{pmatrix} \frac{e^{-\omega_1\zeta_1 t_1}}{\omega_1\sqrt{1-\zeta_1^2}}\sin(\omega_1\sqrt{1-\zeta_1^2}t_1) \\ \frac{e^{-\omega_1\zeta_1 t_2}}{\omega_1\sqrt{1-\zeta_1^2}}\sin(\omega_1\sqrt{1-\zeta_1^2}t_2) \\ \vdots \\ \frac{e^{-\omega_1\zeta_1 t_T}}{\omega_1\sqrt{1-\zeta_1^2}}\sin(\omega_1\sqrt{1-\zeta_1^2}t_T) \end{pmatrix} \begin{pmatrix} \frac{e^{-\omega_2\zeta_2 t_1}}{\omega_2\sqrt{1-\zeta_2^2}}\sin(\omega_2\sqrt{1-\zeta_2^2}t_1) \\ \frac{e^{-\omega_2\zeta_2 t_2}}{\omega_2\sqrt{1-\zeta_2^2}}\sin(\omega_2\sqrt{1-\zeta_2^2}t_2) \\ \vdots \\ \frac{e^{-\omega_2\zeta_2 t_T}}{\omega_2\sqrt{1-\zeta_2^2}}\sin(\omega_2\sqrt{1-\zeta_2^2}t_T) \end{pmatrix} \\ \cdots \begin{pmatrix} \frac{e^{-\omega_N\zeta_n t_1}}{\omega_N\sqrt{1-\zeta_N^2}}\sin(\omega_N\sqrt{1-\zeta_N^2}t_1) \\ \frac{e^{-\omega_N\zeta_n t_2}}{\omega_N\sqrt{1-\zeta_N^2}}\sin(\omega_N\sqrt{1-\zeta_N^2}t_2) \\ \vdots \\ \frac{e^{-\omega_N\zeta_n t_T}}{\omega_N\sqrt{1-\zeta_N^2}}\sin(\omega_N\sqrt{1-\zeta_N^2}t_T) \end{pmatrix} \end{bmatrix}^+ \begin{pmatrix} h(t_1) \\ h(t_2) \\ \vdots \\ h(t_T) \end{pmatrix} \tag{8.16}$$

In equation D.3, the impulse responses $h(t)$ must correspond to a displacement to obtain the right residues. In the case of velocities, the terms $\frac{e^{-\omega_n\zeta_n t}}{\omega_n\sqrt{1-\zeta_n^2}}\sin(\omega_n\sqrt{1-\zeta_n^2}t)$ of the inverse matrix of equation must be derived one time with respect to time. In the case of acceleration, these terms must be derived two times with respect to time.

Determination of the complex and real mode shapes

To obtain the complex residues, the matrix form of the residues given by equation 8.1 is taken. So following the frequency method of extraction :

$$\begin{pmatrix} H(\omega_1) \\ H(\omega_2) \\ \vdots \\ H(\omega_F) \end{pmatrix} = \begin{bmatrix} \begin{pmatrix} \frac{1}{j\omega_1-\lambda_1}+\frac{1}{j\omega_1-\bar{\lambda}_1} \\ \frac{1}{j\omega_2-\lambda_1}+\frac{1}{j\omega_2-\bar{\lambda}_1} \\ \vdots \\ \frac{1}{j\omega_F-\lambda_1}+\frac{1}{j\omega_F-\bar{\lambda}_1} \end{pmatrix} \begin{pmatrix} \frac{1}{j\omega_1-\lambda_2}+\frac{1}{j\omega_1-\bar{\lambda}_2} \\ \frac{1}{j\omega_2-\lambda_2}+\frac{1}{j\omega_2-\bar{\lambda}_2} \\ \vdots \\ \frac{1}{j\omega_F-\lambda_2}+\frac{1}{j\omega_F-\bar{\lambda}_2} \end{pmatrix} \cdots \begin{pmatrix} \frac{1}{j\omega_1-\lambda_N}+\frac{1}{j\omega_1-\bar{\lambda}_N} \\ \frac{1}{j\omega_2-\lambda_N}+\frac{1}{j\omega_2-\bar{\lambda}_N} \\ \vdots \\ \frac{1}{j\omega_F-\lambda_N}+\frac{1}{j\omega_F-\bar{\lambda}_N} \end{pmatrix} \end{bmatrix} \begin{pmatrix} \mathbf{A_1} \\ \mathbf{A_2} \\ \vdots \\ \mathbf{A_N} \end{pmatrix} \tag{8.17}$$

By inverting equation 8.17, one obtains :

$$\begin{pmatrix} \mathbf{A_1} \\ \mathbf{A_2} \\ \vdots \\ \mathbf{A_N} \end{pmatrix} = \begin{bmatrix} \begin{pmatrix} \frac{1}{j\omega_1-\lambda_1}+\frac{1}{j\omega_1-\bar{\lambda}_1} \\ \frac{1}{j\omega_2-\lambda_1}+\frac{1}{j\omega_2-\bar{\lambda}_1} \\ \vdots \\ \frac{1}{j\omega_F-\lambda_1}+\frac{1}{j\omega_F-\bar{\lambda}_1} \end{pmatrix} \begin{pmatrix} \frac{1}{j\omega_1-\lambda_2}+\frac{1}{j\omega_1-\bar{\lambda}_2} \\ \frac{1}{j\omega_2-\lambda_2}+\frac{1}{j\omega_2-\bar{\lambda}_2} \\ \vdots \\ \frac{1}{j\omega_F-\lambda_2}+\frac{1}{j\omega_F-\bar{\lambda}_2} \end{pmatrix} \cdots \begin{pmatrix} \frac{1}{j\omega_1-\lambda_N}+\frac{1}{j\omega_1-\bar{\lambda}_N} \\ \frac{1}{j\omega_2-\lambda_N}+\frac{1}{j\omega_2-\bar{\lambda}_N} \\ \vdots \\ \frac{1}{j\omega_F-\lambda_N}+\frac{1}{j\omega_F-\bar{\lambda}_N} \end{pmatrix} \end{bmatrix}^+ \begin{pmatrix} H(\omega_1) \\ H(\omega_2) \\ \vdots \\ H(\omega_F) \end{pmatrix} \tag{8.18}$$

It is possible to extract the complex mode shapes by means of the complex residues. Considering a vibratory system with N modes and with c degrees of freedom, and j representing the driven point, then :

$$\mathbf{A_n} = \begin{pmatrix} A_{n1} \\ A_{n2} \\ \vdots \\ A_{nj} \\ \vdots \\ A_{Nc} \end{pmatrix} \tag{8.19}$$

Then, the complex mode shapes Ψ_{nk} are given by :

$$\Psi_{nk} = \frac{A_{nk}}{\sqrt{A_{nj}}} \tag{8.20}$$

To determine the complex modal masses, equations 8.3 and 8.20 are used :

$$A_{nk} = \frac{\Psi_{nk}\Psi_{nj}}{2j\omega_n m_n^c} = \frac{1}{2j\omega_n m_n^c}\frac{A_{nk}}{\sqrt{A_{nj}}}\frac{A_{nj}}{\sqrt{A_{nj}}} = \frac{A_{nk}}{2j\omega_n m_n^c} \tag{8.21}$$

That implies :

$$m_n^c = \frac{1}{2j\omega_n} \tag{8.22}$$

Then, one can obtain the real mode shapes by means of the complex mode shapes. To proceed, it must be assumed that the damping matrix is proportional to the mass matrix and to the stiffness matrix [119]. As such, the complex mode shapes are related with the real mode shapes in the following way :

$$\Phi_{nk} = \Re(\Psi_{nk}\sqrt{2j\omega_n}) \tag{8.23}$$

if the damping is not proportional, equation 8.23 is still valid in as much as the modal frequencies are well separated, that is when the distance in terms of frequency between the modes is greater than three times the -3 dB band width [119].

Let us normalise the real mode shapes $m_n^r = 1$. Using equation 8.7:

$$B_{nk} = \frac{\Phi_{nk}\Phi_{nj}}{m_n^r} = \Phi_{nk}\Phi_{nj} \tag{8.24}$$

That implies :

$$\Phi_{nk} = \frac{B_{nk}}{\sqrt{B_{nj}}} \tag{8.25}$$

which can be verified by combining equations 8.24 and 8.25 :

$$B_{nk} = \frac{\Phi_{nk}\Phi_{nj}}{m_n^r} = \frac{B_{nk}}{\sqrt{B_{nj}}}\frac{B_{nj}}{\sqrt{B_{nj}}}\frac{1}{m_n^r} = \frac{B_{nk}}{m_n^r} \tag{8.26}$$

which is consistent with the chosen normalisation, namely that $m_n^r = 1$

E Stability condition of the explicit scheme

The stability condition of the explicit numerical scheme used in equation 3.5 can be derived. To do it, the method presented by Bilbao is used [94]. Let us consider the differential equation 2.36 of the conservative system without its second member. Then, this equation is discretized with a Δt time step :

$$\frac{\mathbf{Q}^{n+1} - 2\mathbf{Q}^{n} + \mathbf{Q}^{n-1}}{\Delta t} = -\boldsymbol{W}\boldsymbol{M}^{-1}\boldsymbol{K}\mathbf{Q}^{n} \Leftrightarrow \mathbf{Q^{n+1}} = (2\mathbf{I} - \Delta t^2 \boldsymbol{W}\boldsymbol{M}^{-1}\boldsymbol{K})\mathbf{Q^{n}} - \mathbf{Q^{n-1}} \tag{8.27}$$

Afterwards, an *Ansatz* in the following form $\mathbf{Q}^n = \phi z^n$ is done to obtain an eigen value equation.

$$\Delta t \boldsymbol{W}\boldsymbol{M}^{-1}\boldsymbol{K}\phi = -(z - 2 + z^{-1})\phi \tag{8.28}$$

It is wished that the roots of this equation be complex conjugate. To respect it, it is shown in [94] that the following condition ought to be respected :

$$\Delta t \leq \frac{2}{\max(\mathrm{eig}(\boldsymbol{W}\boldsymbol{M}^{-1}\boldsymbol{K}))} \tag{8.29}$$

This equation expresses the stability condition of the implemented numerical scheme in equation 3.5.

F Measurement of the key motion

To proceed to the accounted vibratory measurements, the same key trajectory needs to be repeated when it comes to setting into vibration the considered excited string. This repetition is needed to produce the same vibratory input having a fixed vibratory amplitude and the same pitch. In such a way, the different vibratory measurements can be easily comparable. To do it, a device satisfying the excitation repeatability hypothesis is necessary. The DROPIC robotic finger, whose trajectory in terms of displacement and velocity in a 2 dimensional space can be programmed, is used for this purpose [120, 126, 99]. This robotic finger motion is programmed by controlling its articular positions. Its feedback loop leads to a low level control of the current sent to the motors. In figure 8.11, the block diagram of the system is presented including a PID controller (proportional–integral–derivative controller) for the position loop and a PI controller (proportional-integral) for the current loop. This robot is made of 2 arms connected by two pivots (see figure 8.12). The robotic finger has two degrees of freedom. It can reproduce any trajectory in a plane parallel to the axis of the key. Note that the key itself has only one degree of freedom. The length of the robot arms is 45 mm. The area of use is 20×20 mm^2 and the maximum force that can be exerted by the finger is 20 N [120]. The trajectory of the robotic finger is programmed by an external controller. This trajectory is coded in a .txt file (see figure 8.11) by giving the desired x and z position in specific times, respecting the velocity limit (1.21 m.s^{-1}) and the area of use. Then, this file is interpreted by the system in terms of angular positions for each arm.

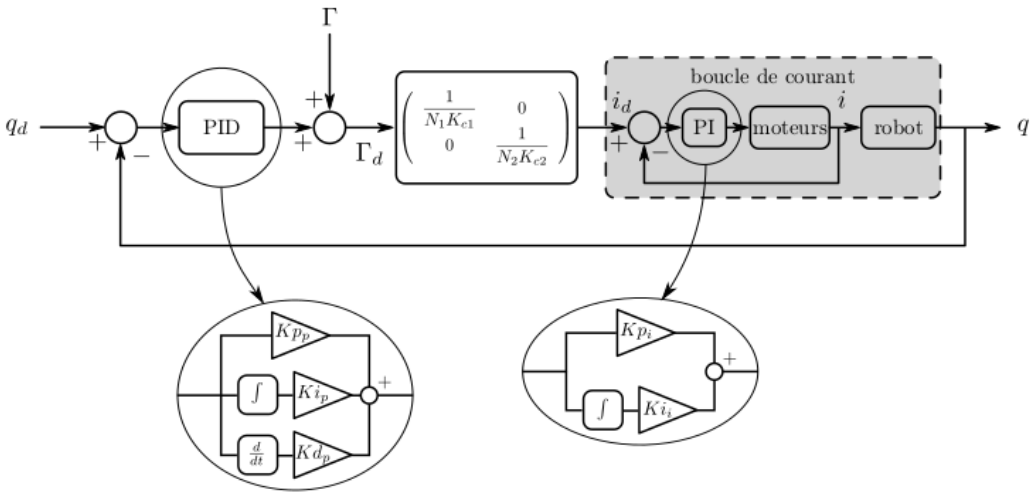

time	x	z	vitesse
0.0000	0.0000	0.0000	0.0000
0.5000	0.0000	0.0050	1.0000
0.5032	-0.0016	0.0050	1.0000
0.5064	-0.0032	0.0050	1.0000
0.5096	-0.0048	0.0050	1.0000
0.5128	-0.0064	0.0050	1.0000
0.5160	-0.0080	0.0050	1.0000

Figure 8.11: Block diagram of the robotic finger system (extracted from [120]) (above), Trajectory given to the controller in a .txt file (below)

To verify the trajectory repetition, it is possible to measure the key displacement as well as the tangent uplift. It is measured by means of a Keyence laser profilometer, functioning by laser triangulation (see figure 8.12). This specific measurement is done on the F_3 key of the LAM1 clavichord. This key displacement measurement is repeated ten times. One kind of a typical finger trajectory is that of a vertical downward motion. Then, the robotic finger trajectory is programmed in view of producing this vertical downward motion with a velocity equivalent to that of a musician's finger.

In figures 8.13 (a) and (b), the F_3 key depth and the tangent uplift with respect to time produced by the robotic finger trajectory are shown. It is possible to differentiate different phases in these key displacement measurements. First, when the key is pressed, the key goes downward until it reaches -6.5 mm at time 0.5 s. Then, it goes back up to -5.5 mm at time 0.55 s. Finally, the key depth remains constant. As a result, the key displacement profile created by the robotic finger trajectory is characterised by a notch followed by a plateau. The notch is caused by the reaction of the string on the tangent, the two substructures behaving like a damped spring-mass once in contact [3]. The tangent displacement in figure 8.13 describe the same shape as that of the key with a homothetic ratio, given that the key is a rigid solid lever. Also, superimposing the ten measurements, the similarity of these ten measurements can be noticed. As a result, the excitation repeatability hypothesis is verified by using the robotic finger. Furthermore, the programmed trajectory yields a reasonable key depth, which can be used for other experiments.

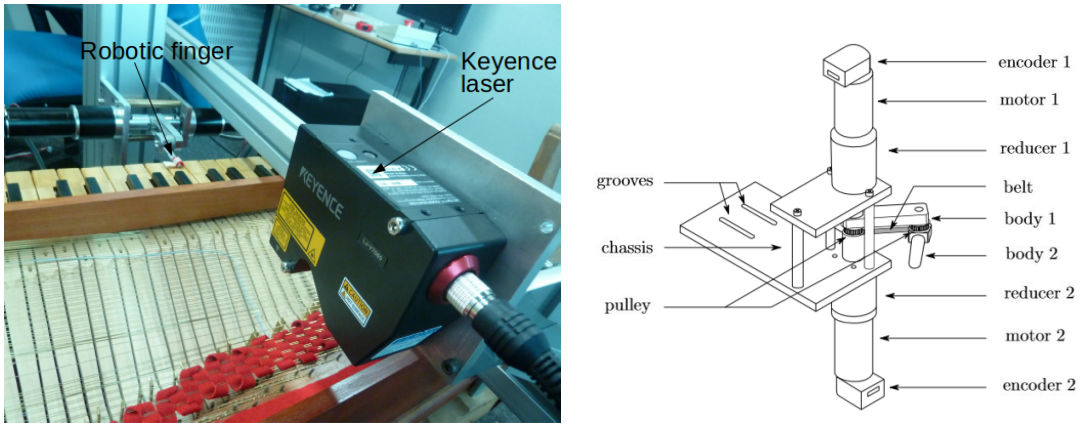

Figure 8.12: Lay out of the Keyence laser profilometer measuring the tangent displacement whose corresponding key is struck by the DROPIC robotic finger (left), Sketch of the robotic finger (extracted from [99]) (right)

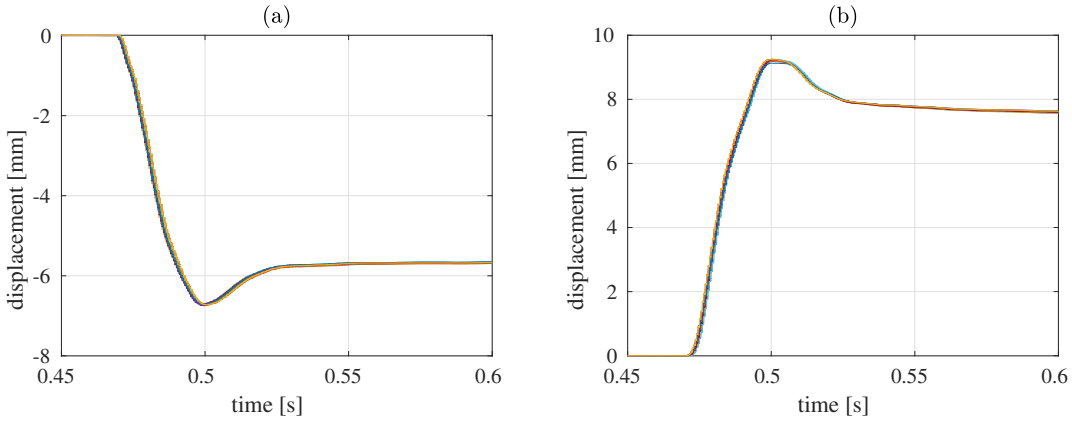

Figure 8.13: Ten measurements of the downward key displacement measured at the extremity of the robotic finger (a) and that of the tangent uplift (b), obtained using the same programmed trajectory.

G Energy and power balance

This annex focuses on an energy analysis of a vibratory system used to verify the precision of its simulation in section 3.3.1. First, the case of a damped spring-mass oscillator is taken to introduce this energetic approach in section G.1. Then, this approach is extended to a vibratory system described by its modal representation in section G.2.

G.1 The damped spring-mass oscillator case

For a damped spring-mass oscillator with one degree of freedom, subjected to a force $F(t)$, the vibratory displacement $y(t)$ is found by the following equation of motion :

$$m\ddot{y}(t) + c\dot{y}(t) + ky(t) = F(t) \tag{8.30}$$

where the equation coefficients can be written in terms of the eigen pulsation ω_0 and the eigen damping ζ_0 of the oscillator, with the damping coefficient $c = 2m\omega_0\zeta_0$ and the stiffness coefficient $k = m\omega_0^2$. To compute the energy associated to the oscillator motion, the two sides of the equation 8.30 are multiplied by $\dot{y}(t)$:

$$m\ddot{y}(t)\dot{y}(t) + ky(t)\dot{y}(t) = F(t)\dot{y}(t) - c\left[\dot{y}(t)\right]^2 \tag{8.31}$$

All the terms of equation 8.31 represent a power. Note that :

$$\ddot{y}(t)\dot{y}(t) = \frac{d}{dt}\left(\frac{1}{2}\left[\dot{y}(t)\right]^2\right); \quad \dot{y}(t)y(t) = \frac{d}{dt}\left(\frac{1}{2}\left[y(t)\right]^2\right) \tag{8.32}$$

The left side of equation 8.31 represents the temporal derivative of the oscillator mechanical energy $E_m(t) = E_c(t) + E_p(t)$, composed of the kinetic energy $E_c(t) = \frac{1}{2}m\left[y(t)\right]^2$ and the potential energy $E_p(t) = \frac{1}{2}k\left[y(t)\right]^2$. At the right side, the power provided by the excitation force $\dot{E}_e(t) = F(t)\dot{y}(t)$ and that provided by the oscillator damping $\dot{E}_d(t) = c\left[\dot{y}(t)\right]^2$ are found :

$$\frac{d}{dt}\left(E_c(t) + E_p(t)\right) = \dot{E}_e(t) - \dot{E}_d(t) \tag{8.33}$$

Equation 8.33 represents the oscillator power balance. Note that, without the excitation force and the damping, the oscillator mechanical energy is conserved :

$$\frac{d}{dt}\left(E_m(t)\right) = 0 \Rightarrow E_m(t) = E_c(t) + E_p(t) = \text{Constant} = E_m(0) \tag{8.34}$$

By the way, without the excitation force, the decrease of the mechanical energy takes place over time because of damping :

$$\frac{d}{dt}\left(E_m(t)\right) = -c\left[\dot{y}(t)\right]^2 \tag{8.35}$$

It is possible to obtain the oscillator energy balance by integrating its power balance with respect to time. Integrating with respect to time the two sides of equation 8.33, it yields :

$$E_c(t) + E_p(t) = \int_0^t \dot{E}_e d\tau - \int_0^t \dot{E}_d d\tau \tag{8.36}$$

To summarise, in the case of damped spring-mass oscillator, two options can be considered : either computing the different terms of the power balance or computing that of the energy balance.

G.2 Vibratory system described by its modal representation

In the case of a vibratory system represented by N modes, there are N modal equations associated to this system, each subjected to a modal force $F_n(t)$ with $n = 1, 2, \ldots, N$. The modal amplitudes $q_n(t)$ are computed thus :

$$m_n \ddot{q}_n(t) + c_n \dot{q}_n(t) + k_n q_n(t) = F_n(t), \quad n = 1, 2, \ldots, N \tag{8.37}$$

where these equations' coefficients can be written in terms of the modal pulsations ω_n and the modal dampings ζ_n, with $c_n = 2m_n\omega_n\zeta_n$ and $k_n = m_n\omega_n^2$. In equations 8.37, the modal forces are given by the projection of the physical forces on the system modal basis. Assuming that the excitation is exerted on the system point located at x_e, then the modal forces are given in the following way :

$$F_n(t) = F(t)\phi_n(x_e), \quad n = 1, 2, \ldots, N \tag{8.38}$$

By the way, the system physical displacement at any location x_r is given by the recombination of the modal responses :

$$y(x_r, t) = \sum_{n=1}^{N} \phi_n(x_r) q_n(t) \tag{8.39}$$

Regarding this system, the energy balance is done for each individual mode, by computing either the power terms or the energy terms.

Power balance

At each time step t_i, the formulation is applied for each mode $n = 1, 2, \ldots, N$:

$$\dot{E}_{cn}(t_i) + \dot{E}_{pn}(t_i) = \dot{E}_{en}(t_i) - \dot{E}_{dn}(t_i) \tag{8.40}$$

with :

$$\begin{aligned} \dot{E}_{cn}(t_i) &= m_n \ddot{q}_n(t_i)\dot{q}_n(t_i) \\ \dot{E}_{pn}(t_i) &= k_n \dot{q}_n(t_i) q_n(t_i) \\ \dot{E}_{en}(t_i) &= F_n(t_i)\dot{q}_n(t_i) \\ \dot{E}_{dn}(t_i) &= c_n \left[\dot{q}_n\right]^2 \end{aligned} \tag{8.41}$$

If the power balance is correct for all modes, then it is also correct for the whole system :

$$\sum_{n=1}^{N} \dot{E}_{cn}(t_i) + \sum_{n=1}^{N} \dot{E}_{pn}(t_i) = \sum_{n=1}^{N} \dot{E}_{en}(t_i) - \sum_{n=1}^{N} \dot{E}_{dn}(t_i) \tag{8.42}$$

Energy balance

At each time step t_i, the formulation is applied for each mode $n = 1, 2, \ldots, N$:

$$E_{cn}(t) + E_{pn}(t) = E_{en}(t) - E_{dn}(t) \tag{8.43}$$

with :

$$\begin{aligned} E_{cn}(t_i) &= \frac{1}{2} m_n \left[\dot{q}_n(t_i)\right]^2 \\ E_{pn}(t_i) &= \frac{1}{2} k_n \left[q_n(t_i)\right]^2 \\ E_{en}(t_i) &\approx E_{en}(t_{i-1}) + F_n(t_i)\dot{q}_n(t_i)\Delta t \\ E_{dn}(t_i) &\approx E_{dn}(t_{i-1}) + c_n \left[\dot{q}_n(t_i)\right]^2 \Delta t \end{aligned} \tag{8.44}$$

Also, the modal energy balance guaranties the system global energy balance :

$$\sum_{n=1}^{N} E_{cn}(t_i) + \sum_{n=1}^{N} E_{pn}(t_i) = \sum_{n=1}^{N} E_{en}(t_i) - \sum_{n=1}^{N} E_{dn}(t_i) \tag{8.45}$$

Nonlinear terms of the string

The string nonlinear terms are all conservatives, because it has to do with additional stiffness terms. Then the modal nonlinear terms are added to the mode potential energy. The generalised modal equations become :

$$m_n \ddot{q}_n(t) + c_n \dot{q}_n(t) + k_n q_n(t) = F_n(t) - F_n^{NL}(t), \quad n = 1, 2, \ldots, N \tag{8.46}$$

where $F_n^{NL}(t)$ represents the sum of all geometrical nonlinear terms of the n^{th} modal equation. Then, for each mode $n = 1, 2, \ldots, N$, the modal potential powers become :

$$\dot{E}_{pn}(t_i) = \dot{E}_{pn}^{L}(t_i) + \dot{E}_{pn}^{NL}(t_i) \quad \text{with} \quad \begin{cases} \dot{E}_{pn}^{L}(t_i) = k_n q_n(t_i)\dot{q}_n(t_i) \\ \\ \dot{E}_{pn}^{NL}(t_i) = F_n^{NL}(t_i)\dot{q}_n(t_i) \end{cases} \tag{8.47}$$

and the corresponding modal potential energies can be computed :

$$E_{pn}(t_i) = E_{pn}^{L}(t_i) + E_{pn}^{NL}(t_i) \quad \text{with} \quad \begin{cases} E_{pn}^{L}(t_i) = \frac{1}{2} k_n \left[q_n(t_i)\right]^2 \\ \\ E_{pn}^{NL}(t_i) \approx E_{pn}^{NL}(t_{i-1}) + F_n^{NL}(t_i)\dot{q}_n(t_i)\Delta t \end{cases} \tag{8.48}$$

H Key moment of inertia

Some interesting features of a clavichord key can be measured. These information will be possibly used to enhance the modeling of the key. One of the features describing the rotating motion of the key is the moment of inertia. The experimental protocol to measure the key moment of inertia is similar to that elaborated by Lozada [127] and Roy [120]. To proceed to this measurement, the A_2 key, which is a typical key of the LAM1 clavichord, is chosen. It is hung on a plastic wire tensed by two gibbets (see figure 8.14). A small accelerometer (PCB 352C23 SN LW 245598) is placed on the key, by means of which the rotating frequency of key can be measured when the key is put into free oscillation. The experience is laid out in such a way that the key rotating motion remains unperturbed as far as possible. The key is hung on the plastic wire at the level of its rotating center O (see figure 8.15). As a result, when the key is rotating with respect to the polarization measured by the sensor, the key frequency of oscillation rotating with respect to point O is measured.

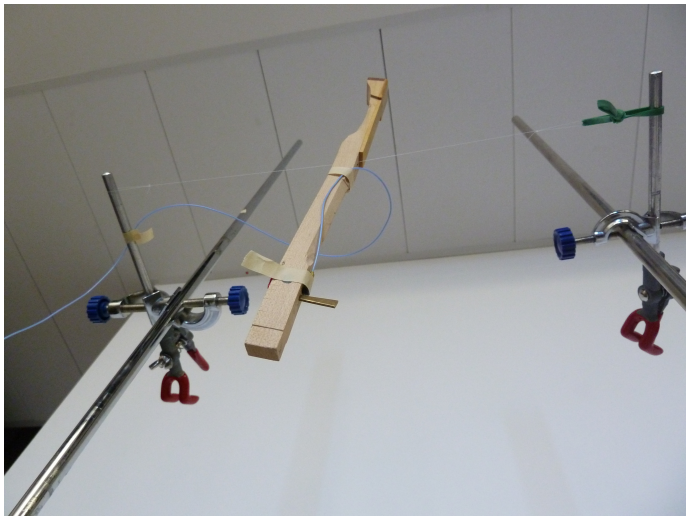

Figure 8.14: The LAM1 clavichord A_2 key hung on a plastic wire tensed by two gibbets.

Then, the moment of inertia I_O with respect to point O is computed :

$$I_O = mgl\frac{T}{2\pi} \tag{8.49}$$

Where m is the key mass, g is the gravitational acceleration, l is the distance between the center of mass G and the rotational center O, and T is the oscillation period. To compute the moment of inertia I_G with respect to the center of mass G, the Huygen's theorem is used :

$$I_G = I_O - ml^2 \tag{8.50}$$

Having the following values for the key :

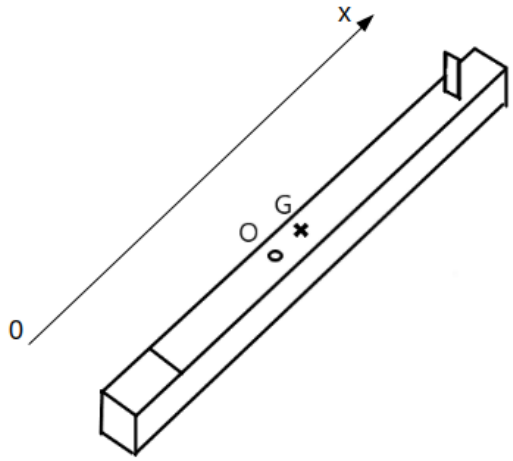

Figure 8.15: Outline of the LAM1 clavichord A2 key

$$\begin{aligned}
\text{Length of the key : } L &= 28,9cm \\
\text{Rotational center position : } L_O &= 11,7cm \\
\text{Position of the tangent : } L_T &= 25.4cm \\
\text{Position of the center of mass : } L_G &= 13.5cm \\
\text{Mass of the key : } M_t &= 30g
\end{aligned}$$

Measuring the rotational frequency of the key, it comes down to these results :

$$\begin{aligned}
I_O &= 7.1937.10^{-4} kg.m^2 \\
I_G &= 7.0737.10^{-4} kg.m^2
\end{aligned}$$

These measured values are similar to those found in the case of keys of keyboard instruments [127, 120].

I Verification of the crossed admittances

Modal parameters of the bridge needed to be extracted out of vibratory measurements. One of the assumption for this is that the considered vibratory system is linear. This can be verified by describing some of the specific features of a linear vibratory system. Also, vibratory measurements on the clavichord bridge are not simple. Because of the proximity of the strings and the way they are laid out, the bridge end up being a cluttered space upon which the sensors cannot be put easily. When it comes to measuring the bridge vibrations in two polarizations, strings need to be moved away from their respecting bridge hitch pins. So this verification is also a way to validate the experimental protocol used to obtain good quality measured vibratory signals on the bridge. First, a nomenclature is used to clarify the terms referring to the measured FRF's. In figure 8.16, the set of axis (x,y) is indicated to point out the two polarizations. The term Y_{xy} referring to a specific FRF is to be read in such a way : the FRF is measured with a hammer impact oriented along the x axis and with the sensor measuring the vibratory response in the y axis.

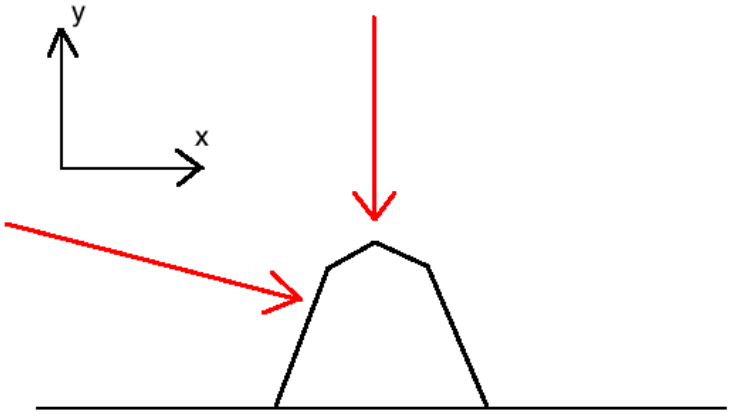

Figure 8.16: Simplified scheme of a LAM1 clavichord bridge with a set of axis.

Two different experimental approaches are tested to establish an experimental protocol adapted to measure the mobility of the bridge in the two polarizations of motion y and x, hence leading to the verification of the linearity of the system. The measurements are done with small accelerometers (PCB 352C23 SN LW 245598 and 233544) and with a PCB 086E80 impact hammer. Because of their little size, these accelerometers sensibility is smaller compared to larger sensors. All results are obtained by calculating the mean value of a set of ten measurements.

Considering a linear system with two polarizations of motion, the mobility matrix $\mathbf{Y}$ is written :

$$\mathbf{Y} = \begin{pmatrix} Y_{yy} & Y_{yx} \\ Y_{xy} & Y_{xx} \end{pmatrix} \tag{8.51}$$

To obtain this matrix, four FRF's need to be measured. In each measurement, the impact axis and the response measurement axis are changed. There are two criteria to comply with in order to end up with a linear system matrix $\mathbf{Y}$:

- Y_{xx} and Y_{yy} must have the same poles, that is the same modal frequencies and modal dampings. these former represent a global feature of the vibratory system. No matter where the measurement in the bridge take place, the same modes need to be present in the measurements. What depends on the location on the system is the amplitude of vibration of these modes, which refers to the mode shapes. Therefore, the modal frequencies and modal dampings need to be the same between Y_{xx} and Y_{yy}.
- The curves representing Y_{yx} and Y_{xy} need to be superimposed by virtue of the reciprocity principle coming from the linearity of the vibratory system. Whether the impact is oriented with respect to one of the axis and the measured response with respect to the other one, as long as the two points of considerations used either for the excitation or the measurement are the same, the two FRF's resulting from these measurement need to be the same.

Once these two criteria are verified, the reliability of the measurements in the two polarizations will be validated and the linearity of the system will be confirmed.

I.1 First approach : two accelerometers laid out on the bridge

The second approach consists in laying out the two accelerometers directly on the bridge. In any case, it is mandatory to move the strings away from their corresponding pins with this approach (see figure 8.17). In such a situation, the y and x axis vibratory responses are directly measured. Note that because of the geometry of the bridge, the sensors are inclined by a small angle relative to the y and x axis. Since the sensors cannot be placed in a plan orthogonal to the axis, at least some differences between Y_{yx} and Y_{xy} are expected.

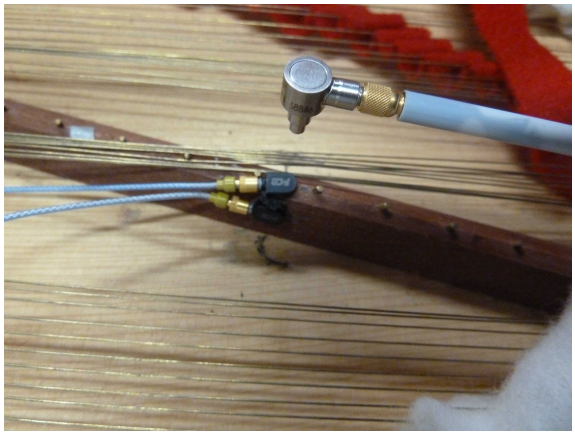

Figure 8.17: Layout of the accelerometers on the bridge measuring the vibratory response with respect to the x and y axis respectively.

Figures 8.18 shows the results obtained with this approach. The good equivalence between Y_{yx} and Y_{xy} can be noticed. Therefore, the reciprocity principle is checked in the case of the LAM1 clavichord bridge. The modes of vibration between Y_{yy} and Y_{xx} are globally the same. That being said, it might be that some of the modes have been displaced between of the difference in impact intensity of the hammer in the two different measurements. The verification of the reciprocity principle confirms the good quality of the measurements and it supports the assumption that the system is linear.

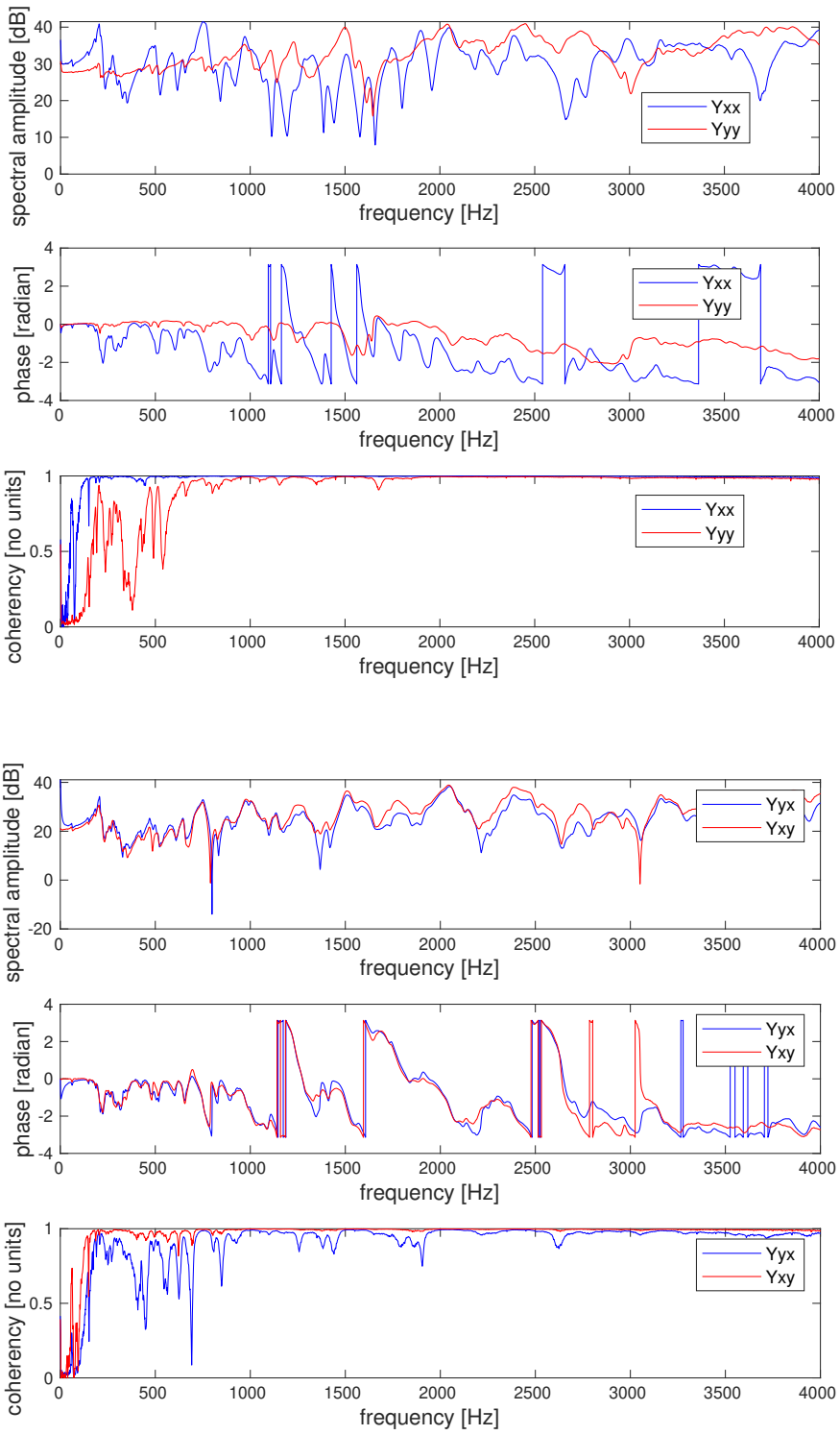

Figure 8.18: Spectral amplitude, phase and coherency of Y_{yy} and Y_{xx} with the approach where two accelerometers are laid out on the two sides of the bridge (left), Spectral amplitude, phase and coherency of Y_{yx} and Y_{xy} with the approach where two accelerometers are laid out on the bridge (right).

I.2 Second approach : two accelerometers laid out on the two sides of the bridge

It is assumed that the mobility of the bridge at its top is equivalent to the mean value of the mobilities at its two sides[1]. In figure 8.19, the specific layout of the accelerometers is shown. Under this assumption, the approach consists in obtaining the vibratory response at the bridge top (which is separated by a distance H from the soundboard, see figure 8.19) in the y and x axis. To do it, an impact is given with respect to the y and x axis measuring the vibratory response in the y axis at the sides of the bridge (separated by a distance D) by means of the two aforementioned accelerometers. Considering $a_r(t)$ and $a_l(t)$ the acceleration measured at the right side and at the left side of the bridge respectively, the acceleration in the y axis $a_y(t)$ and that in the x axis $a_x(t)$ are thus computed (see [82]) :

$$a_y(t) = \frac{1}{2}(a_r(t) + a_l(t)) \tag{8.52}$$

$$a_x(t) = \frac{H}{D}(a_r(t) - a_l(t)) \tag{8.53}$$

Figure 8.20 shows results obtained out of the measurements and equations 8.52 and 8.53. Note that the reciprocity principle is not obtained with this approach because the computed Y_{yx} and Y_{xy} are not equivalent. The reason of this mismatch can be accounted for by putting into question the assumption of this approach, namely that the vibration at the top of the bridge cannot be obtained by means of two accelerometers placed at its two sides measuring the y axis response. The complexity of the vibratory behaviour of this structure is the cause of this non-equivalence.

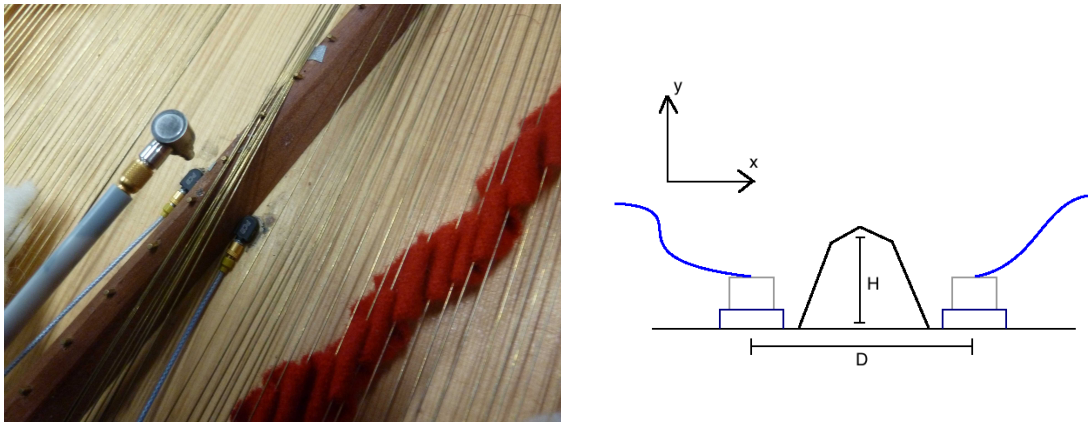

Figure 8.19: Layout of the accelerometers at the two sides of the bridge (left), Simplified scheme of a LAM1 clavichord bridge with a set of axis, with the two accelerometers laid out at its two sides (right).

[1]This approach was proposed by Jose Antunes by means of a personal communication

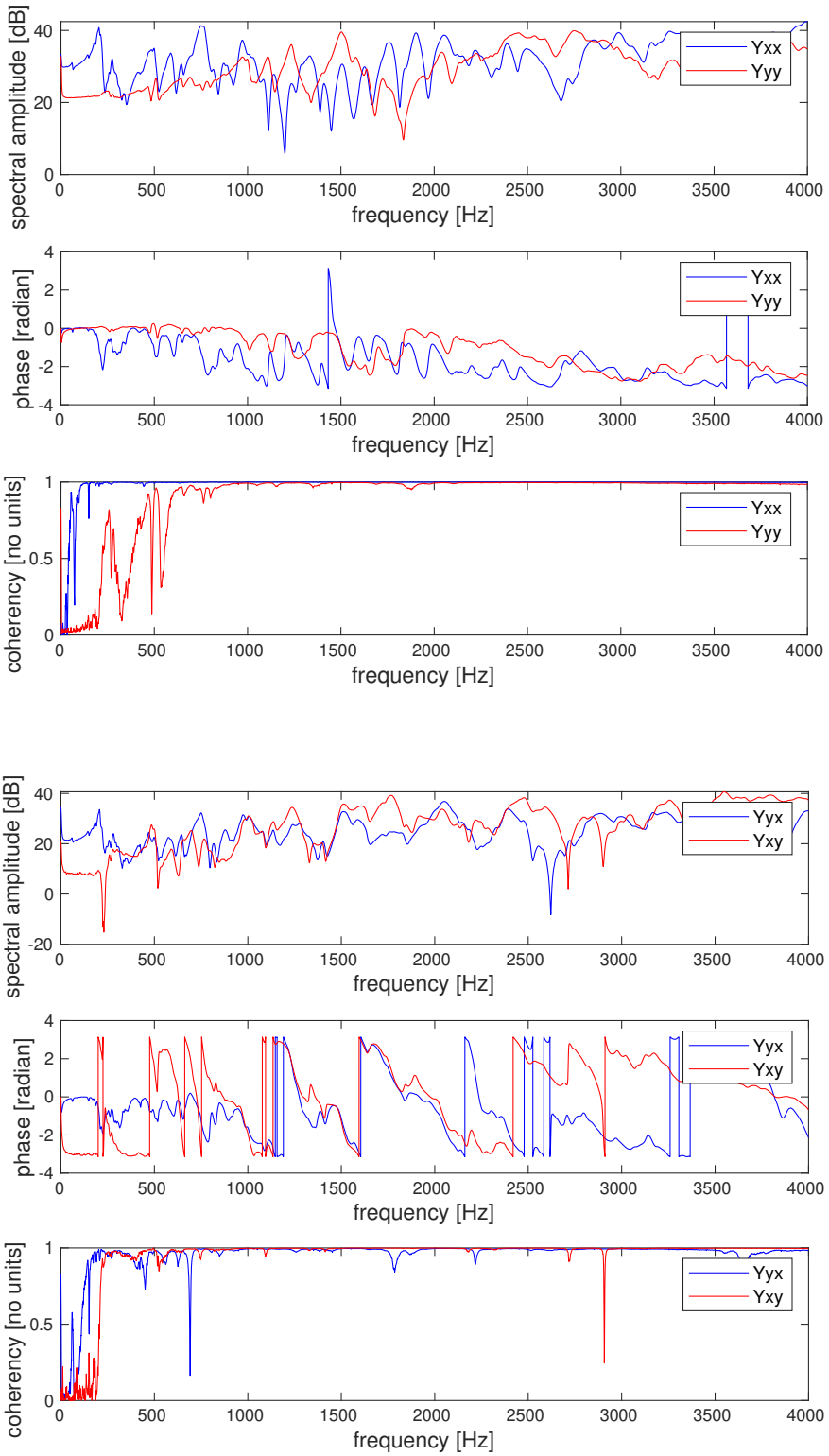

Figure 8.20: Spectral amplitude, phase and coherency of Y_{yy} and Y_{xx} with the approach where two accelerometers are laid out on the two sides of the bridge (left), Spectral amplitude, phase and coherency of Y_{yx} and Y_{xy} with the approach where two accelerometers are laid out on the two sides of the bridge (right).

Part VII

Publications

Preprint of the paper in the ***Journal of the Acoustical Society of America***

Non-linear modelling of the string-tangent dynamics with application to time-domain synthesis of the clavichord

Jean-Théo Jiolat,[1] Christophe d'Alessandro,[1] Jean-Loic Le Carrou,[1] and José Antunes-Vieira[2]
[1] *Sorbonne Université, CNRS, Institut Jean Le Rond d'Alembert, Équipe Lutheries-Acoustique-Musique, F-75005 Paris, France*
[2] *Centro de Ciências e Tecnologias Nucleares, Instituto Superior Técnico, Universidade de Lisboa, Estrada Nacional 10, Km 139.7, 2695-066 Bobadela LRS, Portugal*

String excitation by the tangent in the clavichord is a unique mechanism. The tangent, keeping in contact with the string after the initial strike, controls continuously the string tension. Four main flexible subsystems are considered in the clavichord: the tangent-key subsystem, the strings subsystem, the bridge-soundboard subsystem, the string damper subsystem. A modal description of the dynamics of these subsystems is proposed. Parameters of the subsystems are estimated on a copy of a historical instruments by Hubert (1784). The different subsystems and their coupling are modeled using a modal Udwadia-Kalaba formulation. A non-linear Kirchhoff-Carrier model of the string is used for capturing the string-tangent interaction dynamics. Realistic string, soundboard and tangent motions are obtained using a time-domain synthesis scheme that computes the dynamics of the uncoupled subsystems and the constraints resulting from coupling between them. Simulated motions of the model in response to a driving force on the key are analysed. The results are consistent with experimental measurements and published data on the dynamics of the clavichord. The model is able to reproduce the main acoustic features of the instrument: force on the key for intonation control, key velocity for dynamic nuances control, constant spectral slope for varying dynamic nuance.

 [http://dx.doi.org(DOI number)]

[XYZ] Pages: 1–13

I. INTRODUCTION

The clavichord is highly prized as a practice instrument among keyboard players, because of its superior ability to encourage a polished technique[?] . Its sound itself is weak and sometime a little disappointing at the first contact with the instrument. One explanation for its special appreciation of the clavichord as a wonderful coach of finger technique lies in the refined string control allowed by its simple and direct action. In the piano or harpsichord keyboard families (including tangent pianos, tangentenfluegel), the string/excitation mechanism (hammer, plectra) interaction is relatively short compared to tone duration. The interaction is interrupted after the hammer strike or plectra pluck, the string being allowed to vibrate freely, independently of the key motion until the finger is lowered and the string damped. On the contrary in the clavichord, the string and tangent stay in contact, i.e. are mechanically coupled as long as the key remains depressed (see[1] for a thorough presentation of the instrument). This feature has important consequences on the sound and the dynamic of the instrument[2]. The tangent-string contact during the whole tone is responsible to the specific (and much appreciated) expressive features of the clavichord, particularly expressive pitch control, a unique feature among keyboard instruments. Variations of finger force exerted on the key change the string tension, allowing for effects like vibrato, melodic accents of fine tuning. The aim of the present research is to develop a physical model of the clavichord that is able to account for, and synthesize the specific feature of the clavichord's action.

Relatively few acoustic studies on the clavichord have been published so far. The first ones[3][4] mainly reports descriptions of sound features (level, spectrum) due to the tangent action compared to the piano and harpsichord actions[4]. From the player point of view, a study on the clavichord touch and action is developed in[5]. Hardness of touch and pitch stability are related to string tension and key balance parameters. Some aspects of the physics of the instrument are investigated in[6]: soundboard and cavity coupling, tangent velocity profile and string displacement, sound decay rate, string pair coupling effects (as predicted by[7]). A simple linear string model is used for qualitative explanation of the tangent velocity profile (modeled as an exponential decaying function), string motion and sound decay rate. Based on these results a comparison with the piano and harpsichord through a simple synthesis model is derived in[8].

Focusing on the string excitation mechanism, the dynamics of the clavichord is revisited in[2]. Oscillation of the key/tangent and string system is modeled as mass-spring-damper model. Using a quasi-static approxima-

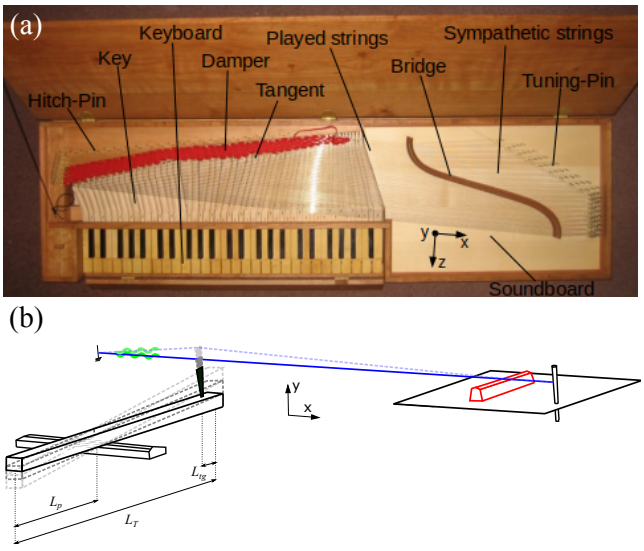

FIG. 1. (a) Description of a clavichord and (b) Sketch of the clavichord's mechanism in three positions of the touch: at rest, the tangent flushing the string and after excitation

tion of the string motion under the tangent action and a delay-line linear model of the string, results on the excitation dynamics are derived and compared to experimental data. The main conclusions are: both the tangent velocity and the tangent displacement appear important for playing the clavichord; a linear relationship between tangent velocity and the sound pressure level is shown; String displacement (and then variation of string tension) has a significant effect on fundamental frequency; The spectral slope does not vary much with tangent velocity or displacement. Measurement on 4 clavichords are in good agreement with these finding[9]. In a subsequent study on clavichord playing technique, musical consequences of the needed joint tangent displacement/velocity controls for the clavichord playing technique are studied in terms of the so-called "clavichord's paradox"[10].

As for sound synthesis, two approaches for physical modeling have been published so far. The first approach is based on commuted wave-guide synthesis[11]. In this signal processing based approach, string/tangent interaction is partly based on sampling of real sounds (for a realistic knock sound) and partly on additional filters accounting for the variable string tension during a tone.

Another approach for sound synthesis considers the clavichord as a particular case of a piano. A complete physical model of the piano[12,13] allows for real-time sound synthesis and refined variations of the physical parameters of the considered instrument model (e.g. hammer felt density and thickness, soundboard dimensions and wood etc.). The clavichord is considered in this framework among many historical pianos, harpsichords, or hybrid instruments models[?] . The model is simulated using a finite element approach, with particular attention on the constraining forces responsible for the coupling between the string and the bridge. The specific features of clavichord excitation are not published, but it seems that a hard metallic hammer is simulated for the initial tangent strike. An additional after-touch effect seems to account for the maintained tangent/string contact.

Although experimental data on the dynamics of the clavichord have been published, only simple linear physical models have been proposed so far. A new model for sound synthesis of the clavichord, paying special attention to non-linear tangent/string dynamics is developed in the present article. A time-domain synthesis scheme using the Udwadia-Kalaba (U-K) formulation that proved successful for modeling of other stringed instruments[14] seemed appropriate for this purpose. A functional description of the clavichord in terms of vibrating subsystems results in a simplified one string model. Parameters are identified using experimental measurements on a copy of a historical instruments (Part II). A model of tangent/string interaction based on the Kirchhoff-Carrier string representation and the U-K formulation for coupled dynamical system is developed for the one-string clavichord model (Part III). The modal equations of the U-K model can be solved by means of a simple finite difference time discretization scheme. Synthesis results are compared to the measured dynamic behaviour of the real clavichord using experiments and published data (Part IV).

II. VIBRATORY AND ACOUSTIC SUBSYSTEMS IN THE CLAVICHORD

A. Principle of the clavichord and tangent action

A clavichord and its parts are described in Figure 1-(a), a recent (2007) instrument inspired by a historical clavichord by Hubert (1784). The main parts of the instrument are indicated on the picture. At the center of the instrument, the sound of the clavichord results from string vibration. The strings, organized in pairs, are stretched between the hitch-pins and tuning pins and attached to the radiating soundboard through the bridge and bridge pin. Strings are functionally divided into three sections. The "damped section", between the hitch-pin and the tangent. This section is partially covered by strips of cloth. Then, after the initial tangent excitation, its vibration is rapidly damped. The "played section" vibrates between the tangent and bridge, as long as the tangent stays in contact with the string after the initial tangent strike. When the key is released, the tangent contact is lost and the string vibration is damped by the cloth strips. The "resting section" between the bridge and the tuning pin, is not directly excited by the tangent, but as it is not damped in the clavichord (contrary to e.g. the square piano), partial transmission of the played section vibration results in sympathetic vibration[15,16]. The strings are pressed vertically on the bridge and pressed horizontally on the pins laid out along the bridge. This contact leads to the soundboard/string coupling. The

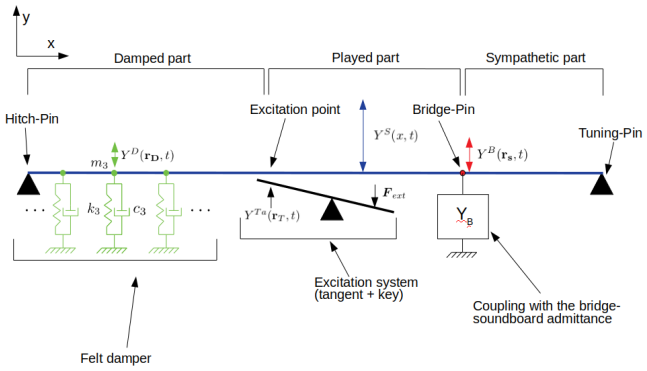

FIG. 2. Schema of the modeled G#3 string being excited by the tangent.

soundboard vibrates under the action of the string, and because of its large surface sound is radiated in the air.

A complete study of the instrument is out of the scope of the present work: only the simplified model displayed in Figure 1-(b) will be studied in depth. This simplified model is made of only one string (the chosen string is the first string of the G3# choir) and the corresponding key, tangent and damper. In this model the string is stretched between the hitch-pin and tuning pin and in contact with the bridge at the bridge pin. The soundboard and bridge are those of the whole instrument, because it is important to consider this part in its integrity even for modeling a unique string. Other aspects of the instrument, like the case and lid, are not considered in the present study, because their vibratory and acoustic functions are only of second order.

B. Vibratory and acoustic subsystems

For modelling purposes, the model can be considered as an assembling of four vibrating subsystems as displayed in Figure 2. The initial force for playing the instrument is provided by the player's finger. The player moves the tangent/key subsystem, the first subsystem, providing the string excitation. The strings, second subsystem, act as the vibratory engine of the instrument. Attached to the left side of the strings are the cloth dampers, a third attached subsystem. Attached to right side of the strings, is the bridge/soundboard subsystem, fourth subsystem.

The string is the central subsystem of the instrument. Let $Y^S(x,t)$ (resp. $Y^D(r_D,t)$, $Y^{Ta}(r_T,t)$, $Y^B(r_s,t)$) be the string displacement (resp. damper/string contact point displacement, string/tangent contact point displacement, string/bridge contact point displacement) at position x (resp. r_D, r_T, r_s). The vibratory subsystems are coupled to the string at points r_D, r_T, r_s (damper, tangent and bridge).

The first subsystem, the tangent/key subsystem, can be considered as a rigid rod which tilts with respect to a pivot. When the tangent strikes the string, the elastic string reacts and the whole system oscillates. The tangent has a mass $M_{Tg} = 5$ g, the key has a mass $M_k = 30$ g. The length of the key is $L_T = 28.9$ cm. The pivot of the key (balance point) is situated at a distance $L_p = 17.2$ cm of the back of the key, the finger presses the key at a distance $L_f = 27.9$ cm of the back of the key, and the tangent is located at a distance $L_{tg} = 3.5$ cm of the back of the key, see Figure 1-(b). Associated modal parameters for the tangent/key subsystem (k_{Ta}, m_{Ta}, c_{Ta}) are used.

The string, second subsystem, is characterized by its mass, elasticity and damping factors. Between the hitch pin and excitation point, the cloth strips damper, third subsystem, is represented by N (typically N=65) parallel damped oscillators characterized by their spring, mass and viscous damping coefficients (k_D, m_D, c_D). The bridge/soundboard subsystem, fourth subsystem, is characterized by its coupling admittance Y_B.

In the remaining of this part, parameters of the subsystems in Figure 2 are estimated on a copy of a historical instruments by Hubert (1784) displayed in Figure 1-(a). Parameter for the G$\#_3$ string are identified (see table I). These parameters will be used for numerical simulation and evaluation. Three functional parts of the string can be identified: between $x = 0$ m and $x = 0.2$ m, is the damped part of the string, with a cloth damper coiled up between $x = 3.4$ mm and $x = 13.7$ mm. The played part of the string is between $x = 0.2$ m and $x = 0.53$ m. The sympathetic part rest of the string is between the bridge pin $x = 0.53$ m and tuning pin $x = 0.84$ m.

C. The key-tangent subsystem

The modal parameters of the key-tangent subsystem are determined by their vibratory characteristics. The tilting mode of the G$\#_3$ key equipped of its tangent is measured with the help of an impulse hammer and accelerometers. The measured frequency are $f_{Ta} = 1.2$ Hz. Its modal mass, determined in section III B, is $m_{Ta} = 1.17 \times 10^{-2}$ kg, its modal stiffness is $k_{Ta} = 4\pi^2 f_1^2 m_{Ta} = 0.63$ N.m^{-1} and its modal damping is $c_{Ta} = 2.5$ kg.s^{-1}.

D. The string subsystem

The string modal damping characteristics are obtained by measurements of the vibrating string stretched on a string bench. This bench allows for string vibration measurement without any coupling of the string with another vibratory structure. The string is excited by a copped wire that breaks at a given tension when lifted vertically. The vibratory displacement of the string is measured at the other extremity by means of optical forks[17]. For the right (sympathetic) part of the G$\#_3$ string ($L = 31.7$ cm, $d_s = 0.33$ mm, $f_0 = 396.9$ Hz), damping for 23 partials between 396.9 Hz to 9354 Hz are analysed using the high-resolution algorithm ESPRIT[18], following the methodology described in[19,20].

ρ (kg.m^{-3})	E (Pa)	δ_{ve-te}
7000	62×10^9	$1{,}5 \times 10^{-4}$
Q_{struc}	η_{air} (kg.m^{-1}.s^{-1})	ρ_{air} (kg.m^{-3})
5×10^4	$1{,}8 \times 10^{-5}$	1,2

TABLE I. String's parameters used to simulate the string damping coefficients

The measured damping coefficients are matched with the Valette and Cuesta model (see section III C 3), with the parameters reported in Table I, where of E and ρ corresponds to brass, η_{air} and ρ_{air} are taken from the previous data[21].

E. Bridge and soundboard subsystems

To simulate the vibratory motion of the bridge, the modal parameters (mass matrix, stiffness matrix, damping matrix, mode shapes) of this subsystem need to be known. As no classical continuous model (like the beam) has a similar modal basis as that of the bridge, these modal parameters need to be extracted out of modal analysis. Modal parameters (mass matrix, stiffness matrix, damping matrix, mode shapes) are estimated using experimental modal analysis and measurement of the bridge Frequency Response Function (FRF). The FRF are obtained by measurement of the response at the coupling point between the bridge and the G#$_3$ string (using a PCB M352C65 accelerometer and an acquisition system with a sample rate of 51.2 kHz and a 24 bit depth) to impulses given by an automatic impact hammer (force sensor PCB 086E80). The accelerometer is placed above the hitch-pin and measures its vertical acceleration. All the other strings are damped by strips of cloth woven on both sides of strings (above the soundboard on the right size and above the keyboard on the left size). Modal analysis between 100 Hz and 600 Hz is conducted in two steps. A first step is the estimation of physical poles containing the modal frequencies and damping coefficients of the analysed structure, using the Least square rational function (LSRF) estimation method (Matlab signal processing toolbox[22]). The second step is the estimation of residues which encapsulate the mode shapes and modal masses of the system. Normalizing modal masses to $m_n = 1$ kg for modes $n = 1{,}2{,}...{,}N_B$, the corresponding mode shapes are estimated from the residues. The estimated and measured FRF at the G#$_3$ string/bridge coupling point are plotted on figure 3.

F. The damper subsystem, coupling between subsystems and activation

The damper in the model is a series of 65 dashpots. The parameters c_D, m_D and k_D are chosen so that the damping effect exerted on the string once the key is released can be reproduced. The values chosen are

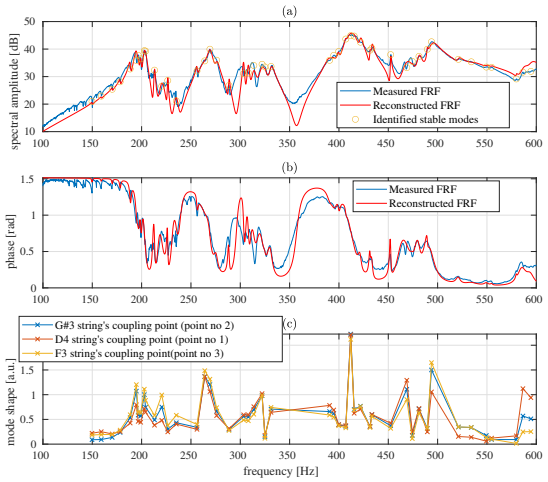

FIG. 3. Comparison of the spectral amplitude (Ref 1 dB : 1 m.s^2.N^{-1}) of the measured FRF (blue line) with its reconstruction (red line) by means of modal analysis at the driving point (point n°2) coupling the bridge with the G#3 string (a), Unwrapped phase of the measured FRF (blue line) and its reconstruction (red line) by means of modal analysis (b), Mode shapes extracted out of this modal analysis (c).

$m_D = 1.0 \times 10^{-2}$ kg, $k_D = 0$ N.m^{-1} and $c_D = 8.0 \times 10^2$ kg.s^{-1}.

The four subsystems are coupled through the string: the string is coupled to the damper at the damper location; it is coupled to the bridge at the bridge pin location; it is coupled to the tangent/key subsystem during its contact at the tangent location. All these coupling conditions assume a continuity of displacement between the string at the coupling position and the other subsystem involved.

Finally, the whole vibratory system is activated by an external force that represents the action of the finger on the key. The finger force profile is typically a step with given attack and release times.

III. PHYSICAL MODELING USING THE U-K FORMULATION

A. U-K formulation for the clavichord

In this section, the clavichord model in terms of four coupled vibratory subsystems is modeled using a modal U-K formulation[14,23], a formalism that has been successfully used for physical modeling of the guitar and Portuguese guitar[24,25]. Let us consider a mechanical system with mass matrix $\mathbf{M}$ which is subjected to a force vector $\mathbf{F_e}(t)$ including all constraint-independent internal and external forces. This system is also subjected to constraining forces $\mathbf{F_c}(t)$. Denoting the dynamical solution $\mathbf{y_u}(t)$ of the unconstrained system and $\mathbf{y}(t)$ of the con-

strained system, the motion equations of the constrained system derived by Udwadia and Kalaba[14,26] are:

$$\ddot{\mathbf{y}} = \ddot{\mathbf{y}}_u + \mathbf{M}^{-1/2}\mathbf{B}^{+}(\mathbf{b} - \mathbf{A}\ddot{\mathbf{y}}_\mathbf{u}), \quad \ddot{\mathbf{y}}_u = \mathbf{M}^{-1}\mathbf{F}_e(t) \quad (1)$$

where $\mathbf{A}$ is the constraint matrix, $\mathbf{b}$ is a known constrained vector. The generalized Moore-Penrose inverse matrix $\mathbf{B}^{+}$ of $\mathbf{B} = \mathbf{A}\mathbf{M}^{1/2}$ can be rendered numerically robust, even for a singular constraint matrix. For a particular external (finger) excitation $\mathbf{F}_e(t)$ these equations are solved using a suitable time-step integration scheme. A modal version of the U-K formulation suitable for continuous flexible systems proved successful for musical instruments modeling[14]. Assuming a set of S vibrating subsystems defined in terms of their unconstrained modal basis and coupled through P kinematic constraints, one obtains[14].

$$\ddot{\mathbf{q}} = \boldsymbol{W}\tilde{\mathbf{M}}^{-1}(-\tilde{\mathbf{C}}\dot{\mathbf{q}} - \tilde{\mathbf{K}}\mathbf{q} + \mathbf{F}_\mathbf{ext}) \quad (2)$$

where $\mathbf{q}$ represent the vector of modal displacements, $\tilde{\mathbf{M}}$, $\tilde{\mathbf{K}}$, $\tilde{\mathbf{C}}$ are respectively the modal mass matrix, modal stiffness matrix, and modal damping matrix, while $\boldsymbol{W} = \mathbf{1} - \tilde{\mathbf{M}}^{-1/2}\boldsymbol{B}^{+}\boldsymbol{A}$ is a convenient global transformation matrix (which is computed before the time loop), where $\boldsymbol{A}$ is the modal constraint matrix, and $\mathbf{F}_\mathbf{ext}$ are the external modal forces applied on the system.

B. Key-tangent modelling

A mode shape is associated to the key-tangent subsystem to model the tilting motion of the key. The modal representation of this system is given by the following equations :

$$Y^{Ta}(\mathbf{r}, t) = \phi^{Ta}(x)q^{Ta}(t) \quad (3)$$

where Y^{Ta} is the displacement of the key-tangent substructure, ϕ^{Ta} is its mode shape and q^{Ta} is its modal amplitude, "Ta" standing for "tangent", and,

$$m_{Ta}\ddot{q}^{Ta}(t) + c_{Ta}\dot{q}^{Ta}(t) + k_{Ta}q^{Ta}(t) = F_{ext}(t) \quad (4)$$

where m_{Ta}, c_{Ta} and k_{Ta} are respectively the modal mass, modal damping and modal stiffness of the key-tangent subsystem, and F_{ext} is the modal excitation force that the musician exerts on the key. The mode shape ϕ^{Ta} is given in the following way :

$$\phi^{Ta}(x) = \frac{L_T - x}{L_T - L_p} - 1 \quad (5)$$

Considering that the linear density of the key is $\rho_k = \frac{M_k}{L_T}$, the modal mass of the key-tangent substructure m^{Ta} can be found thus :

$$m_{Ta} = M_{Tg}\phi^{Ta}(L_{tg})^2 + \int_0^{L_T} \rho_k \phi^{Ta}(x)^2 dx \quad (6)$$

After some calculations, it gives :

$$\begin{aligned} m_{Ta} = M_{Tg}\left(\frac{L_T - L_{tg}}{L_T - L_p} - 1\right)^2 \\ + M_k \frac{3L_p^2 - 3L_pL_T + L_T^2}{3\left(L_T - L_p\right)^2} \end{aligned} \quad (7)$$

C. String modelling

1. Modal description of the string

To comply the string model with the modal U-K formulation, a modal representation of the string is given in this section. A modal expansion of the string displacement Y^S is done :

$$Y^S(x,t) = \sum_{n=1}^{N_s} \phi_n^S(x) q_n^S(t) \quad (8)$$

where ϕ_n^S are the mode shapes of the string, q_n^S are its modal amplitudes, and N_s is the string's number of modes so that $n = 1, 2, ..., N_s$. Considering that the boundary conditions of the clavichord string are pined-pined, it leads to the following string's mode shapes :

$$\phi_n^S(x) = \sin\left(\frac{n\pi x}{L}\right) \quad n = 1, 2, \ldots, N \quad (9)$$

where L refers to the string length between the hitchpin and the tuning-pin. Also, if the static displacement is large enough, the geometrical non-linear force $\boldsymbol{F}_{nl}^S$ related to the string's variation of tension also needs to be taken into account. That yields the following string's modal equations :

$$\boldsymbol{M}^S\ddot{\mathbf{q}}^S + \boldsymbol{C}^S\dot{\mathbf{q}}^S + \boldsymbol{K}^S\mathbf{q}^S + \boldsymbol{F}_{nl}^S(\mathbf{q}^S, \dot{\mathbf{q}}^S) = \mathbf{0} \quad (10)$$

where $\boldsymbol{M}^S$, $\boldsymbol{C}^S$ and $\boldsymbol{K}^S$ are the modal mass matrix, the modal damping matrix and the modal stiffness matrix of the string respectively, and $\mathbf{q}^S$ is the modal amplitude vector of the string. The expression of the geometrical non-linear forces can be expressed by means of the kirchhof-Carrier model, which is the topic of the next section.

2. Non-linear string dynamics in string tangent interaction

The string-tangent interaction in the clavichord results in geometrical deformations of the string (the tangent lifts the string after the initial contact) and consequently in an increased string tension. This displacement

can be quite significant in the clavichord, up to 3-5 mm, inducing a substantial rise in pitch. The string uplift results in a geometrical deformation of the string and thus non-linear forces that must be considered in the dynamics of the instrument. For dynamic modeling of the non-linear forces, the Kirchhoff-Carrier non-linear model for the string is used[27,28], following previous work on the twelve-string Portuguese guitar[24,25]. According to the mode shapes in Equation 9, the kirchhoff-Carrier model leads to geometric non-linear terms creating the dynamic tension T_{dyn} : +

$$T_{dyn}(t) = \frac{ES}{2L}\int_0^L \left[\left(\frac{\partial Y^S(x,t)}{\partial x}\right)^2\right] dx \tag{11}$$

which gives rise to the non-linear differential equation of motion :

$$\rho S\frac{\partial^2 Y^S(x,t)}{\partial t^2} - (T_0 + T_{dyn}(t))\frac{\partial^2 Y^S(x,t)}{\partial x^2} = 0 \tag{12}$$

The force F^{nl} due to geometric non-linear terms are :

$$F^{nl}(x,t) = T_{dyn}(t)\frac{\partial^2 Y^S(x,t)}{\partial x^2} \tag{13}$$

Thereby, it yields the nonlinear modal force terms :

$$F_n^{nl}(t) = \int_0^L F^{nl}(x,t)\phi_n(x)dx \tag{14}$$

Using equations 8 and 9 and calculating the integrals in equation 11, it leads to a dynamic tension that depends quadratically on the modal response amplitudes:

$$T_{dyn}(t) = \frac{ES\pi^2}{4L^2}\sum_{n=1}^{N} n^2\left(q_n(t)\right)^2 \tag{15}$$

Then, calculating the integral in equation 14, the cubic modal force terms are deduced[24] :

$$F_n^{nl} = \frac{ES\pi^4}{8L^3}n^2 q_n(t)\sum_{m=1}^{N} m^2 q_m(t)^2 \tag{16}$$

Equation 16 represents the modal non-linear forces for the string due to the vertical displacement resulting from the tangent lift. In contrast to the quasi-static situation, the force in Equation 16 can be computed in dynamic modeling of this interaction.

The increase of tension due to tangent height Y_e is an important parameter, particularly for the player, as it is related to the hardness of touch[5], the key force feedback felt by the player.

Note that in a quasi-static approximation the string lifted by the tangent is in the shape of a triangle (neglecting the string stiffness). The resulting quasi-static tension T_{stat} can be expressed using simple geometry[2] :

$$\Delta T_{stat} = ES\left(\frac{\sqrt{L_l^2 + Y_e^2} + \sqrt{L_r^2 + Y_e^2}}{L} - 1\right) \tag{17}$$

where $L_l = x_e$ and $L_r = L - x_e$ are the lengths of the left (resp. the right) side of string relative to the excitation point x_e, and Y_e is the vertical heights of the string. As the tangent heights is small compared to the string length, it can be assumed that $\frac{Y_e}{L_l} \ll 1$ and $\frac{Y_e}{L_r} \ll 1$. Simplifying equation 17 using a Taylor expansion, the quasi-static tension is proportional to the square of the tangent heights :

$$\Delta T_{stat} = Y_e^2\frac{ES}{2x_e(L - x_e)} \tag{18}$$

The same result can be derived by using the Kirchhoff-Carrier model. Under static conditions, in equation 15, the modal displacements q_n^S are computed by noticing that:

$$\begin{aligned} Y^S(x) &= \sum_{n=1}^{N}\phi_n^S(x)q_n^S \\ \Rightarrow \int_0^L Y(x)\phi_n^S(x)dx &= \int_0^L \left[\phi_n^S(x)\right]^2 q_n^S dx \end{aligned} \tag{19}$$

so that the modal displacements created by the string displacement field are given by:

$$q_n^S = \frac{\int_0^L Y(x)\phi_n^S(x)dx}{\int_0^L \left[\phi_n^S(x)\right]^2 dx}, \quad n = 1, 2, ..., N \tag{20}$$

which gives :

$$q_n^S = Y_e\frac{\int_0^{x_e}\frac{x}{x_e}\phi_n^S(x)dx + \int_{x_e}^L\frac{L-x}{L-x_e}\phi_n^S(x)dx}{\int_0^L \left[\phi_n^S(x)\right]^2 dx}, \quad n = 1, 2, ..., N \tag{21}$$

Because the physical displacement of the string is given by :

$$Y(x) = \begin{cases} \frac{x}{x_e}Y_e & 0 \leqslant x \leqslant x_e \\ \\ \frac{L-x}{L-x_e}Y_e & x_e \leqslant x \leqslant L \end{cases} \tag{22}$$

using Equation 9 for computing the integrals in equation 21, one obtains :

$$q_n^S = \frac{2L^2 \sin\left(\frac{n\pi x_e}{L}\right)}{n^2\pi^2 x_e\left(L - x_e\right)} Y_e, \quad n = 1, 2, ..., N \tag{23}$$

Then, replacing equation 23 in equation 15

$$T_{dyn}(Y_e) = Y_e^2 \frac{ESL^2}{\pi^2 x_e^2 \left(L - x_e\right)^2} \sum_{n=1}^{N} n^2 \left(\frac{1}{n} \sin\left(\frac{n\pi x_e}{L}\right)\right)^2 \tag{24}$$

Notice that when the number of modes N is large enough, then :

$$\begin{aligned} \sum_{n=1}^{N} \left(\frac{1}{n} \sin\left(\frac{n\pi x_e}{L}\right)\right)^2 &\approx \sum_{n=1}^{\infty} \left(\frac{1}{n} \sin\left(\frac{n\pi x_e}{L}\right)\right)^2 \\ &\approx \frac{\pi^2}{2} \frac{x_e}{L} \left(1 - \frac{x_e}{L}\right) \end{aligned} \tag{25}$$

replacing equation 25 in equation 24 gives the same result as Equation 18, showing that a same tangent height gives a same string tension at for the quasi-static approach and the non-linear Kirchhoff-Carrier approach.

3. Model of string's modal dampings

To bestow a proper damping coefficient to each string's mode, the string damping model elaborated by Valette and Cuesta[29] is chosen. The air friction, the visco-elastic and thermo-elastic friction as well as the structural friction are taken into account. They are denoted respectively by the quality factor $Q_{n,air}$, $Q_{n,ve-te}$ and Q_{struc}.

$$\begin{aligned} Q_n^{-1} &= Q_{n,air}^{-1} + Q_{n,ve-te}^{-1} + Q_{struc}^{-1} \\ &= \frac{R}{2\pi\rho_L} (nf_0)^{-1} + \frac{4\pi^2 \rho_L E I \delta_{ve}}{T^2} (nf_0)^2 + Q_{struc}^{-1} \end{aligned} \tag{26}$$

where R designates the mechanical resistance

$$R = 2\pi\eta + 2\pi d_s \sqrt{\pi \eta_{air} \rho_{air} f} \tag{27}$$

and where ρ_{air} and η_{air} corresponds to the dynamic viscosity and the density of the air respectively, and d_s represents the string's diameter. Then, Q_n^{-1} represent the damping coefficient associated to the n^{th} mode of the string. E is the Young modulus of the string, I is the second moment of inertia of the string, T is the string's tension, ρ_L is the linear density of the string, and δ_{ve-te} is the imaginary part of the strin's Young modulus. The term $\delta_{ve-te} = \delta_{ve} + \delta_{te}$ encapsulates visco-elastic effects δ_{ve} and thermo-elastic ones δ_{te}, taking the same approach as Paté[20]. Q_{struc} is a constant value. Using $\zeta_n = \frac{Q_n^{-1}}{2}$, one can obtain the damping ζ_n coefficients of the string.

D. Bridge modelling

The motion of the bridge is modelled by means of its modal equations. So considering the modal expansion of the bridge displacement :

$$Y^B(\mathbf{r}, t) = \sum_{n=1}^{N_B} \phi_n^B(x) q_n^B(t) \tag{28}$$

where $\mathbf{r}$ is the location vector, N_B is the number of bridge modes, ϕ_n^B are the mode shapes of the bridge and q_n^B are the modal amplitudes of the bridge. Then, the modal equations governing the bridge's vibratory motion are :

$$\boldsymbol{M}^B \ddot{\mathbf{q}}^B + \boldsymbol{C}^B \dot{\mathbf{q}}^B + \boldsymbol{K}^B \mathbf{q}^B = \mathbf{0} \tag{29}$$

where $\boldsymbol{M}^B$, $\boldsymbol{C}^B$ and $\boldsymbol{K}^B$ are the modal mass matrix, the modal damping matrix and the modal stiffness matrix of the bridge respectively, and $\mathbf{q}^B$ is the modal amplitude vector of the bridge. Because of the complexity of the structure, as opposed to the string, there is no continuous model that can yield analytically the expression of the bridge's modal parameters. These could be derived numerically by means of finite element method by reproducing the geometry and the material properties of the bridge, as it was done for instance in the case of the piano[12]. Experimental modal analysis of the bridge is done in section II E to give numerical values to the bridge's modal parameters.

E. Damper modelling

The damper is modeled by coupling a portion of string with a number of mass-spring-dampers assuming a continuity of displacement between the dampers and the string at their contact points. All theses mass-spring-damper are considered independent to one another. Let N_D is the chosen number of dampers D:

$$\boldsymbol{M}^D \ddot{\mathbf{q}}^D + \boldsymbol{C}^D \dot{\mathbf{q}}^D + \boldsymbol{K}^D \mathbf{q}^D = \mathbf{0} \tag{30}$$

Where $\mathbf{q}^D$ is the amplitude vector of the damper responses. Matrices $\mathbf{M}^D$, $\mathbf{C}^D$ and $\mathbf{K}^D$ are square diagonal with identical coefficients m_D, c_D and k_D, respectively.

All the mass-spring-dampers associated to the cloth damping device have the same mass, stiffness and damping coefficients. So all the mass-spring-dampers have the same frequency and the same damping. These mass-spring-dampers representing the cloth damper are coupled with a certain length of the string, as it is modeled in section III F 3.

F. Couplings between subsystems

The individual subsystems are described with the help of a modal representation. The modal constraint

matrix $\boldsymbol{A}$ and the vector $\mathbf{b}$ of the constrained system is given $\boldsymbol{A}\ddot{\mathbf{Q}} = \mathbf{b}$ with: with

$$\boldsymbol{A} = \begin{bmatrix} \boldsymbol{A}_B \\ \boldsymbol{A}_{Ta} \\ \boldsymbol{A}_D \end{bmatrix}, \mathbf{b} = \begin{bmatrix} \mathbf{b}_B \\ \mathbf{b}_{Ta} \\ \mathbf{b}_D \end{bmatrix}, \quad \ddot{\mathbf{Q}} = \begin{bmatrix} \ddot{\mathbf{q}}^S \\ \ddot{\mathbf{q}}^B \\ \ddot{\mathbf{q}}^{Ta} \\ \ddot{\mathbf{q}}^D \end{bmatrix} \tag{31}$$

where $\boldsymbol{A}_B$ is the matrix coupling the string with the bridge with $\mathbf{b}_B$ its associated vector, $\boldsymbol{A}_{Ta}$ is the matrix coupling the string with the key-tangent subsystem with $\mathbf{b}_{Ta}$ its associated vector, and $\boldsymbol{A}_D$ is the matrix coupling the string with the damper with $\mathbf{b}_D$ its associated vector. By giving the continuity conditions related to all these couplings, these matrices and vectors are determined in sections III F 2, III F 1 and III F 3.

1. String and key-tangent subsystem coupling

To model the contact between the tangent and the string, the approach developed by Antunes *et al* is adopted[23]. This contact is considered to be a coupling between the tangent and the string at the moment when the tangent touches the string. At the contact location, assuming a continuity of displacement between the two subsystems, this yields the following coupling conditions :

$$Y^S(x_{ext}, t) - Y^{Ta}(\mathbf{r}_T, t) = 0 \tag{32}$$

$$[\boldsymbol{\Phi}^S(x_{ext})]^T \mathbf{q}^S(t) - [\boldsymbol{\Phi}^{Ta}(\mathbf{r}_T)]^T \mathbf{q}^{Ta}(t) = 0 \tag{33}$$

where Y^{Ta} is the displacement of the tangent, x_{ext} is the position where the string is excited, $\mathbf{r}_T$ is the location of contact on the tangent. The tangent is initially located below the string with respect to axis y. The whole string is initially at rest at altitude $y = 0$. At the moment when the tangent reaches altitude $y = 0$, $\boldsymbol{A}_{Ta}$ can be modified to couple the two subsystems. The contact is thus modeled by this coupling written within matrix $\boldsymbol{A}$ at this moment in time. Then, the conditions for this coupling are written as follows :

$$\begin{cases} Y^{Ta}(\mathbf{r}_T, t) < Y^S(x_{ext}, t) & \mathbf{b}_{Ta} = 0 \qquad \boldsymbol{A}_{Ta} = \mathbf{0} \\ Y^{Ta}(\mathbf{r}_T, t) = Y^S(x_{ext}, t) & \mathbf{b}_{Ta} = 0 \\ \boldsymbol{A}_{Ta} = \left[[\boldsymbol{\Phi}^S(x_{ext})]^T 0 \dots 0 - [\boldsymbol{\Phi}^{Ta}(\mathbf{r}_T)]^T 0 \dots 0\right] \end{cases}$$

where $\boldsymbol{\Phi}^{\mathbf{S}}_{\mathbf{c}}$ and $\boldsymbol{\Phi}^{\mathbf{Ta}}_{\mathbf{c}}$ represent respectively the string's mode shape vector and that of the key-tangent subsystem at the coupling point. The U-K formulation apply constraints on the system's acceleration. It means that, when simulating the model, the constraints on the system's acceleration are respected. However, respecting these constraints does not imply respecting the constraints on the system's displacement and on the system's velocity. Without the implementation of stabilization techniques, numerical drifts are taking place during the simulation, because of the constraint's violation in terms of displacement and velocity. The technique elaborated by Yoon *et al*[30] can be used to eliminate the aforementioned violations. It is based on a geometric projection approach applied after each time step. The displacement constraint violations are eliminated by correcting the constrained system displacement :

$$\mathbf{y}_c = \mathbf{y} + \Delta\mathbf{y} \quad \Rightarrow \quad \mathbf{y}_c = \mathbf{y} - \mathbf{A}\boldsymbol{\varphi}_{\boldsymbol{p}}(\mathbf{x}, t) \tag{34}$$

$$\Rightarrow \quad \mathbf{q}_c = \mathbf{q} - \boldsymbol{A}\boldsymbol{\varphi}_{\boldsymbol{p}}(\mathbf{x}, t) \tag{35}$$

Then, the same procedure is done when it comes to the velocity constraint violations :

$$\begin{aligned} \dot{\mathbf{y}}_c = \dot{\mathbf{y}} + \Delta\dot{\mathbf{y}} \quad &\Rightarrow \quad \dot{\mathbf{y}}_c = \dot{\mathbf{y}} - \mathbf{A}\boldsymbol{\Psi}_{\boldsymbol{p}}(\dot{\mathbf{x}}, t) \\ &\Rightarrow \quad \dot{\mathbf{q}}_c = \dot{\mathbf{q}} - \boldsymbol{A}\boldsymbol{\Psi}_{\boldsymbol{p}}(\dot{\mathbf{q}}, t) \end{aligned} \tag{36}$$

where $\mathbf{y}_c$ and $\dot{\mathbf{y}}_c$ represent respectively the corrected displacements and velocity, $\Delta\mathbf{y}$ and $\Delta\dot{\mathbf{y}}$ represent respectively the correction of the displacement and that of the velocity, $\boldsymbol{\varphi}_{\boldsymbol{p}}(\mathbf{y}, t)$ and $\boldsymbol{\Psi}_{\boldsymbol{p}}(\dot{\mathbf{y}}, t)$ are respectively the displacement and velocity constraints.

2. String-Bridge coupling

The interaction of the string with the bridge is modeled by means of coupling. It is assumed that the displacement of the string is continuous with that of the bridge at the coupling location. Therefore, one can express the necessary coupling conditions to model the constraints of the system. This continuity implies that the string's displacement $Y^S(x_B, t)$ must be the same as that of the bridge $Y^B(\mathbf{r}_B, t)$, "S" standing for "string" and "B" standing for "bridge", x_B is the location of the coupling point on the string and $\mathbf{r_B}$ is the vector of location of the coupling point on the bridge. Thus :

$$Y^S(x_B, t) - Y^B(\mathbf{r_B}, t) = 0 \tag{37}$$

with modal coordinates, it leads to :

$$[\Phi^S(x_B)]^T \mathbf{q}^S(t) - [\Phi^B(\mathbf{r_B})]^T \mathbf{q}^B(t) = 0 \tag{38}$$

with the mode shape vectors :

$$\begin{aligned} \Phi^S(x_B) &= [\phi_1^S(x_B)\phi_2^S(x_B) \dots \phi_{N_S}^S(x_B)]^T, \\ \Phi^B(\mathbf{r_B}) &= [\phi_1^B(\mathbf{r_B})\phi_2^B(\mathbf{r_B}) \dots \phi_{N_B}^B(\mathbf{r_B})]^T \end{aligned} \tag{39}$$

where N_B is the number of bridge's modes, N_S is the number of string's modes. As a result, defining N_c as the number of strings of the system, equation 38 leads to the following matrix $\boldsymbol{A}_B$ and vector $\mathbf{b}_B = \mathbf{0}$:

$$\boldsymbol{A}_B = \begin{bmatrix} [\Phi^S(x_B)]^T & -[\Phi^B(\mathbf{r_B})]^T & 0 & \dots & 0 \end{bmatrix} \tag{40}$$

Equation 40 shows the coupling matrix $\boldsymbol{A}_B$ and the associated vector $\mathbf{b}_B$ used to couple the strings with the bridge.

3. String-Damper coupling

Like the string-bridge coupling, the continuity of the string's displacement $Y^S(x_D,t)$ with that of the damper $Y^D(\mathbf{r}_s,t)$ is assumed, "D" standing for "damper", x_D being the location of the damper on the string and r_D being the vector locating the damper. Thus :

$$Y^S(x_D,t) - Y^D(\mathbf{r_D},t) = 0 \qquad (41)$$

$$[\Phi^S(x_D)]^T\mathbf{q}^S(t) - [\Phi^D(\mathbf{r_D})]^T\mathbf{q}^D(t) = 0 \qquad (42)$$

Then, equation 42 leads to the following matrix $\boldsymbol{A}_D$ and vector $\mathbf{b}_D = \mathbf{0}$:

$$\boldsymbol{A}_D = \begin{bmatrix} [\Phi^S(x_{D_1})]^T & 0 \ldots 0 & -1 & 0 & \ldots & 0 \\ [\Phi^S(x_{D_2})]^T & 0 \ldots 0 & 0 & -1 & \ldots & 0 \\ \vdots & \vdots \vdots \vdots & \vdots & \vdots & \ddots & \vdots \\ [\Phi^S(x_{D_{N_D}})]^T & 0 \ldots 0 & 0 & 0 & \vdots & -1 \end{bmatrix}$$

where $\Phi^S(x_{D_j})$ is the mode shape of the string coupled with the n^{th} damper at the x_{D_j} location.

IV. SIMULATION AND EVALUATION OF THE CLAVICHORD MODEL

The one-string model developed in Section III, using the experimental data of Section II, is discussed in this section. A finite element approach is chosen for simulation. Following a preliminary convergence study, not detailed her, an appropriate the time step is $\Delta t = 2\times10^{-6}$ s using $N_s = 100$ string modes. Assessment of the model is performed in 3 steps: 1/ visualisation of string motion; 2/ visualisation of subsystems vibrations and comparison with experimental data: 3/ comparison on the dynamics of the model, previous models and experimental data on the dynamics of the clavichord.

A. String motion

The string motion of the clavichord is shaped by the specific excitation mechanism of the instrument. Time domain simulation of the system allows for visualisation of the string motion. Simulation of the G#$_3$ string motion is displayed in Figure 4, in response to a 6 N excitation force. The top panel represent the initial 35 ms, i.e. the beginning of the motion. The tangent (represented by circles at x=0.6m, sampled with a period of 0.1 ms) comes in contact with the string and lifts the string to a maximum. When the tangent strikes the string, an angular point is created and propagates to the bridge. At the same time, the string is uplifted by the tangent. After the arrival of the angular point at the bridge, it is reflected back and then reflected again by the tangent. As the mechanical impedance of the bridge and that of the tangent are high compared to the string mechanical impedance, most of the wave energy is reflected. At

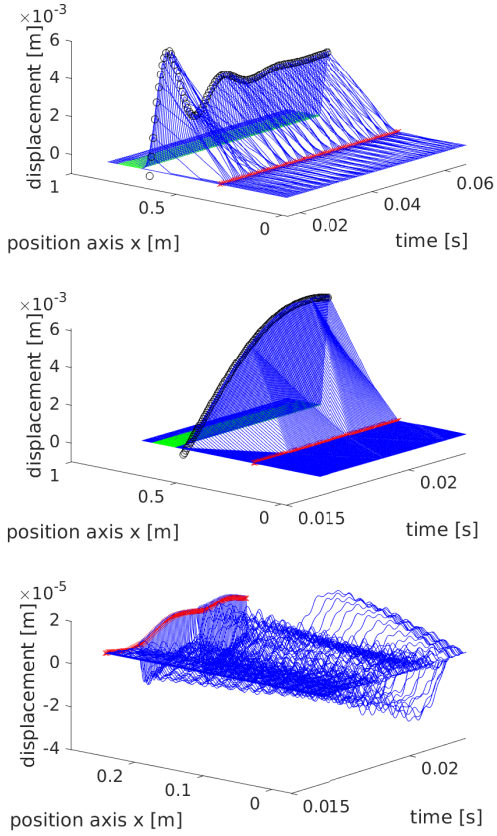

FIG. 4. History of the transverse motion for the G#3 string.x axis: time (s); y axis : string length; z axis: transverse string motion. Top panel: full string between $t = 0.0164$ s and $t = 0.0759$ s . Middle panel: full string between $t = 0.0164$ s and $t = 0.0224$ s. bottom panel: sympathetic part alone, between $t = 0.0164$ s and $t = 0.0224$ s.

vibration amplitude (then the sound amplitude level) depends on the angle of the angular point, and then on the ratio of wave velocity in the string and tangent velocity, as discussed in[2], and then on the steepness of the tangent motion slope. In the middle panel of Figure 4 the string motion history is displayed between 35 and 200 ms (sampled with a period of 1 ms). The low frequency (62.5 Hz) oscillation of the key-tangent subsystem because of the elasticity of the string is observed. Bottom panel of Figure 4 shows vibration by sympathy of the part of string between the bridge and tuning pin, corresponding to the circle in the middle panel, between 35 and 200 ms (sampled with a period of 1 ms). Note that the sympathetic vibration is two order of magnitude lower than the played part of the string, between 10^{-5} - 10^{-6} m, and that the string motion looks rather disorganized compared to more regular motion between the tangent and bridge pin. No direct measurement of the whole string motion are available to the best of our knowledge. Comparison with high-speed videos of the string motion in the vicinity of the tangent[?] show good agreement with

the simulation:the same "zipper" motion of the angular point on the string can be observed in high-speed videos and Figure 4.

B. Bridge motion

The bridge is a key point in sound production, because it moves the soundboard, and then produces the sounds. For assessment of the model, simulated and measured bridge motions are compared. The acceleration at the bridge pin for the string is measured using the same PCB M352C65 accelerometer and the same acquisition system as in section II E. For this measurement, all the other strings are muffled using felt strips. Measured and simulated signals oscillograms and spectrograms are displayed in Figure 5. The results are on the whole in very good agreement. The main difference between the two signals is in the attack transition. The real acceleration exhibit a sharper attack transient. This could be explained by the "drum noise" that is present in a real clavichord but not in the model. The drum noise is the structural noise due to the shock of the tangent on the string, that excites all the body (structure) of the instrument. This is a well known effect, not simulated here, the string being isolated from the structure. Otherwise, the essential features of simulation and measurement are very similar, and the orders of magnitude of these accelerations are the same.

The forces applied to the key and the response at the bridge are analyzed with the help of Figure 6. A step force of 6 N is applied on the key for 1 s. The constraint force at the contact point between the tangent and strings is computed. Note that the tangent force is lower than the force applied to the key, because of the leverage ration on the pivoting key (since $x_f - x_p$ is smaller than $x_p - x_{tg}$). Two conditions are studied in the simulation with and without damper. The middle panel shows the simulated force at the bridge. As expected, the force is lowered during the tone, because the tangent lifts the string, and then release the string pressure on the bridge. When dampers are removed, the string appears less constrained, and the force lowering is higher. String vibration is apparent in the force signal. The top panel shows the vibration displacement. As expected, the string is raised in response to the tangent lift, and raised higher when the dampers are withdrawn. The vibratory magnitude is surprisingly low (a maximum of about 0.015 mm). Displacement measurements were subsequently performed on the G#$_3$ string using a Keyence (LJ-V7060) profilometer. The same order of magnitude were observed: a bridge lift of 0.010-0.020 mm and a maximal vibratory amplitude of about 0.010-0.015 mm, in good agreement with the simulated motions. After the key release, the tangent loses contact with the string. The remaining vibration after the key release correspond to the sympathetic vibration between the bridge and tuning pin, and in the non-damped situation to the vibration of all the length of the string. In this latter situation, the magnitude is larger.

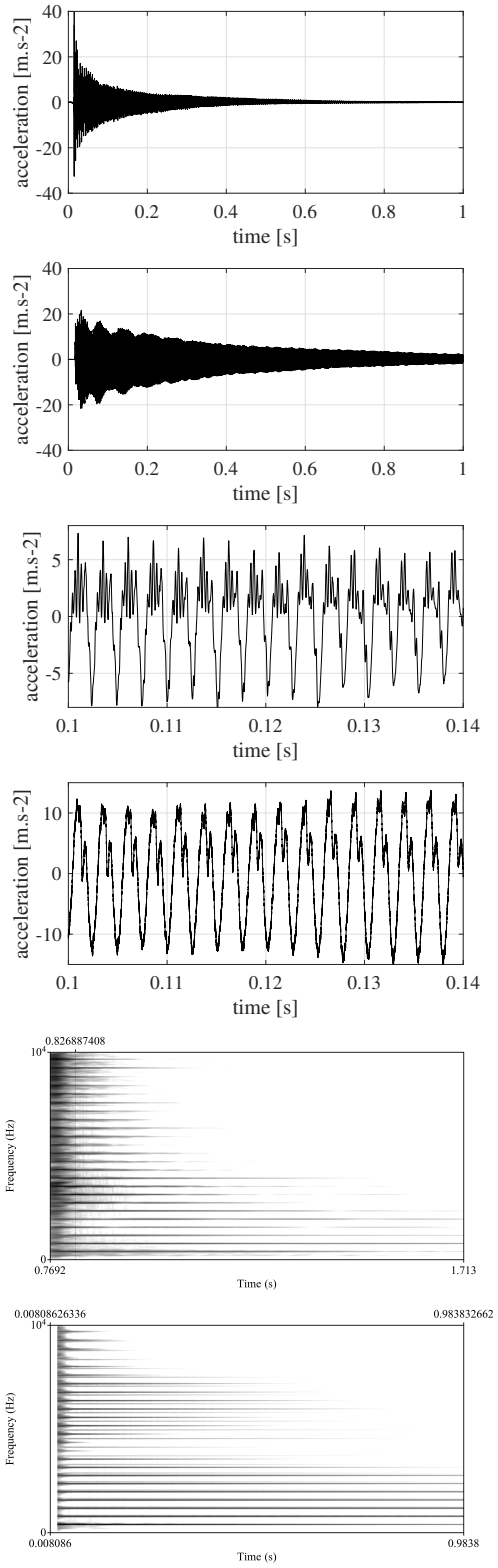

FIG. 5. Comparison of simulated and measured acceleration at the bridge. The first plot of each pair corresponds to measurement and the second corresponds to simulation. Top: oscillogram for 1s; Middle: zoom on a 40 ms section; Bottom: spectrogram

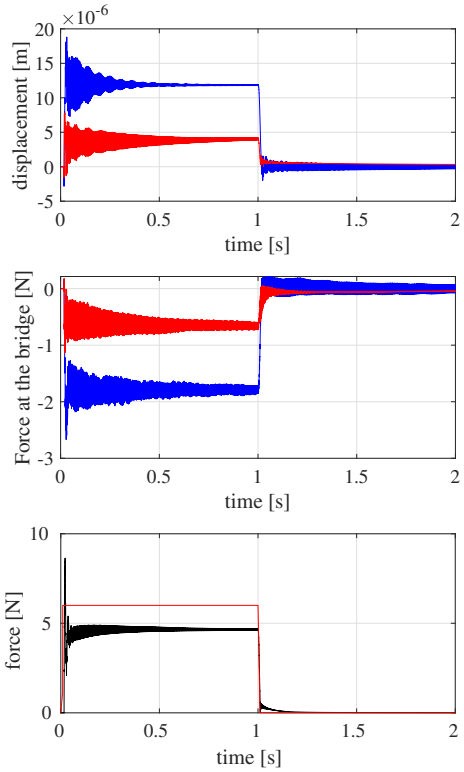

FIG. 6. Bottom: force applied on the key and resulting force on the tangent. Middle: force on the bridge with (red) and without (blue) dampers. Top: bridge displacement with (red) and without (blue) dampers.

C. Tangent-string dynamics

Figure 7 shows the effect of the tangent-string interaction on string tension. The key is activated by the robotic finger. As expected, the key-tangent interaction exhibit some oscillation due essentially to the string elastic reaction to the tangent strike. The 60 Hz oscillation rate obtained is consistent with the 30 Hz oscillation reported[2] in experiments with another clavichord. The corresponding change in the measure[31] fundamental frequency is consistent, showing that the acoustic effect of the string-tangent interaction is well rendered by the model. Dynamic and quasi-static tension simulation give almost identical results, consistent with measurements. This shows the validity of the dynamic approach.

To study the effect of tangent velocity on acceleration at the bridge, the force $\boldsymbol{F}_{ext}$ applied on the key-tangent subsystem is varied. The impact velocity and the average acceleration are computed by the model. Similarly to the sound pressure level (SPL) the acceleration level is computed as the logarithm of acceleration integrated over 250 ms. Figure 8 shows a linear relationship between the logarithm of the impact velocity and the acceleration level in dB. This is in good agreement with experimental results obtained for impact velocity and sound pressure

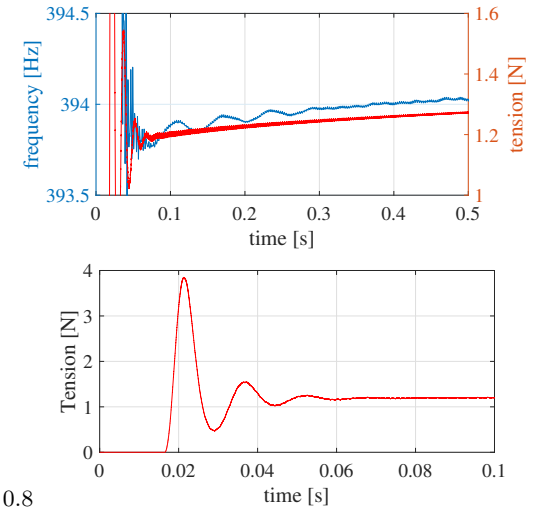

0.8

FIG. 7. Top: Dynamic tension of the string and corresponding fundamental frequency for a 0.5s note. Bottom: Dynamic tension of the string in the firsts 0.1 s.

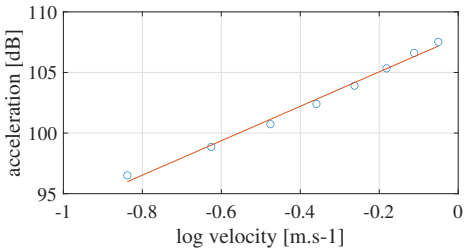

FIG. 8. Force profiles used to obtain the simulated impact velocities and the associated bridge acceleration (a), Time average of the bridge acceleration (ref 1 dB : 1 m.s^{-2}) at the G#3 string coupling point with respect to the logarithm of the tangent impact velocity (b).

level and with predictions by a linear model of string-tangent dynamics[2]: playing louder is playing faster.

The influence of the impact velocity on the timbre of the bridge acceleration is studied. Spectral slopes of the acceleration spectrum for different impact velocities are presented in Figure 9. Two effects are noticeable. First, increasing the excitation force leads to increasing the static displacement of the string, hence the fundamental frequency. This accounts for the frequency shift of the partials in figure 9. Second, the spectral slopes for the different spectra remain approximately the same, an average spectral slope can represent spectral slope for all the spectra. Then, the timbre of the simulated bridge acceleration, so to speak, does not change much with respect to the tangent impact velocity, a result reported in a previous experimental study[2].

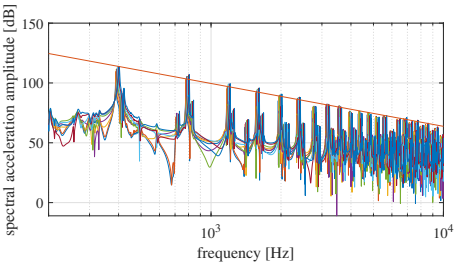

FIG. 9. Spectral amplitude of the different bridge accelerations at the G#3 string coupling point with respect to time (ref 1 dB : 1 m.s^{-2}), for different impact velocity of the key-tangent subsystem (0.4433 m.s^{-1}, 0.535 m.s^{-1}, 0.622 m.s^{-1}, 0.698 m.s^{-1}, 0.769 m.s^{-1}, 0.834 m.s^{-1}, 0.894 m.s^{-1} and 0.951 m.s^{-1}), with the average spectral slope.

V. CONCLUSION AND PERSPECTIVES

In summary, the essential features of the non-linear dynamics of the string-tangent interaction are well captured by the U-K model for the clavichord. A very simplified instrument is considered here. At least four important vibroacoustic characteristics of this instrument are missing and must be worked out : 1/ coupling between the two unison strings of a choir; 2/ effect of free strings between the bridge and tuning pins, that bring sympathetic vibration and resonance; 3/ effect of the lid, sound radiation aspects; 4/ other source of sound by vibration of the structure. Part of this research program is currently in progress, aiming at a fully parametric physical clavichord model that would be desirable for historical instrument simulation and analysis, performance studies and new music instrument design.

[1] Bernard Brauchli. *The clavichord*. Cambridge University Press, 1998.

[2] Christophe d'Alessandro. On the dynamics of the clavichord: From tangent motion to sound a. *The Journal of the Acoustical Society of America*, 128(4):2173–2181, 2010.

[3] Ferdinand Trendelenburg, E. Franz, and Erich Thienhaus. *Zur Klangwirkung von Klavichord, Cembalo und Flügel*. 1940.

[4] R.A. Hands. A scientific approach to the clavichord. *The Galpin Society Journal*, pages 89–98, 1967.

[5] Peter Bavington. *Keylever, tangent and string—a preliminary analysis of clavichord touch and action*. na, 1998.

[6] Suszanne Thwaites and Neville H. Fletcher. Some notes on the clavichord. *The Journal of the Acoustical Society of America*, 69(5):1476–1483, 1981.

[7] Gabriel Weinreich. Coupled piano strings. *The Journal of the Acoustical Society of America*, 62(6):1474–1484, 1977.

[8] Donald E Hall. String excitation: piano, harpsichord and clavichord. In *Proceedings of the 1993 Stockholm Music Acoustics Conference*, pages 309–314, 1993.

[9] Christophe d'Alessandro, Charles Besnainou, and Luc Ginieis. Tonal portrait of the clavichord. In *De Calvicordio VIII*, pages 201–213, 2008.

[10] Christophe d'Alessandro. Le paradoxe du clavicorde. In *Congrès Français d'Acoustique (CFA 2016)*, pages 2263–2269. Société Française d'Acoustique, 2016.

[11] Vesa Välimäki and Cumhur Erkut. Commuted waveguide synthesis of the clavichord. *Computer Music Journal*, 27(1):71–82, 2003.

[12] Juliette Chabassier. *Modélisation et simulation numérique d'un piano par modèles physiques*. PhD thesis, 2012.

[13] Antoine Chaigne. Modélisation du piano et couplage cordes-chevalet. *Proceedings of 12ème Congrès Français d'Acoustique*, pages 1085–1091, 2014.

[14] Jose Antunes and Vincent Debut. Dynamical computation of constrained flexible systems using a modal udwadia-kalaba formulation: Application to musical instruments. *The Journal of the Acoustical Society of America*, 141(2):764–778, 2017.

[15] Christophe d'Alessandro and Brian F.G. Katz. Tonal quality of the clavichord: The effect of sympathetic strings. In *Proceedings of the International Symposium on Musical Acoustics ISMA '04*, pages 21–24, 2004.

[16] Jean-Théo Jiolat, Christophe d'Alessandro, and Jean-Loic Le Carrou. L'effet acoustique des cordes mortes du clavicorde. In *Congrès Français d'Acoustique, CFA 2018*, pages 233–239, 2018.

[17] Jean-Loïc Le Carrou, Delphine Chadefaux, Léonard Seydoux, and Benoit Fabre. A low-cost high-precision measurement method of string motion. *Journal of Sound and Vibration*, 333(17):3881–3888, 2014.

[18] Richard Roy and Thomas Kailath. Esprit-estimation of signal parameters via rotational invariance techniques. *IEEE Transactions on acoustics, speech, and signal processing*, 37(7):984–995, 1989.

[19] Jean-Loïc Le Carrou, François Gautier, and Roland Badeau. Sympathetic string modes in the concert harp. *Acta Acustica united with Acustica*, 95(4):744–752, 2009.

[20] Arthur Paté, Jean-Loïc Le Carrou, and Benoît Fabre. Predicting the decay time of solid body electric guitar tones. *The Journal of the Acoustical Society of America*, 135(5):3045–3055, 2014.

[21] Arthur Paté. *Lutherie de la guitare électrique solid body: aspects mécaniques et perceptifs*. PhD thesis, Paris 6, 2014.

[22] Ahmet Arda Ozdemir and Suat Gumussoy. Transfer function estimation in system identification toolbox via vector fitting. *IFAC-PapersOnLine*, 50(1):6232–6237, 2017.

[23] Jose Antunes, Vincent Debut, Laurent Borsoi, Xavier Delaune, and Philippe Piteau. A modal udwadia-kalaba formulation for vibro-impact modelling of continuous flexible systems with intermittent contacts. *Procedia engineering*, 199:322–329, 2017.

[24] V. Debut, J. Antunes, M. Marques, and M. Carvalho. Physics-based modeling techniques of a twelve-string portuguese guitar: A non-linear time-domain computational approach for the multiple-strings/bridge/soundboard coupled dynamics. *Applied Acoustics*, 108:3–18, 2016.

[25] Vincent Debut and Jose Antunes. Physical synthesis of six-string guitar plucks using the udwadia-kalaba modal formulation. *The Journal of the Acoustical Society of America*, 148(2):575–587, 2020.

[26] Ara Arabyan and Fei Wu. An improved formulation for constrained mechanical systems. *Multibody System Dynamics*, 2(1):49–69, 1998.

[27] Gustav Kirchhoff. *Vorlesungen Uber Mechanik*. BG Teubner, 1883.

[28] GF Carrier. On the non-linear vibration problem of the elastic string. *Quarterly of Applied Mathematics*, 3(2):157–165, 1945.

[29] Christian Cuesta and Claude Valette. Mécanique de la corde vibrante. *Paris: Hermes*, 520, 1993.

[30] S. Yoon, R.M. Howe, and D.T. Greenwood. Geometric elimination of constraint violations in numerical simulation of lagrangian equations. 1994.

[31] Alain De Cheveigné and Hideki Kawahara. Yin, a fundamental frequency estimator for speech and music. *The Journal of the Acoustical Society of America*, 111(4):1917–1930, 2002.

Proceeding in the *Congrès Français d'acoustique* (CFA)

L’effet acoustique des cordes mortes du clavicorde

J.-T. Jiolat[a], C. d’Alessandro[a] et J.-L. Le Carrou[b]
[a]Sorbonne Université, Centre National de la Recherche Scientifique, Institut Jean Le Rond d’Alembert, F-75005 Paris, France
[b]Sorbonne Université, CNRS, Institut Jean Le Rond d’Alembert, Equipe LAM, F-75005 Paris, France
jean-theo.jiolat@heywood.dalembert.upmc.fr

Le clavicorde est un instrument à clavier particulièrement expressif, mais de faible niveau sonore. Lorsqu'une des touches du clavier est enfoncée, un élément de métal (appelé tangente) percute une paire de cordes et reste en contact avec elle, la tangente jouant le rôle à la fois d'excitateur et de sillet. La portion des cordes mortes, entre le chevalet et les chevilles d'accord est laissée libre dans le clavicorde. Ces cordes mortes sont assez longues, et elle entre en vibration par sympathie, à cause du mouvement du chevalet, venant ajouter de la réverbération et un renforcement du son. Le but de ce travail est d'étudier et de quantifier l'effet des cordes mortes. Les mesures sont conduites sous 2 conditions : avec cordes mortes libres et avec cordes mortes étouffées. Les résultats montrent la manifestation de deux phénomènes distincts : l'un est l'effet de réverbération, que l'on peut modéliser par un système vibratoire linéaire ; l'autre est l'effet de sympathie, caractérisé par le couplage entre les partiels des cordes jouées et mortes.

1 Introduction

1.1 Présentation du clavicorde

Le clavicorde est un instrument à clavier particulièrement expressif, mais dont le niveau sonore est assez faible (d'où son surnom "d'épinette sourde" au XVIIème siècle chez Marin Mersenne) [1]. La mécanique est simple : les touches à balancier sont équipées de lames de laiton, les tangentes, qui font office de sillet et excitent les cordes à leurs extrémités. Lorsque l'on relâche la touche, une bande de tissu située à droite de la tangente étouffe la vibration de la corde. Le niveau de pression sonore du clavicorde est faible, proportionnel au logarithme de la vitesse d'impact de la tangente, directement liée à celle du doigt (contrairement au piano qui multiplie la vitesse grâce à la mécanique) [6]. Le niveau mesuré 30 cm au dessus du centre de la table d'harmonie est au maximum de 60 dB SPL, pour l'instrument que nous étudions ici, ce qui est typique des valeurs mesurées pour d'autres clavicordes. On trouvera des mesures de niveau sonore et de durée pour toutes les notes de 4 clavicordes jouées avec diverses nuances dans [5]. Une façon d'augmenter la durée ou le niveau du son dans le clavicorde est d'utiliser les parties mortes des cordes, entre le chevalet et les chevilles d'accord (voir Figure 1) comme des cordes sympathiques, c'est à dire des cordes qui ne sont pas directement mises en vibration par l'excitation, mais qui sont entraînées par la vibration des cordes jouées [8].

1.2 Fonctionnement acoustique

Le clavicorde est muni d'un unique chevalet. Toutes les cordes sont toutes couplées par ce chevalet, qui les divise en deux segments : la partie "corde jouée", excitée par la tangente, entre la tangente (sillet) et le chevalet, et la partie "corde morte", entre le chevalet et les chevilles (voir figure 1). Lorsque les cordes jouées sont excitées, il y a un transfert d'énergie vibratoire vers les cordes mortes par le biais du couplage avec le chevalet. Ceci provoque la vibration des cordes mortes, de la tables d'harmonie, et de la masse d'air sous la table d'harmonie (qui, jointe à la cavité forme un résonateur de Helmoltz). L'énergie vibratoire est transférée à la table d'harmonie qui rayonne le son dans la salle où se trouve l'instrument. (voir figure 2).

Les cordes mortes sont laissées libres dans le clavicorde, contrairement par exemple au piano (le piano carré est très proche du clavicorde du point de vue de la facture, et les cordes mortes y sont étouffées [4]). Des mesures acoustiques ont montré que ces cordes mortes apportent un halo sonore à l'instrument, un effet que l'on peut comparer à la réverbération d'une salle : ce premier effet de vibration sympathique, que nous nommons ici "réverbération" ne privilégie pas de fréquence précise, mais une zone fréquentielle large (dans le gamme de 450 Hz à 1000 Hz environ pour l'instrument étudié dans [7]). Par ailleurs, lorsque les rapports de fréquence sont favorables, une ou plusieurs cordes mortes peuvent être susceptibles de renforcer la vibration d'une corde jouée, par couplage mécanique à travers le chevalet : nous réservons désormais le mot de "sympathie" pour ce couplage mécanique, effet qui a été observé et modélisé dans d'autres instruments.

Dans le cas de la harpe de concert, il a été montré que les harmoniques des cordes dont la fondamentale est en dessous de celle de la corde excitée viennent contribuer à la vibration par sympathie [9]. Dans certains modèles de pianos, au premier rang desquels les pianos à queue Steinway & Sons, se trouvent des cordes mortes dénommées cordes "duplex", localisées à l'avant et à l'arrière des parties jouées, pour l'ensemble de son ambitus. Ces cordes contribuent au timbre du son rayonné [10].

1.3 Positionnement du problème

Le présent travail est une première approche pour mettre en évidence et caractériser ces deux effets dans le cas du clavicorde, en mesurant les phénomènes vibratoires dues à la mise en vibration indirecte des cordes mortes. L'instrument étudié est une copie inspirée d'un clavicorde historique (Christian Gottlob Hubert, Ansbach, 1784, conservé dans la Russel Collection, Edimbourg) construit par un des auteurs en 2008 dans l'atelier Marc Ducornet. L'instrument présente 51 touches de Do1 à Ré5, les notes sont liées par 2 à partir de Mi2, et il possède donc 37 chœurs de 2 cordes, soit 74 cordes pour les 51 notes. Il est accordé à La3=415 Hz. Jouer une note met donc en vibration deux cordes jouées et 74 cordes mortes. L'approche expérimentale porte sur deux volets. Dans un premier temps, l'effet de réverbération est étudié, en négligeant le couplage au chevalet. En faisant l'hypothèse que les cordes mortes fonctionnent comme un système passif, ou système linéaire invariant dans le temps, c'est à dire qu'il n'y a pas de tranfert d'énergie des cordes mortes vers les cordes jouée (donc pas de sympathie, mais seulement réverbération), une première expérience caractérise la réponse impulsionnelle de la table d'harmonie dans différentes configurations. Dans un second temps, les effets de couplage entre cordes jouées et cordes mortes sont étudiés en situation de jeu. Pour cela la réponse des cordes jouées avec les cordes mortes libres est comparée avec la réponse des cordes jouée avec les cordes mortes étouffées convoluée par la réponse impulsionnelle des cordes mortes libres. Dans l'hypothèse d'un couplage par sympathie, la première réponse devrait durer davantage que la seconde.

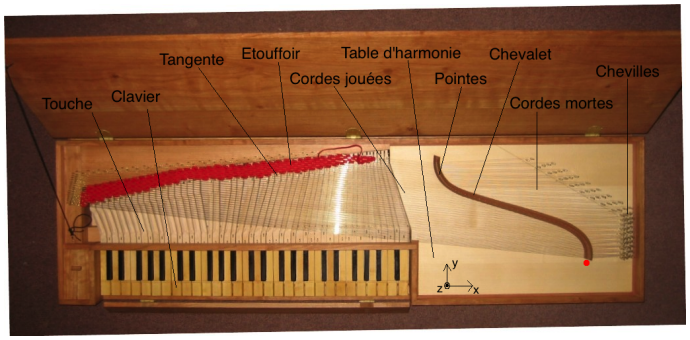

FIGURE 1 – Vue du dessus du clavicorde Hubert avec des légendes, le point rouge correspondant à la position où se trouve l'accéléromètre.

2 Réponse impulsionnelle

Des mesures acoustiques de réponses impulsionnelles ont été décrites dans [7]. Il s'agissait du son rayonné, en réponse à des impulsions par un marteau sur la table, en combinant toutes les conditions de cordes mortes étouffées, cordes jouées étouffées, cavité étouffée. Les résultats (sous l'hypothèse d'une réponse linéaire, sans couplages mécaniques au chevalet) montrent un effet de réverbération dans le son. De plus l'ensemble des cordes jouées contribue en basse fréquence, ce qui est connu des facteurs de clavicorde comme "effet tambour". Les cordes jouées sont en effet toutes couplées par la bande d'étouffoir, et un choc sur la structure les met en vibration, avec un son grave de "tambour". La cavité joue un rôle, avec une résonance de Helmoltz vers 50-200 Hz environ.

2.1 Protocole expérimental

Nous souhaitons mesurer la réponse impulsionnelle de la table d'harmonie en un point de la structure. Pour mettre en place cette mesure vibratoire, nous plaçons un accéléromètre (PCB M352C65) en bas du chevalet là où auront lieu les impacts effectués par le marteau d'impact (PCB 086C01) (voir figure 1). Le marteau d'impact envoie un signal E en entrée et on mesure le signal d'accélération a en sortie 3. Les mesures de réponse en fréquence seront donc co-localisées. Nous sommes à même d'étouffer les cordes mortes grâce à la disposition de feutres faisant office d'étouffoir. Par conséquent, nous pouvons mesurer la réponse impulsionnelle de notre système lorsque les cordes mortes sont libres et lorsque ces cordes sont étouffées. Nous ne nous intéresserons ici qu'à l'étouffement des cordes mortes, et pas à l'effet tambour.

2.2 Méthode d'analyse

Considérons le système vibratoire "cordes, chevalet, table". Nous faisons l'hypothèse que les sous-structures de notre système vibratoire sont découplées. Cela implique que nous pouvons décomposer notre système vibratoire en différents sous-systèmes, comme on peut le voir sur la figure 3.

Notre système d'étude est alors linéaire. On peut donc caractériser une réponse impulsionnelle pour chaque sous-structure de la figure 3. L'ensemble de ces différentes réponses impulsionnelles caractérise la réponse impulsionnelle du système vibratoire globale. De plus, on considère que notre système vibratoire ne se déplace selon une seule direction, ici l'axe z (voir figure 1). Ce qui implique que notre système ne possède qu'un seul degré de liberté. Sous couvert de ces hypothèses, nous pouvons calculer nos fonctions de réponse en fréquence par simple division fréquentielle, et ainsi obtenir la réponse impulsionnelle correspondante par transformée de Fourier.

2.3 Analyse de la Réponse impulsionnelle des cordes mortes

Ayant mesuré les réponses impulsionnelles de notre système vibratoire selon que les cordes mortes soient libres ou étouffées, on effectue une déconvolution de nos signaux dans le domaine de Fourier. Ainsi, nous enlevons la contribution de tous les éléments vibrants dans le signal vibratoire si ce n'est celle des cordes mortes. Nous montrons ce que nous obtenons comme signal résultant sur la figure 4. On remarque que la bande de fréquence d'influence des cordes mortes va de 350 Hz à 4500 Hz. On montre sur la figure 5 la répartition des fréquences des cordes mortes et des cordes jouées selon le nom de la note de chaque corde. On remarque que les fréquences des cordes mortes vont de 350 Hz à 1200 Hz environ. La borne inférieure de 350 Hz pour la zone fréquentielle des cordes mortes est cohérente avec celle trouvé par le biais de la figure 4. Le reste de l'énergie spectrale au-dessus de 1200 Hz est dû aux harmoniques de toutes les cordes mortes. L'énergie spectrale au dessous de 350 Hz provient probablement de la vibration des cordes graves jouées, qui elles n'ont pas été totalement soustraites (cet effet, le "tambour" a été décrit dans [7], il est d'une amplitude notable dans le grave du spectre).

3 Étude en situation de jeu

3.1 Protocole expérimental

Nous voulons aussi analyser le comportement de la partie morte des cordes de notre clavicorde d'étude lors de la production de sons musicaux. Nous gardons la même disposition expérimentale que précédemment. Ici nous utilisons un doigt robotique (voir Figure 6) pour enfoncer les touches correspondant aux cordes Si2 et Sol4. Ce doigt peut effectuer une trajectoire programmée et la répéter de façon identique [3]. Cette trajectoire est programmée par la position et la vitesse du doigt robotisé selon le plan (y,z) (voir figure 1). Les mesures obtenues sont les réponses vibratoires de la table d'harmonie dues aux excitations de ces deux cordes en répétant la même trajectoire d'enfoncement de la touche. Une excitation particulière est considérée, celle où le doigt relâche directement la touche après l'avoir enfoncé. La trajectoire en question est effectué de telle façon à ce que la touche soit enfoncée de 7 mm environ et que la vitesse d'enfoncement soit de l'ordre de 0,6 $m.s^{-1}$. Cette valeur de vitesse d'enfoncement est équivalente à celle qui est utilisée dans [6], où c'est le doigt du musicien qui enfonce la touche. On considère alors que la trajectoire du doigt robotisé utilisée ici est équivalente que celle d'un musicien.

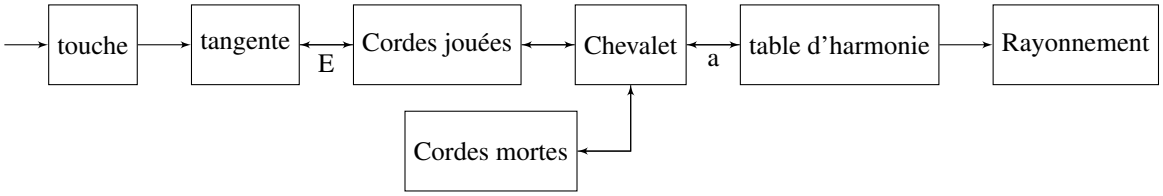

FIGURE 2 – Schéma bloc du fonctionnement acoustique du clavicorde, *E* représentant l'entrée du système vibratoire et *a* correspondant au signal vibratoire mesuré par l'accéléromètre.

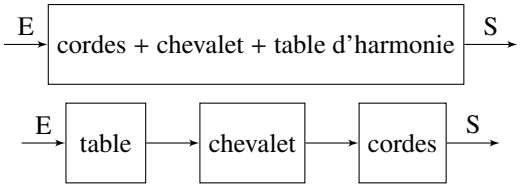

FIGURE 3 – Schéma bloc du système vibratoire linéaire, où E est le signal d'entrée et S est le signal de sortie.

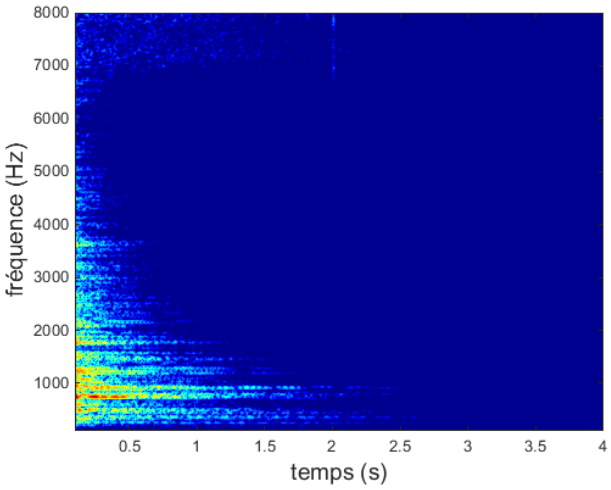

FIGURE 4 – Réponse impulsionnelle des cordes mortes du clavicordes.

3.2 Analyse temporelle

Nous effectuons une comparaison entre les formes d'onde des signaux mesurés dans des conditions différentes. Sur la figure 7 (haut), on montre les signaux vibratoires mesurés lors de l'excitation de la corde de Si2 lorsque les cordes mortes sont libres (bleu) et lorsqu'elles sont étouffées (rouge). Qualitativement, on peut remarquer que le signal correspondant à la condition "libre" dure plus longtemps que le deuxième signal. Cela met en exergue le fait que la contribution vibratoire des cordes mortes permet l'allongement du signal vibratoire. Aussi, nous effectuons sur la figure 7 (bas) la même comparaison lorsque l'on excite la corde de Sol4. On peut en tirer la même conclusion. En revanche, quantitativement, le signal correspondant à la situation où les cordes mortes sont libres dure encore plus longtemps que le deuxième signal. Cette différence de longueur en temps est plus accrue que dans le cas de l'excitation de la corde de Si2. Ceci peut s'expliquer par un effet de couplage. La corde de Sol4 est couplée avec certaines cordes mortes par le biais de relation fréquentielle entre leur première harmonique, ce qui n'est pas le cas pour la corde de Si2 (voir figure 5). Ceci a pour conséquence que

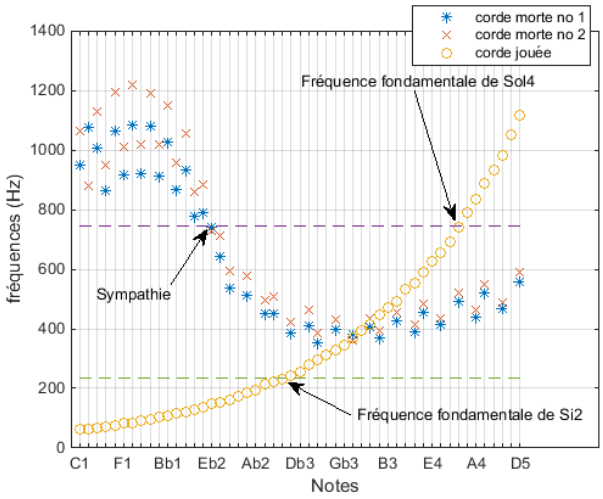

FIGURE 5 – Fréquences fondamentales des cordes mortes et des cordes jouées. Les fondamentales des cordes mortes se situent entre 350Hz et 1200 Hz environ. Deux zones fréquencielles apparaissent : un zone ou les cordes jouées sont en dessous des cordes mortes, et une zone ou elles sont dans la même gamme de fréquences fondamentales.

FIGURE 6 – Doigt robotisé pour le jeu automatique et reproductible du clavier.

le signal de Sol4 possède des composantes fréquentielles plus élevées en énergie que celles du signal de Si2.

La figure 8 représente les signaux du Si2 et du Sol4 dans les conditions cordes mortes libres (bleu) et cordes mortes étouffées convolués par la réponse impulsionnelle des cordes mortes libres seules (rouge). Pour la note Si2 les deux signaux se superposent bien. Cela indique que les cordes mortes joue un rôle de système linéaire, puisque la convolution par leur réponse impulsionnelle du signal étouffé est proche du signal libre. Au contraire, pour la note Sol4, les deux signaux se superposent mal.

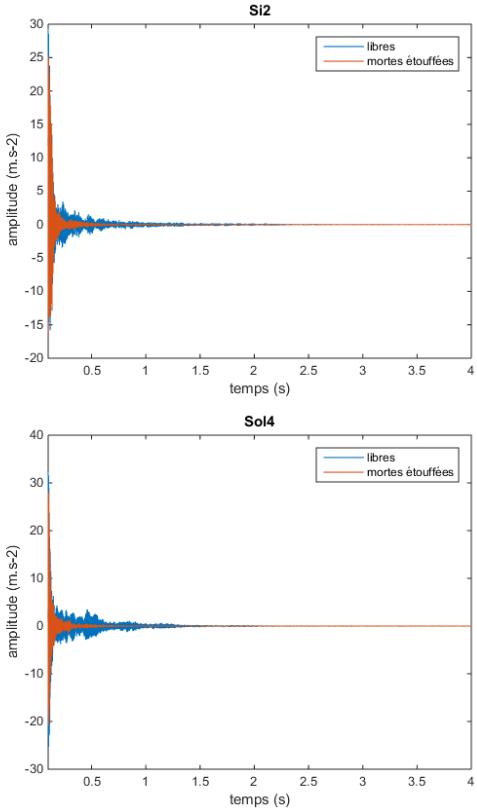

FIGURE 7 – Signal d'accéleration sur la table, note jouée Si2 (haut) et Sol4 (bas), mortes étouffées et cordes mortes libres.

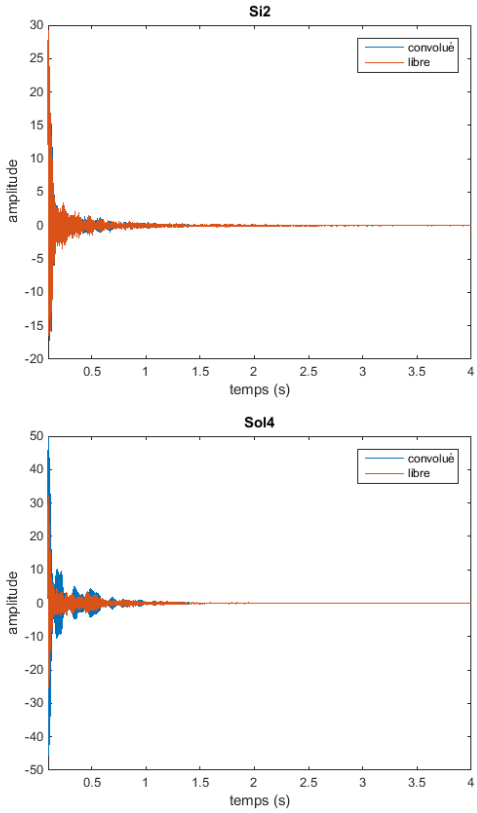

FIGURE 8 – Signal d'accéleration sur la table, note jouée Si2 (haut) et Sol4 (bas) avec les cordes mortes mortes étouffées, et cordes mortes mortes étouffées convoluées par la réponse impultionnelle de la table.

Donc une simple convolution ne suffit pas pour expliquer l'effet des cordes mortes. Un phénomène non-linéaire, comme un couplage mécanique au chevalet entre les cordes jouées et les cordes mortes, prend certainement place dans l'interaction des cordes jouées et des cordes mortes. Une analyse temps-fréquence permet de visualiser cet effet.

3.3 Analyse spectro-temporelle

Sur la figure 9, on montre la comparaison entre le signal de la réponse du système vibratoire avec les cordes mortes étant libres et avec l'excitation de la corde de Sol4 (spectrogramme A), et le signal de celle où la corde de Si2 est excitée (spectrogramme B). Les harmoniques du premier signal possèdent plus d'énergie spectrale que ceux du deuxième. On remarque que les partiels de fréquences 1480 Hz, 2188 Hz, 2967 Hz, 3656 Hz, et 4468 Hz sont assez prépondérants dans le signal de la note Sol4. En revanche, peu de partiels se distinguent nettement sur le signal correspondant à la note Si2, si ce n'est légèrement les partiels 2553 Hz et 4688 Hz.

Toujours sur la figure 9, on fait une comparaison semblable à la précédente, tout en ayant étouffé les cordes mortes (spectrogramme C et D). Dans les deux cas, on remarque que toutes les hautes fréquences sont fortement atténuées. Les partiels susmentionnés des deux signaux ne sont plus présents. Seuls les partiels en deçà de 350 Hz restent inchangés par rapport à la situation précédente. Par comparaison entre les spectrogrammes A et C, on peut constater de nouveau que l'effet des cordes mortes se trouve principalement dans la bande de fréquence allant de 350 Hz à 4500 Hz.

3.4 Mise en évidence de la sympathie

Pour évaluer les contributions de la réverbération et de la sympathie, nous utilisons les signaux où l'on a convolué la réponse impulsionnelle des cordes mortes avec un signal vibratoire de la réponse de la table d'harmonie où les cordes mortes sont étouffées. Nous le faisons dans le cas où l'on excite la corde de Sol4 et celle de Si2. Les signaux obtenus sont affichés sur les spectrogrammes E et F de la figure 9. Dans le cas du spectrogramme E, on remarque la résurgence des partiels de Sol4 comme on l'avait noté sur le spectrogramme A. Par contre, ces partiels durent bien moins longtemps que dans le cas de notre mesure vibratoire où les cordes mortes sont libres. Dans le cas du spectrogramme F, le signal convolué est assez proche du spectrogramme B, tout en notant l'absence de la légère prééminence des partiels de hauteur 2553 Hz et 4688 Hz dans le signal convolué.

En ayant utilisé un système de filtre linéaire invariant dans le temps, on a montré que la convolution de la réponse impulsionnelle des cordes mortes du système avec le signal de la corde de Si2 donnait une réponse vibratoire cohérente. En revanche, cette modélisation ne semble pas satisfaisante dans le cas de la convolution avec le signal de la corde de Sol4. Or, cette modélisation implique qu'entre le chevalet et les cordes mortes, la transmission d'énergie vibratoire est unidirectionnelle seulement. Il n'y a pas de couplage entre la corde excitée et les cordes mortes, ne permettant pas une transmission vibratoire réciproque.

Par conséquent, dans le cas du signal de la corde de Si2, on a un transfert d'énergie vibratoire majoritairement à perte, où toute l'énergie est transférée à toutes les cordes

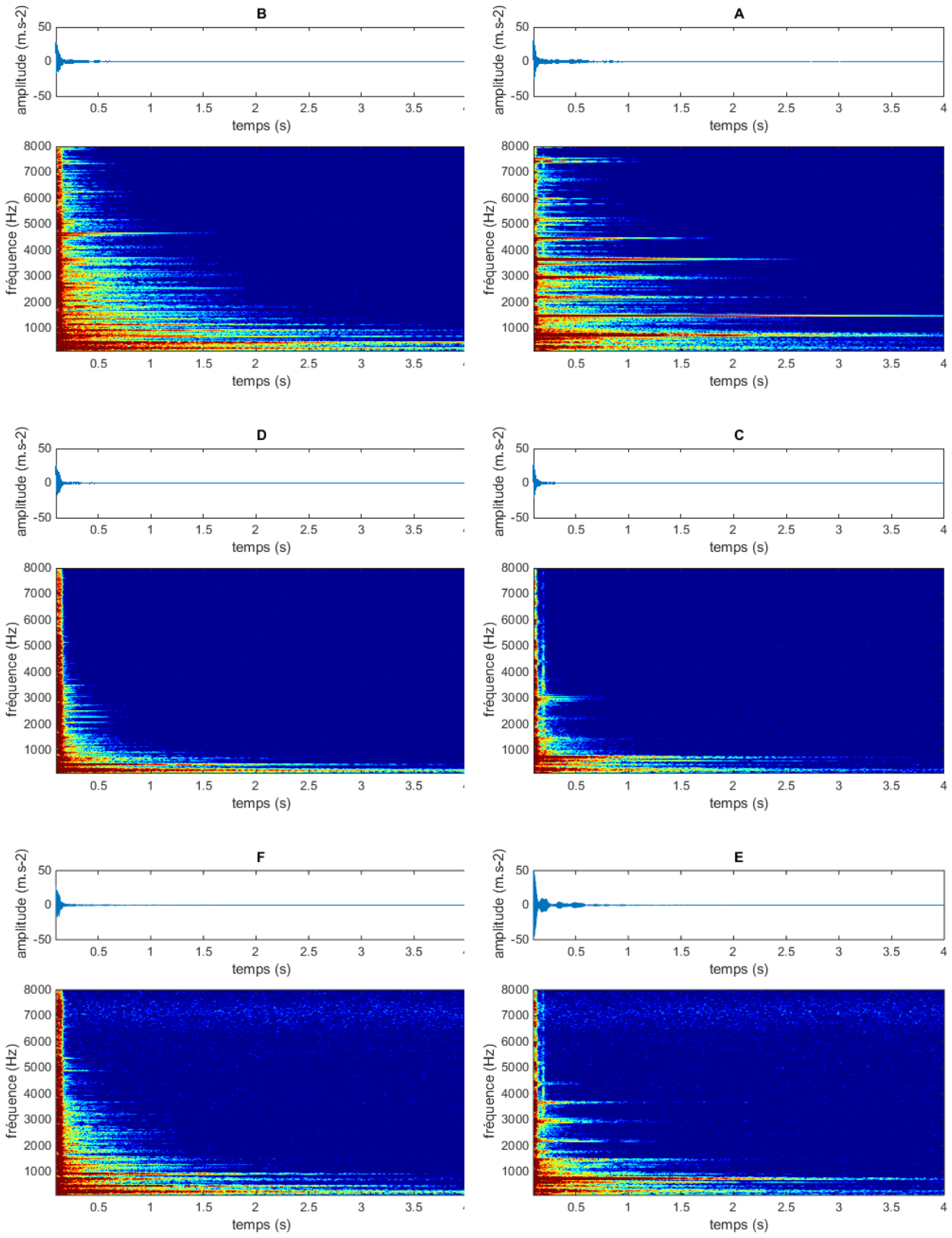

FIGURE 9 – Comparaison entre les spectrogrammes du signal de la réponse vibratoire de la table d'harmonie lorsqu'on excite les notes si2 et Sol4 : avec les cordes mortes libres (spectrogramme A et B) ; avec les cordes mortes étouffées (spectrogramme C et D) ; en ayant convolué avec la réponse impulsionnelle des cordes mortes (spectrogramme E et F).

mortes sans effet de couplage. Cette distribution directe à toutes les cordes mortes est responsable du halo sonore, résultant de l'ensemble des contributions vibratoires de toutes ces cordes. La création de ce halo sonore est ce que l'on appelle l'effet de réverbération. Cet effet se retrouve aussi dans le cas de l'excitation de la corde de Sol4. En revanche, Il y a en plus un effet de couplage entre certaines cordes mortes et la corde de Sol4, où certains partiels de cette corde échangent de l'énergie avec d'autres partiels de même fréquence des cordes mortes concernées. Ceci permet à ces partiels d'obtenir plus d'énergie. Ce transfert d'énergie réciproque par effet de couplage se réfère à l'effet de sympathie.

4 Conclusion

Dans cette étude, nous avons mené une approche expérimentale afin d'étudier l'effet de sympathie du clavicorde, en particulier en prenant comme instrument d'étude une réplique d'un clavicorde Hubert. Deux expériences distinctes ont été effectuées : une qui consistait à mesurer la réponse impulsionnelle de la table d'harmonie de notre instrument dans deux configurations différentes, c'est-à-dire avec cordes mortes libres et puis avec ces cordes étouffées ; la deuxième consistait à mesurer la réponse de la table d'harmonie en enfonçant les touches Sol4 et Si2 du clavicorde par le biais d'un doigt robotique reproduisant la même trajectoire. La première expérience nous a permis de caractériser la réponse impulsionnelle de notre système vibratoire en utilisant un système de filtre linéaire invariant dans le temps. Lors de la deuxième, nous avons pu étudier les différentes réponses de notre système d'étude selon la fréquence fondamentale de la corde excitée et selon l'étouffement ou non des cordes mortes. Dans le cas de l'excitation de la corde de Si2, le système utilisé permet de donner une réponse semblable au signal mesuré. Par contre, ce système présente ses limites dans le cas de l'excitation de la corde de Sol4. Ceci nous permet de mettre en évidence l'existence d'un effet de couplage potentiel qui renvoie à l'effet de sympathie.

Dans le cas du clavicorde, les cordes mortes permettent d'allonger le signal et d'ajouter un halo sonore grâce à l'effet de réverbération, similaire à celui que l'on trouve en acoustique des salles [7]. Nos mesures confirment ces résultats, et les précisent : par déconvolution, la réponse impulsionnelle du filtre linéaire associé aux cordes mortes à été mesurée. On peut ainsi caractériser et comparer de façon simple cet aspect de la sonorité d'un instrument.

En plus de la réverbération un effet de sympathie a été mis en evidence. L'effet de sympathie se caractérise ici par la mise en vibration indirecte d'une corde par l'accord ou le couplage entre certains partiels de cette dernière et avec ceux de la corde excitée. La harpe de concert notamment présente ce phénomène de sympathie, et des travaux ce sont attachées à caractériser expérimentalement et théoriquement la sympathie sur cet instrument [2, 9]. Au delà de la mise en évidence du phénomène, nos travaux futurs porterons sur l'analyse fréquentielle des modes qui contribuent à la sympathie et sur la modélisation mécanique du couplage au chevalet.

Références

[1] Bernard Brauchli. *The clavichord*. Cambridge University Press, 1998.

[2] Jean-Loïc Le Carrou, Francois Gautier, Nicolas Dauchez, and Joël Gilbert. Modelling of sympathetic string vibrations. *Acta Acustica united with Acustica*, 91(2) :277–288, 2005.

[3] Delphine Chadefaux, Jean-Loïc Le Carrou, Marie-Aude Vitrani, Sylvère Billout, and Laurent Quartier. Harp plucking robotic finger. In *Intelligent Robots and Systems (IROS), 2012 IEEE/RSJ International Conference on*, pages 4886–4891. IEEE, 2012.

[4] Christophe D'Alessandro. The acoustics of tangent-string interaction in the clavichord, with a comparison to hammer-string interaction in the fortepiano. In *De Clavicordio IX*, pages 83–90, 2011.

[5] Christophe D'Alessandro, Charles Besnainou, and Luc Ginieis. Tonal portrait of the clavichord. In *De Calvicordio VIII*, pages 201–213, 2008.

[6] Christophe d'Alessandro. On the dynamics of the clavichord : From tangent motion to sound a. *The Journal of the Acoustical Society of America*, 128(4) :2173–2181, 2010.

[7] Christophe d'Alessandro and Brian FG Katz. Tonal quality of the clavichord : The effect of sympathetic strings. In *Proceedings of the International Symposium on Musical Acoustics ISMA '04, Nara, Japan*, pages 21–24, 2004.

[8] Charles Besnainou et Michèle Castellengo. De le résonance, une étude acoustique du phénomène sympathique. In Christophe Coin, editor, *Amour et sympathie.* Tenu á Limoge les 28 et 29 novembre 1992 (p. 53-61). L'ensemble baroque de Limoge.

[9] Jean-Loïc Le Carrou, François Gautier, and Roland Badeau. Sympathetic string modes in the concert harp. *Acta Acustica united with Acustica*, 95(4) :744–752, 2009.

[10] Fredrik Öberg and Anders Askenfelt. Acoustical and perceptual influence of duplex stringing in grand pianos. *The Journal of the Acoustical Society of America*, 131(1) :856–871, 2012.

Proceeding in the *International Modal Analysis Conference* (IMAC)

Modelling of sympathetic string vibrations in the clavichord using a modal Udwadia-Kalaba formulation

J.T. Jiolat[1] , J.L. Le Carrou[1] , J. Antunes[2] , C. d'Alessandro[1]

[1] Sorbonne Université, Centre National de la Recherche Scientifique, Institut Jean Le Rond d'Alembert, 4, Place Jussieu 75252 Paris, France

[2] Centro de Ciencias e Tecnologias Nucleares, Instituto Superior Técnico, Universidade de Lisboa, Estrada Nacional 10, Km 139.7, Bobadela LRS, 2695-066, Portugal

Abstract

The vibratory and acoustic modeling of musical instruments is important for several purposes in cultural heritage preservation, performance studies and musical creation. On the one hand, building a model helps understanding the key features of an instrument, and then is useful for evaluation, documentation and preservation of historical models. On the other hand, modeling and simulation can help for improving existing instruments, or even designing new instruments by extension of the model. The clavichord is an early keyboard instrument equipped with a very simple mechanics. The strings are excited by small metal wedges or blades (the tangents) placed at the end of the keys. The tangent remains in contact with the strings for the duration of the note, defining the vibrating length of the string. All strings are coupled at a same bridge. A string is divided into three sections: a damped section (DS) between the hitch-pin and the tangent; the played section (PS), excited by the tangents, between the tangent and the bridge; and the resting section (RS) between the bridge and the tuning pin. Because of the coupling through the bridge of the PS and RS, the RS is set into vibration, acting as sympathetic strings. The vibratory responses of the RS is modelled using a modal approach based on the Udwadia-Kalaba formulation. Firstly, a review of the method is presented, accompanied with measurements performed on an instrument (copy of a Hubert 1784 fretted clavichord), which include an experimental modal analysis at the instrument bridge and measurements of string motions. Then, simulation results are reported and compared with experimental measurements.

Keywords: Sympathetic vibration, Clavichord, Udwadia-Kalaba formulation, String coupling, Modal analysis

1 Introduction

The sound of string instruments results of the vibratory behavior of coupled mechanical subsystems. These couplings can be studied by using physical modeling of several kinds. For instance, in the case of the concert harp, the coupling of the strings and the soundboard has been modeled by means of transfer matrices [3]. Also, it could be modeled by using finite element methods or experimental modal analysis, in particular using substructure techniques. In the case of the guitar, the couplings have been modeled by extracting the modal parameters of the soundboard at the bridge locations where the strings and the structure motions are coupled [1]. In the clavichord, a string is divided into three functional sections: a damped section (DS) between the hitch-pin and the tangent; the played section (PS), excited by the tangents, between the tangent and the bridge; and the resting section (RS) between the bridge and the tuning pin (see figure 1). The RS of the string is not directly excited by the tangent but is subjected to the motion constraint at the bridge. Then it is set into vibration, acting as sympathetic strings. Our objective is to predict the vibratory response of the RS of strings, set indirectly into vibration as a consequence of the excitation of one PS. To proceed accordingly, we first present the Udwadia-Kalaba (U-K) formulation and its modal extension, in order to compute the vibratory responses of a set of coupled mechanical substructures. Then, having extracted the necessary experimental modal parameters from our studied clavichord, we present some results from our numerical simulation.

2 Model U-K

The U-K formulation was originally obtained from the Gauss principle of least action. Then, in the papers by Arabyan and Wu [2] and Laulusaand Bauchau [5], an original algebraic approach was found for deriving the U-K formulation for constrained systems from the classical formulation with Lagrange multipliers [1]. Let us consider a mechanical system with mass matrix $\mathbf{M}$ which is subjected to an external force vector $\mathbf{F_e}(t)$, which includes all constraint-independent internal and external forces. This system is also subjected to a set of P holonomic and non-holonomic constraints which depend on the system displacement $\mathbf{x}(t)$ and velocity $\mathbf{v}(t)$. Denoting the dynamical solution $\mathbf{x_u}(t)$ of the unconstrained system and the one $\mathbf{x}(t)$ of the constrained system, which depends on the constraining forces $\mathbf{F_c}(t)$, and following [2], one obtains the motion equations of the constrained system proposed by Udwadia and Kalaba [1, 2] :

$$\ddot{\mathbf{x}} = \ddot{\mathbf{x}}_u + \mathbf{M}^{-1/2}\mathbf{B}^{+}(\mathbf{b} - \mathbf{A}\ddot{\mathbf{x}}_\mathbf{u}). \tag{1}$$

$$\ddot{\mathbf{x}}_u = \mathbf{M}^{-1}\mathbf{F}_e(t) \tag{2}$$

where $\mathbf{A}$ is the constraint matrix, $\mathbf{b}$ is a known constrained vector, $\mathbf{B}^{+}$ is the Moore-Penrose inversion of matrix $\mathbf{B} = \mathbf{A}\mathbf{M}^{1/2}$. The original character of this approach is that it can be used for conservative or dissipative, linear or non-linear systems. Moreover, the generalized inverse $\mathbf{B}^{+}$ can be rendered numerically robust, even when the constraint matrix is singular. For a particular excitation $\mathbf{F}_e(t)$, we can solve these equations using a suitable time-step integration scheme. Next, we adapt the U-K formulation in order to deal with continuous flexible systems whose dynamics will be described in terms of modal coordinates. We assume a set of S vibrating subsystems, each one defined in terms of its unconstrained modal basis and being coupled through P kinematic constraints. Then, using the usual modal equations that govern the physical motion of the subsystems, we end up with similar equations of motion, which are described now in terms of modal parameters [1].

$$\ddot{\mathbf{q}} = \boldsymbol{W}\tilde{\mathbf{M}}^{-1}(-\tilde{\mathbf{C}}\dot{\mathbf{q}} - \tilde{\mathbf{K}}\mathbf{q} + \mathbf{F_{ext}}) \tag{3}$$

where $\mathbf{q}$ represent the vector of modal displacements, $\tilde{\mathbf{M}}$, $\tilde{\mathbf{K}}$, $\tilde{\mathbf{C}}$ are respectively the modal mass matrix, modal stiffness matrix, and modal damping matrix, while $\boldsymbol{W} = \mathbf{1} - \tilde{\mathbf{M}}^{-1/2}\boldsymbol{B}^{+}\boldsymbol{A}$ is a convenient global transformation matrix (which is computed before the time loop), where $\boldsymbol{A}$ is the modal constraint matrix, and $\mathbf{F_{ext}}$ are the external modal forces applied on the system. In order to proceed to the computation of the vibratory response of the constraint system, for a given external force vector, we need to obtain the modal parameters of each unconstrained subsystem. For the strings, we consider the classical mode shapes that we find theoretically for a flexible string. We also use a theoretical formulation for the damping of the string [4]. For the simulation, we decide to take 50 modes for each strings, covering a frequency range up to 24.5 kHz. Concerning the modal parameters of the instrument soundboard, which were measured at the bridge, these were obtained through experimental modal identification, using 37 points for the discretization along the bridge. Once we measured the vibratory frequency response functions (between a reference location and each point of the bridge), we proceeded to the modal identification using a frequency-domain approach called LSRF (Least-squares rational function estimation method), implemented in Matlab [6]. This modal analysis was performed within a frequency band going from 40 Hz to 800 Hz, leading to 12 identified modes.

3 Results and conclusion

To compare our model with experimental data, we used a vibrometer to measure the vibratory velocity of the RS of the C5 string, at two centimeters from the bridge, induced by the tangent excitation of PS of the F3 string (i.e. playing the F3 key), all the other strings being muffled. The vibratory response is only measured in the vertical polarization of the motion of the string, since the model developed gives the response in just one polarization of motion. Our first step was to model the F3 PS and the G4 and C5 RS being coupled with the bridge (see figure 1). We choose these two strings because their RS have harmonic frequency relations with the harmonics of the PS of the F3 string: therefore a significant vibratory coupling should be expected. We produced numerically a realistic string excitation such that the response of the played string was as close as possible to the experimental response. In figure 2, we compare the spectral response of the C5 RS given by the numerical simulation with the measured one. In both results, we see the fundamental frequency peak of the F3 string which is at 328 Hz and all its harmonics, which are the partials transmitted to the C5 RS by means of the coupling with the bridge. Also, we note the presence of the fundamental frequency peak of the C5 RS which is at 491 Hz and its harmonics, being present because of the impulse response given to all substructures by the tangent excitation. Figure 2 shows a good agreement between

the numerical simulation and measurement. So with this simplified model, we can take account of much of the physics being involved despite of the complexity of this instrument. For example, the coupling of the string with the bridge is quite simplified in the model. However, some spectral components do not have the same spectral amplitudes. In particular, we see that the partial at 200 Hz is absent in the simulation. We conjecture that this frequency peak comes from a soundboard mode of the clavichord which was not taken into account in the model. As for the other partials, their lack of spectral energy is probably due to a lack of precision in the estimation of the damping of the strings, and/or from some inaccuracy of the simulated string excitation. To further improve the model, we should consider all the 74 sympathetic strings of the Hubert clavichord in our simulation, which implies much longer computations. However, repeating the same measurement with all strings being free, the vibratory response of the RS of the C5 string remains quite unchanged. So we may not need to consider all the strings in the model to obtain a better result. Also, to improve our results, we should proceed to a more precise study of the damping of the strings and of the excitation features, to have a better estimation of the spectral amplitude of each partial of the computed response.

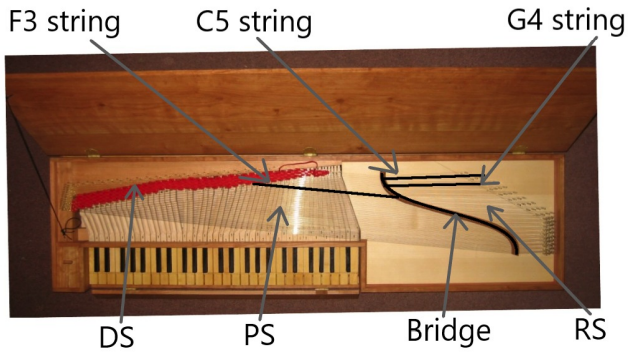

Fig. 1: Photo from above of the Hubert clavichord, with indications as to the substructures being modeled in our numerical simulations

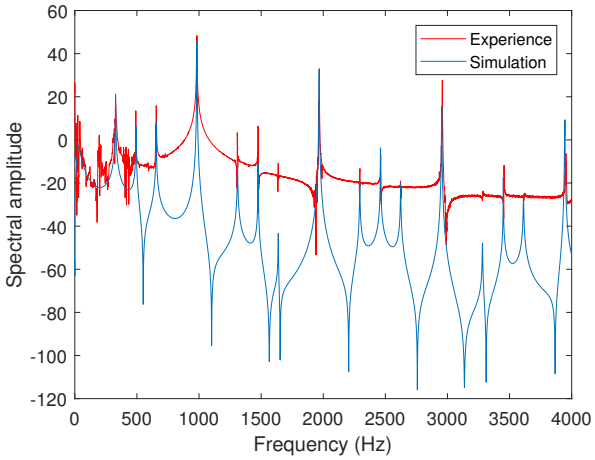

Fig. 2: Spectral comparison between the experimental signal measured with the vibrometer and the simulation of the C5 string having excited the F3 string of the Hubert clavichord

References

[1] Jose Antunes and Vincent Debut. Dynamical computation of constrained flexible systems using a modal udwadia-kalaba formulation: Application to musical instruments. *The Journal of the Acoustical Society of America*, 141(2):764–778, 2017.

[2] Ara Arabyan and Fei Wu. An improved formulation for constrained mechanical systems. *Multibody System Dynamics*, 2(1):49–69, 1998.

[3] Jean-Loïc Le Carrou, Francois Gautier, Nicolas Dauchez, and Joël Gilbert. Modelling of sympathetic string vibrations. *Acta Acustica united with Acustica*, 91(2):277–288, 2005.

[4] C Cuesta and C Valette. Mécanique de la corde vibrante. *Paris: Hermes*, 520, 1993.

[5] André Laulusa and Olivier A Bauchau. Review of classical approaches for constraint enforcement in multibody systems. *Journal of Computational and Nonlinear Dynamics*, 3(1):011004, 2008.

[6] Ahmet Arda Ozdemir and Suat Gumussoy. Transfer function estimation in system identification toolbox via vector fitting. *IFAC-PapersOnLine*, 50(1):6232–6237, 2017.

Proceeding in the *International Symposium on Music Acoustics* (ISMA)

PROCEEDINGS of ISMA 2019
International Symposium on Music Acoustics

13 - 17 September 2019 in Detmold, Germany

A parametric study of finger motions when playing the clavichord : towards characterization of expressive control.

Jean-Théo JIOLAT, Jean-Loïc LE CARROU, Christophe d'ALESSANDRO

[1]Sorbonne Université, CNRS, Institut Jean le Rond d'Alembert, Équipe LAM, France,
{jean-theo.jiolat,jean-loic.le_carrou,christophe.dalessandro}@sorbonne-universite.fr

Abstract

The clavichord is considered to be the most demanding keyboard instrument in terms of finger control. This is because of its direct mechanisms: the key works as a lever. When the finger presses the key, the tangent (metal blade) on the key's extremity goes up and strike the string. And as long as the finger remains pressed on the key, the tangent remains in contact with the string, leading to string's tone variation. The loudness of the sound is proportional to the velocity of the key's displacement. Then there is a duality between loudness and pitch accuracy. This is the paradox of the clavichord. The objective of the study is to analyze experimentally the vibro-acoustical consequences of the instrument with respect to the gestural strategies of the finger. To proceed, an experimented player performs in different configurations two main gestures: the pushed and pulled gesture. A robotic finger is used to simulate different trajectories in terms of downward displacement and velocity. The study shows that the pushed and pulled gestures have opposed influences on the fundamental frequency and on the sound level. The robotic finger demonstrates that a rise in sound level without a rise in fundamental frequency is possible.

Keywords: Clavichord, gesture, robotic finger

1 INTRODUCTION

1.1 The clavichord's paradox

The clavichord is the earliest stringed keyboard instruments, dating back to the XVth century [1]. Its sound level is low compared to other stringed instruments, and it is the only keyboard instrument allowing for some pitch control. When a key is pressed, the corresponding pair of strings is impacted by a small metal blade (the tangent) placed at the end of the key. As long as the key is pressed, the tangent remains in contact with the strings. The tangent is at the same time the nut (i.e. one extremity) of the string and the string exciter (the string is then excited at a vibration node). It has been showed experimentally that the sound level of the clavichord is proportional to the tangent velocity at impact [7]. So the faster the key is pressed, the louder the sound becomes. However, when a key is pressed with a high velocity, the key's displacement tends to be higher. The tangent raises the string, then increases its tension, and thereby increases the vibration fundamental frequency. As a result, playing louder ends up in raising the pitch, if the key is pressed in a simple vertical motion. To control independently loudness and intonation would require a paradoxical gesture: at the tangent-string contact, the tangent should have enough velocity, but should not raise the string. In other words, the key should transfer all the tangent momentum to the string, but without raising it, or losing contact. This dependence between loudness and pitch accuracy is coined "the clavichord's paradox"[4, 5]. It is difficult, at least for human players, to achieve exactly such a motion. However compromises between tangent impact velocity and string displacement are possible.

1.2 Historical clavichord techniques

The clavichord is considered as the most demanding among keyboards instruments in terms of finger control. This is because every nuance of pressure of the finger on the key is likely to change loudness and intonation. In addition both finger velocity and displacement must be controlled because of the clavichord's paradox. To

Figure 1. Photo from above of the Hubert clavichord.

deal with these constraints, specific performance practice have been elaborated. Because of these constraints, the clavichord has always been highly praised as a pedagogical instrument. Several texts describing clavichord performance around Johann Sebastian Bach's circle, "Every Players first Grammatica" to quote J.G. Walther (1732) (see [12], page 169), mention a specific technique called "Schnellen" [11], which can be translated in French by "tire" [5] and in English by "pulled" (see for instance, J.J. Quantz, 1752, C.P.E. Bach 1752, Forkel 1802). In this technique, the finger tip is drawn back quickly after contact with the key, in a sliding motion.

1.3 Measurement and simulation of fingers motions

In a preceding work [4], the effect of vertical finger motion ("pushing motion") and sliding finger motion ("pulling") on loudness and pitch of clavichord tones have been studied. It has been shown that the pulling gesture is a better compromise for dealing with the clavichord's paradox: loudness and pitch are controlled more independently with pulled than with pushed motions. The aim of the present work is to study the clavichord's paradox with the help of new measurement techniques and robotic simulation: 1/ to measure accurately finger trajectories and their consequences on vibration and sound patterns (Section 2); 2/ to reproduce these trajectories using a robotic finger, in order to study the limits of the clavichord's paradox, and then the "optimal" trajectories, decoupling key velocity at impact and string displacement (Section 3).

2 MEASUREMENTS OF FINGER AND VIBRATORY MOTIONS

2.1 Experimental setup

The instrument under study has been built by C. d'Alessandro and C. Besnainou, and completed in 2007 (at The Paris Workshop, led by M. Ducornet, in Montreuil). It is based on a kit designed by E. Dancet and M. Ducornet after XVIIIth century unfretted clavichord models by G. Hubert. The instrument is not an exact copy of an historical model. It has been built especially for acoustic investigations, but it has occasionally been played in concert. The instrument has 51 keys, from C to d3, with double strings in brass. Its dimensions are 1267 mm x 358 mm x 112 mm. It is tuned at A=415 Hz, in a Kirnberger II temperament. Vibrating string lengths C = 1097mm, c = 926mm, c1 = 509mm, c2 = 262mm, c3 = 122mm.

The objective is to measure the vibration of the excited string resulting from the motion of the musician's finger. In preceding works, measurements were performed with the help of an accelerometer near the tangent, a string-tangent contact signal and a measurement microphone. It appeared necessary to measure directly the finger motion and the string motion, using non-invasive measurement devices. Finger motions are filmed by a high-speed camera (Phantom Miro M 120) with a 2000 frame per second rate. Several marks are placed on the finger. Trajectories of these marks are estimated thanks to image processing.

String vibrations are measured with the help of calibrated opto-switch sensors [8]. These sensors are optical

forks, positioned around the string. The string motion in one direction is measured with accuracy and without contact. Only the vertical displacement of the string is considered here (although the horizontal displacement can also be significant). The string chosen for our measurements is the G2 string (length is 70 cm, fundamental frequency 185 Hz). The sensor is placed at 2 cm from the extremity of the string, near the bridge in order to be within its measurement range. Sound pressure is measured with the help of an omnidirectional DPA 4006-TL microphone placed at 30 cm above the soundboard. A set of 8 trajectories are recorded, using index and middle fingers, pulled and pushed motions for long and short notes.

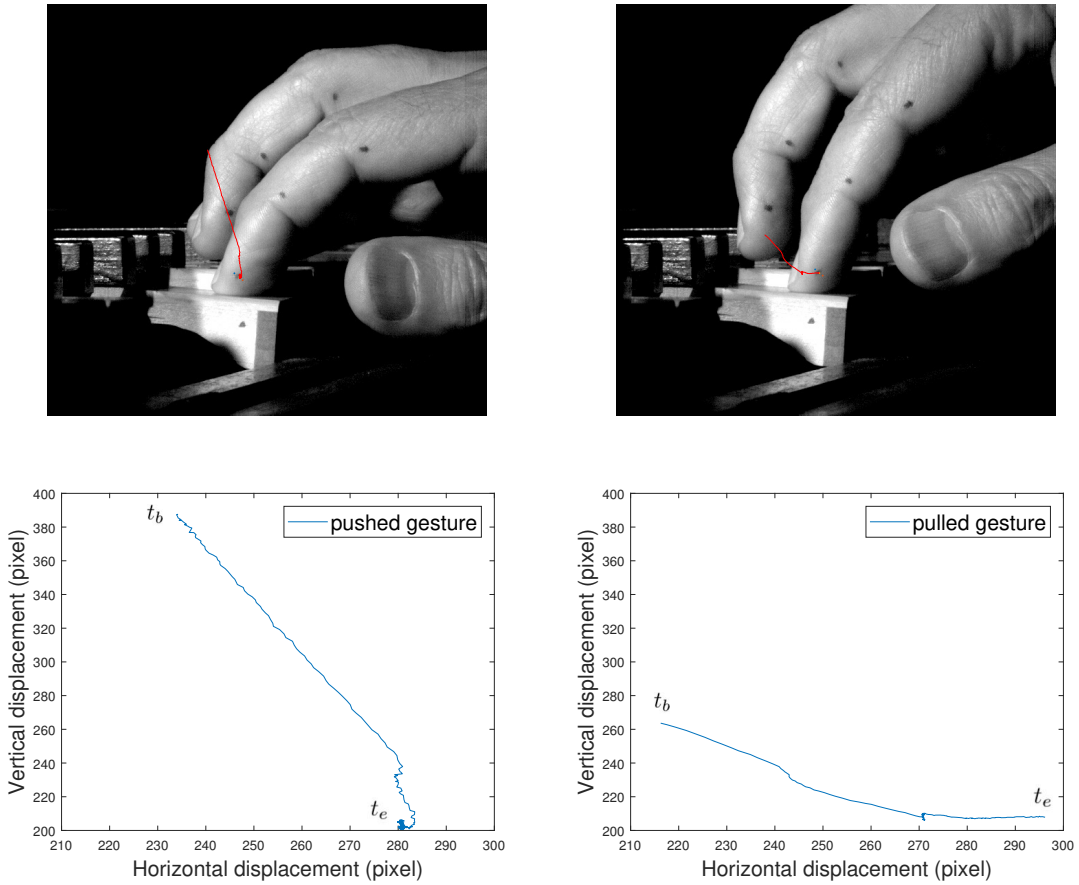

Figure 2. (Top) Images of the pushed (left-hand side) and the pulled gesture (right-hand side) performed by the index finger. (Bottom) Trajectories of the pushed (left-hand side) and the pulled gesture (right-hand side) performed by the index finger (with t_b the beginning time and t_e the ending time).

2.2 Results

In figure 2, we used the videos to extract the trajectories representative of the two distinct motions : the pushed and pulled gestures. The pushed motion refers to a vertical trajectory, the finger going mostly downward. The pulled motion corresponds to a vertical and horizontal trajectory, the finger sliding on the key and going downward at the same time. Figure 2 displays a selection of extracted trajectories. Note that the key depression is shallower in the second case.

Example of string vibration pattern are displayed in figure 3 and 4 for the pushed and pulled gestures by the index finger. As the sensor is placed near the bridge, the vibratory motion is of small amplitude, about 0.2 mm.

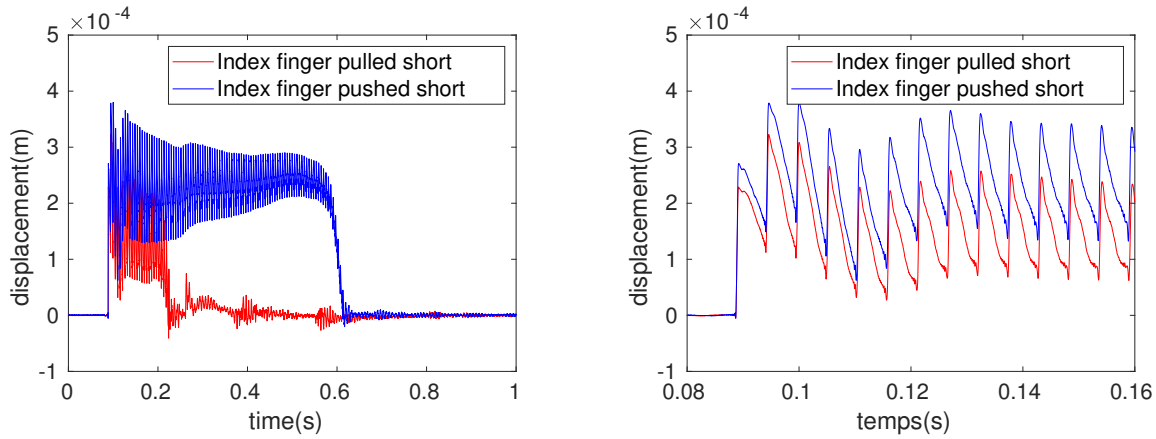

Figure 3. Vibratory signal of the G2 string excited by means of the two different trajectories done by the index finger with a short length (left-hand side), with a zoom at the beginning of the signals (right-hand side).

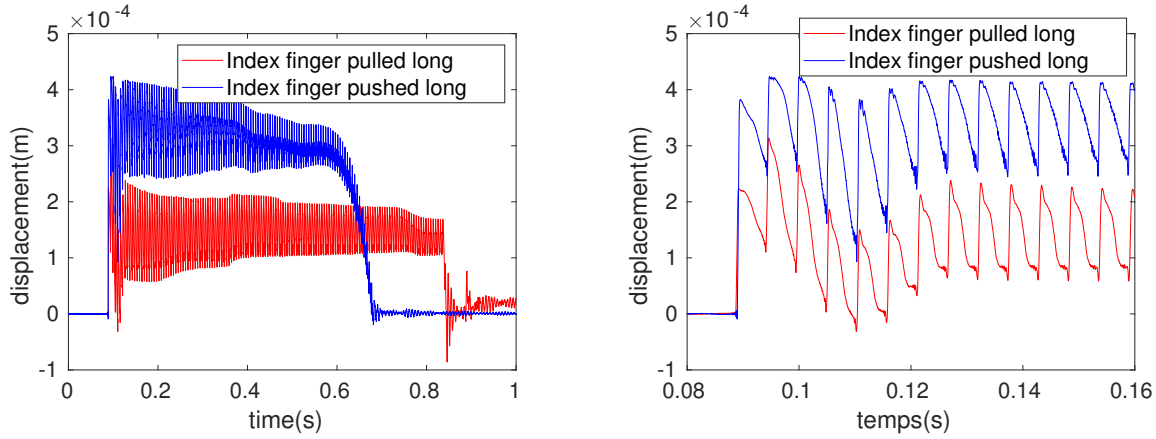

Figure 4. Vibratory signal of the G2 string excited by means of the two different trajectories done by the index finger with a long length (left-hand side), with a zoom at the beginning of the signals (right-hand side).

The string height is also small at this position, about 0.2-0.3 mm. It is much larger at the tangent position. The string is much more elevated in the case of the pushed gesture than the pulled one (see figure 3 and 4). Because of this difference in string height, the string tension and then the sound fundamental frequency is higher for the pulled motion. Note that the vibration amplitude is also larger in the case of the pushed gesture, resulting in a louder tone. Fundamental frequency is measured on the sound and vibration signals using the Yin algorithm [6] implemented in Matlab. Fundamental frequency with respect to time (G2 string) is displayed in figure 5. As predicted, the fundamental frequency is higher for the pushed gesture compared to the pulled gesture. The difference between the pushed and the pulled gesture is more than 4 cents for some conditions. Such a difference is perceptually noticeable. Fundamental frequency gives information about the way the musician deals with the contact between the tangent and the string with respect to time. In figure 5, one can observe that the fundamental frequency for the pushed gesture decreases with respect to time, whereas that of the pulled gesture remains around the same fundamental frequency although with some little hills. This shows that the key control differs for both gestures. These variations of finger depth after the string-tangent contact are certainly perceived in terms of quality of touch.

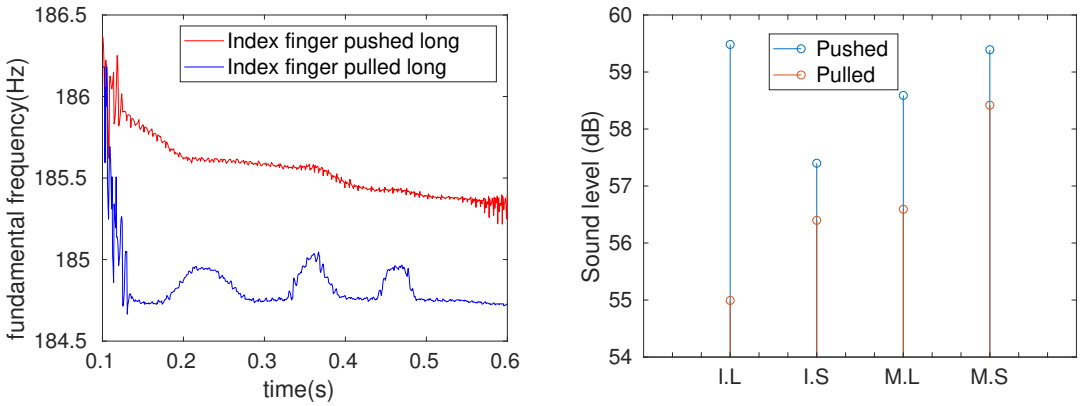

Figure 5. Fundamental frequency of the signals in the case of the pushed and pulled gesture done by the middle finger and the index finger (left-hand side). Sound level of the different exciting configurations (right-hand side) (I : Index finger, M : Middle finger, S : Short, L : Long).

Figure 6. Measurement devices: (left-hand side) optical forks for string displacement. (right-hand side) DRoPi-Crobotic finger for key trajectory control.

The sound level in dB for the different microphone signals are displayed in figure 5 (integration time 250 ms). Pushed gestures produce higher sound levels than pulled gestures. This has already been observed on the signal amplitude in figure 3 and 4.

In summary, different gestures, corresponding to different finger trajectories, are producing different vibratory patterns of the string, and then different sounds. In the small set of recordings available, the pushed motions always produce a larger string displacement : the string is always raised higher, and the amplitude of vibration is larger. A larger amplitude of vibration results in a louder sound. A higher string height results in a higher fundamental frequency. For the same reasons, the finger motion in the case of pulled gestures gives lower fundamental frequencies and also weaker sounds. Note that in previous studies it has been shown that pulled motions, to some extent, allows for independent loudness and pitch control, a result that cannot be observed here, because no sample have similar loudness. These measurements are the first direct measurements of string height, and are in good agreement with the theory developed in [7].

3 ROBOTIC SIMULATION OF FINGERS MOTIONS

3.1 Experimental setup: the robotic finger

Measurements of finger motion show the dependence between string height, sound radiated and fundamental frequency. As predicted by the clavichord's paradox, it seems difficult to control simultaneously the key (then tangent, then string) velocity and displacement. The pulled motion provides a better control and a better management of the clavichord's paradox, because the finger trajectory is more complex: pressure on the string can be released after the tangent-string impact.

It is interesting to study the clavichord's paradox with the help of controlled and reproducible key trajectories. For this purpous, a robotic finger is used. The DROPIC robot [9] has been initially developed for simulation of finger trajectories in plucking gesture of harps [3, 2]. It has been applied to keyboard instruments in studies of the plectra effects for the harpsichord. [10]. The robotic finger has two degrees of freedom. It can reproduce any trajectory in a plane parallel to the axis of the key. Note that the key itself has only one degree of freedom. The effort for depressing a key is relatively weak, less than 2 N.

For a given starting trajectory, two parameters are considered and modified: downward displacement (resulting in string height) and its maximal velocity (corresponding to loudness). The A2 string (length is 59.1 cm, fundamental frequency 205Hz) is studied. The initial position of the robotic finger above the key is set before modifying either the velocity or the displacement. A joint measure of the string vibration by means of calibrated opto-switch sensors is performed. Three different velocities with the same displacement, and three different downward displacements with the same velocity have been programmed. The displacement of the key corresponding to a referent trajectory performed by the robotic finger is displayed in figure 8. The trajectory has a typical shape with a notch followed by a plateau. It is possible to adjust independently the depth of the notch and the height of the plateau, that correspond roughly to the key velocity at contact and to the string height.

3.2 Trajectories simulation and sound results

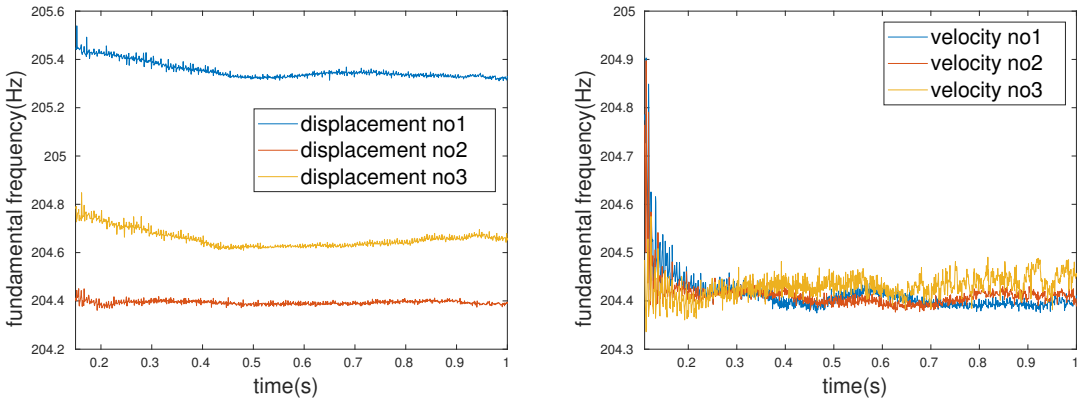

Figure 7. Tracking of the fundamental frequencies of the signals in the case where we modify the displacement of the key (left-hand side) and in the case where we modify its velocity (right-hand side).

Systematic variations of displacement and velocity are performed. Note that in this second experiment, the note studied is A2 instead of G2 studied in Section 2. These two notes are close enough to be compared. In figure 8, the key velocity is varying but the key depth is constant. The key depth is about 5-6 mm in this case. The resulting average string elevation is 0.1 mm.

Figure 7 displays the fundamental frequency of the different signals measured when the key is played with

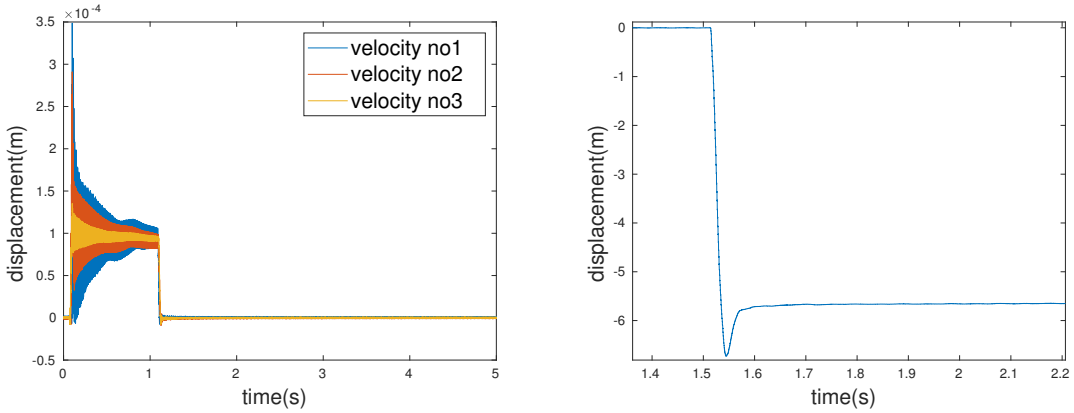

Figure 8. Temporal signals of the A2 string produced by the different velocities of the key (left-hand side). Displacement of the key in the case of the referent trajectory performed by the robotic finger (right-hand side).

the robotic finger. The resulting fundamental frequency does not change, while the amplitude of the signal increases. This shows that the trajectory of the finger is well repeated by the robot no matter the change in velocity. Moreover, it demonstrates that the clavichord's paradox can be managed with appropriate trajectories. These results also confirm that the displacement of the key is directly linked to the string's fundamental frequency. Conversely, changing the displacement of the key but maintaining the same velocity produces changes in fundamental frequency. However, fundamental frequency is very stable in the case of the robotic finger compared to a musician's finger (compare figures 7 and 5).

These results demonstrate that a robotic control is able to manage the clavichord's paradox. Whether human and robotic control are comparable is questionable. In the present experiment, the robotic finger has no haptic or sound feedback: the trajectories are optimized directly, without any perceptual loop. On the contrary, human control relies much on audio and haptic feedback. The musicians tend to control the contact between the tangent and the string after the excitation by modifying the key position according to the perceived effect of their initial motion. This variation in time of the key position is probably an essential feature of the specific style of a musical performance. Another difference between the robotic finger and human finger is their mechanical and dynamical properties. Human fingers have a much limited range of velocity and acceleration than the robot. Oscillations of the key-string-finger system that are observed in human control [7] seem negligible in the case of the robotic finger (see the displacement of the key in figure 8).

4 CONCLUSIONS

This work presents two experiments addressing the clavichord's paradox, i.e. simultaneous control of velocity and displacement of the string and tangent when playing the instrument. In a first part, new measurements using a new methodology is used. Two types of finger trajectories have been used for performing two different motions : the pushed and the pulled gesture. This experiment confirms the dependence of displacement and velocity, and the possibility to modulate this dependence with appropriate gestures. In the second experiment, a robotic finger is used to further optimize the key trajectory, by modifying in terms of velocity and downward displacement a referent trajectory. In this case it seems possible to manage the clavichord's paradox, and to control independently velocity and displacement, i.e. intonation and loudness of the instrument. Whether a musician would be able to effectively perform this type of movement remains an open question.

ACKNOWLEDGEMENTS

The authors thank Sebastien Guy and Laurent Quartier for their help during the measurements.

REFERENCES

[1] B. Brauchli. *The clavichord*. Cambridge University Press, 1998.

[2] D. Chadefaux, J.-L. Le Carrou, and B. Fabre. A model of harp plucking. *The Journal of the Acoustical Society of America*, 133(4):2444–2455, 2013.

[3] D. Chadefaux, J.-L. Le Carrou, M.-A. Vitrani, S. Billout, and L. Quartier. Harp plucking robotic finger. In *Intelligent Robots and Systems (IROS), 2012 IEEE/RSJ International Conference on*, pages 4886–4891. IEEE, 2012.

[4] C. D'Alessandro. Le paradoxe du clavicorde. In *Congrès Français d'Acoustique (CFA 2016)*, pages 2263–2269. Société Française d'Acoustique, 2016.

[5] C. D'Alessandro. Le paradoxe du clavicorde et la technique de Bach au clavier. *Revue musicale OICRM*, 6(1):87–112, 2019.

[6] A. De Cheveigné and H. Kawahara. Yin, a fundamental frequency estimator for speech and music. *The Journal of the Acoustical Society of America*, 111(4):1917–1930, 2002.

[7] C. d'Alessandro. On the dynamics of the clavichord: From tangent motion to sound a. *The Journal of the Acoustical Society of America*, 128(4):2173–2181, 2010.

[8] J.-L. Le Carrou, D. Chadefaux, L. Seydoux, and B. Fabre. A low-cost high-precision measurement method of string motion. *Journal of Sound and Vibration*, 333(17):3881–3888, 2014.

[9] J.-L. Le Carrou, D. Chadefaux, M.-A. Vitrani, S. Billout, and L. Quartier. Dropic: A tool for the study of string instruments in playing conditions. In *Acoustics 2012*, 2012.

[10] A. Paté, J.-L. Le Carrou, A. Givois, and A. Roy. Influence of plectrum shape and jack velocity on the sound of the harpsichord: an experimental study. *The Journal of the Acoustical Society of America*, 141(3):1523–1534, 2017.

[11] M. Van Delft. Schnellen. a quintessential articulation technique in eighteenth-century keyboard playing. *The Keyboard in Baroque Europe*, Christopher Hogwood (dir.)(1):187–197, 2003.

[12] J. G. Walther. *Musicalisches Lexicon oder Musicalische Bibliothec*. Wolfgang Deer, 1732.

Abstract

The objective of this PhD is to study the vibro-acoustic behaviour of the clavichord, from its excitation system to the sympathetic strings vibration. The Udwadia-Kalaba formulation is used to model the instrument as a coupled mechanical system, reduced to its main vibratory substructures: the key-tangent substructure, the string, the damper and the bridge-soundboard. The Kirchhoff-Carrier model is introduced to model the non-linear geometric deformation of the clavichord string responsible for the change in its fundamental frequency when it is excited by the tangent. Simulation of this model give satisfactory results compared to the measurements and experimental results found in the literature. The main features of the excitation system are satisfactorily reproduced: the pitch shift caused by the string uplift, the linearity between the vibratory level and the logarithm of the impact velocity as well as the link between spectral slope and impact velocity. The "clavichord paradox", referring to the demanding gesture of the musician's finger to balance between pitch shift and sound level, is studied experimentally with the help of a clavichord player and by means of a robotic finger on a specific clavichord, made from a model conceived by C.G. Hubert. Sympathetic string vibration in the clavichord create two different vibro-acoustic effects: the reverberation effect similar to that found in room acoustics, and string resonance occurring when frequency coincidence between two string partials take place. These two effects are studied experimentally and numerically. The comparison between simulations and measurements are consistent and put forward the veering of the partial frequency and damping at resonance. It highlights the relation between the mechanical properties of the string-bridge coupling and string resonance, putting forward the acoustic features of this instrument and the adjustment part done by the instrument maker.

Keywords : clavichord, Udwadia-Kalaba formulation, coupled system, experimental study, sympathy, reverberation, resonance

Résumé

L'objectif de cette thèse consiste à étudier le comportement vibro-acoustique du clavicorde, depuis le système d'excitation jusqu'à la vibration des cordes sympathiques. La formulation Udwadia-Kalaba est utilisée pour modéliser l'instrument comme un système mécanique couplé réduit à ses sous-structures vibratoires principales : la sous-structure tangente-touche, la corde, les étouffoirs et le système chevalet-table. Le modèle de Kirchhoff-Carrier est introduit pour modéliser les déformations géométriques non-linéaires de la corde du clavicorde à l'origine du changement de sa fréquence fondamentale lors de l'excitation par la tangente. La simulation du modèle donne des résultats satisfaisants comparés aux mesures et aux résultats expérimentaux de la littérature. Les caractéristiques principales de l'excitation sont reproduites : le changement de fréquence fondamentale causé par le soulèvement de la corde, la linéarité entre le niveau vibratoire et le logarithme de la vitesse d'impact, ainsi que le lien entre la pente spectrale et la vitesse d'impact. Le « paradoxe du clavicorde », faisant référence à l'exigence du geste du doigt du musicien en vue d'un compromis entre l'augmentation de la fréquence fondamentale et le niveau sonore, est étudié expérimentalement avec l'aide d'un clavicordiste et d'un doigt robotique sur un clavicorde d'étude, fabriqué à partir d'un modèle de C.G. Hubert. La vibration des cordes sympathiques du clavicorde créent deux effets vibro-acoustiques différents : l'effet de réverbération similaire à celui présent en acoustique des salles, et la résonance se manifestant dès lors qu'une coïncidence fréquentielle entre deux partiels de corde a lieu. Ces deux effets sont étudiés expérimentalement et numériquement. La comparaison entre les simulation et les mesures sont cohérentes et mettent en évidence la déviation de la fréquence et de l'amortissement du partiel à la résonance. Ceci montre la relation entre les propriétés mécaniques du couplage corde-chevalet et la résonance de la corde, mettant en avant les spécificités sonores de cet instrument et la part de réglage du facteur.

Mots-clefs : clavicorde, formulation Udwadia-Kalaba, système couplé, étude expérimentale, sympathie, réverbération, résonance.